Separation of Colloidal Particles from Groundwater by Cross-Flow Electro- Filtration Process for Improving the Analysis of Lead

C.P. Huang (Principle Investigator)
Y.T. Lin (Graduate Research Assistant)
Department of Civil and Environmental Engineering
University of Delaware
Newark, Delaware 19716

Final Report

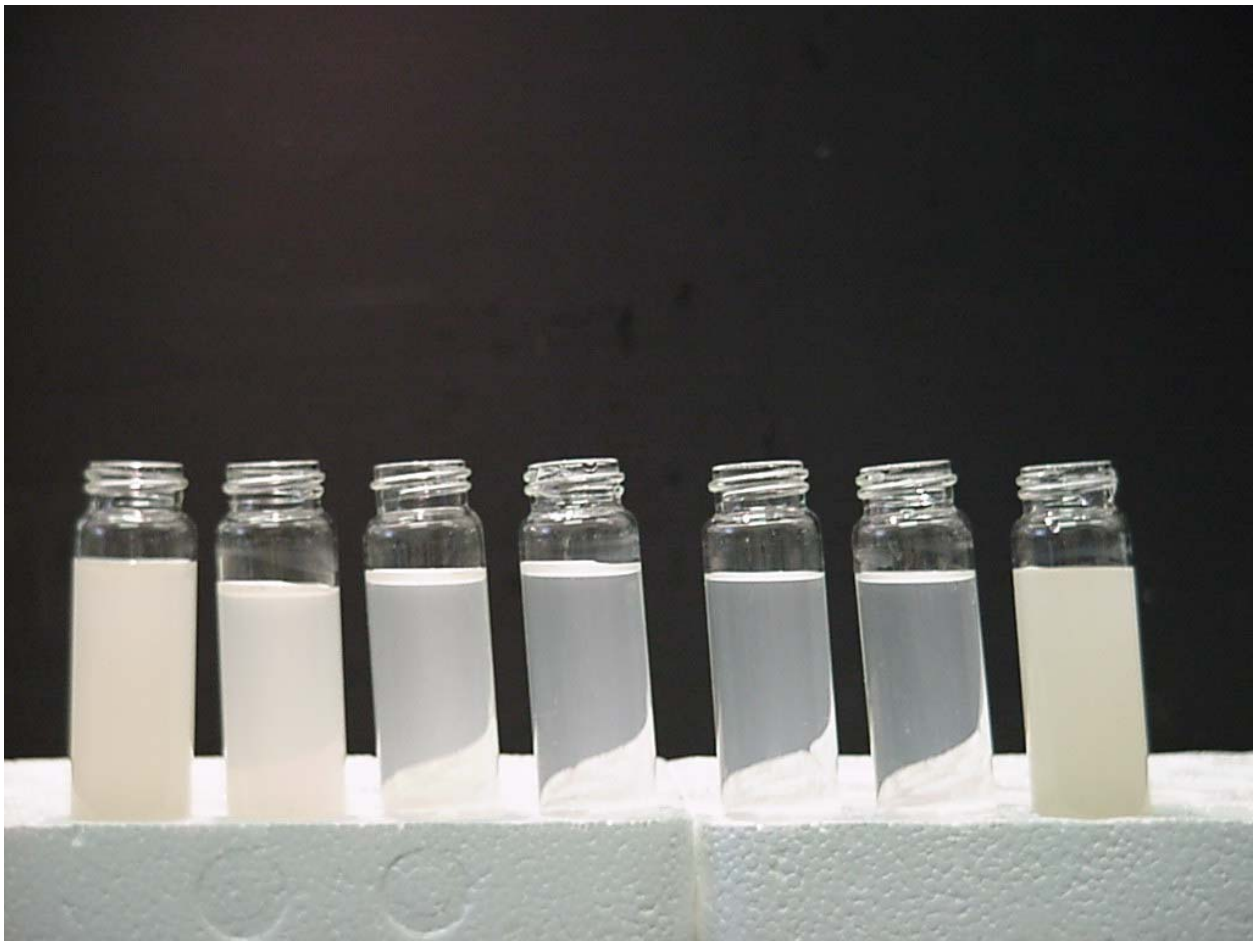

November 28, 2001

Project Officer
Paul F. Sanders
Division of Science & research
Department of Environmental Protection
Trenton, New Jersey 08625

TABLE OF CONTENTS

Table of Content i

Executive Summary xvii

1.0 Introduction 1

1.1. Groundwater Monitoring 1

1.2. Lead in the Environment 2

1.3. Objectives 6

2.0 Cross Flow Electro Filtration Module 8

2.1. Introduction 8

2.2. Design and Construction of CFEF Module 10

2.3. Basic Principles of Operation 11

3.0 Preliminary Assessment of the CFEF unit 16

3.1. Particle and Characterization 16

3.2. Operation of the EFCF Module 16

3.3. Clogging 17

3.4. Flux Production 17

3.5. Quality of Flux 18

3.6. Backwash Frequency 18

3.7. Effect of Electrostatic Field Applied 18

3.8. Effect of γ-Al_2O_3 Concentration 20

3.9. Effect of Filtration Rate 20

3.10. Effect of pH 21

4.0 Field Studies 22

4.1. Field Sampling 22

4.2. Nationally occurring Particulate 22

4.2.1. Particle Size 22

4.2.2. The Electrophoretic Mobility of Particles 23

4.3. Total Solid, Soluble Lead and Total Lead 24

4.4. Operation and Performance of EFEF Module 26

4.4.1. Operation of EFCF Module 26

4.4.2. Clogging 27
4.4.3. Quality of Flux 28
4.4.4. Backwash Frequency 28
4.4.5. Effect of Electrostatic Field Applied 29
4.4.6. Effect of pH 31
4.4.7. The Particle Size Distribution of Filtrate and Concentrate 32
4.4.8. The Total and Soluble Lead Concentration of Filtrate and Concentrate 33
4.4.9. The Speciation of Lead 34
4.4.9.1.Introduction 34
4.4.9.2.Materials and Methods 35
4.4.9.3.Results 37
5.0 Comparison with experimental Results 41
5.1. Effect of Particle size distribution 41
5.2. Effect of Electrostatic Field 41
6.0 Conclusions 45
7.0 References 49

LIST OF TABLES

Table 1. The summary of the cross-flow electrostatic-filtration module under various experiments: γ-Al_2O_3 53
Table 2. List of field samples 54
Table 3. Diameter of naturally occurring particles in well waters 55
Table 4. Major chemical characteristics 55
Table 5. The summary of performance of the cross-flow electrostatic-filtration module under various experimental conditions with groundwater samples 56
Table 6. The concentration of total and soluble lead in the filtrate and concentrate of CFEF operation 58
Table 7. The Tessier sequential extraction procedures for lead speciation 59
Table 8. Concentration of sequentially extracted and total lead as affected by electrostatic field strength in particles of well waters sample 10IB01 60
Table 9. Concentration of sequentially extracted and total lead as affected by electrostatic field strength in particles of well waters sample 10IL01 60
Table 10. Concentration of sequentially extracted and total lead as affected by electrostatic field strength in particles of well water sample 5SIIB03 61
Table 11. Concentration of sequentially extracted and total lead as affected by electrostatic field strength in particles of well water sample 5IIL02 62
Table 12. Concentration of sequentially extracted and total lead as affected by electrostatic field strength in particles of well water sample MW3IB03 63

LIST OF FIGURES

Figure 1. Main unit of the CFEF module 64
Figure 2. Power supply 65
Figure 3. Milipore (model M12: cross flow filter) units 65
Figure 4. Micro-computer for flow control 66
Figure 5 The total arrangement of the CFEF module 66
Figure 6. Schematic presentation of the flow diagram of the CFEF system 67
Figure 7. Schematic presentation of flow direction and location of sampling 78
Figure 8. Collection section of CFEF. 69
Figure 9. Theoretical removal as a function of applied electrostatic field. Particle size = 200 nm; surface charge = 18 $\mu C/m^2$ 70
Figure 10. Theoretical removal as a function of surface charge. Electrostatic field strength = 1560 V/m; particle size = 200 nm 71
Figure 11 Theoretical removal as a function of applied electrostatic field and particle size. Surface charge = 5 mC/m2 72
Figure 12 Theoretical removal as a function of particle size under various surface charges. Electrostatic field strength = 1,560 V/m 73
Figure 13. Zeta Potential of γ-Al_2O_3 as a function of pH
Experimental conditions: 100 mg /L γ-Al_2O_3; varying $NaClO_4$ concentration 74
Figure 14. Effect of electrostatic field. Experimental conditions: 100 mg /L γ-Al_2O_3; pumping speed 15% (or filtration rate 0.46 mL/min) 75
Figure 15. Effect of filtration rate on removal of colloidal particle. Experimental conditions: 100 mg/L γ-Al_2O_3; initial pH = 5.6; E = 96.8V/cm 76
Figure 16. Effect of pH on the removal of colloidal particle. Experimental conditions: pumping speeding 15% (or filtration rate 0.46 mL/min); E = 96.8V/cm 77
Figure 17. Zeta potential of naturally occurring particles as a function of pH (Well #10, bailing sample, 10IB01) 78
Figure 18. Zeta potential of naturally occurring particles as a function of pH (Well #10, low flow purging sample, 10IL01) 79
Figure 19. Zeta potential of naturally occurring particles as a function of pH (Well #5S, bailing sample, 5SIB01) 80
Figure 20. Zeta potential of naturally occurring particles as a function of pH (well #5S, low flow purging sample, 5SIL01) 81
Figure 21. Zeta potential of naturally occurring particles as a function of pH (Well #5S, bailing sample, 5SIIB03) 82
Figure 22. Zeta potential of naturally occurring particles as a function of pH (Well #5S, low flow purging sample, 5SIIL01) 83
Figure 23. Zeta potential of naturally occurring particles as a function of pH (Well #MW3, bailing sample, MW3IB03) 84
Figure 24. Zeta potential of naturally occurring particles as a function of pH (Well #MW3, low flow purging sample, MW3IL01) 85
Figure 25. Visual comparison of water sample on the various electrostatic field (Well#5S, low flow purging sample) 86

Figure 26. Change of filtrate turbidity as a function of time under various electrostatic field values (I). Experimental condition: pH = 6.5; Sample = 10IB01 87
Figure 27. Change of filtrate turbidity as a function of time under various electrostatic field values (II). Experimental condition: pH = 6.5; Sample = 10IB01 88
Figure 28. Removal efficiency as a function of time at various electrostatic field values. Experimental condition: pH = 5; Sample = 10IL01 89
Figure 29. Removal efficiency as a function of time at various electrostatic field values. Experimental condition: pH = 5; Sample = 10IL01 90
Figure 30. Removal efficiency as a function of time at various electrostatic field values. Experimental condition: pH = 6.7; Sample = 5SIL02 91
Figure 31. Removal efficiency as a function of time at various electrostatic field values. Experimental condition: pH = 7.9; Sample = MW3IB02 92
Figure 32. Steady state removal efficiency as a function of pH. Experimental conditions: pH = 5 (electrostatic field = 32.3V/cm); pH = 7 (electrostatic field = 48.4V/cm); pH = 9 (electrostatic field = 48.4V/cm); Sample = 10IB01 93
Figure 33. Steady state removal efficiency as a function of pH. Experimental condition: electrostatic field = 97.8V /cm; Sample = 5SIIB03 94
Figure 34. Steady state removal efficiency as a function of pH. Experimental conditions: pH = 5 (electrostatic field=10.3V/cm); pH = 7 (electrostatic field=13.2V/cm); pH = 9 (electrostatic field=14.8V/cm); Sample = MW3B02 95
Figure 35. Steady state removal efficiency as a function of pH. Experimental conditions: pH = 5 (electrostatic field=32.3V/cm); pH = 7 (electrostatic field=48.4V/cm); pH = 9 (electrostatic field=48.4V/cm); Sample = 10IL01 96
Figure 36. Steady state removal efficiency as a function of pH (I). Experimental condition (electrostatic field = 97.8 V/cm); Sample = 5SIL02 97
Figure 37. Distribution of particle size as affected by electrostatic field. Experimental condition: pH = 6.5; Sample = 10IB01 98
Figure 38. Distribution of particle size as affected by electrostatic field. Experimental condition: pH = 6.5; Sample = 10IL01 99
Figure 39. Distribution of particle as affected by electrostatic field. Experimental condition: pH = 6.6; Sample = 5SIIB03 100
Figure 40. Distribution of particle size as affected by electrostatic field. Experimental condition: pH = 6.7; Sample = 5SIIL02 101
Figure 41. Distribution of particle size as affected by electrostatic field. Experimental condition: pH = 7.9; Sample = MW3IB01 102
Figure 42. Distribution of particle size as affected by pH. Experimental conditions: pH = 5 (electrostatic field=32.3V/cm); pH = 7 (electrostatic field=48.4V/cm); pH = 9 (electrostatic field=48.4V/cm); Sample = 10IB01 103

Figure 43. Distribution of particle size as affected by pH. Experimental conditions: pH = 5 (electrostatic field = 32.3 V/cm); pH = 7 (electrostatic field = 48.4 V/cm); pH = 9 (electrostatic field = 48.4 V/cm); Sample = 10IL01 104
Figure 44. Distribution of particle size as affected by pH. Experimental conditions: electrostatic field = 97.8 V/cm; Sample = 5SIIB03 105
Figure 45. Distribution of particle size as affected by pH. Experimental condition: electrostatic field = 97.8 V/cm; Sample = 5SIIL02 106
Figure 46. Distribution of particle size as affected by pH. Experimental conditions: pH = 5 (electrostatic field = 10.3 V/cm); pH = 7 (electrostatic field = 13.2 V/cm); pH = 9 (electrostatic field = 14.8 V/cm); Sample = MW3IB01 107
Figure 47. Distribution of lead species in particulate collected from well water sample 10IB01 as affected by electrostatic field. Experimental condition: pH = 6.5 108
Figure 48. Distribution of lead species in particulate collected from well water sample 10IL01 as affected by electrostatic field. Experimental condition: pH = 6.5 109
Figure 49. Distribution of lead species in particulate collected from well water sample 5SIIL02 as affected by electrostatic field. Experimental condition: pH = 6.7 110
Figure 50. Distribution of lead species in particulate collected from well water sample MW3IB03 as affected by electrostatic field. Experimental conditions: pH = 7.9 111
Figure 51. Distribution of lead species in particulate collected from well water sample 10IB01 as affected by pH. Experimental conditions: pH = 5 (electrostatic field = 32.3 V/cm); pH = 7 (electrostatic field = 48.4 V/cm); pH = 9 (electrostatic field = 64.5 V/cm) 112
Figure 52. Distribution of lead species in particulate collected from well water sample 10IL01 as affected by pH. Experimental conditions: pH = 5 (electrostatic field = 32.3 V/cm); pH = 7 (electrostatic field = 48.4 V/cm); pH = 9 (electrostatic field = 48.4 V/cm) 113
Figure 53. Distribution of lead species in particulate collected from well water sample 5SIIB03 as affected by pH. Experimental conditions: pH = 5 (electrostatic field = 97.8 V/cm); pH = 7 (electrostatic field = 97.8 V/cm); pH = 9 (electrostatic field = 97.8 V/cm) 114
Figure 54. Distribution of lead species in particulate collected from well water sample 5SIIL02 as affected by pH. Experimental conditions: pH = 4.5 (electrostatic field = 97.8 V/cm); pH = 6.5 (electrostatic field = 97.8 V/cm); pH = 9.0 (electrostatic field = 97.8 V/cm) 115
Figure 55. Distribution of lead species in particulate collected from well water sample as affected by pH. Experimental conditions: pH = 5 (electrostatic field = 10.3 V/cm); pH = 7 (electrostatic field = 13.2 V/cm); pH = 9 (electrostatic field = 14.8 V/cm) 116
Figure 56. Predicting the removal of γ-Al_2O_3 as a function of applied electrostatic field. Theoretical values using Equations 15, 21 and 30 versus measured values 117

Figure 57. Predicting the removal of naturally occurring particles in well water sample 10IB01 as a function of applied electrostatic field. Theoretical values using equations 15, 21 and 30 versus measured values 118
Figure 58. Predicting the removal of naturally occurring particles in well water sample 10IL0 as a function of applied electrostatic field. Theoretical values using equations 15, 21 and 30 versus measured values 119
Figure 59. Predicting the removal of naturally occurring particles in well water sample 5SII03 as a function of applied electrostatic field. Theoretical values using equations 15, 21 and 30 versus measured values 120
Figure 60. Predicting the removal of naturally occurring particles in well water sample 5IIL02 as a function of applied electrostatic field. Theoretical values using equations 15, 21 and 30 versus measured values 121
Figure 61. The concept of resistance distribution of the CFEF unit 122

APPENDIX
LIST OF TABLES

Table A1. The effect of electrostatic field on the change of turbidity (I) 123
Table A2. The effect of electrostatic field on the removal of Al_2O_3 (II) 124
Table A3. Effect of electrostatic field on the change of turbidity (III) 125
Table A4. Effect of electrostatic field on the removal of Al_2O_3 (IV) 125
Table A5. The effect of concentration on the change of turbidity (I) 126
Table A6. The effect of concentration on the removal of Al_2O_3 (II) 127
Table A7. The effect of filtrate rate on the change of turbidity (I) 128
Table A8. The effect of filtrate rate on the removal efficiency of Al_2O_3 (II) 128
Table A9. The effect of pH on the change of turbidity (I) 129
Table A10. The effect of pH on the removal of Al_2O_3 (II) 130
Table A11. The effect of electrostatic field on the change of turbidity (I) Sample: 10IB01 131
Table A12. The effect of electrostatic field on the removal efficiency (I) Sample: 10IB01 131
Table A13. The effect of electrostatic field on the change of turbidity (II) Sample: 10IB01 132
Table A14. The effect of electrostatic field on the removal efficiency (II) Sample: 10IB01 132
Table A15. The effect of pH on the change of turbidity Sample: 10IB01 133
Table A16. The effect of pH on the removal efficiency Sample: 10IB01 133
Table A17. The effect of electrostatic field on the change of turbidity Sample: 10IL01 134
Table A18. The effect of electrostatic field on the removal efficiency Sample: 10IL01 134
Table A19. The effect of pH on the change of turbidity Sample: 10IL01 135
Table A20. The effect of pH on the removal efficiency Sample: 10IL01 135
Table A21. The effect of electrostatic field on the change of turbidity Sample: 5SIIB03 136
Table A22. The effect of electrostatic field on the removal efficiency Sample: 5SIIB03 136
Table A23. The effect of pH on the change of turbidity Sample: 5SIIB03 137
Table A24. The effect of pH on the removal efficiency Sample: 5SIIB03 137
Table A25. The effect of electrostatic field on the change of turbidity Sample: 5SIIL02 138
Table A26. The effect of electrostatic field on the removal efficiency Sample: 5SIIL02 138
Table A27. The effect of pH on the change of turbidity

Sample: 5SIIL02 139
Table A28. The effect of pH on the removal efficiency
Sample: 5SIIL02 139
Table A29. The effect of electrostatic field and pH on the change of turbidity
Sample: MW3IB02 140
Table A30. The effect of electrostatic field and pH on the removal efficiency
Sample: MW3IB02 140

APPENDIX
LIST OF FIGURES

Figure A1.	Filtration flow rate versus pumping speed	141
Figure A2.	Calibration curve for γ-Al_2O_3 as measured by turbidity (NTU)	142
Figure A3.	Effect of electrostatic field (I). Experimental conditions: 100 mg /L γ-Al_2O_3; pumping speed 20% (or filtration rate 0.77 mL/min)	143
Figure A4.	Effect of electrostatic field (II). Experimental conditions: 100 mg /L γ- Al_2O_3; pumping speed 20% (or filtration rate 0.77 mL/min)	144
Figure A5.	Effect of electrostatic field (III). Experimental conditions: 100 mg /L γ- Al_2O_3; pumping speed 15% (or filtration rate 0.46 mL/min)	145
Figure A6.	Effect of electrostatic field (IV). Experimental conditions: 100 mg /L γ- Al_2O_3; pumping speed 15% (or filtration rate 0.46 mL/min)	146
Figure A7.	Effect of γ- Al_2O_3 concentration (I). Experimental conditions: pumping speed 15% (or filtration rate 0.46 mL/min); E = 16.1V/cm	147
Figure A8.	Effect of γ- Al_2O_3 concentration (II). Experimental conditions: pumping speed 15% (or filtration rate 0.46 mL/min); E = 16.1V/cm	148
Figure A9.	Effect of filtration rate on change of turbidity. Experimental conditions: 100mg/L γ- Al_2O_3; initial pH = 5.6; E = 96.8V/cm	149
Figure A10.	Effect of filtration rate on removal of colloidal particles (I). Experimental conditions: 100 mg/L γ- Al_2O_3; initial pH = 5.6; E = 96.8V/cm	150
Figure A11.	Effect of pH on the change of turbidity. Experimental conditions: 100mg/L γ- Al_2O_3; pumping speed 15% (or filtration rate 0.46 mL/min); E = 96.8V/cm	151
Figure A12.	Effect of pH on the removal of colloidal particles (I). Experimental conditions: 100mg/L γ- Al_2O_3; pumping speeding 15% (or filtration rate 0.46 mL/min); E = 96.8V/cm	152
Figure A13.	Calibration curve for turbidity (NTU) and particulate concentration of well water. (Well #10, bailing sample, 10IB01)	153
Figure A14.	Calibration curve for turbidity (NTU) and particulate concentration of well water. (Well#10, low flow purging sample, 10IL01)	154
Figure A15.	Calibration curve for turbidity (NTU) and particulate concentration of well water. (Well#5S, bailing sample, 5SIB01)	155
Figure A16.	Calibration curve for turbidity (NTU) and particulate concentration of well water. (Well#5S, low flow purging sample, 5SIL02)	156
Figure A17.	Calibration curve for turbidity (NTU) and particulate concentration of well water. (Well#5S, bailing sample, 5SIIB03)	157
Figure A18.	Calibration curve for turbidity (NTU) and particulate concentration of well water. (Well#5S, low flow purging sample, 5SIIL01)	158
Figure A19.	Calibration curve for turbidity (NTU) and particulate concentration of well water. (Well#MW3, bailing sample, MW3IB03)	159
Figure A20.	Calibration curve for turbidity (NTU) and particulate concentration of well water. (Well#MW3, low flow purging sample, MW3IL01)	160

Figure A21. Change of filtrate turbidity as a function of time under various electrostatic field values (I). Experimental condition: pH = 6.5; Sample = 10IB01 161
Figure A22. Change of filtrate turbidity as a function of time under various electrostatic field values (II). Experimental condition: pH = 6.5; Sample = 10IB01 162
Figure A23. Change of filtrate turbidity as a function of time under various electrostatic field values (II). Experimental condition: pH = 6.5; Sample = 10IB01 163
Figure A24. Change of filtrate turbidity as a function of time under various electrostatic field values (III). Experimental condition: pH = 6.5; Sample = 10IB01 164
Figure A25. Turbidity changes as a function of time at various electrostatic field values. Experimental condition: pH = 6.6; Sample = 5SIIB03 165
Figure A26. Removal efficiency as a function of time at various electrostatic field values (I). Experimental condition: pH = 6.6; Sample = 5SIIB03 166
Figure A27. Turbidity changes as a function of time at various electrostatic field values. Experimental condition: pH = 7.9; Sample = MW3IB02 167
Figure A28. Removal efficiency as a function of time at various electrostatic field values (I). Experimental condition: pH = 7.9; Sample = MW3IB02 168
Figure A29. Turbidity changes as a function of time at various electrostatic field values. Experimental condition: pH = 5; Sample = 10IL01 169
Figure A30. Removal efficiency as a function of time at various electrostatic field values (I). Experimental condition: pH = 5; Sample = 10IL01 170
Figure A31. Turbidity changes as a function of time at various electrostatic field values. Experimental condition: pH = 6.7; Sample = 5SIIL02 171
Figure A32. Removal efficiency as a function of time at various electrostatic field values (I). Experimental condition: pH = 6.7; Sample = 5SIL02 172
Figure A33. Change of turbidity as a function of time at various pH values. Experimental conditions: pH = 5 (electrostatic field = 32.3V/cm); pH = 7 (electrostatic field = 48.4V/cm); pH = 9 (electrostatic field = 48.4V/cm); Sample = 10IB01 173
Figure A34. Removal efficiency as a function of time at various pH values (I). Experimental conditions: pH = 5 (electrostatic field = 32.3V/cm); pH = 7 (electrostatic field = 48.4V/cm); pH = 9 (electrostatic field = 48.4V/cm); Sample = 10IB01 174
Figure A35. Turbidity changes as a function of time at various pH values. Experimental condition: electrostatic field = 97.8 V/cm; Sample = 5IIB03 175
Figure A36. Removal efficiency as a function of time at various pH values (I). Experimental condition: electrostatic field = 97.8 V/cm; Sample = 5SIIB03 176
Figure A37. Turbidity changes as a function of time at various pH values. Experimental conditions: pH = 5 (electrostatic field=10.3V/cm); pH = 7 (electrostatic field=13.2V/cm); pH = 9 (electrostatic field=14.8V/cm); Sample = MW3IB02 177

Figure A38. Removal efficiency as a function of time at various pH values (I). Experimental conditions: pH = 5 (electrostatic field=10.3V/cm); pH = 7 (electrostatic field=13.2V/cm); pH = 9 (electrostatic field=14.8V/cm); Sample = MW3IB02 178
Figure A39 Turbidity changes as a function of time at various pH values. Experimental conditions: pH = 5 (electrostatic field = 32.3V/cm); pH = 7 (electrostatic field = 48.4V/cm); pH = 9 (electrostatic field = 48.4V/cm); Sample = 10IL01 179
Figure A40. Removal efficiency as a function of time at various pH values (I). Experimental conditions: pH = 5 (electrostatic field=32.3V/cm); pH = 7 (electrostatic field=48.4V/cm); pH = 9 (electrostatic field=48.4V/cm); Sample = 10IL01. 180
Figure A41. Turbidity changes as a function of time a t various pH values. Experimental condition: electrostatic field = 97.8 V/cm; Sample = 5SIL02 181
Figure A42. Removal efficiency as a function of time at various pH values (I). Experimental condition: electrostatic field = 97.8 V/cm; Sample = 5SIL02 182
Figure A43. Changes in particle size distribution during filtration operation. Experimental conditions: Electrostatic field = 32.3 V/cm; pH = 6.5; Sample: 10IB01 183
Figure A44. Changes in particle size distribution during filtration operation. Experimental conditions: electrostatic field = 48.4 V/cm; pH = 6.5; Sample = 10IB01 184
Figure A45. Changes in particle size distribution during filtration operation. Experimental conditions: electrostatic field = 64.5 V/cm; pH = 6.5; Sample = 10IB01 185
Figure A46. Changes in particle size distribution during filtration operation. Experimental conditions: pH = 5; electrostatic field = 32.3 V/cm; Sample = 10IB01 186
Figure A47. Changes in particle size distribution during filtration operation. Experimental conditions: pH = 7; electrostatic field = 48.4 V/cm; Sample = 10IB01 187
Figure A48. Changes in particle size distribution during filtration operation. Experimental conditions: pH = 9; electrostatic field = 48.4 V/cm; Sample = 10IB01 188
Figure A49. Changes in particle size distribution during filtration operation. Experimental conditions: electrostatic field = 32.3 V/cm; pH = 6.5; Sample = 10IL01 189
Figure A50. Changes in particle size distribution during filtration operation. Experimental conditions: electrostatic field = 48.4 V/cm; pH = 6.5; Sample = 10IL01 190
Figure A51. Changes in particle size distribution during filtration operation. Experimental conditions: electrostatic field = 64.5 V/cm; pH = 6.5; Sample = 10IL01 191

Figure A52. Changes in particle size distribution during filtration operation. Experimental conditions: pH = 5; electrostatic field = 32.3 V/cm; Sample = 10IL01 192
Figure A53. Changes in particle size distribution during filtration operation. Experimental conditions: pH = 7; electrostatic field = 48.4 V/cm; Sample = 10IL01 193
Figure A54. Changes in particle size distribution during filtration operation. Experimental conditions: pH = 9; electrostatic field = 48.4 V/cm; Sample = 10IL01 194
Figure A55. Changes in particle size distribution during filtration operation. Experimental conditions: electrostatic field = 32.3 V/cm; pH = 6.6; Sample = 5SIIB03 195
Figure A56. Changes in particle size distribution during filtration operation. Experiment conditions: electrostatic field = 64.5 V/cm; pH = 6.6; Sample = 5SIIB03 196
Figure A57. Changes in particle size distribution during filtration operation. Experimental conditions: electrostatic field = 97.8 V/cm; pH = 6.6; Sample = 5SIIB03 197
Figure A58. Changes in particle size distribution during filtration operation. Experimental conditions: electrostatic field = 129 V/cm; pH = 6.6; Sample = 5SIIB03 198
Figure A59. Changes in particle size distribution during filtration operation. Experimental conditions: electrostatic field = 156.8 V/cm; pH = 6.6; Sample = 5SIIB03 199
Figure A60. Changes in particle size distribution during filtration operation. Experimental conditions: pH = 5; electrostatic field = 97.8 V/cm; Sample = 5SIIB03 200
Figure A61. Changes in particle size distribution during filtration operation. Experimental conditions: pH = 7; electrostatic field = 97.8 V/cm; Sample = 5SIIB03 201
Figure A62. Changes in particle size distribution during filtration operation. Experimental conditions: pH = 9; electrostatic field = 97.8 V/cm; Sample = 5SIIB03 202
Figure A63. Changes in particle size distribution during filtration operation. Experimental conditions: electrostatic field = 32.3 V/cm; pH = 6.7; Sample = 5SIIL02 203
Figure A64. Changes in particle size distribution during filtration operation. Experimental conditions: electrostatic field = 64.5 V/cm; pH = 6.7; Sample = 5SIIL02 204
Figure A65. Changes in particle size distribution during filtration operation. Experimental conditions: electrostatic field = 97.8 V/cm; pH = 6.7; Sample = 5SIIL02 205
Figure A66. Changes in particle size distribution during filtration operation. Experimental conditions: electrostatic field = 129 V/cm; pH = 6.7; Sample = 5SIIL02 206

Figure A67. Changes in particle size distribution during filtration operation. Experimental conditions: electrostatic field = 156.8 V/cm; pH = 6.7; Sample = 5SIIL02 207
Figure A68. Changes in particle size distribution during filtration operation. Experimental conditions: pH = 4.5; electrostatic field = 97.8 V/cm; Sample = 5SIIL02 208
Figure A69. Changes in particle size distribution during filtration operation. Experimental conditions: pH = 6.5, electrostatic field = 97.8 V/cm; Sample = 5SIIL02 209
Figure A70. Changes in particle size distribution during filtration operation. Experimental conditions: pH = 9; electrostatic field = 97.8 V/cm; Sample = 5SIIL02 210
Figure A71. Changes in particle size distribution during filtration operation. Experimental conditions: electrostatic field = 17.1 V/cm; pH = 7.9; Sample = MW3IB01 211
Figure A72. Changes in particle size distribution during filtration operation. Experimental conditions: pH = 5; electrostatic field = 10.3 V/cm; Sample = MW3IB01 212
Figure A73. Changes in particle size distribution during filtration operation. Experimental conditions: pH = 7; electrostatic field = 13.2V /cm; Sample = MW3IB01 213
Figure A74. Changes in particle size distribution during filtration operation. Experimental conditions: pH = 9; electrostatic field = 14.8 V/cm; Sample = MW3IB01 214
Figure A75. Distribution of lead species in particulate collected from well water sample 10IB01 215
Figure A76. Distribution of lead species in particulate collected from well water sample 10IB01 at constant pH value. Experimental conditions: electrostatic field = 32.3 V/cm; pH = 6.5 216
Figure A77. Distribution of lead species in particulate collected from well water sample 10IB01 at constant value. Experimental conditions: electrostatic field = 48.4 V/cm; pH = 6.5 217
Figure A78. Distribution of lead species in particulate collected from water sample 10IB01 at constant pH value. Experimental conditions: electrostatic field = 64.5 V/cm; pH = 6.5 218
Figure A79. Distribution of lead species in particulate collected from well water sample 10IB01 at constant electrostatic field. Experimental conditions: electrostatic field = 32.3V/cm; pH = 5 219
Figure A80. Distribution of lead species in particulate collected from well water sample 10IB01 at constant electrostatic field. Experimental conditions: electrostatic field = 48.4 V/cm; pH = 7 220
Figure A81. Distribution of lead species in particulate collected from well water sample 10IB01 at constant electrostatic field. Experimental conditions: electrostatic field = 64.5 V/cm; pH = 9. 221
Figure A82. Distribution of lead species in particulate collected from well sample 10IL01 222

Figure A83. Distribution of lead species in particulate collected from well water sample 10IL01 at constant pH value. Experimental conditions: electrostatic field = 32.3 V/cm; pH = 6.5 223
Figure A84. Distribution of lead species in particulate collected from well water sample 10IL01 at constant pH value. Experimental conditions: electrostatic field = 48.4 V/cm; pH = 6.5 224
Figure A85. Distribution of lead species in particulate collected from well water sample 10IL01 at constant pH value. Experimental conditions: electrostatic field = 64.5 V/cm; pH = 6.5 225
Figure A86. Distribution of lead species in particulate collected from well water sample 10IL01 at constant electrostatic field. Experimental conditions: pH = 5; electrostatic field = 32.3 V/cm 226
Figure A87. Distribution of lead species in particulate collected from well water sample 10IL01 at constant electrostatic field. Experimental conditions: pH = 7; electrostatic field = 48.4 V/cm 227
Figure A88. Distribution of lead species in particulate collected from well water sample 10IL01 at constant electrostatic field. Experimental conditions: pH = 9; electrostatic field = 48.4 V/cm 228
Figure A89. Distribution of lead species in particulate collected from well water sample 5SIIB03 229
Figure A90. Distribution of lead species in particulate collected from well water sample 5SIIB03 at constant electrostatic field. Experimental conditions: pH = 5; electrostatic field = 97.8 V/cm 230
Figure A91. Distribution of lead species in particulate collected from well water sample 5SIIB03 at constant electrostatic field. Experimental conditions: pH = 7; electrostatic field = 97.8 V/cm 231
Figure A92. Distribution of lead species in particulate collected from well water sample 5SIIB03 at constant electrostatic field. Experimental conditions: pH = 9; electrostatic field = 97.8 V/cm 232
Figure A93. Distribution of lead species in particulate collected from well water sample 5SIIL02 233
Figure A94. Distribution of lead species in particulate collected from well water sample 5SIIL02 at constant pH values. Experimental conditions: electrostatic field = 32.3 V/cm; pH = 6.7 234
Figure A95. Distribution of lead species in particulate collected from well water sample 5SIIL02 at constant pH values. Experimental conditions: electrostatic field = 64.5 V/cm; pH = 6.7 235
Figure A96. Distribution of lead species in particulate collected from well water sample 5SIIL02 at constant pH values. Experimental conditions: electrostatic field = 97.8 V/cm; pH = 6.7 236
Figure A97. Distribution of lead species in particulate collected from well water sample 5SIIL02 at constant pH values. Experimental conditions: electrostatic field = 129.0 V/cm; pH = 6.7 237
Figure A98. Distribution of lead species in particulate collected from well water sample 5SIIL02 at constant pH values. Experimental conditions: electrostatic field = 156.8 V/cm; pH = 6.7 238

Figure A99. Distribution of lead species in particulate collected from well water sample 5SIIL02 at constant electrostatic field. Experimental conditions: pH = 4.5; electrostatic field = 97.8 V/cm 239
Figure A100. Distribution of lead species in particulate collected from well water sample 5SIIL02 at constant electrostatic field. Experimental conditions: pH = 6.5; electrostatic field = 97.8 V/cm 240
Figure A101. Distribution of lead species in particulate collected from well water sample 5SIIL02 at constant electrostatic field. Experimental conditions: pH = 9; electrostatic field = 97.8 V/cm 241
Figure A102. Distribution of lead species in particulate collected from well water sample MW3IB03 242
Figure A103. Distribution of lead species in particulate collected from well water sample MW3IB03. Experimental conditions: electrostatic field = 17.1 V/cm; pH = 7.9 243
Figure A104. Distribution of lead species in particulate collected from well water sample MW3IM03 at constant electrostatic field. Experimental conditions: pH = 5; electrostatic field = 10.3 V/cm 244
Figure A105. Distribution of lead species in particulate collected from well water sample MW3IM03 at constant electrostatic field. Experimental conditions: pH = 7; electrostatic field = 13.2 V/cm 245
Figure A106. Distribution of lead species in particulate collected from well water sample MW3IM03 at constant electrostatic field. Experimental conditions: pH = 9; electrostatic field = 14.8 V/cm 246

Executive Summary

This project was officially begun on October 1, 2000. During this project period, research effort was concentrated on the construction of a cross-flow electro-filtration (CFEF) devise, testing of the CFEF unit with model colloid particle, γ-Al_2O_3, and field water samples. Groundwater samples were collected with bailers and the low flow purging technique (LFP) from three of the five wells at the Denzer-Schaefer site, Toms River, NJ. Experiments were conducted to characterize the performance of the CFEF module under various conditions specifically, pH and applied voltage. The filtrated water, concentrated water and the solids collected were further analyzed for soluble lead and total lead. The solid particles collected were characterized for particle size distribution and surface charge. The solid particles collected were also subjected to sequential extraction for lead. Analytical procedures for the analysis of chemical species followed those of the Standard Methods for the Examination of Water and Wastewater (1995) or the SW846 methods. The quality assurance (QA) management and quality control (QC) technique were applied throughout the experiments.

The main CFEF filter unit consists of an external tube (insulated), an inner electrically charged cathodic filter membrane, and a co-centric anodic rod. The external tube has a diameter of 8.9 cm, the inner filter has a diameter of 3.0 cm and the co-centric rod is a 0.5-cm stainless wire. The total module is 22.5 cm long. This module has a total filtration surface area of 212 cm^2. The cathode and the anode are connected to an A.C. power supply. The CFEF filter unit is feed from a Millipore cross flow module, model

ProFlux M12. A computer with necessary software is used to control the filtration rate and flow direction.

In the early phase of the project, we selected γ-Al_2O_3 as the surrogate colloidal particle. The γ-Al_2O_3 has a pH_{zpc} of 9.2 and mean particle size of 0.3 μm. Laboratory experiments using γ-Al_2O_3 were conducted first to evaluate the performance of the CFEF unit. The results show that the prototype CFEF unit is functioning properly. There is no clogging problem encountered. The final pressure at the inlet and outlet are always identical and equal to the initial pressure. Therefore, it is not necessary to backwash the CFEF unit any time under the experimental conditions of this study. The results show that optimum filtration rate of the CFEF unit is 0.46 L/min at a experimental conditions: γ-Al_2O_3 concentration of 100 mg/L and electrostatic field of 96.8 V/cm. The removal of γ-Al_2O_3 particles is faster during the first 1 to 3 minutes. The removal efficiency increases with increasing electrostatic field. There is a pH-dependent γ-Al_2O_3 removal efficiency as expected since pH affects the surface charge of the colloidal particles. When the pH value of solution is less than 9.2, pH_{zpc}, the surface of γ-Al_2O_3 will be positively charged. Decreasing pH will increase the surface charge of the γ-Al_2O_3 particles. Consequently, under otherwise identical conditions, the particle removal efficiency is enhanced as pH decreases.

As indicated above, groundwater samples were collected with bailers and the low flow purging technique (LFP) from three of the five wells at the Denzer-Schaefer site, Toms River, NJ. Naturally occurring particles collected from water samples are negatively charged under the pH condition of the groundwater. The naturally occurring particles have a pH_{zpc} of approximately 1 to 2. The results show that the particle appear

to be monodispered. The average particle size is in the range of 490 to 774 nm. Another observation is that the particle size in well #5S are slightly larger than in well #10 and #MW3. The total lead in the water collected from the three wells is 24-29, 45-116 and <1 μg/L in well #10, #5S and #MW3 respectively. The soluble lead is 4, <1-13, <1 μg/L in well #10, #5S and #MW3, respectively. Water sampling technique, i.e. bailing and low flow purging, appears to have little effect on the particle characteristics in this case. This can be preliminarily attributed to the problem encountered during sampling. Due to high solid content in the well water, the groundwater is disturbed twice during low flow purging.

The removal rate of particle in water samples is faster during the first 1 to 4 minute. The removal efficiency increases with increasing electrostatic field. The final removal efficiency was 84% and 75%, respectively, at electrostatic field of 161.3 v/cm and 64.5 V/cm for #10 water sample by the bailing and low flow purging sampling. The final removal efficiency was 95% and 94%, respectively, at electrostatic field of 156.5 v/cm and 156.85 V/cm for #5S water sample by the bailing and low flow purging sampling. The average particle size of particles in the filtrate for water sample collected by bailing and low flow purging sampling in well #10, #5S and #MW3 is almost below 400 nm and smaller than those of the raw water and collected in the concentrate stream. The average particle size of particle in the concentrate stream of water sample collected by bailing and low flow purging sampling in well #10, #5S and #MW3 is in the range of 470 to 2,881 nm and larger than those of raw and filtrate.

The soluble and total lead concentration in the filtrate of groundwater sample is < 1 μg/L. The total lead concentration in the concentrate stream of groundwater sample is

higher than both the total lead concentration in the filtrate and the soluble lead concentration in the concentrate stream. From the results, we can identify the high lead concentration is attributive to high particle loading.

The lead species accumulated in particulate were divided into five major geochemical forms: (1) exchangeable; (2) bound to carbonate phase; (3) bound to iron-manganese oxides; (4) bound to organic matter; and (5) residual metal phase. Results indicate that lead was mostly concentrated in the residual, organic matter and Fe-Mn oxide fractions.

We also analyze the performance of the CFEF module. Results indicate that the electrostatic field and surface charge are two essential parameters governing the removal efficiency of particle. These results observed agree well with those predicted. Results also indicate that it is possible to separate the naturally occurring particle by adjusting the pH (or surface charge) and/or applied electrostatic field of the CFEF unit.

1.0 Introduction

1.1. Groundwater Monitoring

Groundwater monitoring collects necessary data for environmental site investigation. Past practice depends on existing water supply wells for water sample collection. However, the function and characteristics of a supply well are different from those of a monitoring well. A water supply well does not always satisfy the special requirements of environmental monitoring. Water supply wells harvest water from the best available aquifer; whereas, environmental monitoring wells are always located at critically geological formation.

Numerous studies have demonstrated that the presence of colloidal material in groundwater may facilitate the transport of organic and inorganic contaminants (Sheppard et al., 1979; Means and Wjayaratne, 1982; Takayanagi and Wang, 1984; Chiou et al., 1986). Colloidal material having a diameter in the range of 0.01 to 10 μm (Stumm and Morgan, 1981) may originate from macromolecular components of dissolved organic carbons, such as humic acids, biological materials, micro-emulsions of non aqueous phase liquids (NAPL) and weathering products. The effect of colloidal material on contaminants in the saturated zone depends on the nature of the interactions between the contaminants and colloids, the groundwater, and the soil matrix. As a general rule, metals tend to attach onto negatively charged colloids.

Conventional groundwater sampling procedures stress speedy pumping and rely on filtration to separate the particles from water in order to determine the soluble concentration of a chemical species. The validity of the resulting samples is therefore questionable (Kearl et al., 1992). Vigorous bailing of groundwater samples may increase oxygen concentrations and disturb particles and colloids in the influence zone of the well. This agitation of the monitoring well may generate additional colloids or particulate with adsorbed organic and inorganic

chemicals of concern. It is generally accepted that the water in the well casing may not be representative of the formation water, so it needs to be purged prior to collecting the water samples. Traditional sampling methods rely on purging and sampling with bailers or high-speed pumps to remove 3 to 5 well casing volumes. This can lead to excessive drawdown, accelerated groundwater flow, aeration of water in the well, stirring up of sediments in the well, and abrasion of the well casing. Following this purge, there is a cursory evaluation of water quality stability, usually pH, temperature, and specific conductivity (Puls and Barcelon, 1994).

Finally, the water samples are collected. These water samples need to be filtered to compensate for the excess turbidity. Filtering is done a default filter pore size, typically 0.45 μm that is the middle of the size range for colloids. The method does not take into account site-specific factor, which might include larger- than-0.45 μm particulate (Puls and Barcelon, 1994).

Low flow purging sampling was developed to allow for collection of samples while causing as little disturbance in the well and the surrounding formation as possible, and to base the collection of the water samples on continuous observations of stability parameters during purging. In this manner, representative unfiltered samples can be collected. The major feature of the low flow purge method is velocity with which water enters the pump intake and is imparted to the formation (Puls and Barcelon, 1994). However, this technique is slow and expensive.

1.2. Lead in the Environment

Lead has been an important metal in human society for many thousand years. Unique physical characteristics such as low melting point, good workability and durability made lead a popular construction material in our early society. The use of lead, however, has increased dramatically since the early days of the industrial revolution. Annual lead production has

stabilized at the annual rate of 2.5 million tons per annum. As many as 40 countries worldwide have workable lead deposits, with Russia, USA, Australia and Canada (ca. 60 % of the total) being the four major lead producing countries. Mining, smelting and refining of lead, as well as the production and use of lead-based products give rise to the release of lead into the environment. This takes the form primarily of either lead-rich aqueous effluent streams, or emission of fumes and dusts into air. A large part of the lead discharged into surface waters is rapidly incorporated into suspended and bottom sediments and most of this lead will ultimately be found in marine sediments. Of greater concern, however, is the emission of lead into atmosphere. The fine aerosol particles may be transported long distances from their sources before deposition onto land or sea. Although the magnitude of the resulting pollution is very small at large distances, significant concentrations in soils and vegetation can occur close to a major source of lead, such as a smelter or busy highway. Most of this lead will ultimately be found in marine sediments. When incorporated in the soil, lead is very low mobility. Hence once contaminated, a soil is liable to remain polluted with lead.

Soil contamination by lead can cause potential groundwater pollution problem. Stumm and Bilinski (973) divided the lead species into three groups: soluble (< 0.001 μm), colloidal (0.001 μm) and particulate (> 1 μm). Soluble lead species are free lead ion, ion pairs or organic complexes. Colloidal lead species are those bound to high molecular weight organic ligands and those adsorbed on colloids such as hydrous oxides of Fe and Mn. Particulate lead species are those incorporated with organic particles, remains of microorganisms, and lead precipitates. The current method for the determination of dissolved lead (or heavy metals) uses 045 μm filters. This is in the mid size range of colloids.

Groundwater monitoring is an important part of site remediation and environmental risk assessment. However, very little is understood of the aqueous chemistry of lead. Using 0.45 μm filters as the criteria, lead in groundwater can be divided into dissolved and particulate fractions. As mentioned above, the dissolved lead includes mainly free Pb(II) and its hydrolysis species, ion-pairs, and organic-lead complexes. Particulate lead is a collection of all lead species that are associated with greater than 0.45 μm particulates. Chemically, particulate lead can be further fractionated into the following forms: (1) adsorbed at particles surface; (2) present as discrete carbonate minerals or co-precipitated with major carbonate phases; (3) occlude in iron and/or manganese oxyhydroxide; (4) bound with organic matter, in either living or detritus form; (5) bound with amorphous authigenic sulfides or in more crystalline forms; or (6) bound in lattice positions in aluminosilicates, in resistant oxides or in resistant sulfides.

Lead has a strong tendency to form ion pairs, principally $PbHCO_3^+$ and $PbCO_3^0$ under the prevailing pH range of most waters. The formation of lead ion pairs increases the concentration of total dissolved lead in water. Lead can also form strong complexes with organic matter such as the humic acid and fulvic acid, and increase the concentration of lead in water.

Lee (1975) has proposed that colloidal hydrous ferric and manganese oxides can scavenge lead and pH plays an important role on the adsorption of lead onto hydrous ferric and manganese oxides. This is an important linkage in the hydrogeochemical cycle of lead. Hydrous ferric and manganese oxides are readily reduced and hence become soluble under anaerobic conditions; consequently, lead will become mobilized. However, there may be concomitant formation of metal sulfides which are even less soluble than hydrous oxides of ferric and manganese. Conceptually, the solid material can be partitioned into specific factor; sequential extractions with appropriate reagents can then be devised to leach successive fractions

selectively from the particulate sample. The method of Tessier et al. (1979) is one of the most throughly researched and widely used methods to evaluate the possible chemical associations of metals.

Soils contamination by lead can cause potential groundwater pollution problems. Lead in soil-water systems is mostly associated with solids, i.e. colloidal or particulate state. During site investigation water sample are taken from monitoring wells for chemical analysis, i.e. lead. Particulate material in water can range from 1 to 5,000 μm. At the same time, colloidal material ranges from 0.01 to 10 μm. There is an overlap of particles in the range of 1 to 10 μm which has resulted in the rejection of filtration data. This complicates the process in segregating dissolved and particulate matter. An investigation of the overlap pore size may result in a protocol that would allow the use of filtered samples in site investigations. It is proposed that lead contaminated groundwater samples from wells containing high particulate levels be subjected to a serious of filter sizes from 0.45 μm up to 10 μm. This data should be compared to conventionally collected bailer samples and low flow purge collected samples. An acceptable filtering procedure would be one that eliminates the presence of artificially introduced particulate material while still allowing naturally occurring colloid material to be determined.

Traditional methods depend on speed pumping and bailers. This sampling practice tends to disturb colloidal material and bring it into water samples. The water is generally filtered, especially for metal analysis, then analyzed for dissolved constituents such as lead. Current technique uses 0.45 μm filters to divide dissolved from particulate chemical constituents. This will include colloidal material between 0.01 to 0.45 μm and exclude the 0.45 to 10 μm portion of colloids in the determination of dissolved lead. Moreover, due to the small size, it is difficult to filter groundwater of high solid concentration (or turbidity). The New Jersey Department of

Environmental Protection (NJDEP) has used a low flow purge technique to minimize the introduction of particulate into groundwater samples. This technique is effective, but it is also slow and expensive. In order to determine the lead speciation in groundwater, it is necessary to separate the colloids then analyze the lead content.

1.3. Objectives

This project was officially begun on October 1, 2000. During this project period, research effort was concentrated on the construction of a cross-flow electro-filtration (CFEF) devise, testing of the CFEF unit with model colloid particle, γ-Al_2O_3, and field water samples. Groundwater samples were collected with bailers and the low flow purging technique (LFP) from three of the five wells at the Denzer-Schaefer site, Toms River, NJ. Experiments were conducted to characterize the performance of the cross-flow electrofiltration module under various conditions, specifically, pH and applied voltage. The filtrated water, concentrated water and the solids collected were further analyzed for soluble lead and total lead. The solid particles collected were characterized for particle size and surface charge. The solid particles collected were also subjected to sequential extraction for lead. Analytical procedures for the analysis of chemical species followed those of the Standard Methods for the Examination of Water and Wastewater (1995) or the SW846 methods. The quality assurance (QA) management and quality control (QC) technique were applied throughout the experiments.

The major objective of this research project is to develop an innovative solid-liquid separation technique that will allow the use of filtered water samples in site investigation. The technique should be capable of separating the naturally occurring colloids. The following are specific objectives:

1. To design and operate a cross-flow electro-filtration (CFEF) process for the separation of naturally occurring colloidal material from groundwater. An instrument based on the principle of cross-flow electro-filtration process is to be constructed and operated. The CFEF unit will eliminate all problems associated with conventional dead-end filtration process.
2. To study the major factors controlling the operation of the cross-flow electro-filtration process. Factors such as filtration rate, applied electrostatic field strength, influent water quality and characteristics that may affect the performance of the CFEF unit will evaluated. Performance of the CFEF process will be assessed in terms of effluent quality, rejection, flux rate and backwash.
3. To study the effect of cross-flow electro-filtration on the improvement of lead determination in groundwater. The effectiveness of the CFEF process on the speciation of lead in groundwater will be compared with bailing and low flow purge technique samples.

2.0. Cross Flow Electro Filtration Module

2.1 Introduction

In order to analyze the lead species in groundwater, it is necessary to separate the naturally occurring colloidal material from groundwater samples. This is generally achieved by filtration. By flow pattern, filtration processes can be divided into two groups: dead-end and cross-flow. In the dead-end filtration mode, both the water flux or permeate, or filtrate) and the solid (or rejection) pass through a filter medium (or membrane) in the same direction. In the cross-flow filtration mode, the feed water and the filtrate passes the membrane in a different direction; generally, at almost a right angle.

The cross-flow filtration has the intrinsic merit of minimizing the solid contact with the filter membrane. However, since the particles of interest are of the micron or submicro size, further improvement of solid separation efficiency can be made by the application of an electrostatic field. In the presence of an electrostatic field, the particles are collected on the surface of an electrode, usually an anode, as most particulate in water is negatively charged.

Manegolg (1973) was the first to study the process of combining conventional pressure filtration and electrophoresis. It was not until 1977 when Henry provides a fundamental analysis of the cross-flow electro-filtration process (Henry et al., 1977). Moulik (1977) applied an electrostatic field to microfilters and reported excellent removal of colloidal particles such as bentonite and algal cells. Archer et al. (1993) designed an electrode capable of generating non-uniform electrostatic fields over a large surface area to separate yeast cells from water. They reported that a linear relationship between dielectrophoretic collection and pulse length over the range 0 to 100 sec. Lo et al. (1993) separated Al_2O_3 colloids from non-aqueous solution using cross-flow electro-filtration process. The effect of feed rate, driving pressure, and electrostatic

field strength on the filtration rate and total solid deposition rate on the collection electrode was evaluated. Results indicate that extent of filter fouling is greatly decreased. Majmudar and Manohar (1994) reported the separation of TiO_2 from aqueous solution by electrophoretic filtration. Experiments were carried out at different voltages and flow rates. It was observed that voltages lower than 10 V and higher than 200 mL/h flow rate. It was further observed that 96% separation was the maximum obtainable. Wakeman and Sabri (1995) reported that direct current electrostatic field reduce cake formation in cross-flow membrane filtration. Operating parameters such as filtration pressure, cross-flow velocity, electrostatic field gradient, pH and feed concentration can affect filter performance. Verdegan (1996) studies the separation of fine particles (<10 μm) from nonpolar liquids by cross-flow electro-filtration process. He reported that cross-flow electro-filtration has many distinct advantages over conventional separation processes: high removal for all particle size, long life, and minimal power requirement. Akay and Wakeman (1996) reported enchanced removal of a double chain cationic surfactant (diocatadecyldimethylammonium chloride) in water using the cross-flow electro-filtration process. Wakeman reported electrophoretically assisted cross-flow microfiltration of bovine serum albumin (BSA), ovalbumin and denatured lactalbumin (1998). It is shown that the stead state flux is higher when an electrostatic field is applied than it is with conventional cross-flow microfiltration. The flux is almost independent of the membrane pore size. Finer pore sizes enable steady state flux and rejection condition conditions to be reached sooner.

Von Zumbusch et al. (1998) reported that the alternating electrostatic field diminished membrane fouling and hence yields a higher specific filtrate flux. The effect of the electrostatic field depends on frequency (0.5 to 50 Hz), field strength (0 to 80 V/cm), conductivity (1 to 10 mS^{-1}), and protein concentration (0.1 to 5 w%). Low frequency and high electrostatic field

strength yield the best result for electroultrafiltration with alternating fields. The effevtness of the electrostatic field increases with rising conductivity up to the point where a limiting electrolytic current is reached. Increasing protein concentration diminishes the effect of the electrostatic field.

Houtain et al. (1999) reported that applying an electrostatic field across cross-flow filtration can greatly increases the flux rate. Weigert et al., (1999) conducted the first pilot plant study on microfiltration of mineral and biological slurry with cross-flow filtration, coupled with constant and pulsed fields and reported that the specific permeate rate markedly increases compared to the value without an electrostatic field. For mineral slurry, the increase in flux rate was more than 10 fold. An estimation of the specific energy input demonstrates the cost-saving potential of this technique.

2.2 Design and Construction of CFEF Module

During this project period, we have designed and constructed a prototype cross-flow electro-filtration system. As indicated in Figure 1 the main filter unit consists of an external tube (insulated), an inner electrically charged cathodic filter membrane, and a co-centric anodic rod. The external tube has a diameter of 8.9 cm, the inner filter has a diameter of 3.0 cm and the co-centric rod is a 0.5-cm stainless wire. The total module is 22.5 cm long. This module has a total filtration surface area of 212 cm^2. The cathode and the anode are connected to an A.C. power supply (Figure 2). The CFEF filter unit is feed from a Milipore cross flow module, model ProFlux M12 (Figure 3). A computer with necessary software is used to control the filtration rate and flow direction (Figure 4). Figure 5 shows the total CFEF system. Figure 6 illustrates the schematic presentation of flow direction and sampling points.

2.3 Basic Principles of Operation

The basic forces that act on the particles in the CFEF unit are gravity, the viscous resistance, and electrostatic attraction. The gravity is proportional to the volume for particles of constant density ($\propto D^3$). Thus the ratio of gravity to resisting force is proportional to (D^3/D) or D^2. As diameter decreases, this ratio falls rapidly. For electrostatic force, the resisting force is still the Stokes viscous drag force, but the electrostatic force is proportional to the square of particle diameter, i.e., D^2. Thus the ratio of electrostatic force to resisting force is proportional to (D^2/D) or to the diameter D. Thus it is harder for the CFEF unit to collect small particles. The degree of difficulty is proportional to 1/D rather than to $1/D^2$ as in the case of gravity as driving force. For small particle, the main driving force would be electrostatic force in the CFEF unit. When the particles are sufficiently charged, an electric field is applied to the flow region, exerting an attractive force to the particles and causes them to migrate toward the oppositely charged electrode at right angles to the flow direction.

Referring to figure 1, the raw water enters from the bottom and flows upward through the cylindrical collector portion of the CFEF unit. As the flow moves upward, electrostatic force directs the particles to migrate to the collector electrode. The clean water passes through the filter medium and emerges from the top of the unit.

Accordingly, charged particles migrate toward the collector electrode under the action of an electric field between the electrodes. Figure 7 shows a cross section of the CFEF with a boundary layer in which the particles are captured.

When a charged particle with a solid charge, qp, is located in the region where an electric field of strength, Ec, is present, a force, Fq, will exert on the particle (Figure 8). The magnitude of this force is given by the following expression:

$$F_e = q_p E_c \quad \textbf{(1)}$$

Next, let us consider the case of a laminar flow around a particle. Under such circumstance, the drag force can be obtain by the expression:

$$F_d = 3\pi\mu d v_t \quad \textbf{(2)}$$

Where μ is the viscosity of the fluid; d is the diameter of particle; v_t is the velocity of particle.

For small particles, its terminal velocity will soon be reached under the action of these forces. When an equilibrium state is reached, the terminal velocity becomes:

$$v_t = \frac{F_e}{3\pi\mu d} = \frac{q_p E_c}{3\pi\mu d} \quad \textbf{(3)}$$

In the CFEF system, the distance that a particle travels relative to fixed coordinates is the same distance as it travels relative to the flow (Δz in both cases). If the particle is at its terminal velocity, vt, relative to the surrounding flow, where flow is moving at an opposite direction with velocity, vz= Qf /($\Delta x \Delta y$), then the velocity of the particle relative to the fixed coordinate of the CFEF unit is:

$$v_p = v_t - v_z = \frac{q_p E_c}{3\pi\mu d} - v_z \quad \textbf{(4)}$$

Referring to figure 8, a particle, which enters the capture zone adjacent to the wall, will migrate a distance "dz" toward the wall while it moves a distance "dx" in the axial direction. Since the time required for moving these two distances is identical, one has:

$$dz = v_p dt = v_p \frac{dx}{v_x} \quad \textbf{(5)}$$

We shall assume that the effect of the turbulent flow in the duct will be to distribute the particles uniformly across any section. Also, we shall allow the field strength at the collector electrode, Ec, to vary along the length of the collection section. The fraction of particles that will

be captured in distance "dx" is the ratio of the area within the capture zone to the total cross-sectional area, that is:

$$-\frac{dN}{N}=\frac{pdz}{A}=\frac{p}{A}\frac{v_p}{v_x}dx \qquad \textbf{(6)}$$

Upon integration of equation (6), and under the following boundary condition, N = N0 at x = 0 and allow vt to vary with x, one has:

$$N = N_0 \exp\left(-\frac{p}{Av_x}\int_0^x v_D dx\right) \qquad \textbf{(7)}$$

The theoretical removal efficiency then becomes:

$$\eta=\frac{N_0-N}{N_0}=1-\exp\left(-\frac{p}{Av_x}\int_0^L v_p dx\right) \qquad \textbf{(8)}$$

By substituting vp term in equation (4) to the equation (8), one has:

$$\eta=1-\exp\left(-\frac{p}{Av_x}\int_0^L\left(\frac{q_p E_c}{3\pi\mu d}-v_z\right)dx\right)=1-\exp\left(-\frac{p}{Av_x}\left(\frac{q_p}{3\pi\mu d}\int_0^L E_c dx-v_z L\right)\right) \qquad \textbf{(9)}$$

Noting that Avx = Qc and that the product pL is equal to the collection surface area, Ac, Equation (9) may be written as:

$$\eta=1-\exp\left(-\frac{q_p A_c}{3\pi\mu d Q_c}\frac{1}{L}\int_0^L E_c dx+\frac{A_c v_z}{Q_c}\right) \qquad \textbf{(10)}$$

Next, we define the mean electric field strength at the collector electrode, Ecm, as

$$E_{cm}=\frac{1}{L}\int_0^L E_c dx \qquad \textbf{(11)}$$

Then equation (10) becomes:

$$\eta = 1 - \exp\left(-\frac{q_p A_c}{3\pi\mu d Q_c} E_{cm} + \frac{A_c V_z}{Q_c} \right) \quad \textbf{(12)}$$

Noting that $V_z = Q_f / (\Delta x \Delta y) = Q_f / A_f$ (filtration surface area) and q_p is equal to $\pi d^2 \sigma_o$ (σ_o being the surface charge of particle). Equation (12) may be written as:

$$\eta = 1 - \exp\left(-\frac{\sigma_o d A_c}{3\mu Q_c} E_{cm} + \frac{Q_f A_c}{Q_c A_f} \right) \quad \textbf{(13)}$$

Let Q_f/Q_c be equal to ϕ, and the ratio of the area within the capture zone to the filtration is known as:

$$\frac{A_c}{A_f} = \frac{2\pi r L}{2\pi R L} \quad \textbf{(14)}$$

Where r is the radius of capture zone; R is the radius of filtration area.

The equation (13) then becomes:

$$\eta = 1 - \exp -\frac{\sigma_o d A_c}{3\mu Q_c} E_{cm} + \phi \frac{r}{R} \quad \textbf{(15)}$$

Assuming that a particle with a diameter 200 μm has a surface charge 18 mC/m^2. From equation 15, the removal efficiency of particle is about 80% at an electrostatic field of 6,000 V/m. Figure 9 shows the removal efficiency of particle as a function of electrostatic field. The removal efficiency increases as the electrostatic field strength increases. These results agree well with those results obtained experimentally. If we keep a constant electrostatic field strength, for example 1560 V/m, the removal efficiency of particle is about 64% at a surface charge 5 mC/m^2 under the same conditions previously. Figure 10 shows the removal efficiency of particle as a function of surface charge. From figures 9 and 10, it is indicated that the high electrostatic field and high surface charge will enhance the removal efficiency of particle. The results agree well with those results obtained experimentally. Figure 11 shows the removal efficiency of particle as

a function of particle size at various levels of electrostatic field. Figure 12 shows the removal efficiency of particle as a function of particle size at various levels of surface charge. Based on results presented in figures 11 and 12, it is possible to separate the naturally occurring particles by adjusting the pH (or surface charge) and/or applied electrostatic field of the CFEF unit.

3.0. Preliminary assessment of the CFEF unit

During the early phase of the project, we selected γ-Al_2O_3 as the surrogate colloidal particle for studies. Laboratory experiments using γ-Al_2O_3 were conducted first to evaluate the performance of the CFEF unit.

3.1. Particle and Characterization

The γ-Al2O3 was obtained from the Degussa Company (Darmstadt, Germany). The electrophoretic mobility of γ-Al2O3 was determined by using the Laser Zee Meter (Brookhaven Instrument Co.). The average particle size of γ-Al2O3 was determined by light-scattering measurement using ZetaPALS instruction, Brookhaven Instruments Co. (Holtsville, NY, USA) and a value of 0.3 μm was obtained. Figure 13 shows the pH dependence of the zeta potential for γ-Al2O3. According to Figure 13, the pHzpc for γ-Al2O3 is approximately 9.2. This value agrees well with these reported by other (Huang and Stumm, 1973, and Hsieh, 1984).

3.2. Operation of the EFCF Module

The sample solutions were prepared with 100 mg γ-Al_2O_3 /L deionized-distilled water at different ionic strengths of 10^{-3}M, 10^{-2}M, 10^{-1}M $NaClO_4$. The initial pH values were measured while the suspension was being stirred. Then the pH was adjusted to the range from 2.0 to 11.0 with 0.1 N $HClO_4$ and 0.1 N NaOH. About 15 mL of pH-adjusted sample was injected into the electrophoresis chamber. Laboratory experiments were then conducted to evaluate the performance of the crossflow electrofiltration unit. The following operational conditions were evaluated: (1) clogging, (2) flux production, (3) quality of flux, and (4) backwash frequency. The

degree of filter clogging can be measured in terms of several properties including pressure drop and water quality of the filtrate, i.e. turbidity. During the course of the filtration, the pressure of the system was monitored continuously. Flux production is expressed in terms of mass (or volume) of water produced per time per unit area of the filter, i.e. cm^3/cm^2-min. The turbidity of the filtrate was measured during filtration. The frequency of the filter backwash was evaluated.

Laboratory experiments were run under the following conditions: (1) filtration rate; (2) pH; (3) γ-Al2O3 concentration; (4) initial electrostatic field applied. The filtration rate was from 2.4 cm3/cm2-min to 14.2 cm3/cm2-min. The pH value of solution was adjusted to the range between 4.0 and 8.0 with 0.1 N HClO4 and 0.1 N NaOH. The γ-Al2O3 concentrations were from 50 mg/L to 200 mg/L. The electrostatic field strength applied was at 0, 12.9 V/cm (40 voltage), 16.1 V/cm (50 voltage), 32.3 V/cm (100 voltage), 48.4 V/cm (150 voltage), 64.5 V/cm (200 voltage), 80.6 V/cm (250 voltage), 96.8 V/cm (300 voltage), individually.

3.3. Clogging

During the course of filtration, the pressures of the system were monitored continuously. The initial pressure of inlet and outlet were controlled at 2 and 1 psi, respectively. At the end of all experiments, the pressure of inlet and outlet always remain at the same level. For evaluating long time clogging, we run two hours at the pump speed of 15%, γ-Al2O3 of 100mg/L, initial pH of 5.6 and electrostatic field strength 96.8 V/cm (300 voltage). The results were the same as above. Results show no difference between the inlet and outlet pressure.

3.4. Flux production

The pumping speed (S, %) cab be correlated to filtration flow rate (Q, L/min) by the equation: Q = -0.47513 + 0.062099*S (Figure A1). Filtration flow rate can be converted to flux production by dividing the filtration flow rate by filter surface area. The flux production of cross-flow electro-filtration unit varied from 2.4 cm^3/cm^2-min to 14.2 cm^3/cm^2-min.

3.5. Quality of flux

Suspended and colloidal matter such as γ-Al2O3, clay, silt, finely divided organic and inorganic matter causes the turbidity in water. The turbidity (NTU unit) of the filtrate was measured against a calibration curve using dilute water sample solutions. Figure A2 shows the calibration curve for turbidity measurement. A linear relationship exits between turbidity and the solid concentration of γ-Al2O3 was observed. The Turbidity (NTU) is related to the γ-Al2O3 concentration (C) by the expressions: NTU = 0.81583 + 0.31515*C with a linear correlation coefficient (R2) of 0.99.

The results show that all water samples have a high refractive index, which contribute turbidity to the water even at very low solid concentrations.

3.6. Backwash Frequency

No clogging was observed in all experiments. Therefore, it is not necessary to backwash the filter.

3.7. Effect of electrostatic field applied

Figure 14 shows the effect of electrostatic field on the removal of γ-Al_2O_3 particles. The corresponding raw data are shown in Tables 1 and Table A1-A4. The removal efficiency of colloidal particle is calculated by the following expression:

$$R_i = \frac{T_o - T_i}{T_o} x100(\%) \quad \textbf{(16)}$$

Where: r_i : removal efficiency at the ith minute;

T_0 : The turbidity of suspension at 0 minute;

T_i : The turbidity of suspension at the ith minute.

For safety consideration, we first applied low electrostatic field strength less than 16.1 V/cm (or 50 voltages). In the absence of an electrostatic field condition (i.e., 0 volt), the final removal efficiency was about 3% after 1-min filtration time and remained at this level afterward. The removal efficiency increases with increasing electrostatic field (voltage). Figures A3 and A6 show the removal of γ-Al_2O_3 as a function of time at various electrostatic field under a pumping speed 20% (or 0.77 mL/min) and γ-Al_2O_3 100 mg/L. Results indicate that the removal of γ-Al_2O_3 is fast during the first 3 minutes. The final removal efficiency at an applied electrostatic field strength is 13% and 18% at electrostatic field strength of 12.9 V/cm and 16.1 V/cm (or voltage of 40 V and 50 V), respectively. It is clear that high electrostatic field will benefit the removal efficiency of γ-Al_2O_3. We then decreased the pumping speed to 15% (or 0.46 mL/min) and adjusted the electrostatic field strength to between 16.1 V/cm to 96.8 V/cm (or voltage between 50 V to 300 V). Figure A6 shows the removal efficiency of γ-Al_2O_3 at these

applied electrostatic field strength and pumping speed of 15% (or 0.46 mL/min). The results show that the removal rate of γ-Al_2O_3 is fast during the first 1 minute. Figure 14 clearly shows that the removal efficiency increases with increasing electrostatic field (voltage). The final removal efficiency is 23, 46, 60, 68, 72, and 80%, respectively, at 16.1, 32.3, 48.4, 64.5, 80.6, and 96.8 V/cm (or 50, 100, 150, 200, 250, 300 V) applied.

3.8. Effect of γ-Al_2O_3 concentration

The effect of the γ-Al_2O_3 concentration is shown in and Figures A7 and A8. Figure A7 gives the residual turbidity of the filtrate and Figure A8 represents the removal efficiency of γ-Al_2O_3 at various concentrations (50, 100, and 200 mg/L). The corresponding raw data are shown in Tables 1 and Table A5-A6. The removal efficiency of γ-Al_2O_3 is 29, 29, and 25%, respectively, at γ-Al_2O_3 concentrations of 50 mg/L, 100 mg/L, and 200 mg/L, respectively, at a filtration time of 15 minutes. The results show that there is no distinct removal efficiency at various γ-Al_2O_3 concentrations within the concentration range tested.

3.9. Effect of filtration rate

Figures A9 and A10 show the effect of filtration rate on the performance of the CFEF unit. The corresponding raw data are list in Table 1 and Table A7-A8. From Figure A10, it is seen that the removal efficiency of γ-Al_2O_3 increases with filtration rate (or pumping speed), reaches a maximum value then decreases with further increase in filtration rate. The maximum removal efficiency was observed at a filtration rate of 0.46 mL/min or pumping speed of 15%. For filtration rate greater than 0.46 mL/min (or pumping speed greater than 15%), the removal efficiency of γ-Al_2O_3 decreases as increasing filtration rate (or pumping speed). Figure 15

summa is the removal efficiency at the 10-minute filtration time as a function of filtration rate. Results indicate that the particle removal percentage was 75, 80, 64, 53, 45, and 46%, at filtration rate of 0.27, 0.46, 0.77, 1.08, 1.39, and 1.70 mL/min (or pumping speed of 12, 15, 20, 30, and 40%) respectively.

3.10. Effect of pH

Figures A11 and A12 shows the effect of pH on the performance of CFEF system. The corresponding raw data are shown in Table 1 and Table A9-A10. Based on Figure A12, the particle removal efficiency increases rapidly in the first minute of filtration to a plateau. Results also show that the removal efficiency increases with decreasing pH. As shown in Figure 16, the pH_{zpc} of γ-Al_2O_3 is 9.2. A pH value less than pH_{zpc} indicates that the particles are positively charged: the larger the pH difference from pH_{zpc} , the greater the surface is charged. The results agree very well with what would be predicted theoretically. Figure 16 summarizes the effect of pH on the percentage of particle removal at the 22-minute operation time. Results show that the particle removal efficiency was 84, 72, 64, 45, and 46%, respectively, at pH 4, 5, 6, 7, and 8.

4.0. Field Studies

4.1. Field Sampling

On December 28, 2001 and April 4, 2001, we made two separate trips to the Denzer-Schaefer site, Toms River, Bayvile, Ocean County, New Jersey, for field sampling. Water samples were taken from three wells, #10, #5S and #MW3. Both bailing and low flow purging techniques were used. The well depths are approximately 27~35 ft. Table 2 shows the description of well water samples.

4.2. Naturally Occurring Particulate

4.2.1. Particle size

It must be noted that the solid content was high in these three well waters, the pump screen was clogged quickly during low flow purging. We had to lift the pump screen head from the well for cleaning frequently during water sampling. As a result, it is possible that the water samples collected may be disturbed.

The average particle size was determined by light-scattering size analyzer using the ZETASIZER 3000HSA particle measurement (Malvern Instrument Ltd., Malvern, Worcs, United Kingdom). The results show that the particles appear to be monodispersed. The average particle diameter is in the range of 490 to 774 nm. Another observation is that the particles in well #5S are slightly larger than those from well #10 and well #MW3. Results also indicate that water-sampling methods appear to impose no effect on the particle size distribution. Table 3 lists the average particle size of the water samples.

4.2.2 The electrophoretic mobility of particles

The electrophoretic mobility of particles in the well water samples was determined by the ZETASIZER 3000HSA zeta potential meter from Malvern Instrument Ltd., Malvern, Worcs, United Kingdom. Figures 17-24 show the zeta potential (surface charge) as a function of ionic strength of naturally occurring particles. Figures 17, 19, 21, and 23 give the zeta potential of naturally occurring particles collected by the bailer of three wells. Figures 18, 20, 22, and 24 show the zeta potential of naturally occurring particles collected by the low flow purge technique of three wells. According to Figures 17-24, the pH_{zpc} is approximately 1~2. Results indicate that the naturally occurring particles are negatively charged under the pH value of the well water. Results also indicate that groundwater-sampling methods appear to impose no effect on the nature of colloidal particles. Again, this can be attributed particularly to the sampling practices as mentioned above.

4.3 Total solid, soluble lead and total lead

Table 4 shows the concentration of total solid, soluble lead and total lead in these three well water samples. Analytical procedures for total solid followed (2540.B) the Standards Methods for the Examination of Water and Wastewater (1995). The total solid concentration is in the range of 0.14 to 11.52 g/L. Results indicate that the total solid concentration of well #5S by bailer sampling method is greater than those of well #10 and #MW3. Results also indicate that the total solid concentration by bailer sampling method was greater than the low flow purging technique. Apparently the disturbance caused by bailing brings about high total lead concentration in the water samples.

Analytical procedures for total lead analysis followed EPA (3020A) SW-846 method. Briefly the following describe the procedures.

- Transfer a 100-mL representative aliquot of the well-mixed sample to 150 mL Griffin beaker and add 3 mL of concentrated HNO_3.
- Cover the beaker with a ribbed watch glass.
- Place the beaker on a hot plate and cautiously evaporate to a small volume (5 mL), making certain that the sample does not boil and that no portion of the bottom of the beaker is allowed to go dry.
- Cool the beaker and add another 3 mL portion of concentrated HNO_3. Cover the beaker with a non-ribbed watch glass and return the beaker to the hot plate. Increase the heating temperature so that a gentle reflux action occurs.

- Continue heating, adding additional acid as necessary, until the digestion is complete (generally indicated when the digestate is light in color or does not change in appearance with continued refluxing).
- When the digestion is complete, evaporate to a low volume (3-mL); use a ribbed watch glass, not allowing any portion of the bottom of beaker to go dry. Remove the beaker and add approximately 10 mL of water, mix, and continue warming the beaker for 10 to 15 minutes to allow additional solubilization of any residue to occur.
- Remove the beaker from the hot plate and wash down the beaker walls. Centrifuge at relative centrifugal force (RCF) 10,621g (10,000 rpm) for 60 minute and (when necessary) filter through a 0.45 μm millipore membrane the sample to remove insoluble material that may interfere with injecting the sample into the graphite furnace atomic absorption spectroscopy (GFAA). Adjust to the final volume of 100 mL with water.

To prepare water sample for soluble lead analysis, after centrifugation at relative centrifugal force (RCF) 10,621 g (10,000 rpm) for 60 minutes, the supernatant was filtrated through a 0.45 μm Milli-pore membrane. The filtrate was collected for lead analysis with GFAA. The particles collected were analyzed for various lead fractions according to the sequential extraction procedures.

Lead concentration was analyzed with an atomic absorption spectrophotometer (PerKinElmer Aanalyst-800, Überlingen, Germany). Before analysis, allow the lamp to warm up for a minimum of 15 minutes. During this period, align the position of the autosampler. Subsequently, light the flame and regulate the fuel and oxidant flows. Run a series of standards during sample analysis. Construct a calibration curve by plotting the concentration of standards

against absorbance. Standards were run each time as a series of samples was run. A standard were run for approximately every 10 sample runs.

Table 4 gives the total lead and soluble lead in these three well waters. The average total lead concentration was 24 and 29 μg/L in water sample collected by bailing and low flow purging respectively in well #10. The range of the average total lead concentration was from 45 to 116 μg/L in water sample collected by bailing and low flow purging in well #5S. The average total lead concentration is under detection limit (ND < 1 μg/L) in water sample collected by the bailing and low flow purging technique, respectively in well #MW3. The soluble lead concentration in well #10 was 4 μg/L for the bailing and the low flow purging samples, respectively. The range of the soluble lead concentration in well #5S was from < 1 to 13 μg/L for both the bailing and the low flow purging samples. The soluble lead concentration in well #MW3 was < 1 μg/L for both the bailing and the low flow purging samples. Results show that the total lead concentrations in water sample collected by bailing are generally greater than those the by low flow purging method.

4.4 Operation and Performance of EFEF Module

4.4.1 Operation of EFCF Module

Since the solid concentration of the water sample exceeds the detection limit of 1,000 nephelometer turbidity units (NTU) and the total volume of each water sample available was about 20 liter. The water samples were diluted. The initial pH values were measured while the suspension was being stirred. Then the pH was adjusted to the range from 4.5 to 9.0 by 5N $HClO_4$ and/or 5N NaOH. Laboratory experiments were conducted to evaluate the performance of the cross-flow electro-filtration unit. The following operational conditions were tested: (1)

clogging, (2) flux production, (3) quality of flux, and (4) backwash frequency. The degree of filter clogging can be measured in terms of several properties including pressure drop and water quality of the filtrate, i.e. turbidity. During the course of the filtration, the pressure of the system was monitored continuously. Flux production is expressed in terms of mass (or volume) of water produced per time per unit area of the filter, i.e. cm^3/cm^2-min. The turbidity of the filtrate was measured during filtration. The frequency of the filter backwash was evaluated.

It is hypothesized that the naturally occurring particles can be separated according to particle size and surface charge. Furthermore, it is expected that pH and applied field control the particle size and surface charge of naturally occurring particulate, laboratory experiments were run under the following conditions: (1) pH and (2) initial electrostatic field applied. The filtration rate was kept constant at 1.1 cm3/cm2-min. The pH value of solution was adjusted to the range between 4.5 and 9.0 with 5N HClO4 and/or 5N NaOH. The electrostatic field strength applied was at 0, 32.3 V/cm (100 voltage), 64.5 V/cm (200 voltage), 96.8 V/cm (300 voltage), 129.1 V/cm (400 voltage), and 161.3 V/cm (500 voltage).

4.4.2 Clogging

The degree of filter clogging can be measured in terms of several properties including pressure drop and water quality of the filtrate i.e. turbidity. During the course of filtration, the pressures of the system were monitored continuously. The initial pressure of inlet and outlet were controlled at 1 and 2 psi, respectively. At the end of experiment, the pressure of inlet and outlet always remained unchanged. This means that the pressure drop is minimal and that the filter is not clogged.

4.4.3 Quality of flux

Suspended and colloidal matter such as clay, silt, finely divided organic and inorganic matter causes the turbidity in water. The turbidity (NTU unit) of the filtrate was measured against a calibration curve using dilute water sample solutions. Figures A13-A20 show the calibration curves for turbidity measurements. A linear relationship exits between turbidity and the solid concentration of water samples. The Turbidity (NTU) is related to the water sample concentration, C (g/L), by the following expressions:

Sample	Empirical Equation	Corr. Coef.
10IB01	NTU = -6.9+ 1266.8C	$R^2 = 0.999$
10IL01	NTU = -1.8+ 1155.6C	$R^2 = 0.999$
5SIB01	NTU = -24.2+ 1457.2C	$R^2 = 0.999$
5SIL02	NTU = -28.2+ 5137.4C	$R^2 = 0.999$
5SIIB03	NTU = -21.2+ 1799.6C	$R^2 = 0.999$
5SIIL01	NTU = -11.2+ 1490.7C	$R^2 = 0.999$
MW3IB03	NTU = -4.2+ 524.5C	$R^2 = 0.999$
MW3IL01	NTU = -2.3+ 810.7C	$R^2 = 0.999$

The results show that all water samples have a high refractive index, which contribute turbidity to the water even at very low concentrations.

4.4.4 Backwash Frequency

The filter has been in operation for 2 hours and no clogging was observed. Therefore, it is not necessary to backwash the filter.

4.4.5 Effect of electrostatic field applied

Figure 25 shows the visual appearance of well #5s for the low flow purging samples under various electrostatic fields. Figure 25 indicates that filtrate is clearer than the raw water sample in the presence of electrostatic field. Figures A21-A32 show the effect of electrostatic field on the removal of particles. The corresponding raw data are show in Tables 5 and Table A11-A14, A17-A18, A21-A22, A25-A26, and A29-A30. The removal efficiency of colloidal particle is shown as equation (16).

Results indicate that the remove rate is fast during the first 4 minutes. The final removal efficiency was 0, 43, 69, 80, 83, and 84%, respectively, at electrostatic field of 0, 32.3, 64.5, 96.8, 129.1, and 161.3 V/cm (or 0, 100, 200, 300, 400, 500V) for well #10 water sample by the bailing sampling (Figures 26-27). The final removal efficiency was 0, 49, 70, and 75% respectively at electrostatic field of 0, 32.3, 48.4, and 64.5 V/cm (or 0, 100, 150, 200V) for well #10 water sample by the low flow purging sampling (Figure 28). The final removal efficiency of an applied electrostatic field strength was 7, 39, 62, 82, 93, 95%, respectively, at electrostatic field of 0, 32.3, 64.5, 96.8, 129.1, and 156.5 V/cm (or 0, 100, 200, 300, 400, 485V) for well #5S water sample by the bailing sampling (Figure 29). The final removal efficiency was 9, 65, 87, 91, 92, and 94%, respectively, at electrostatic field of 0, 32.3, 64.5, 96.8, 129.1, and 156.8 V/cm (or 0, 100, 200, 300, 400, 486V) for well #5S water sample by the low flow purging sampling (Figure 30). It is indicated that high electrostatic field will enhance the removal efficiency of particle as expected.

In the well #MW3 water sample, the electrostatic field strength applied was only at 17.1 V/cm (or 53 voltage) (Figure 31). A higher field strength can not be achieved because its high conductivity (450 μmhos). The conductivity of a solution is a measurement of the ability of a

solution to conduct a current and is directly attributable to the ions in solution. Electric current is transported through solution via the movement of ion, and conductivity increases as ion concentration increase. According to Langelier (1936), ionic strength can be derived from a correction with conductivity or total dissolved solid (TDS).

$$\mu = 2.5\text{x}10^{-5}\,\text{TDS} \tag{17}$$

$$\mu = 1.6\text{x}10^{-5}\nu \tag{18}$$

Where ν is the conductivity (μmho) and TDS in mg/L.

From equations (17) and (18), it is seen that there is relationship between conductivity and TDS. Increasing TDS will increase the conductivity. The resistivity is reversely related to conductivity:

$$\mathbf{R} = \rho\,\frac{\mathbf{1}}{\mathbf{A}} = \frac{1}{\mu}\,\frac{\mathbf{1}}{\mathbf{A}} \tag{19}$$

Where R, ρ, and A are resistance, resistivity, and crosses-section area of conductor, respectively.

According to equations (17), (18), and (19), the resistance will decrease as TDS increases. Based on the *Ohm's law*, we can determine the resistance of the CFEF unit between two points by applying a given potential difference, V, between them and measuring the current, I:

$$\mathbf{V} = \mathbf{IR} \tag{20}$$

Where V is in volts, I is in amperes, and R is in ohms (Ω), respectively.

Equation (20) shows that there is a proportional relationship between V and R at constant I. If the resistance decreases as TDS of solution (or conductivity) increases, the potential difference will decrease under constant current condition. In order words, there is a reverse relationship between potential difference and the conductivity (or TDS) of the solution. The

maximum current of power supply used in our experiment is only 1,000 mA. This is the main reason why we can not increase the voltage to 600V (or electrostatic field) in the well #MW3 water sample. To verify the above hypothesis, we repeatedly run the well #10 water sample and increase the conductivity (or TDS concentration) of solution (Table A13 and A14). The initial turbidity increases from 223 to 799 NTU. The initial conductivity increases from 75 μmho to 122 μmho. The conductivity of concentrate is 240, 285, and 360 μmho, respectively at electrostatic potential of 100, 150, and 194 V (or 32.3, 48.4, 62.6 V/cm) for well #10 water sample by the bailing sampling. The higher electrostatic field can be applied until 194 voltage was applied.

4.4.6 Effect of pH

Figures A33-A42 show the effect of pH on the performance of the CFEF system. The corresponding raw data are shown in Table 5 and Table A15-A16, A19-A20, A23-A24, and A27-A30. The results show that the particle removal efficiency is slightly affected by pH. At a pH value greater than pH_{zpc}, the particles are negatively charged; the larger the difference between pH and pH_{zp}, the greater is the surface charge. The zeta potential of particle present the well #10, 5S, and MW3 water sample are identical in the range of pH 7 to 9. Results agree well with what would be expected.

Figures 32-36 summarize the effect of pH on the solid removal efficiency, for all cases studies, the solid removal efficiency remains high and relatively constant over pH range studied; i.e. 5 to 10. This is because the naturally occurring particles in all well water have a low pH_{zpc}. At the pH values conducted, the surface charge of particles is about identical.

5.4.7 The particle size distribution of filtrate and concentrate

Figures 37-41 shows the effect of electrostatic field on the particle size distribution of filtrate and concentrate. The mean particle diameter is in the range of 490 to 774 nm for well #10, #5S, and #MW3. The average particle size of filtrate for water sample collected by bailing and low flow purging in well #10, #5S, and #MW3 is less than raw and concentrate. The average particle size of filtrate in water sample collected by bailing and low flow purging in well #10, #5S, and #MW3 is almost below than 400 nm. The average particle size of concentrate for water sample collected by bailing and low flow purging in well #10, #5S are larger than those of filtrate. The average particle size of concentrate is in the range of 470 to 1152 nm for water sample collected by bailing and low flow purging in well #10, #5S, and #MW3. Results also indicate the water-sampling methods appear to impose no effect on the particle size distribution of water samples.

Figures 42-46 show the effect of pH on the particle size distribution of filtrate and concentrate. The range of the average particle size of filtrate is from 325 to 520 nm for water sample collected by bailing and low flow purging in well #10, #5S, and #MW3. The average particle size of filtrate for water sample collected by bailing and low flow purging in well #10, #5S, and #MW3 is smaller than raw and concentrate. The average particle size of concentrate is in the range of 473 to 873 nm at pH oh 7 and 9 for water sample collected by bailing and low flow purging in well #10 and #5S. The range of average particle size of concentrate is from 2290 to 2881 nm at pH5 for water sample collected by bailing and low flow purging in well #10 and #5S. The average particle size of concentrate in water sample collected by bailing and low flow purging in well #10, #5S are larger than those of filtrate. The results are almost same as

the effect of electrostatic field, except at low pH (pH=5). When the experiment condition is pH5, the particle size distributions of concentrate wills huge move toward sup-micrometer direction. This phenomenon can be explained by flocculation theory. Detail data on the changes in particle size distribution as affected by electrostatic field and pH are listed in FiguresA43-A73.

4.4.8 The total and soluble lead concentration of filtrate and concentrate

Table 6 shows the total lead and soluble lead concentration of filtrate and concentrate. The total lead and soluble lead concentration of the filtrate and the concentrate are < 1μg/L in well #MW3 water sample collected by the bailing and the low flow purging. The soluble lead concentrations of the filtrate is < 1μg/L in well #5S water sample collected by the bailing and the low flow purging, except at low electrostatic potential applied. The soluble lead concentration of the concentrate is < 1μg/L in well #5S water sample collected by the bailing and the low flow purging, except at an applied electrostatic field strength of 96.8 V/cm for water sample collected by the low flow purging. The range of the total lead concentration of the concentrate is from 9 to 98 μg/L in well #5S water sample collected by the bailing and the low flow purging. The soluble lead and total lead concentration of the filtrate are < 1μg/L in well #10 water sample collected by the low flow purging, except at low electrostatic field applied. The soluble lead concentration of the concentrate is < 1μg/L in well #10 water sample collected by the low flow purging. The total lead concentration of the concentrate are in the range of 75 to 118 μg/L. Results show that the total lead concentration of the concentrate in sample 10IL01, 5SIIL02 and 5SIIB03 are higher than those of the filtrate. Results also show that the total lead concentration of the concentrate in

sample 10IL01, 5SIIL02 and 5SIIB03 are higher than the soluble lead concentration. From the results, we can attribute the high lead concentration to the high particle loading.

4.4.9 The speciation of lead

4.4.9.1 Introduction

Although the total and soluble concentration of heavy metals in contaminated groundwater is of general relevance to assessment of potential toxicity, a key point is to determine how much of heavy metal is mobile or plant-available under nature environmental conditions. Heavy metal mobility and availability in contaminated materials depends to a large extent upon the different chemical and mineralogical forms that present. Toxic trace elements released into aquatic systems are generally bound to particulate matter. However, some of colloid-bound metals may remobilize and be released back to waters with a change of environmental conditions, and impose adverse effects on living organisms. Besides the physical, chemical and biological characteristics of the interstitial water and colloid, the chemical partitioning of trace metals is very important in determining the bio-availability of trace metals (Luoma, 1983). The major mechanism of metal accumulation in particulate can be grouped in five major metal geochemical forms (Tessier et al., 1979: Salomons et al., 1988): (1) exchangeable; (2) bound to carbonate phase; (3) bound to iron-manganese oxides; (4) bound to organic matter; and (5) residual metal phase. These metal fractions have different mobility, biological availability and chemical behaviors. Thus, it is necessary to identify and quantify the metal forms in order to assess the environmental impacts of contaminated groundwater. Many previous studies have attempted to define these forms. Most previous studies frequently used selective extraction analysis (Sims and Patrick, 1978; Miller et al., 1983; Hickey and Kittrick,

1984; Xian, 1989; Xian and Shokohifard, 1989; Clevenger, 1990; Dudka and Chlopecka, 1990; Cholpecka, 1993; Chlopecka et al., 1996; Ramos et al., 1994; Chen et al., 1996; Howard and Shu, 1996; Gee et al., 1997). The method of Tessier et al. (1979) is one of the most throughly researched and widely used methods to evaluate the possible chemical associations of metals.

4.4.9.2 Materials and Methods

The samples were stored at 4 ^{o}C. Experiments were conducted to characterize the performance of cross-flow electro-filtration module under various conditions, specifically, pH, and applied electrostatic field. The solids collected from filtrate water and concentrated water were further separated by centrifuging at 10,000 rpm (about 12,000 g) for 30 minute and then dried at 105 ^{o}C in a drying oven.

The sequential methodology chosen was that of Tessier et al., 1979. The sequential digest used identifies five metal fractions:

1. Exchangeable or adsorbed trace metals:

   These are loosely bound to the substrate and would change in concentration with changes in ionic composition of the overlying water. This fraction is exchanged using magnesium chloride solution at pH 7.0 (1M $MgCl_2$, pH 7.0).

2. Metals bound to detrital carbonates

   Changes in environmental pH would affect the binding of metals to carbonates. It is extracted with sodium acetate at pH 5.0 (1 M NaOAc adjusted to pH 5 with 0.5 M HOAc)

3. Metal coprecipitated with Fe and Mn oxides as coatings on particles

These are extracted using hydroxylamine hydrogen chloride (0.04 M $NH_2OH{\cdot}HCl$ in 25% (v/v) HOAc).

4. Metals associated with organic matter

   Metals can either be incorporated into the tissues of living organisms, deposited as detritus, or can be found as a coating covering grains. Metals associated with organic matter would be released into the environment under oxidizing conditions. The organic fraction was extracted using nitric acid, hydrogen peroxide and ammonium acetate (0.02 M HNO_3, 30% H_2O_2, 3.2 M NH_4OAc).

5. The residual fraction of the heavy metal

   The residual fraction of heavy metals is that trapped in the crystal lattices of primary and secondary minerals. Only released to environment upon complete destruction of the crystal in which they are found. The residual fraction was extracted using a mixture of concentrated hydrofluoric and perchloric acids ($HF\text{-}HClO_4$).]

The selective extraction was conducted in centrifuge tubes (Teflon, 50 mL) to minimize losses of solid material. Between each successive extraction, centrifuging (Labnet, model Z383K), effected separation at (RCF) 10,621 g (10,000 rpm) for 30 min. The supernatant was removed with a pipet and analyzed for heavy metals; whereas the residue was washed with 8 mL of deionized water. After centrifugation for 30 min, this second supernatant was discarded. The volume of rinse water used was kept to minimum as to avoid excessive solubilization of solid material, particularly organic matter. For residual trace metal analysis, the solid was digested with 5:1 mixture of hydrofluoric and perchloric acids. The sample was first digested in a centrifuge tube (Teflon) with a solution of concentrated $HClO_4$ (2mL) and HF (10 mL) to near

dryness; subsequently a second addition of $HClO_4$ (1 mL) and HF (10 mL) was made and again the mixture was evaporated to near dryness. Finally, $HClO_4$ (1 mL) alone was added and the sample was evaporated until the appearance of white fumes. The residue was dissolved in 12 N HCl (5 mL) and diluted to 25 mL. Table 7 shows the detailed procedures of the Tessier procedure method for the sequential extraction of lead.

Lead concentration was analyzed with an atomic absorption spectrophotometer PerKinElmer Aanalyst-800 (Überlingen, Germany). Before analysis, allow the lamp to warm up for a minimum of 15 minutes. During this period, align the position of autosampler. Subsequently, light the flame and regulate the flow of fuel and oxidant. Run a series of standards during sample analysis. Construct a calibration curve by plotting the concentration of standards against absorbance. Standards were run each time as a series of samples was run. A standard were run for approximately every 10 sample runs. Deionized water used in preparing stock solution and each step of leaching procedure was obtained from CORNING MEGA-PURE system MP-290 (New York, USA). All glassware, polypropylene, or Teflon containers, including sample bottles, flasks and pipets, should be washed in the following sequence: detergent, tap water, 1:1 nitric acid, tap water, 1:1 hydrochloric acid, tap water, and reagent water. All acids used in the digestion and sequential extraction procedures were of trace metal grade and all other reagents used were of analytical grade or better.

4.4.9.3 Results

Figures 47-50 show the effect of electrostatic field on the proportions of the lead species, such as exchangeable metals, metals bound to carbonates, metals bound to Fe/Mn oxide, metals bound to organic matter and residual metals in sequential extraction fraction. The corresponding

raw data are shown in Table 8, 9, 11 and 12. Figures 51-55 show the effect of pH on the proportions of the lead in sequential extraction fraction. The corresponding raw data are shown in Table 8-12. Detailed of lead distribution in various geochemical forms is listed in Figures A74-A105.

Exchangeable metal ions are a measure of trace metals that are released most readily into environment. With respect to the total lead content, the exchangeable fraction is a minor component (generally less than 4%) and vary slightly with various electrostatic field and experimental pH condition in all water samples. For well #10 water sample by the bailing sampling method, lead was mostly concentrated in the residual fraction. The percentage of lead associated with various fractions followed the order: residual (45%-57%) > organic matter (32%-40%) > Fe-Mn oxide (2%-11%) > carbonate (0%-11%). For well #10 water sample by the low flow purging sampling method, lead was mostly concentrated in the organic matter and the Fe-Mn oxide fractions. The percentage of lead associated with various fractions followed the order: Fe-Mn oxide (29%-49%) > organic matter (27%-37%) > carbonate (0%-23%) > residual (9%-20%). For well #5S water sample by the low flow purging sampling method, lead was mostly concentrated in the residual and the organic matter fractions. The percentage of lead associated with various fractions followed the order: organic matter (30%-68%) > residual (27%-68%) > Fe-Mn oxide (2%-20%) > carbonate (0%-19%). For well #MW3 water sample by the bailing sampling with various electrostatic field, lead was mostly concentrated in the residual and the organic matter fractions. The percentage of lead associated with various fractions followed the order: residual (53%-72%) > organic matter (27%-46%) > Fe-Mn oxide (less than 1%). For well #MW3 water sample by the bailing sampling method, lead was mostly concentrated in the residual and the organic matter fractions. The percentage of lead associated with different

fractions was in the order: residual (47%-60%) > organic matter (39%-51%) > Fe-Mn oxide (less than 3%).

As far as pH is concerned, for well #10 water sample by the bailing method, lead was mostly concentrated in the residual and the organic matter fractions. The percentage of lead associated with various fractions was in the order: residual (30%-41%) > organic matter (36%-37%) > Fe-Mn oxide (15%-26%). For well #10 water sample by the low flow purging sampling method, lead was mostly concentrated in the organic matter fraction. The percentage of lead associated with various fractions followed the order: organic matter (36%-60%) > carbonate (14%-41%) > residual (4%-32%) > Fe-Mn oxide (9%-10%). For well #5S water sample by the bailing sampling method, lead was mostly concentrated in the residual and the organic matter fractions. The percentage of lead associated with various fractions was in the order: residual (62%-74%) > organic matter (23%-35%) > Fe-Mn oxide (less than 3%). For well #5S water sample by the low flow purging sampling method, lead was mostly concentrated in the residual, the organic matter and the Fe-Mn oxide fractions. The percentage of lead associated with various fractions followed the order: organic matter (26%-55%) > residual (11%-49%) > Fe-Mn oxide (17%-31%) > carbonate (6%-15%).

The bio-availability of lead in particulate is thought to decrease approximately in the order of the extraction sequence, from readily available to unavailable, because the strength of extraction reagents used increases in the sequence. Hence, the exchangeable fraction may indicate the form of the metal that are most available for plant uptake. The second step extracts metals bound to carbonate and specifically adsorbed phases, which can easily become mobile and available under lower pH condition. The remaining three fractions (Fe-Mn oxide, organic matter and residual) are generally strongly held within the particulate and normally unavailable

to plants. Based on the results, it can be seen that the fraction exchangeable/bound to carbonate is minor. This refers to the strong bounding of lead to oxides, organic matters and silicates. This chemical bounding is strong enough to accumulate metal in the particulate and, under natural environmental conditions, the release of lead is not significant.

5.0 Comparison with Experimental Results

Attempt was made to fit experimental data with theoretical prediction. Figures 56-60 show results of such effect. The plot marked "m1" represents data calculated equation (15). Predicted results generally agree with experimental data. Any deviation between experimental and predicted data can be attributed to uncertainly in mean electrostatic field and particle size distribution. Several researches have reported that the electrostatic field strength may not be calculated from the overall applied voltage, since the drop in voltage at electrode-filter-solution interfaces (overpotential) is unknown (Bowen, and Sabuni, 1992; Bowen, and Ahmad. 1997). In the following section, we will discuss the effect of particle size distribution and electrostatic field strength on the application of equation (15).

5.1 Effect of Particle Size Distribution

We use the mean particle size in the equation (15) in our calculation model. An exact approach would be using particle size distribution instead of the mean diameter. The equation (15) can be rewritten as:

$$\eta = \sum_i \left(1 - \exp\left(-\frac{\sigma_o d_i A_c}{3\mu Q_c} E_{cm} + \phi \frac{r}{R} \right) \right) \tag{21}$$

Figures 56-60 also shows the results of calculation based on equation (21) (marked "m2"). Results clearly indicate that equation 21 better than equation 15 in prediction.

5.2 Effect of Electrostatic Field

An important parameter in the design and modeling of crossflow electrofiltration process is the electrostatic field strength, E, which can be easily calculated by its definition:

$$E = \frac{V}{R} \tag{22}$$

where V is the electric potential (voltage) and L is the distance between electrodes. However, in a tubular system equation (22) must be modified. The electrostatic field strength distributions between the two concentric cylinders can be calculated according to equation (23) (Crawford, 1976):

$$E = \frac{q_v r}{2\varepsilon_0} + \frac{V - q_v(r_c^2 - r_0^2)/4\varepsilon_0}{r \ln r_0 / r_c} \tag{23}$$

where V is the electric potential (voltage), r is the radial coordinate, r_0 is the radius of the outer electrode and r_c is the radius of the inner electrode, q_v is the volume charge density (C/m^3) of the reaction channel. If we assume that the volume charge density of the reaction channel is equal to zero, the equation (23) can be further simplified (Wakeman, 1986):

$$E = \frac{V}{r \ln r_0 / r_c} \tag{24}$$

The mean electrostatic field strength (E_{cm}) can be calculated by the expression:

$$E_{cm} = \frac{V}{r_0 - r_c} \tag{25}$$

In general, the electric potential (voltage) may be calculated according to the electric resistance (R) and the electric current (I) (equation (17)). Replacing electric resistance (R) in equation (17) with the conductivity term, from equation (16) becomes:

$$V = RI = \frac{\rho I l}{A} = \frac{I l}{\mu A} \tag{26}$$

where l is the length of each layer. Equation 26 is valid for any layer, or specifically for any feed channel. This is of relevance because the value determining the solid removal of the CFEF is the field strength of the reaction channel, E_r. Figure 61 shows the concept of resistance distribution

of the CFEF unit. A mean electrostatic field strength of the whole CFEF system (calculated using the applied voltage, V_a) would not reflect the real conditions in the reaction channel. The CFEF system acts like a several electric resistances in series and may be described by conductivity (μ), area (A) and distance (l) of each layer. The term ($l/\mu A$) in equation (26) therefore has to be expressed by the specific resistance in the reaction channel, $l_r/\mu_r A_r$, filter layer, $l_f/\mu_f A_f$ and cake layer, $l_c/\mu_c A_c$, respectively.

$$\frac{l}{A\mu} = \left(\frac{l_f}{A_f \mu_f} + \frac{l_r}{A_r \mu_r} + \frac{l_c}{A_c \mu_c}\right) \tag{27}$$

Combination of equation (26) and equation (27) gives the applied voltage V_a

$$V_a = I\left(\frac{l_f}{A_f \mu_f} + \frac{l_r}{A_r \mu_r} + \frac{l_c}{A_c \mu_c}\right) \tag{28}$$

Here, the electrostatic field strength of the reaction channel, E_r, was determined by equation (24) or (25). The applied voltage of the reaction channel may be rewritten as:

$$V_r = \alpha V_a \tag{29}$$

where α will be the effective field factor of CFEC unit. The effective factor is the function of filter characteristic, solution conductivity, solid characteristic and solid concentration. The theoretical removal efficiency (equation (21)) can further modified to:

$$\eta = \sum_i \left(1 - \exp\left(-\frac{\sigma_o d_i A_c}{3\mu Q_c}\alpha E_{cm} + \phi \frac{r}{R}\right)\right) \tag{30}$$

where E_{cm} is equal to ($V_a/(r_r-r_c)$).

Figures 56-60 show the results obtained from equation (30) (plot marked "m2(α)"). Based on experimental data and theoretical value, α can be found from best fit. In this study, we

use α = 0.9 and α = 0.8 for γ-Al_2O_3 and groundwater samples. The results clearly show that equation 30 can best describe the experimental data.

6.0 Conclusion

1. The prototype CFEF unit is functioning properly. There is no clogging problem encountered. The final pressure at the inlet and outlet always remain identical and is equal to the final pressure. Therefore, it is not necessary to backwash the CFEF unit under the experimental conditions of this study.
2. The removal of γ-Al_2O_3 particles is faster during the first 1 to 3 minutes. The removal efficiency increases with increasing electrostatic field. The final removal efficiency of γ-Al_2O_3 at an electrostatic field of 96.8 V/cm is 80% at a γ-Al_2O_3 concentration of 100 mg/L, and filtration rate of 0.43 L/min.
3. In the γ-Al_2O_3 concentration range between 50 mg/L to 200 mg/L, there is no distinct difference in solid removal efficiency.
4. An optimal filtration rate is observed for the separation of colloidal particles. At filtration rate greater or less than 0.46 L/min, the removal efficiency of γ-Al_2O_3 decreases as increasing or decreasing the filtration rate. The results show that optimum filtration rate of the cross-flow electro-filtration unit is 0.46 L/min under the experimental conditions 100 mg/L of γ-Al_2O_3 and an electrostatic field of 96.8 V/cm.
5. The pH dependence of solid removal efficiency of γ-Al_2O_3 observed is as expected since pH affects the surface charge of the colloidal particles. When the pH value of solution is less than 9.2 (pH_{zpc}), the surface of γ-Al_2O_3 is positively charged. Decreasing pH will increase the surface charge of the γ-Al_2O_3 particles. Consequently, under otherwise identical conditions, the particle removal efficiency is enhanced as pH decreases.

6. Groundwater samples were collected with both the bailers and the low flow purging technique (LFP) from three of the five wells at the Denzer-Schaefer site, Toms River, NJ. Naturally occurring particles collected from water samples are negatively charged under the pH condition of the groundwater.The pH_{zpc} is approximately 1 to 2. The particle appear to be monodispered. The avergae particle size is in the range of 490 to 774 nm. Another observation is that the particle in well #5S are slightly larger than those in well #10 and #MW3.
7. A linear relationship exits between the turbidity and the solid concentration of water samples. The linear correlation coefficient (R^2) is 0.99. It is possible to use turbidity measurements as an indication of water quality.
8. The removal rate of particle in water samples is faster during the first 1 to 4 minute. The removal efficiency increases with increasing electrostatic field. The final removal efficiency was 84% and 75%, respectively, at an electrostatic field of 161.3 v/cm and 64.5 V/cm for well #10 water sample by the bailing and the low flow purging sampling methods. The final removal efficiency was 95% and 94%, respectively, at an electrostatic field of 156.5 v/cm and 156.85 V/cm for well #5S water sample by the bailing and the low flow purging sampling techniques.
9. In the well #MW3 water sample, the electrostatic field strength applied was only at 17.1 V/cm. A higher electrostatic field can not be achieved because of its high conductivity. The final removal efficiency was 46% at an electrostatic field of 17.1 V/cm for well #MW3 water sample.
10. It is possible to separate the naturally occurring particles by adjusting the pH and applied field strength of the CFEF unit.

11. The average particle size of filtrate for water sample collected by the bailing and the low flow purging sampling in well #10, #5S and #MW3 is less than 400 nm and smaller than those in the raw and the concentration streams. The average particle size of the concentrate for water sample collected by the bailing and the low flow purging sampling methods in wells #10, #5S and #MW3 is in the range of 470 to 2,881 nm which are larger than those of the raw and the filtrate.
12. At an experimental pH of 5, the particle size distributions of the concentrate will shift toward the sup-micrometer region. This phenomenon can be explained by flocculation theory. That is, the particles become coagulated.
13. The total lead in the water collected from the three wells is 24-29, 45-116 and ND (<1) μg/L in wells #10, #5S and #MW3, respectively. The soluble lead is 4, ND (<1)-13, ND (<1) μg/L in wells #10, #5S and #MW3, respectively. Water sampling technique, i.e. bailing and low flow purging, appears to have little effect on the lead analysis in this case. This can be preliminarily attributed to the problem encountered during sampling. Due to high solid content in the well water, the groundwater is disturbed twice during low flow purging operation.
14. The soluble and total lead concentration of filtrate in water from wells 10IL01, 5SIIL02 and 5SIIB03 are almost < 1 μg/L.
15. Results show that the total lead concentration of the concentrate in water from wells 10IL01, 5SIIL02 and 5SIIB03 is higher than that of the filtrate. Results also show that the total lead concentration of concentrate in water from wells 10IL01, 5SIIL02 and 5SIIB03 are higher than soluble lead concentration. The total lead concentration of the concentrate in water

from well 5SIIL02 increases with increasing the electrostatic field. The high lead concentration can be attributed to high particle loading in water.

16. The exchangeable/bound and the carbonate exchangeable fraction are minor components and vary slightly with electrostatic field and pH at all water samples.
17. Lead was mostly concentrated in the residual, the organic matter and the Fe-Mn oxide fractions. Note that the remaining three fractions (Fe-Mn oxide, organic matter and residual) are generally strongly held within the particulate and normally unavailable to plants. It implies that lead is strongly bound to oxides, organic matters, and silicates. This chemical bounding is strong and, under natural environmental condition, the release of lead to water is not significant.
18. A preliminary model for prediction the solid removal of CFEF unit was established. This model can describe the removal of particles with predicted data agree well with experimental ones.

7.0 References

Archer, G. P., Render, M. C., Bettes, W. B., Sancho, M., 1993. Dielectrophoretic concentration of microorganisms using grid electrodes. Microbiols 76 (309), 237-244

Akay, G., Wakeman, R. J., 1996. Electric field intensification of surfactant mediated separation processes. Chemical Engineering research & design 74 (A5), 517-525.

Chen, W., Tan, S. K., Tay, J. H., 1996. Distribution, fractional composition and release of sediment-bound heavy metals in tropical reservoirs. Water, Air, Soil Pollution 92, 273-287.

Chiou, C. T., Malcolm, R. L., Brinton, T. L., Kile, D. E., 1986. Water solubility enchancement of some organic pollutants and pesticides by dissolved humic and fulvic- acids. Env. Sci. Tech., 20 (5), 502-508.

Clevenger, T. E., 1990. Use of sequential extraction to evaluate the heavy metals in mining wastes. Water, Air, Soil Pollution 50, 241-254.

Chlopecka, A., 1993. Form of trace metals from inorganic source in soils and amounts found in Spring Barley. Water, Air, Soil Pollution 69, 127-134.

Chlopecka, A., Bacon, J. R., Wilson, M. J., Kay, J., 1996. Forms of cadmium, lead, zinc in contaminated soils from southwest Poland. J. Environ. Qual. 25, 69-79.

Crawford M., 1976. Air Pollution Control Theory, 304-312.

Dudka, S., Chlopecka, A., 1990. Effect of soil-phase speciation on metal mobility and phytoavailability in sludge-amended soil. Water, Air, Soil Pollution. 51, 153-160.

Gee, C., Ramsey, M. H., Maskall, J., Thornton, I., 1997. Weathering processes inhistorical smelting slags-factors controlling the release of heavy metals. J. Geochem. Explor. 58, 249-257

Henry, J. D., Lawler, L. F. and Kuo, C. H., 1977. A solid/liquid separation process based on cross flow and electrostation. AIChE., J. 23 (6), 851-859.

Hickey, M. G., Kittrick, J. A., 1984. Chemical partitioning of cadmium, copper, nickel and zinc in soils and sediments containing high levels of hevay metals. J. Environ. Qual. 13, 372-376.

Hsieh, Y. H., 1984. Effect of specific chemical reactions on the dewatering of inorganic slurries. Thesis of University of Delaware.

Huang, C. P., Stumm, W., 1973. Specific adsorption of Cations on hydrous γ-Al_2O_3. J. colloid interface Sci. 43, 409-420.

Huotari, H. M., Tragardh, G., Huisman, I. H., 1999. Crossflow membrane filtration enchanced by an external DC electric field: A review. Chem. Eng. Res. Design 77 (A5), 461-468.

Kearl, P. M., Korte, N. E. and Cronk, T. A., 1992. Groundwater monitoring Review 7 (2), 155.

Lo, YT. S., Gidaspow, D. and Wasan, D. T., 1993. Separation of colloidal particles from nonaqueous media by cross flow electrofiltration. Separation Sci. Tech. 18 (12-12), 1323-1349.

Luoma, S. N. (1983) Bioavailability of trace metals to aquatic organisms: a review. Science of the Total Environment 28, 1-22.

Manegold, E., 1937. The effectiveness of filtration, dialysis, electrophoresis and their intercombination as purification processes. Trans. Faraday Soc. 33.

Majmudar, A. A., manohar, C., 1994. Electrophoretic separation of suspension of TiO_2. Separation Sci. Tech. 29 (7), 845-854.

Means, J. C., Wijayaratne, R., 1982. Role of natural colloids in the transport of hydrophobic pollutants. Science 215(4535), 968-970.

Miller, W. P., McFee, W. W., Kelly, J. M., 1983. Mobility and retention of heavy metals in sandy soils. J. Environ. Qual. 12, 579-584.

Moulik, S. P., 1976. Normal and reverse field induced flow behaviors in electrofiltration. Colloid & polymer Sci. 254, 39044.

Puls, R. W. and Barcelona, M. J., 1996. Low-flow (minimal drawdown) ground-water sampling procedures. EPA/504/S-95/504, EPA, Washington, DC.

Ramos, L., Hernandez, L. M., Gonzalez, M. J., 1994. Sequential fraction of copper, lead, cadmium and zinc in soils from or near Donana national park. J. Environ. Qual. 23, 50-57.

Salomons, W., Kerdlik, H., van Pagee, H., Klomp, R. and Schreur, A. (1988) Behaviou and impact assessment of heavy metals in estuary and coastal zone. In metals in Coastal Environments of Latin America, eds. U. Seeliger, L.D. de Lacerda and S. R. P. Patchineelam, pp. 159-198 Springer, New York.

Sheppard, J. C., Campbell, M. J., Kittrick, J. A., Hardt, T. L., 1979. Retention of neptunium, Americium, and curium by diffusible soil particles. Env. Sci. Tech. 13 (6), 680-684.

Sims, J. L., Patrick, W. H., Jr., 1978. The distribution of micro-nutrient cations in soil under conditions of varying redox potential and pH. Soil Sci. Soc. Am. J. 42, 258-262.

Stumm, W. 1968. Chemical precipitation, stability, and ion exchange, in water purification and wastewater treatment and disposal, Eds. Fair, G. M, Geyer, J. C., and Okun, D. A., John Wiley and sons, New York, NY.

Stumm, W. and Bilinski, H., 1972. Trace metals in natural waters: difficultes of interpretation arising from our ignorance of their speciation, in advances in Water Pollution Research,

Proceedings, 6th international Conference, Jerusalem, Israel. Pergamon Press, Oxford, 39-52.

Takayanagi, K., Wong, G. T., 1983. Organic and colloidal selenium in southern Chesapeake bay and adjacent waters. Marine Chem. 14 (141), 141-148.

Tessier, A., Campbell, P. G. C. and Bisson, M. (1979) Sequential extraction procedure for the speciation of trace metals. Analytical Chemistry 51, 844-851.

Verdegan, B. M., 1996. Cross flow electrofiltration of petroleum oils. Separation Sci. Tech. 21 (6-7), 603-623.

Wakeman, R. J., 1999. Electrically enhanced microfiltration of albumin, food bioproducts process 76 (c1), 53-59.

Wakeman, R. J., and Sabri, M. N., 1995. Utilizing pulsed electric fields in cross-flow microfiltration of titana suspensions. Chem. Eng. Res. Design 73 (A4), 455-463.

Wakeman, R. J. andTarleton, E. S., 1987, Membrance of fouling prevention in crossflow microfiltration, Chem. Eng. Sci., 42(4), 829-842.

Weigert, T., Altmann, J., Ripperger, S., 1999. Crossflow electrofiltration in pilot scale. Journal of membrane science 159 (1-2), 253-262.

Von Zumbusch, P., Kulucke, W. and Brunner, G., 1998. Use of alternating electrical fields as anti-fouling strategy in ultrafiltration of biological suspensions- introduction of a new experimental procedure for crossflow filtration. J. membrane Sci. 142 (1), 75-86.

Xian, X., 1989. Effect of chemical forms of cadmium, zinc, and lead in polluted soils on their uptake by cabbage plants. Plant Soil 113, 257-264.

Xian, X., Shokohifard, G. I., 1989. Effect of pH on chemical forms and plan availability of cadmium, zinc, and lead in polluted soils. Water, Air, Soil Pollut. 45, 265-273.

Table 1. The summary of the cross-flow electrostatic-filtration module under various experiments: γ-Al_2O_3

Variation	Experimental Condition					Turbidity (NTU)		Removal (%)
	Filtration Rate (L/min)	γ-Al_2O_3 (mg/L)	Electrostatic Field (V/cm)	Voltage	pH	Initial	Final	
Electrostatic Field	0.77	100	00.0	00	5.6	29.0	28.0	3
	0.77	100	12.9	40	5.6	29.0	25.2	13
	0.77	100	16.1	50	5.6	29.0	23.8	18
Electrostatic Field	0.46	100	16.1	50	5.6	30.8	23.7	23
	0.46	100	32.3	100	5.6	28.5	15.3	46
	0.46	100	48.4	150	5.6	28.5	11.5	60
	0.46	100	64.5	200	5.6	28.5	9.2	68
	0.46	100	80.6	250	5.6	28.5	8.0	72
	0.46	100	96.8	300	5.6	28.5	5.7	80
γ-Al_2O_3	0.77	50	16.1	50	5.6	16.0	11.3	29
	0.77	100	16.1	50	5.6	30.8	21.9	29
	0.77	200	16.1	50	5.6	58.1	43.6	25
Filtration Rate	0.27	100	96.8	300	5.6	28.5	7.1	75
	0.46	100	96.8	300	5.6	28.5	5.7	80
	0.77	100	96.8	300	5.6	28.5	10.4	64
	1.08	100	96.8	300	5.6	28.5	13.5	53
	1.39	100	96.8	300	5.6	28.5	15.6	45
	1.70	100	96.8	300	5.6	28.5	15.5	46
pH	0.46	100	96.8	300	4.0	29.7	4.9	84
	0.46	100	96.8	300	5.0	29.7	8.3	72
	0.46	100	96.8	300	6.0	29.7	10.7	64
	0.46	100	96.8	300	7.0	29.7	16.2	45
	0.46	100	96.8	300	8.0	29.7	16.0	46

Table 2. List of field samples

Well Name	Sampling Method[a]	Sampling Time	Sample Size (L)	No. Sample (#)	Field Sample ID[b]	Laboratory Sample ID	Weather
10	B	01/10/01	40	1	10-UD-004-01	10IB01	Snowy
	LFP	01/10/01	20	1	LFP-10-UD-009-01	10IL01	Snowy
5S	B	01/10/01	20	1	5S-UD-005-01	5SIB01	Snowy
	LFP	01/10/01	1	1	LFP-5S-UD-012-01	5SIL01	Snowy
				2	LFP-5S-UD-012-02	5SIL02	
				3	LFP-5S-UD-012-03	5SIL03	
				4	LFP-5S-UD-012-04	5SIL04	
				5	LFP-5S-UD-012-05	5SIL05	
				6	LFP-5S-UD-012-06	5SIL06	
				7	LFP-5S-UD-012-07	5SIL07	
				8	LFP-5S-UD-012-08	5SIL08	
				9	LFP-5S-UD-012-09	5SIL09	
				10	LFP-5S-UD-012-10	5SIL10	
	LFP	04/04/01	5	1	LFP-5S-UD-019-01	5SIIL01	Sunny
	LFP	04/04/01	20	2	LFP-5S-UD-019-02	5SIIL02	Sunny
				3	LFP-5S-UD-019-03	5SIIL03	
	B	04/04/01	20	1	5S-UD-021-01	5SIIB01	Sunny
				2	5S-UD-021-02	5SIIB02	
	B	04/04/01	5	3	5S-UD-021-03	5SIIB03	Sunny
MW3	B	04/04/01	20	1	MW3-UD-022-01	MW3IB01	Sunny
				2	MW3-UD-022-02	MW3IB02	
	B	04/04/01	8	3	MW3-UD-022-03	MW3IB03	Sunny
	LFP	04/04/01	8	1	LPF-MW3-UD-024-01	MW3IL01	Sunny
	LFP	04/04/01	20	2	LPF-MW3-UD-024-02	MW3IL02	Sunny
				3	LPF-MW3-UD-024-03	MW3IL03	

a: B: Bailer
LFP: Low flow purge
b: Well-analysis location-sample number
Well Name-Lab Name-Sample Series- Sample Number

Table 3. Diameter of naturally occurring particles in well waters

Unit: nm

Laboratory Sample ID	Run 1	Run 2	Run 3	Average ± SD
10IB01	478	487	505	490 ± 14
10IL01	466	464	497	476 ± 19
5SIB10	554	551	558	554 ± 04
5SIL10	570	578	612	587 ± 22
5SIIB03	724	669	787	727 ± 59
5SIIL02	794	789	740	774 ± 30
MW3IB03	540	471	599	537 ± 64

Table 4. Major chemical characteristics of well waters

Laboratory Sample ID	Ca (mg/L)	Fe (mg/L)	Total Lead (μg/L)	Soluble Lead (μg/L)	Total Solids (g/L)
10IB01	2.1	0.7	24	4	3.687
10IL01	2.8	2.0	29	4	2.954
5SIB10	0.3	5.9	51	11	10.198
5SIL10	0.3	5.6	47	13	2.659
5SIIB03	-	-	116	< 1	11.517
5SIIL02	-	-	45	< 1	3.094
MW3IB03	-	-	< 1	< 1	1.750
MW3IL01	-	-	< 1	< 1	0.136

Table 5. The summary of performance of the cross-flow electrostatic-filtration module under various experimental conditions with groundwater samples

Sample	Experimental Condition			Turbidity (NTU)		Removal (%)
	Electrostatic Field (V/cm)	Voltage	pH	Initial	Final	
10IB01	00.0	00	6.5	223	213	4
	32.3	100	6.5	223	127	43
	64.5	200	6.5	223	68	69
	96.8	300	6.5	223	45	80
	129.1	400	6.5	223	38	83
	161.3	500	6.5	223	35	84
	00.0	00	6.5	799	717	10
	32.3	100	6.5	799	344	57
	48.4	150	6.5	799	272	66
	62.6	194	6.5	799	196	75
	32.3	100	5.0	799	248	69
	48.4	150	7.0	799	239	70
	48.4	150	9.0	799	212	73
10IL01	00.0	00	6.5	548	521	5
	32.3	100	6.5	548	278	49
	48.4	150	6.5	548	164	70
	64.5	200	6.5	548	136	75
	32.3	100	5.0	548	202	63
	48.4	150	7.0	548	144	74
	48.4	150	9.0	548	149	73
5SIIB03	00.0	00	6.6	748	694	7
	32.3	100	6.6	748	456	39
	64.5	200	6.6	748	283	62
	96.8	300	6.6	748	131	82
	129.0	400	6.6	748	51	93
	156.5	485	6.6	748	39	95
	96.8	300	5.0	748	45	94
	96.8	300	7.0	748	56	93
	96.8	300	9.0	748	120	84

Table 5. The summary of performance the cross-flow electrostatic-filtration module under various experimental conditions with groundwater samples (continued)

Sample	Experimental Condition			Turbidity (NTU)		Removal (%)
	Electrostatic Field (V/cm)	Voltage	pH	Initial	Final	
5SIIL02	00.0	00	6.7	939	850	9
	32.3	100	6.7	939	331	65
	64.5	200	6.7	939	125	87
	96.8	300	6.7	939	84	91
	129.0	400	6.7	939	79	92
	156.8	486	6.7	939	55	94
	96.8	300	4.5	939	50	95
	96.8	300	6.5	939	78	92
	96.8	300	9.0	939	95	90
MW3IB 01	00.0	00	7.9	582	514	12
	17.1	53	7.9	582	312	46
	10.3	32	5.0	582	322	45
	13.2	41	7.0	582	303	48
	14.8	46	9.0	582	287	51

Table 6. The concentration of total and soluble lead in the filtrate and concentrate of CFEF operation

Unit: μg/L

Sample	Exper. Condition			Filtrate		Concentrate	
	Electrostatic Field (V/cm)	Voltage	pH	Soluble	Total	Soluble	Total
10IL01	32.3	100	6.5	< 1	3	< 1	91
	48.4	150	6.5	< 1	< 1	< 1	77
	64.5	200	6.5	< 1	< 1	< 1	-
	32.3	100	5.0	< 1	< 1	< 1	75
	48.4	150	7.0	< 1	< 1	< 1	118
	48.4	150	9.0	< 1	< 1	< 1	80
5SIIB03	32.3	100	6.6	< 1	8	-	-
	64.5	200	6.6	< 1	3	-	-
	96.8	300	6.6	< 1	< 1	-	-
	129.0	400	6.6	< 1	< 1	-	-
	156.5	485	6.6	< 1	< 1	< 1	18
	96.8	300	5.0	< 1	< 1	< 1	12
	96.8	300	7.0	< 1	< 1	< 1	9
	96.8	300	9.0	< 1	< 1	< 1	10
5SIIL02	32.3	100	6.7	< 1	4	< 1	24
	64.5	200	6.7	< 1	< 1	< 1	42
	96.8	300	6.7	< 1	< 1	< 1	55
	129.0	400	6.7	< 1	< 1	< 1	72
	156.8	486	6.7	< 1	< 1	< 1	78
	96.8	300	4.5	< 1	< 1	2	73
	96.8	300	6.5	< 1	< 1	< 1	70
	96.8	300	9.0	< 1	< 1	< 1	98
MW3IB 01	17.1	53	7.9	< 1	< 1	< 1	< 1
	10.3	32	5.0	< 1	< 1	< 1	< 1
	13.2	41	7.0	< 1	< 1	< 1	< 1
	14.8	46	9.0	< 1	< 1	< 1	< 1

Table 7. The Tessier sequential extraction procedures for lead speciation

Step	Form/association	Abbr.	Extraction agent	Time	Temperature
1	Exchangeable	EXC	8-mL of 1 M $MgCl_2$, pH 7.0	Shaking 1.0 h	25°C
2	Carbonate	CAB	8-mL of 1 M NaOAc – 0.5 M HOAc, pH 5.0	Soaking 5 h and shaking 3 h	25°C
3	Fe and Mn oxides	FMO	20-mL of 0.04M NH_2OH•HCl, 25% HOAC at 96±3°	Soaking 15 h and shaking 2 h in daylight	96°C
4	Organic matter	ORM	3-mL0.02 M HNO_3, 5-mL 30% H_2O_2, pH 2, mixture was heated at 85±2 °C for 2 h.	2 h	85°C
			A second 3-mL aliquot of 30% H_2O_2 (pH 2 with HNO_3) was added and heated at 85±2 °C for 3 h.	3 h	
			After cooling, 5-mL 3.2 M NH_4OAc in 20% (v/v) HNO_3 was added and diluted to 20-mL and shaking 30 min.	0.5 h	
5	Residual forms	RES	The residue was digested with HF-$HClO_4$ mixture.	-	-

1. The selective extractions were conducted in centrifuge tubes (Teflon, 50 mL) to minimize losses of solid material.
2. Between each successive extraction, separation was effected by centrifuging at (RCF 10,621 g (10,000 rpm) for 30 min.
3. The supernatant was removed with pipet and analyzed for trace metals; whereas the residue was washed with 8-mL of deionized water, after centrifugation for 30 min; this second supernatant was discarded.
4. The volume of rinse water used was kept to a minimum to avoid excessive solubilization of solid material, particularly organic matter.
5. For total or residual trace metal analysis, the solid was digested with a 5:1 mixture of hydrofluoric and perchloric acids. The sediment was first digested in a PTFE beaker with a solution of concentrated $HClO_4$ (2-mL) and HF (10-mL) to near dryness; subsequently a second addition of $HClO_4$ (1-mL) and HF (10-mL) was made and again the mixture was evaporated to near dryness. Finally, $HClO_4$ (1-mL) alone was added and the sample was evaporated until the appearance of white fumes. The residue was dissolved in 5-mL 12 N HCl and diluted to 25-mL.

Table 8. Concentration of sequentially extracted and total lead as affected by electrostatic field strength in particles of well water sample 10IB01

unit: Pb-μg/soil-g

Field strength	E = 00 V/cm (V = 00)	E = 32.3 V/cm (V = 100)	E = 48.4 V/cm (V = 150)	E = 48.4 V/cm (V = 150)	E = 32.3 V/cm (V = 100)	E = 48.4 V/cm (V = 150)	E = 64.5 V/cm (V = 200)
pH	6.50	5.00	7.00	9.00	6.50	6.50	6.50
exchangeable	0.00	1.94	2.33	0.15	0.17	0.15	0.65
carbonate	0.00	0.00	0.00	1.44	1.79	1.10	1.46
Fe-Mn oxide	1.73	3.50	8.32	4.79	0.50	0.41	0.62
organic matter	5.07	8.35	11.45	7.86	6.69	5.95	6.45
Residual form	9.28	9.48	9.61	6.77	7.78	9.43	8.13
Total	16.08	23.28	31.71	21.01	16.94	17.05	17.31

Table 9. Concentration of sequentially extracted and total lead as affected by electrostatic field strength in particles of well water sample 10IL01

unit: Pb-μg/soil-g

Field strength	E = 00 V/cm (V = 00)	E = 32.3 V/cm (V = 100)	E = 48.4 V/cm (V = 150)	E = 48.4 V/cm (V = 150)	E = 32.3 V/cm (V = 100)	E = 48.4 V/cm (V = 150)	E = 64.5 V/cm (V = 200)
pH	6.5	5.0	7.0	9.0	6.5	6.5	6.5
exchangeable	0.00	0.00	0.81	0.00	0.00	0.00	0.00
carbonate	0.00	2.05	24.62	2.53	1.99	1.23	2.91
Fe-Mn oxide	2.29	1.44	5.15	0.99	6.33	2.61	3.62
organic matter	1.78	8.77	26.99	4.08	3.55	3.00	4.48
Residual form	1.04	2.26	2.13	3.55	1.18	1.29	1.62
Total	5.10	14.53	59.71	11.13	13.04	8.12	12.63

Table 10. Concentration of sequentially extracted and total lead as affected by electrostatic field strength in particles of well water sample 5SIIB03

unit: Pb-μg/soil-g

Field Strength	E = 00 V/cm (V = 00)	E = 96.8 V/cm (V = 300)	E = 96.8 V/cm (V = 300)	E = 96.8 V/cm (V = 300)
pH	6.5	5.0	7.0	9.0
exchangeable	0.00	0.00	0.00	0.00
carbonate	0.00	0.00	0.00	0.00
Fe-Mn oxide	0.14	0.11	0.13	0.15
organic matter	1.12	1.44	1.42	1.34
Residual form	3.56	2.60	2.74	4.21
Total	4.82	4.15	4.29	5.69

Table 11. Concentration of sequentially extracted and total lead as affected by electrostatic field strength in particle of well water sample 5IIL02

unit: Pb-μg/soil-g

Field strength	E = 00 V/cm (V=00)	E = 96.8 V/cm (V = 300)	E = 96.8 V/cm (V = 300)	E = 96.8 V/cm (V = 300)	E = 32.3 V/cm (V = 100)	E = 64.5 V/cm (V = 200)	E = 96.8 V/cm (V = 300)	E = 129.0 V/cm (V = 400)	E = 156.8 V/cm (V = 486)
pH	6.5	4.5	6.5	9.0	6.5	6.5	6.5	6.5	6.5
exchangeable	0.00	0.00	0.00	0.00	0.00	0.00	0.00	0.00	0.00
carbonate	0.00	0.63	1.01	1.52	0.15	0.33	1.18	2.31	1.83
Fe-Mn oxide	0.09	3.18	2.06	1.89	0.71	0.64	1.00	1.54	3.13
organic matter	1.09	3.96	3.29	5.54	3.89	3.76	4.73	4.88	5.71
Residual form	2.41	2.49	6.09	1.11	1.00	3.16	2.51	3.17	5.25
Total	3.58	10.26	12.46	10.05	5.74	7.89	9.42	11.89	15.93

Table 12. Concentration of sequentially extracted and total lead as affected by electrostatic field strength in particles of well water sample MW3IB03

unit: Pb-μg/soil-g

Field Strength	E = 00 V/cm (V = 0)	E = 10.3 V/cm (V = 32)	E = 13.2 V/cm (V = 41)	E = 14.8 V/cm (V = 6)	E = 17.1 V/cm (V = 53)
pH	6.5	5.0	7.0	9.0	6.5
exchangeable	0.00	0.00	0.00	0.00	0.00
carbonate	0.00	0.00	0.00	0.00	0.00
Fe-Mn oxide	0.10	0.10	0.08	0.04	0.05
organic matter	1.84	1.72	1.79	2.00	1.71
Residual form	4.88	1.87	1.64	3.03	1.95
Total	6.81	3.69	3.51	5.07	3.71

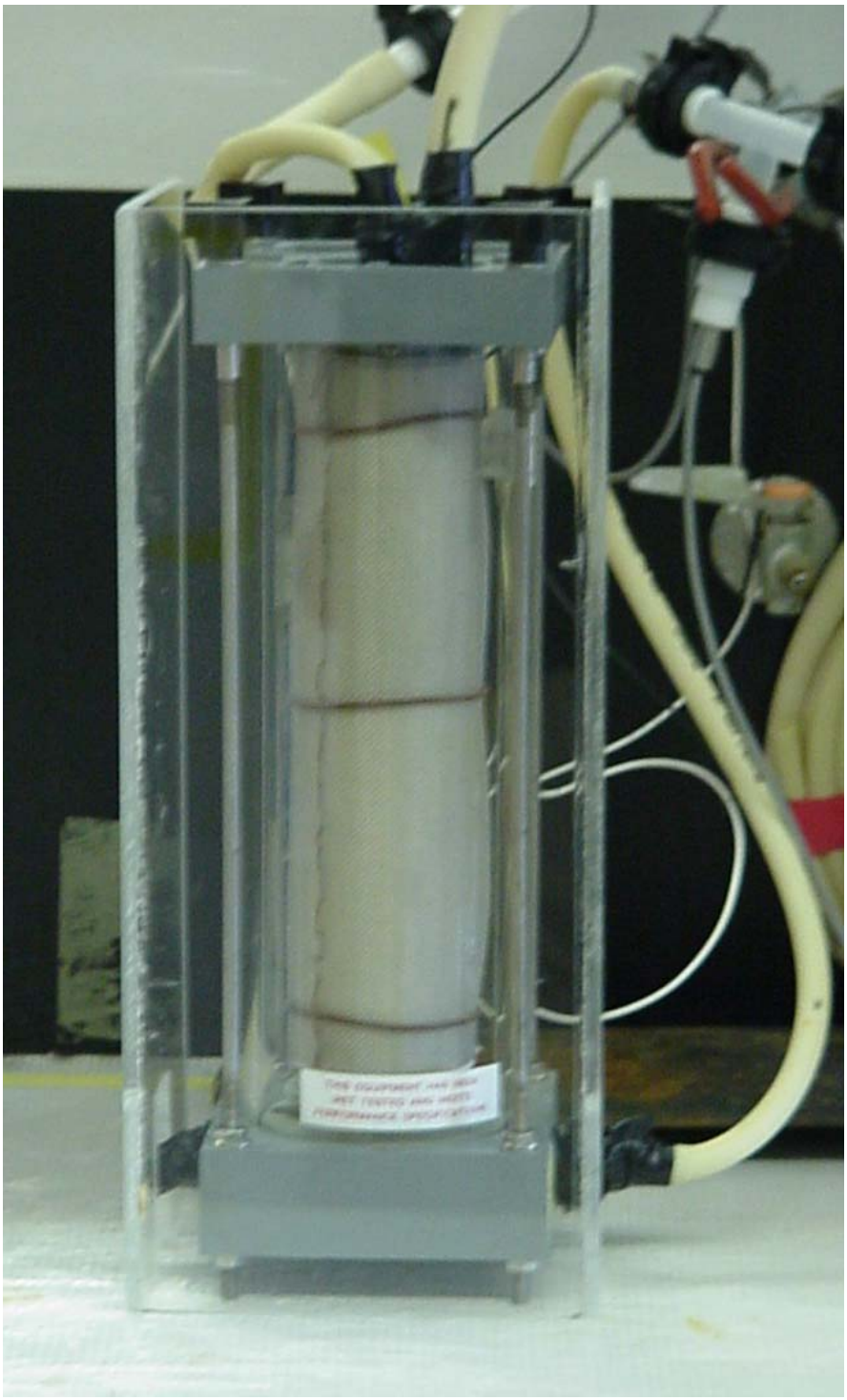

Figure 1. Main unit of the CFEF module. It consists of an external tube (insulated), an inner electrically charged cathodic filter membrane, and a co-centric anodic rod. The external tube has a diameter of 8.9 cm. The inner filter has a diameter of 3.0 cm and the co-centric rod is a 0.5 cm stainless wire. The total module is 22.5 cm long and has a total filtration surface area of 212 cm^2

Figure 2. Power supply

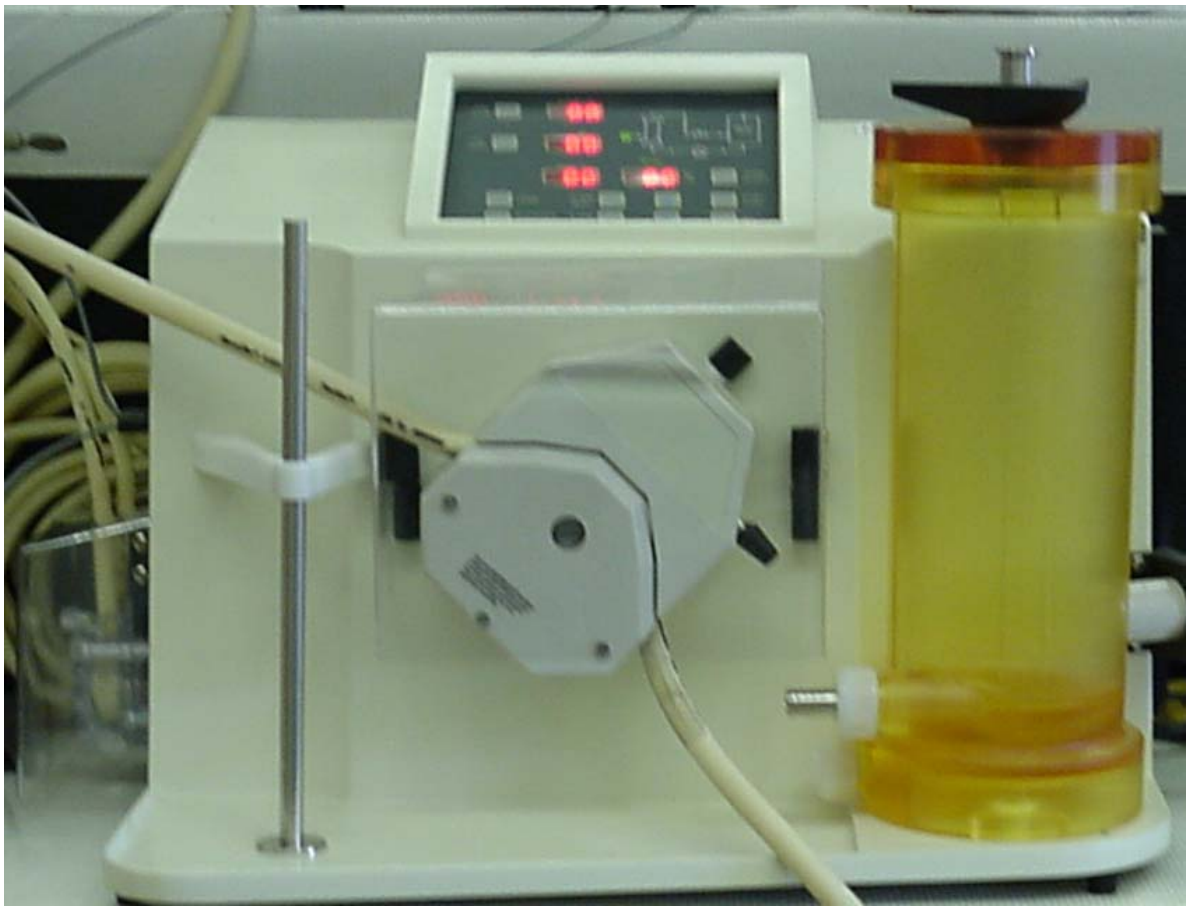

Figure 3. Millipore (model M12: cross flow filter) units

Figure 4. Micro-computer for flow control

Figure 5. The total arrangement of the CFEF module

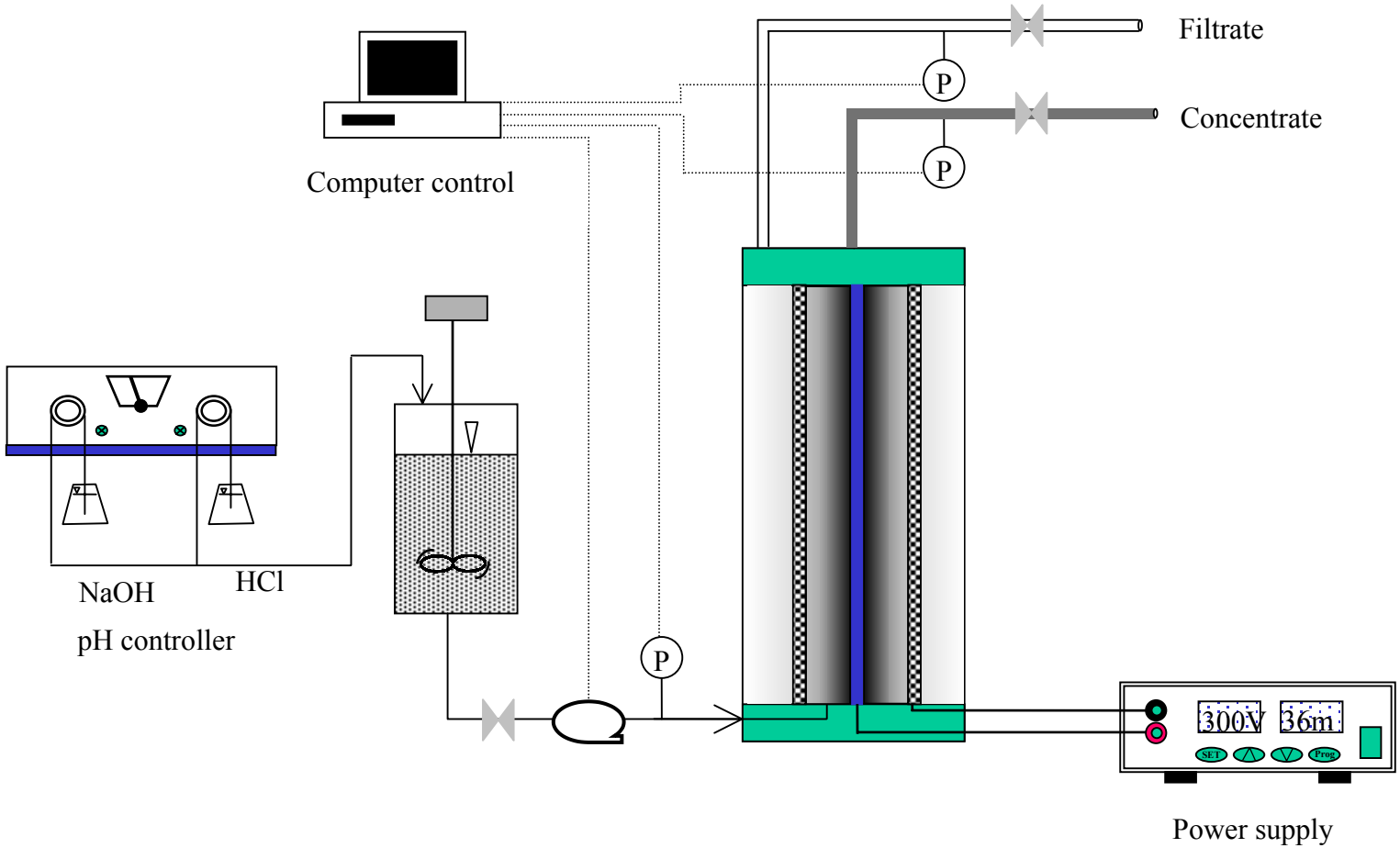

Figure 6. Schematic presentation of the flow diagram of the CFEF system

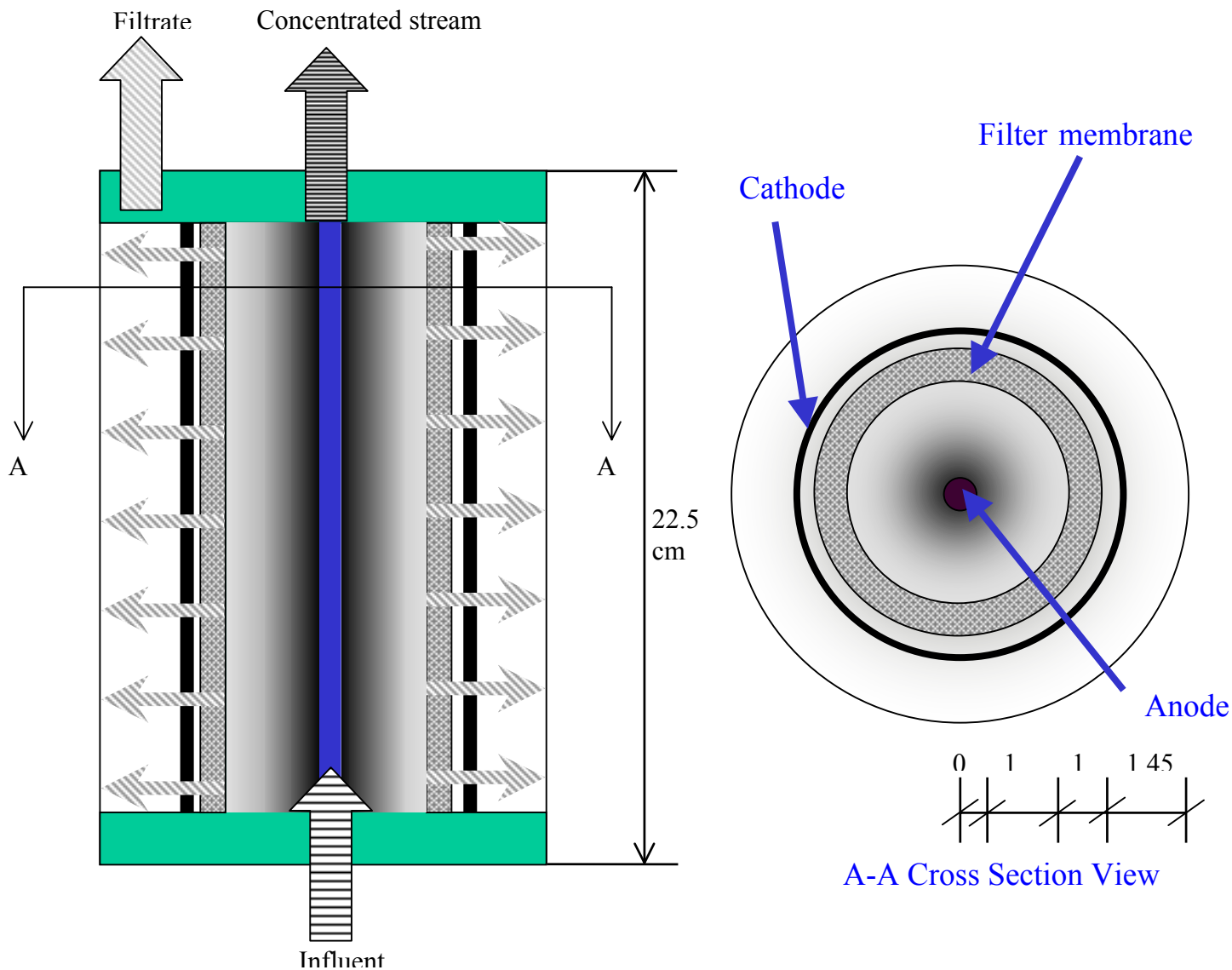

Figure 7. Schematic presentation of flow direction and location of sampling

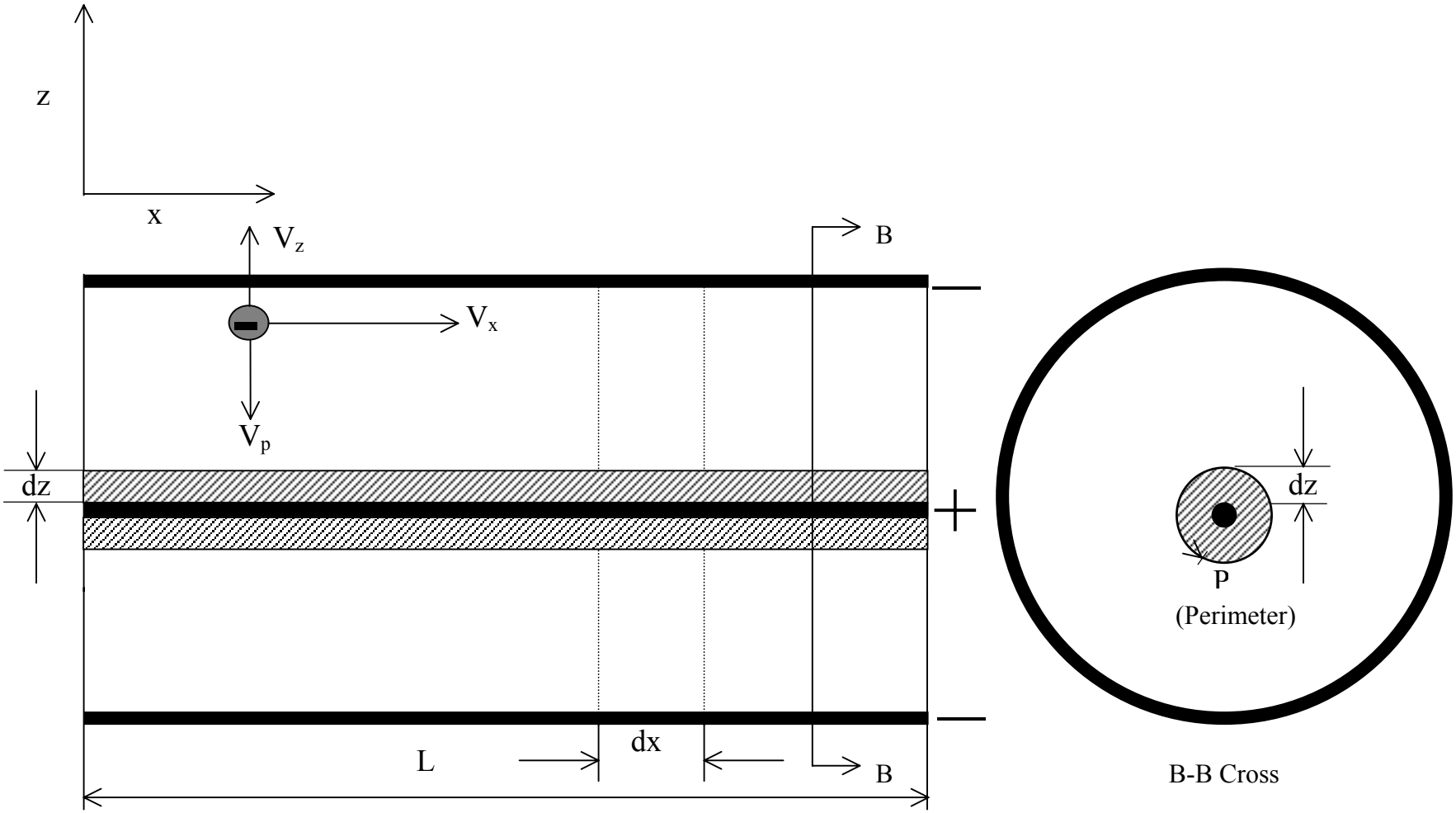

Figure 8. Collection section of CFEF.

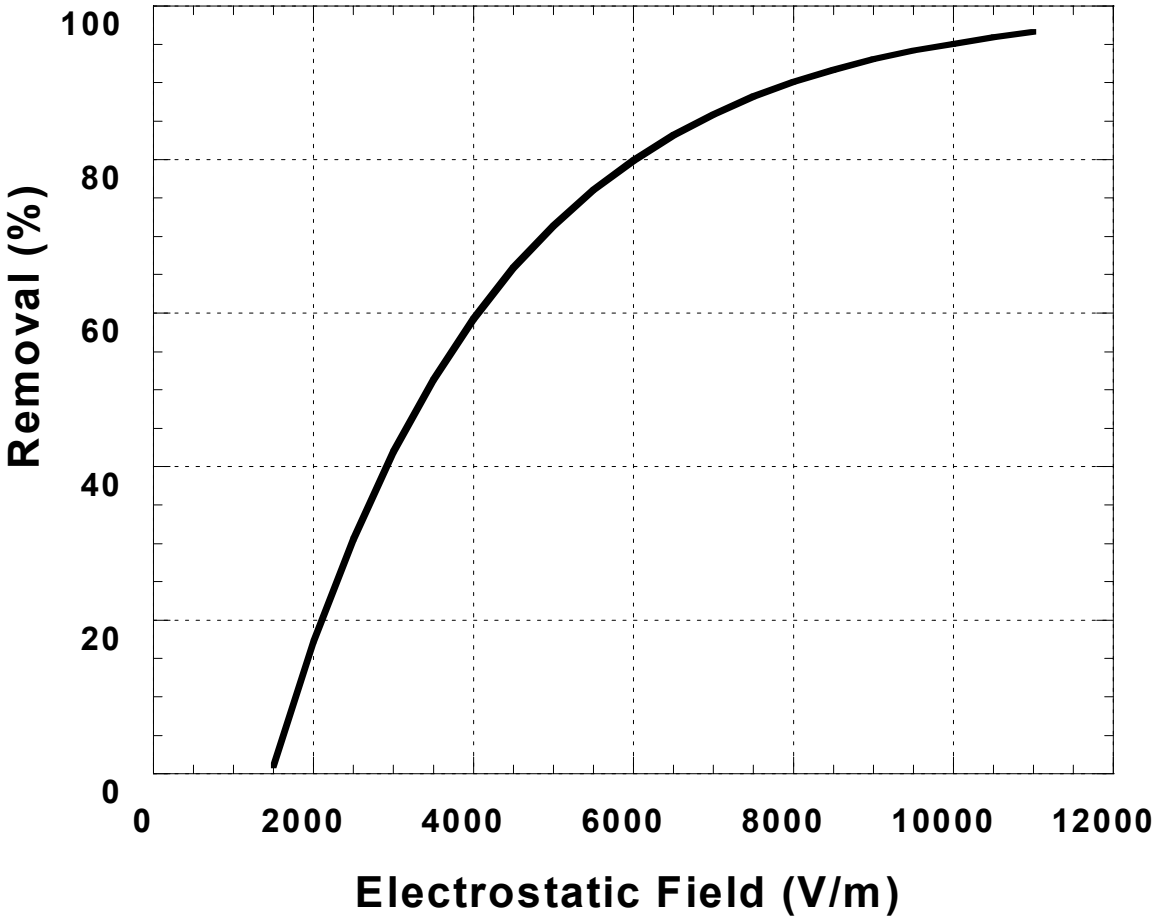

Figure 9. Theoretical removal as a function of applied electrostatic field. Particle size = 200 nm; surface charge = 18 $\mu C/m^2$.

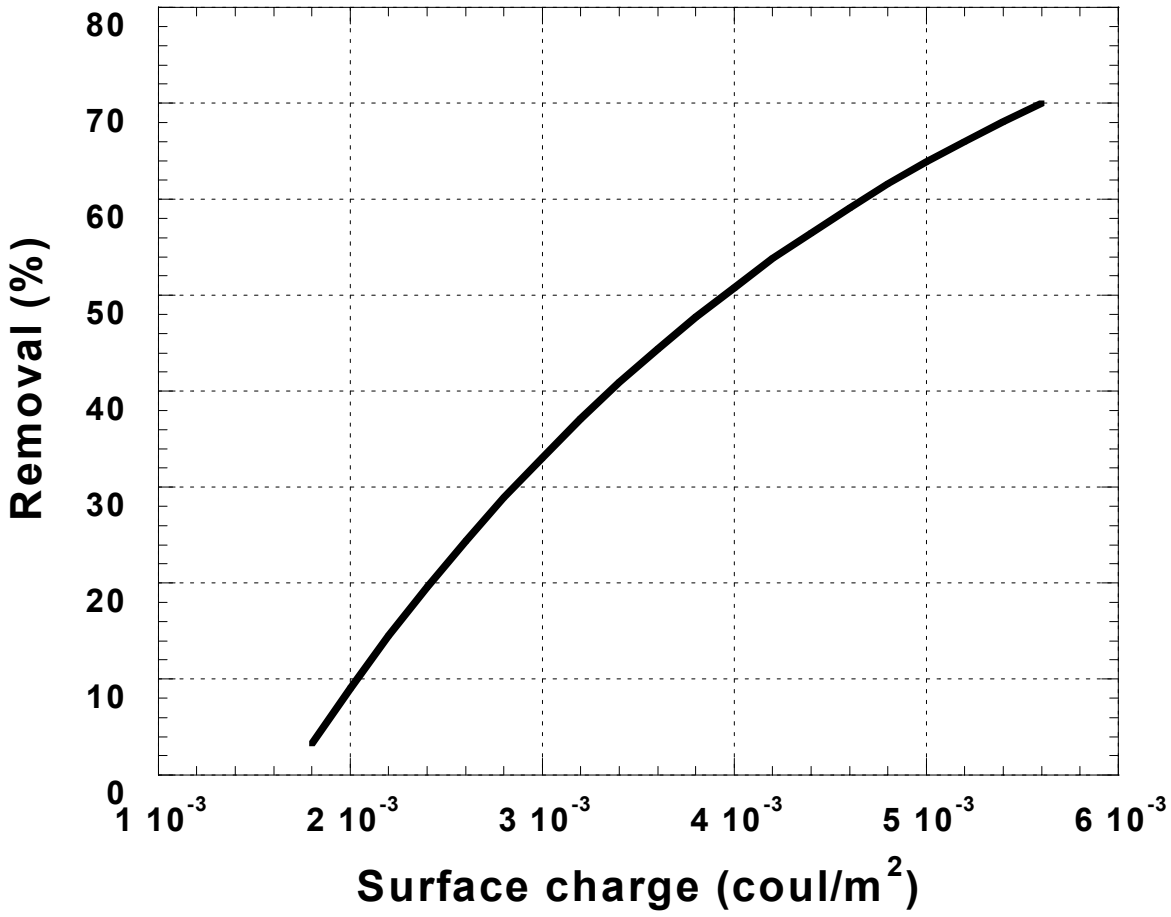

Figure 10. Theoretical removal as a function of surface charge. Electrostatic field strength = 1560 V/m; particle size = 200 nm.

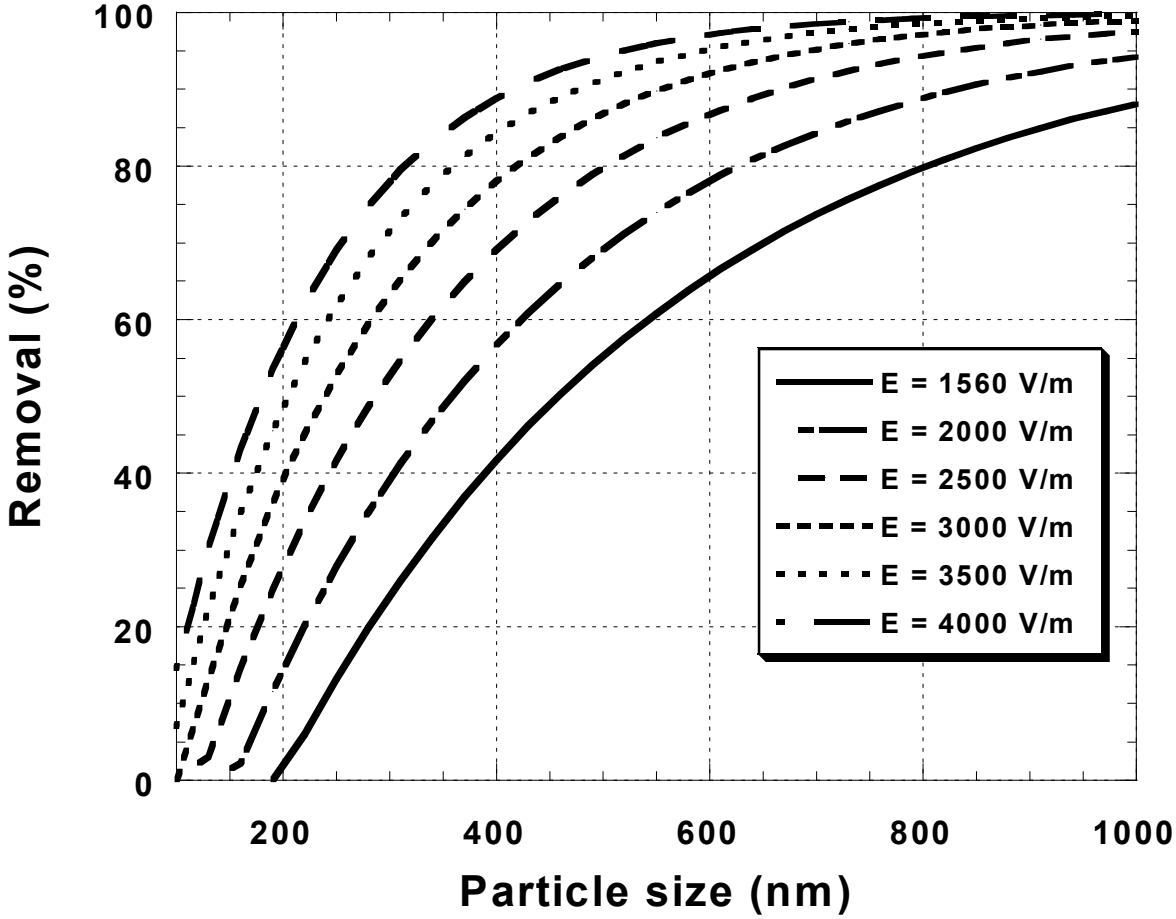

Figure 11. Theoretical removal as a function of applied electrostatic field and particle size. Surface charge = 5 mC/m^2.

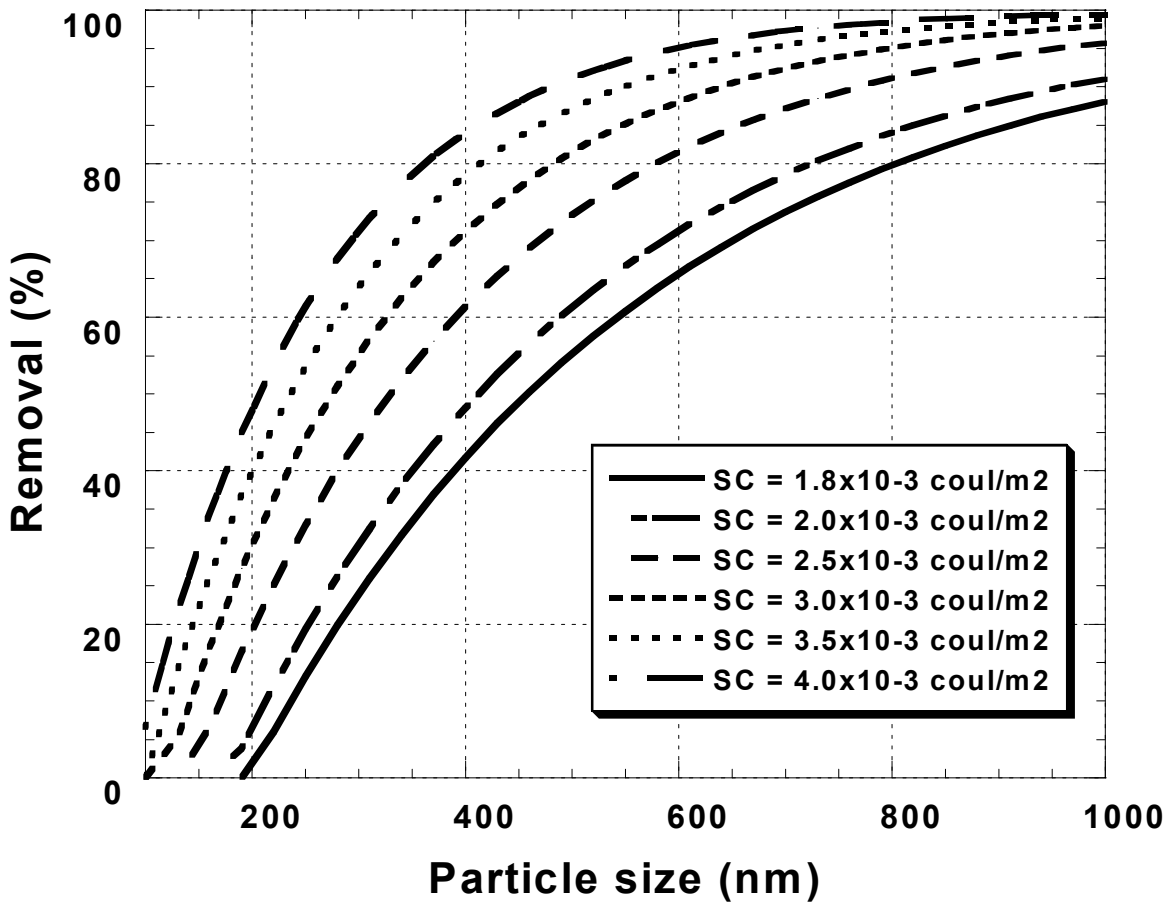

Figure 12. Theoretical removal as a function of particle size under various surface charges. Electrostatic field strength = 1,560 V/m.

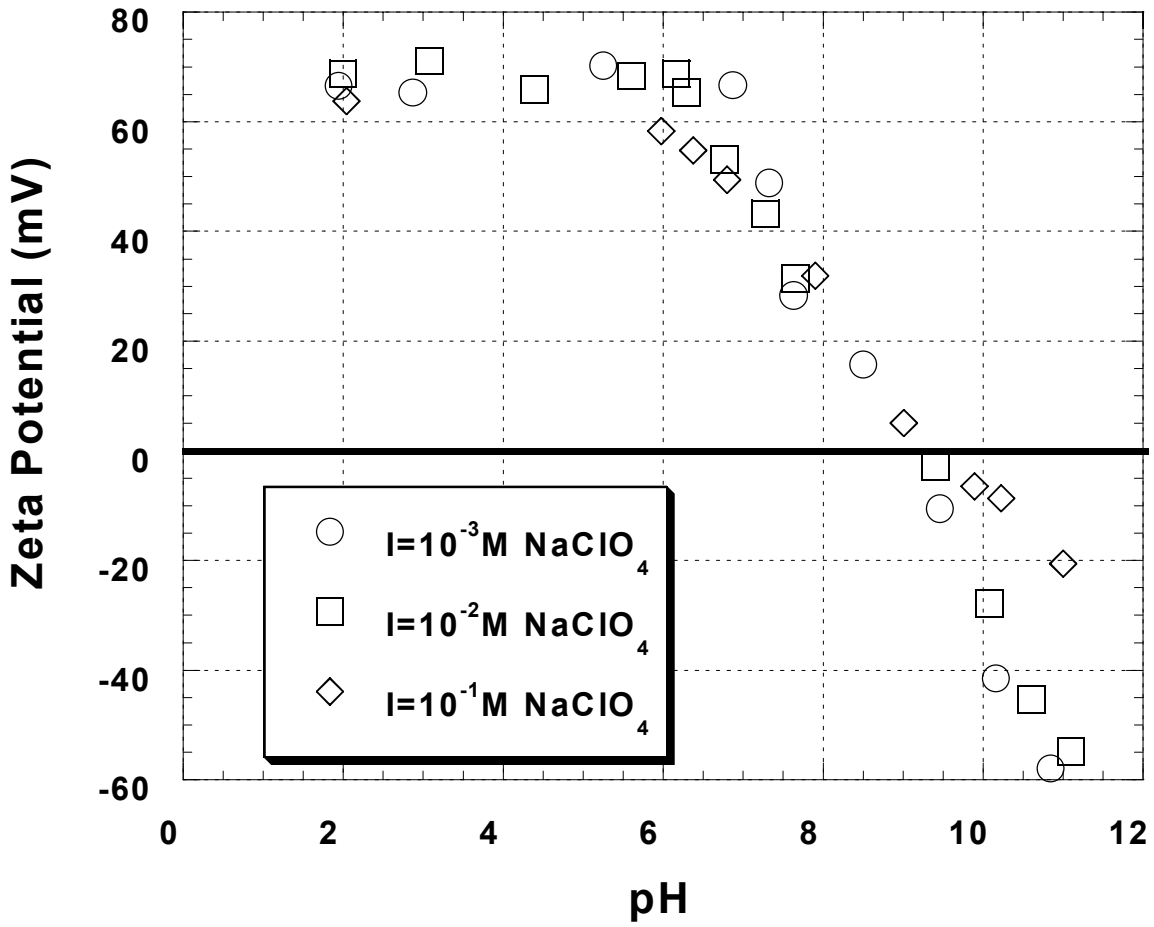

Figure 13. Zeta Potential of γ-Al_2O_3 as a function of pH. Experimental conditions: 100 mg /L γ-Al_2O_3; varying $NaClO_4$ concentration.

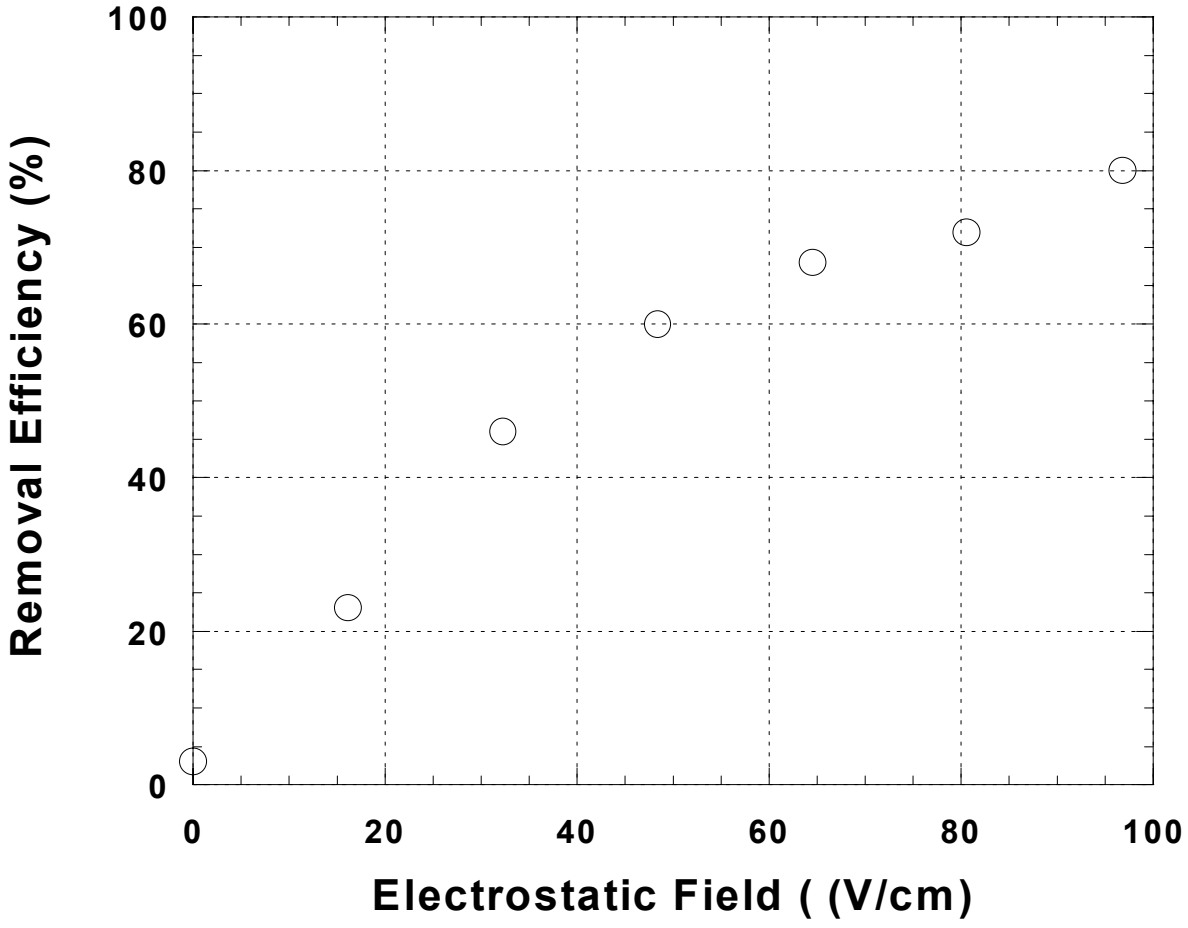

Figure 14. Effect of electrostatic field. Experimental conditions: 100 mg /L γ-Al_2O_3; pumping speed 15% (or filtration rate 0.46 mL/min)

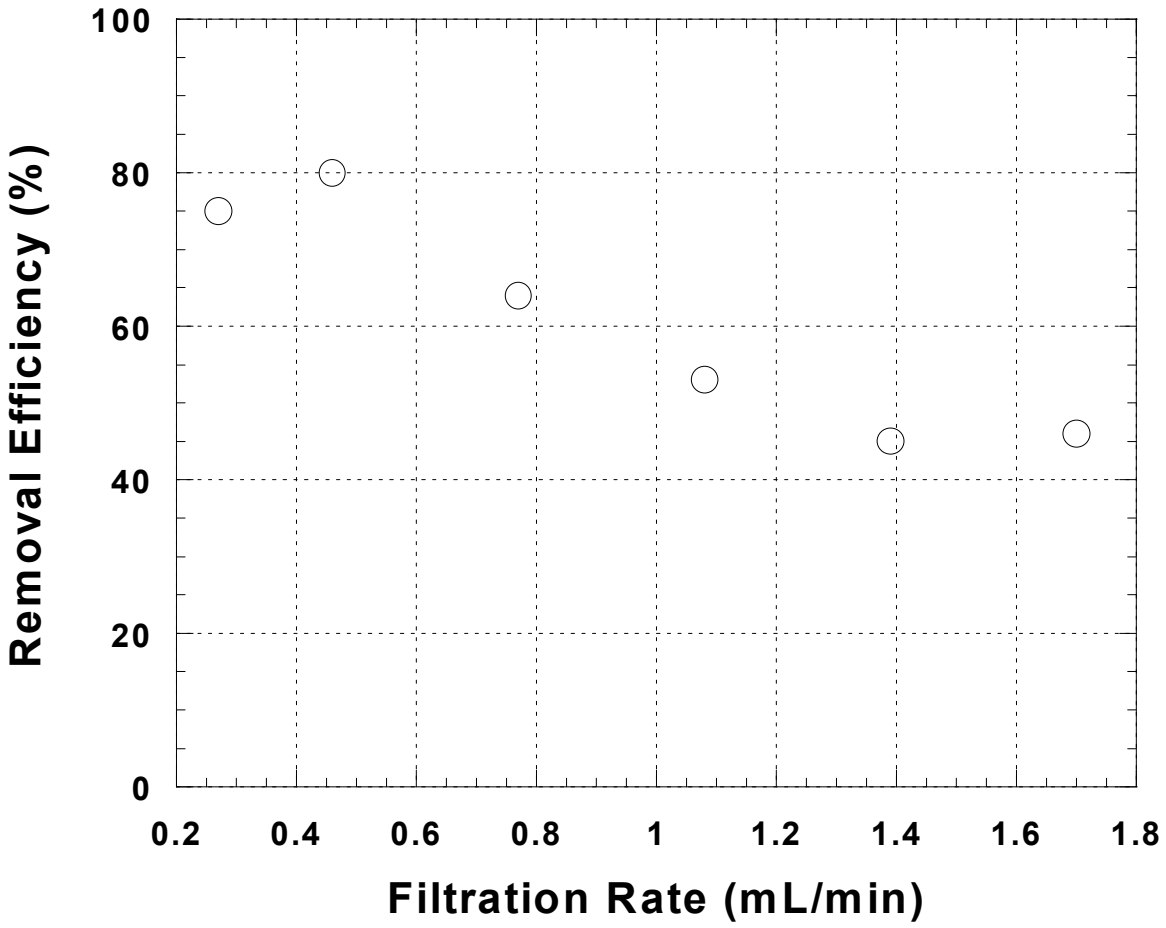

Figure 15. Effect of filtration rate on removal of colloidal particle. Experimental conditions: 100 mg/L γ-Al_2O_3; initial pH = 5.6; E = 96.8V/cm.

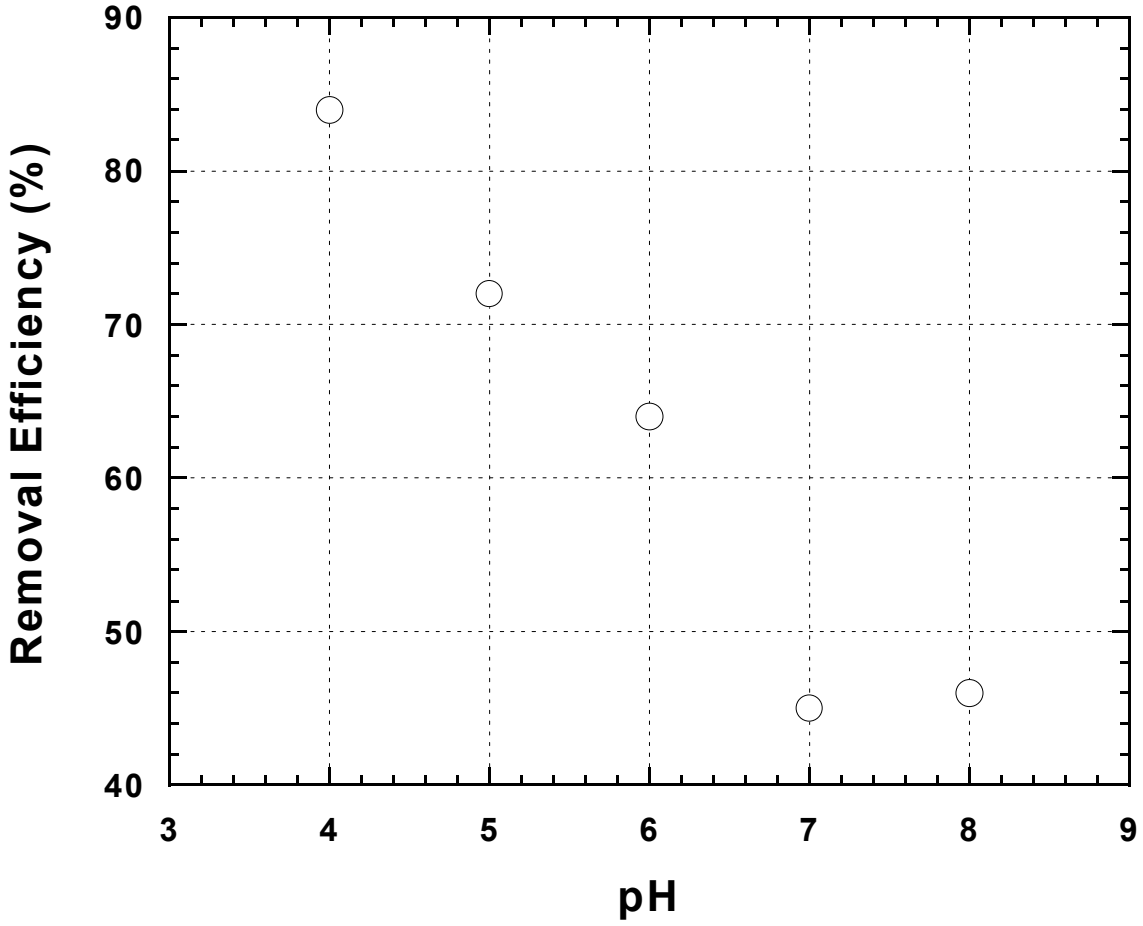

Figure 16. Effect of pH on the removal of colloidal particle. Experimental conditions: pumping speeding 15%(or filtration rate 0.46 mL/min); E = 96.8V/cm.

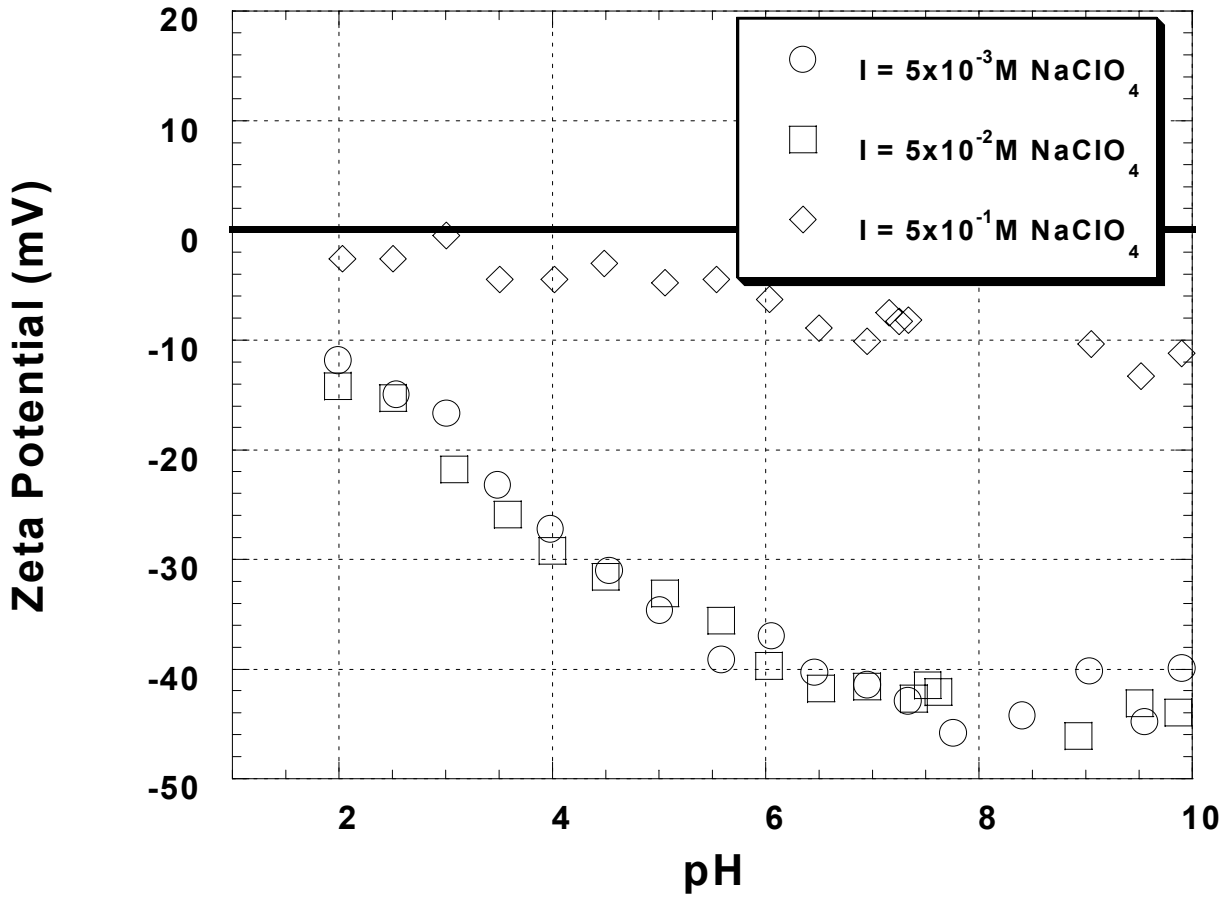

Figure 17. Zeta potential of naturally occurring particles as a function of pH (Well #10, bailing sample, 10IB01).

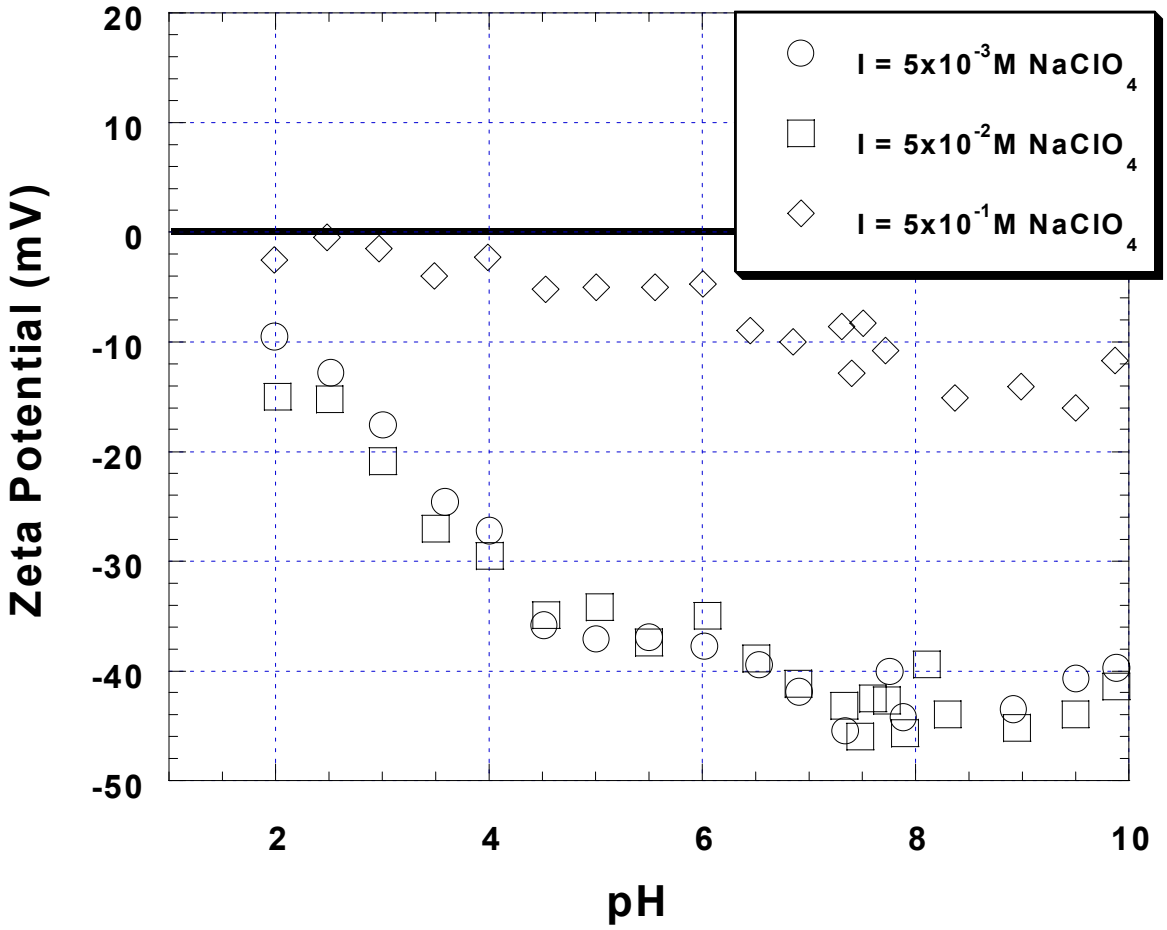

Figure 18. Zeta potential of naturally occurring particles as a function of pH (Well #10, low flow purging sample, 10IL01)

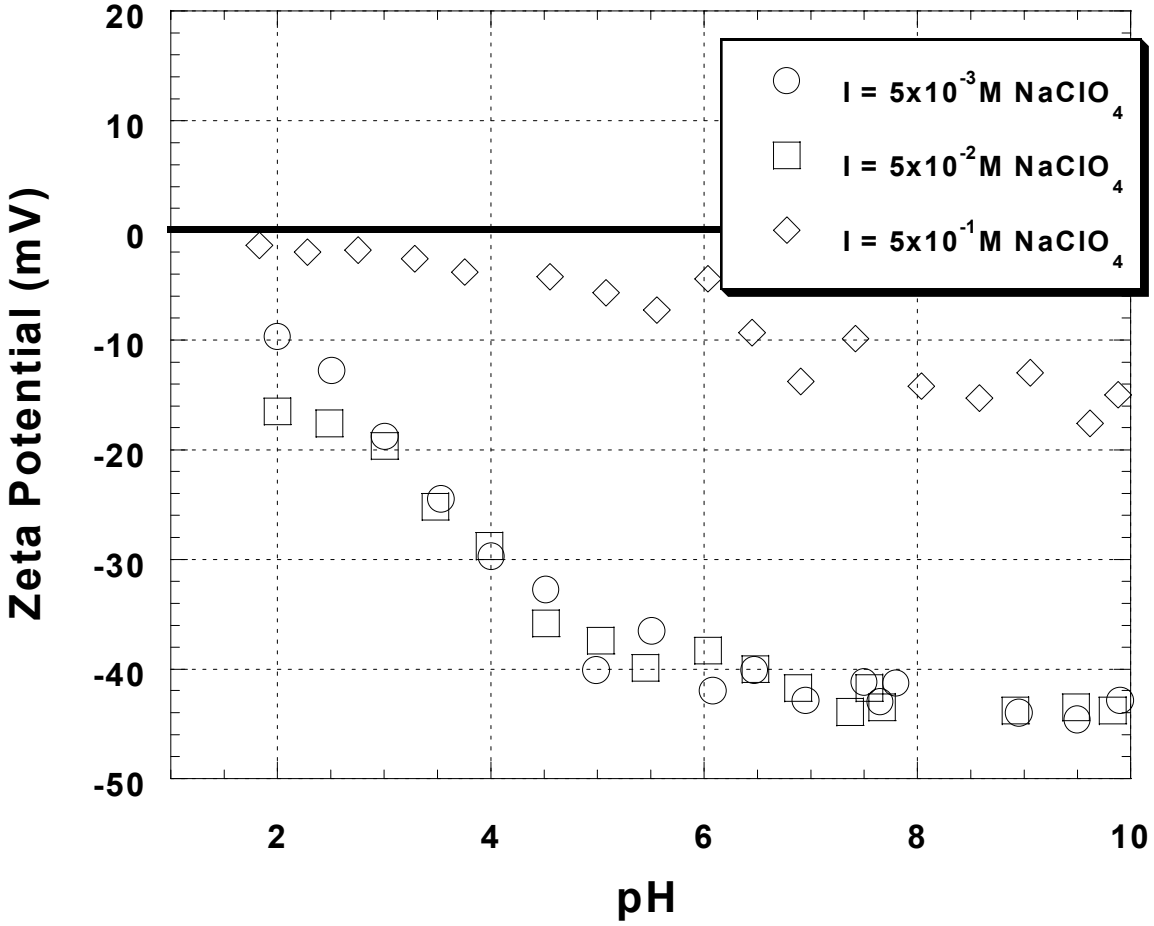

Figure 19. Zeta potential of naturally occurring particles as a function of pH (Well #5S, bailing sample, 5SIB01)

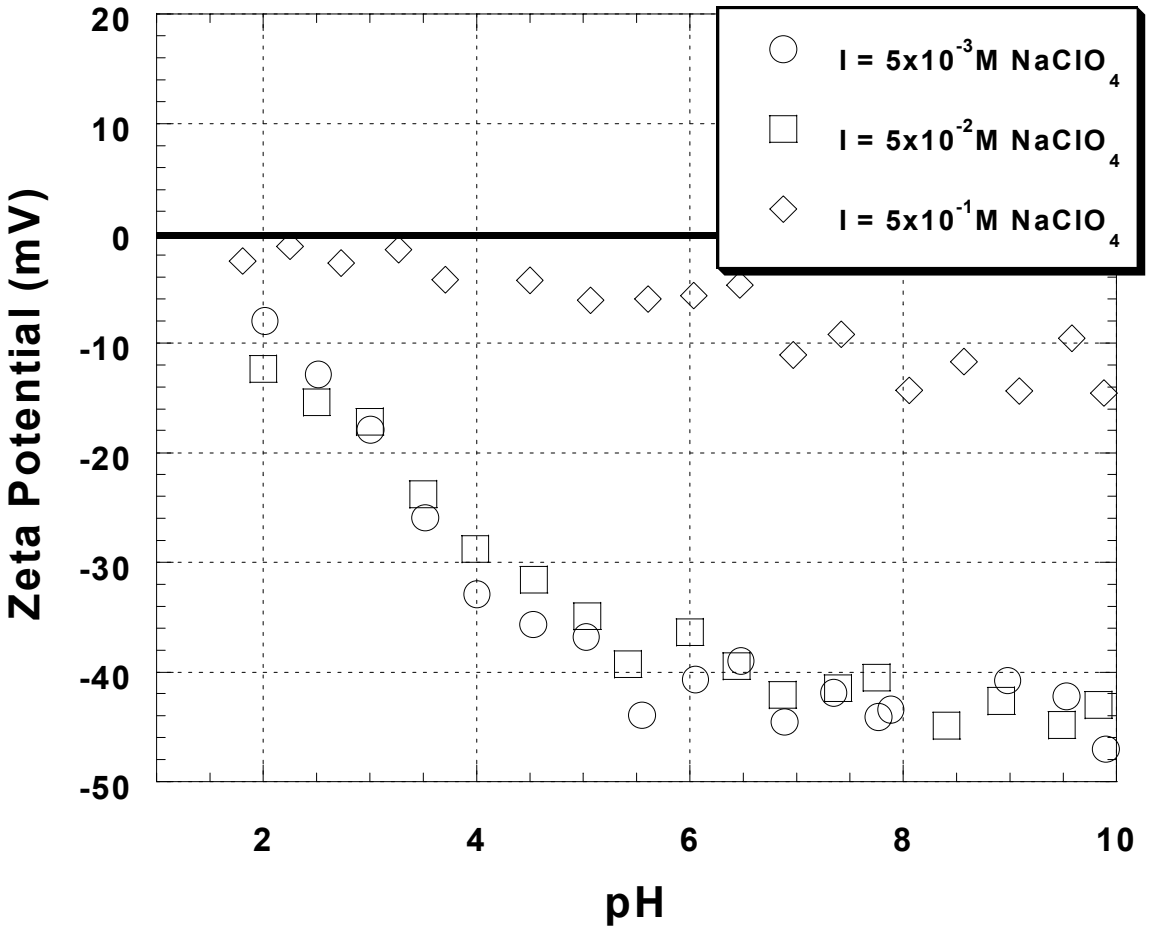

Figure 20. Zeta potential of naturally occurring particles as a function of pH (well #5S, low flow purging sample, 5SIL01).

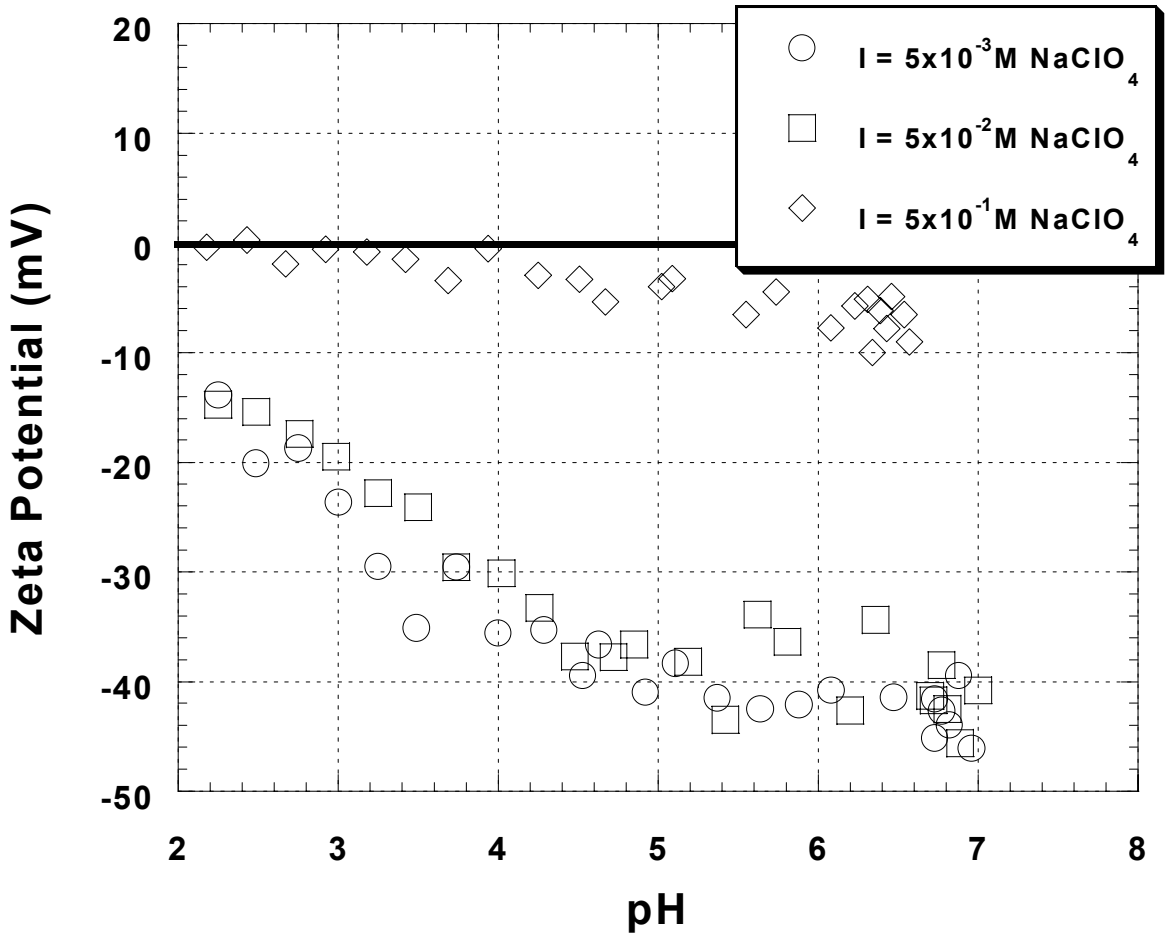

Figure 21. Zeta potential of naturally occurring particles as a function of pH (Well #5S, bailing sample, 5SIIB03).

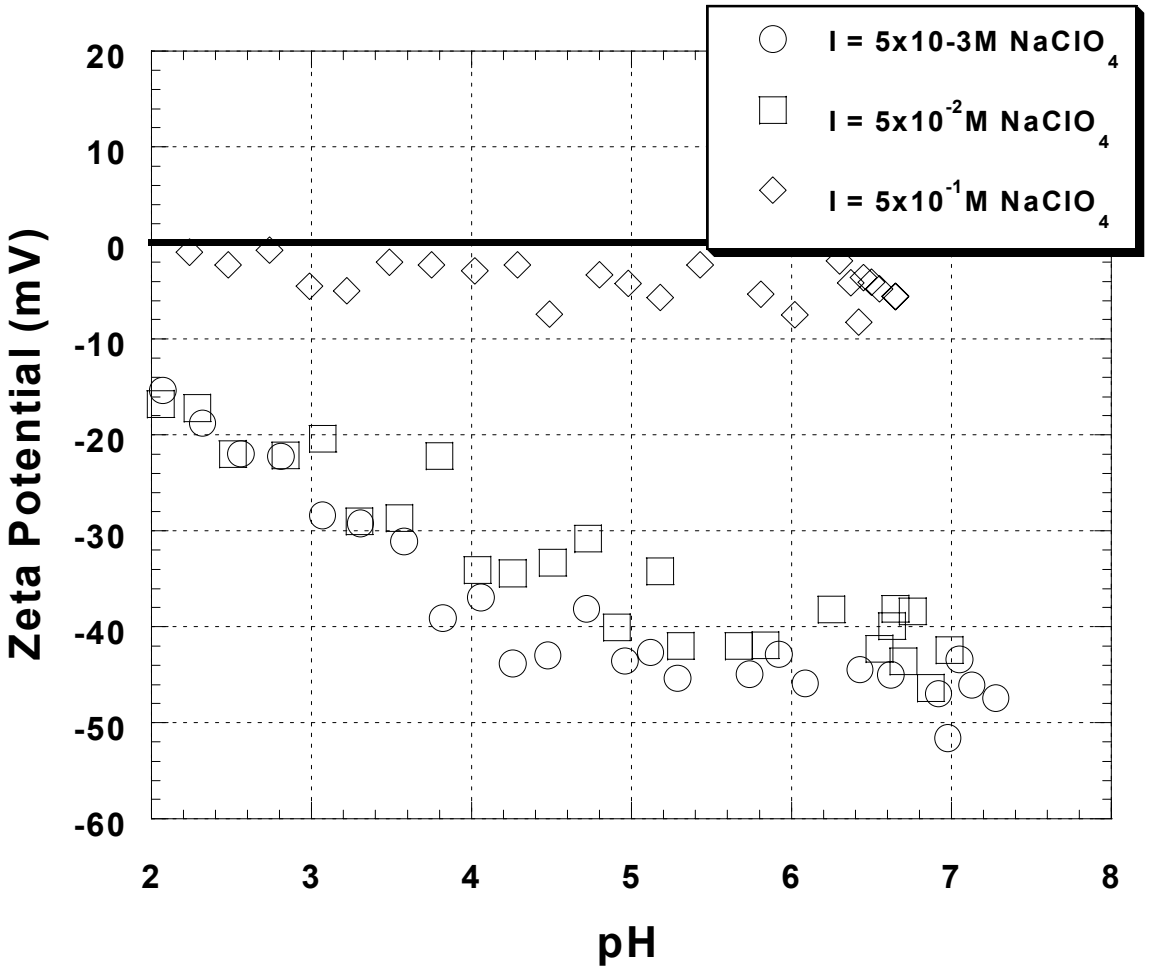

Figure 22. Zeta potential of naturally occurring particles as a function of pH (Well #5S, low flow purging sample, 5SIIL01).

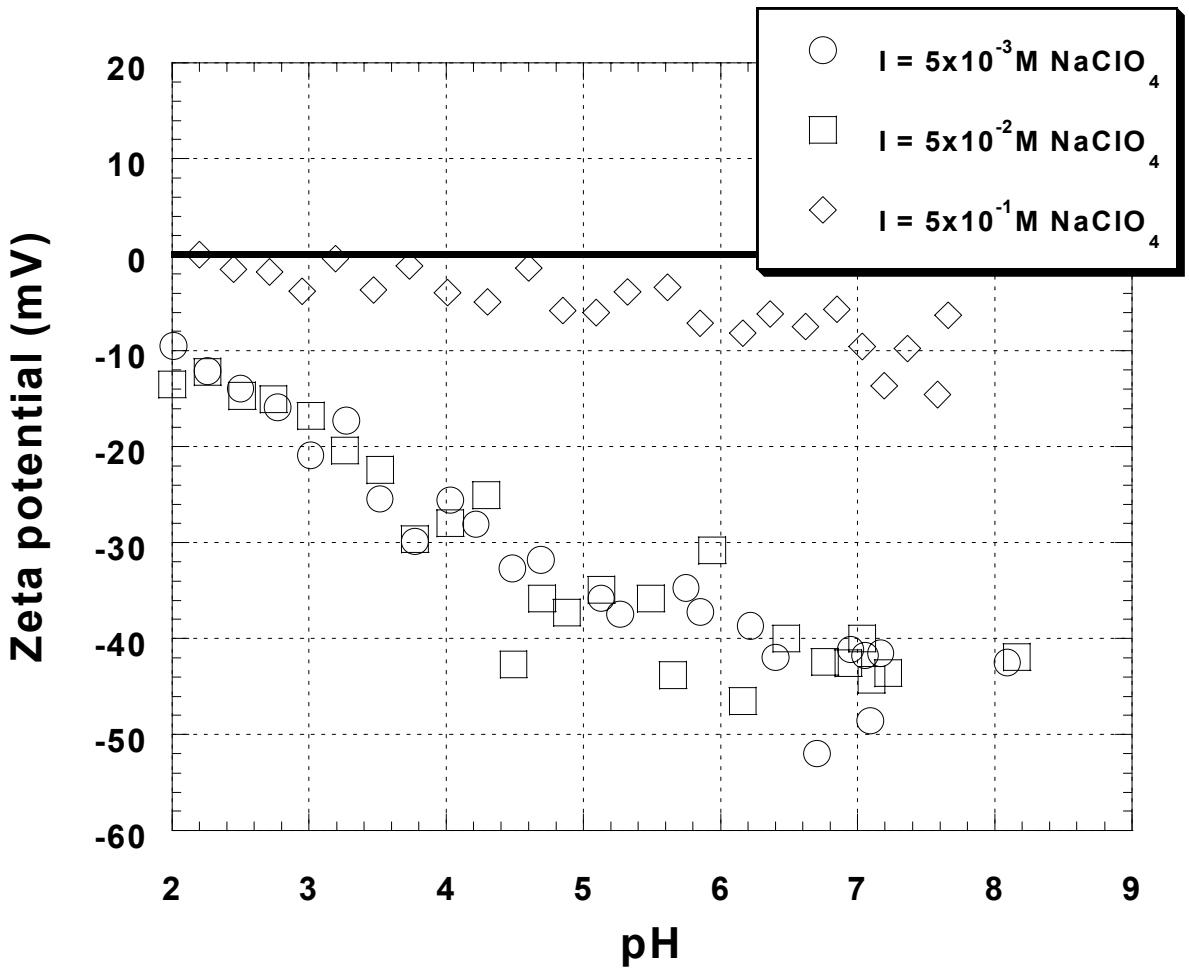

Figure 23. Zeta potential of naturally occurring particles as a function of pH (Well #MW3, bailing sample, MW3IB03).

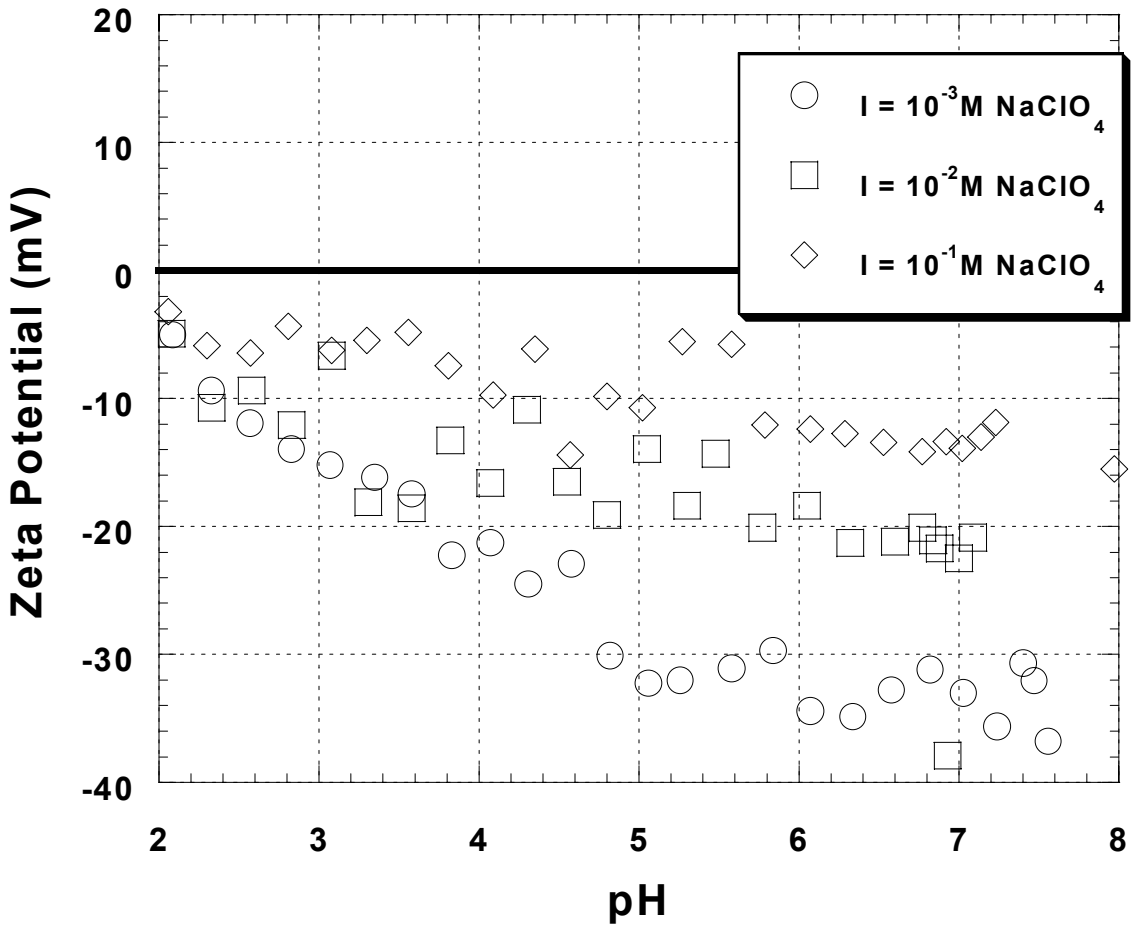

Figure 24. Zeta potential of naturally occurring particles as a function of pH (Well #MW3, low flow purging sample, MW3IL01).

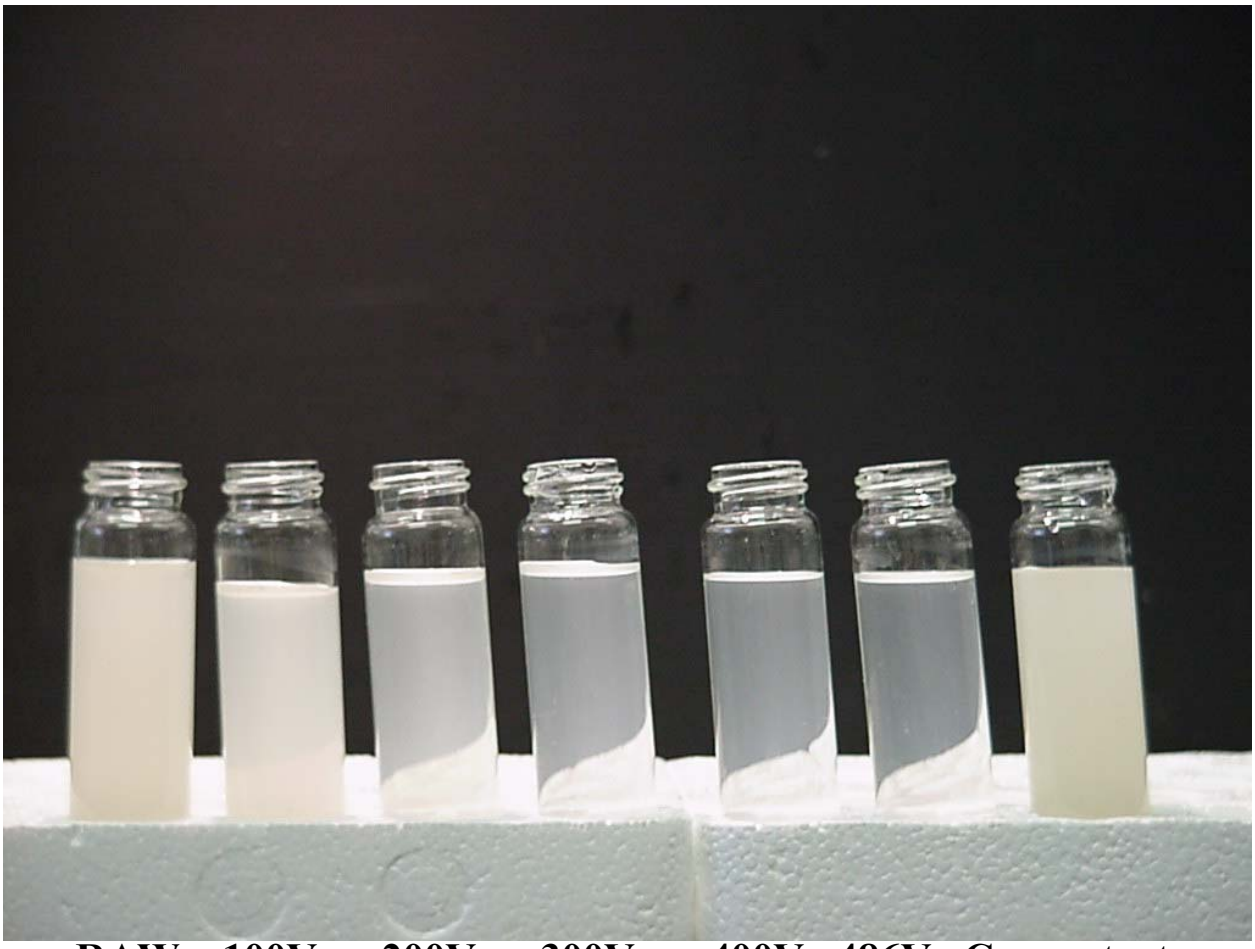

Figure 25. Visual comparison of water sample on the various electrostatic field (Well#5S, low flow purging sample)

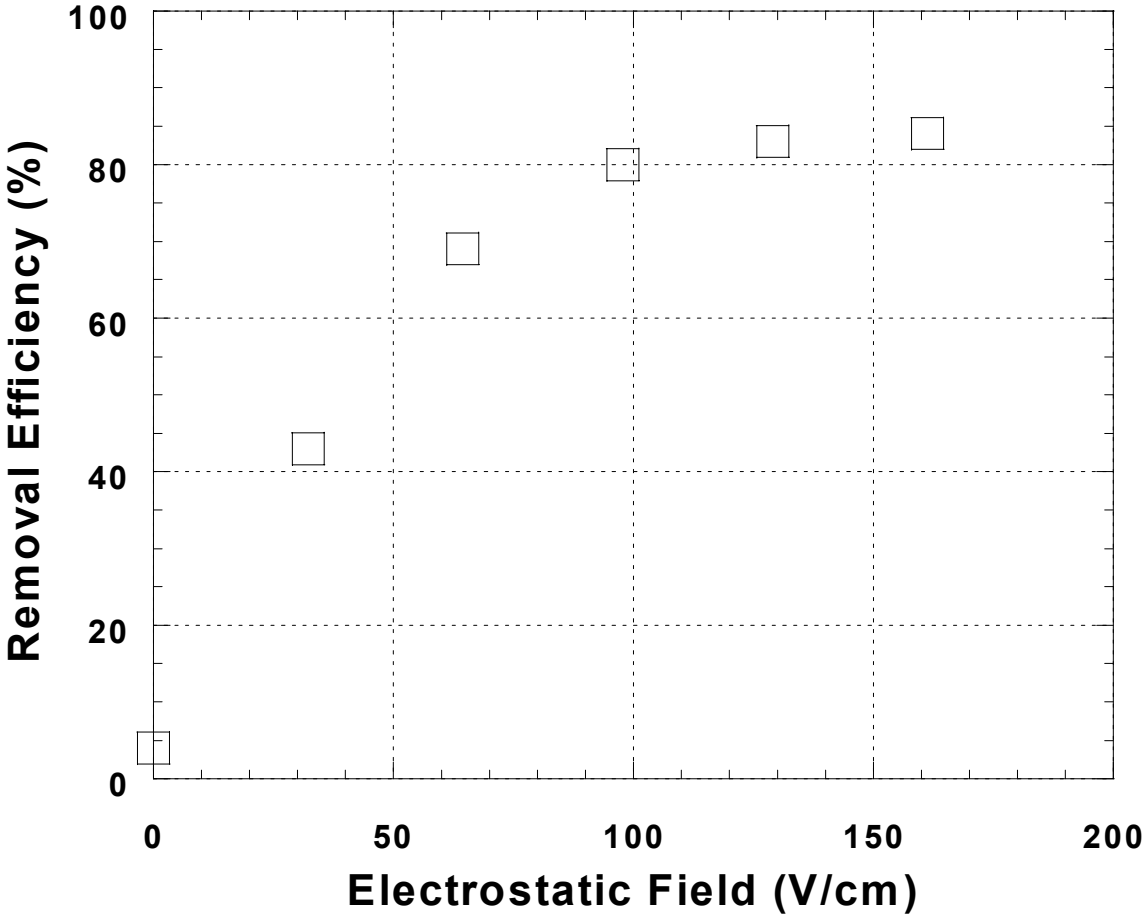

Figure 26. Change of filtrate turbidity as a function of time under various electrostatic fields values (I). Experimental condition: pH = 6.5; Sample = 10IB01.

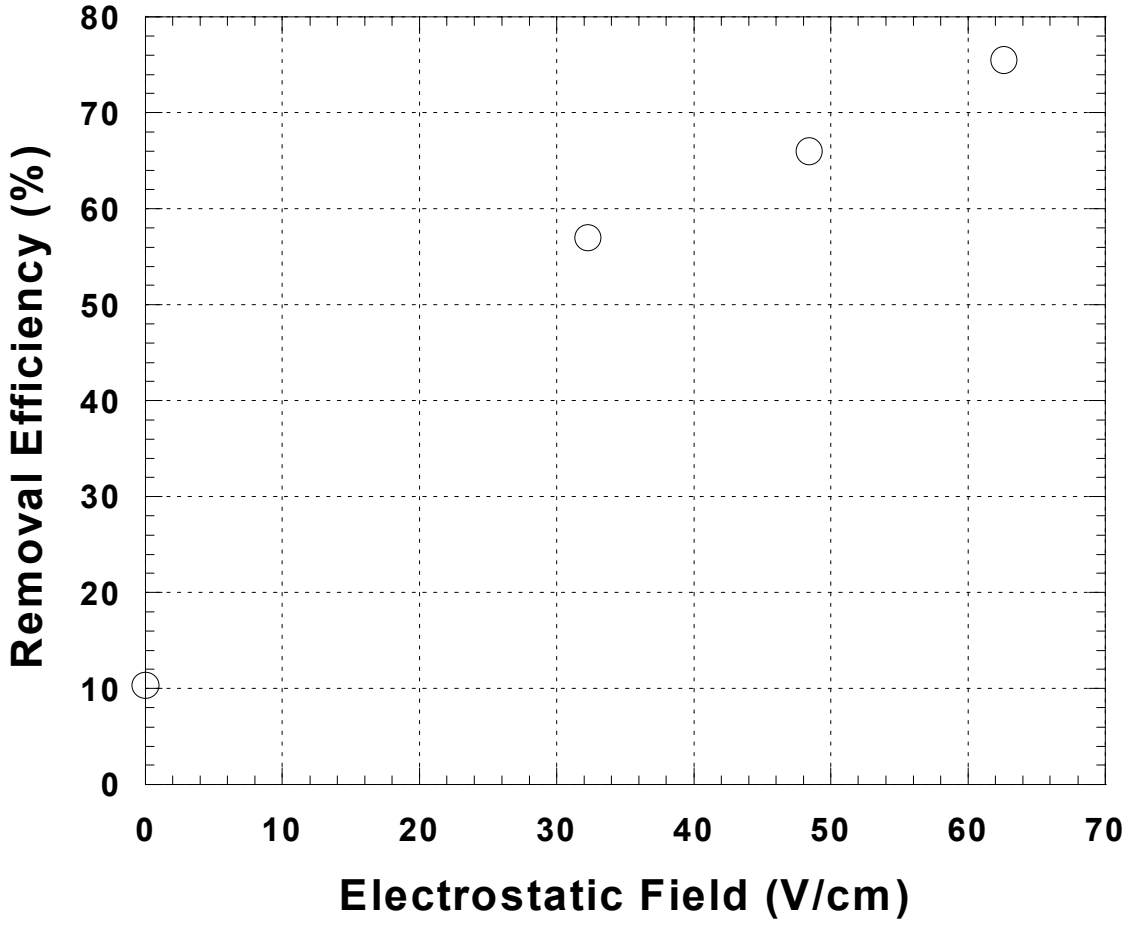

Figure 27. Change of filtrate turbidity as a function of time under various electrostatic field values. Experimental condition: pH = 6.5; Sample = 10IB01.

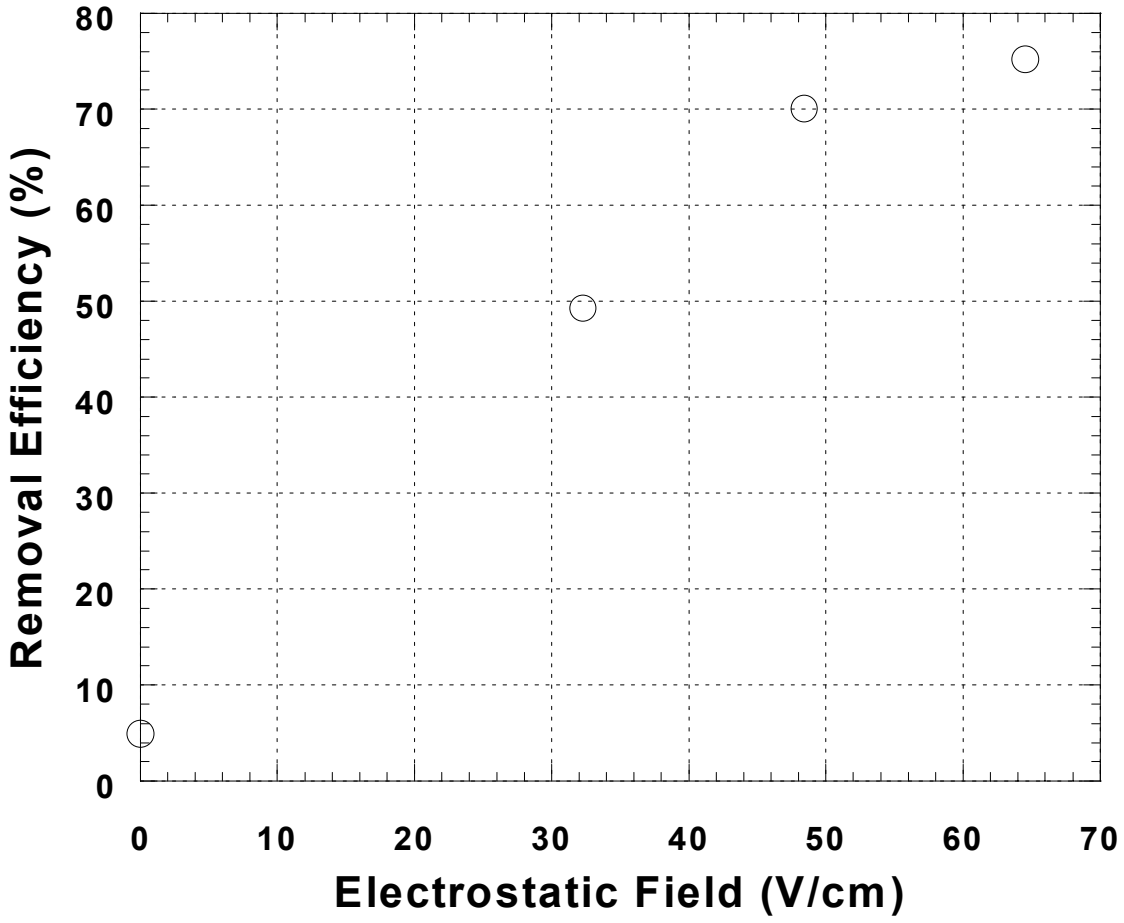

Figure 29. Removal efficiency as a function of time at various electrostatic field values. Experimental condition: pH = 5; Sample = 10IL01.

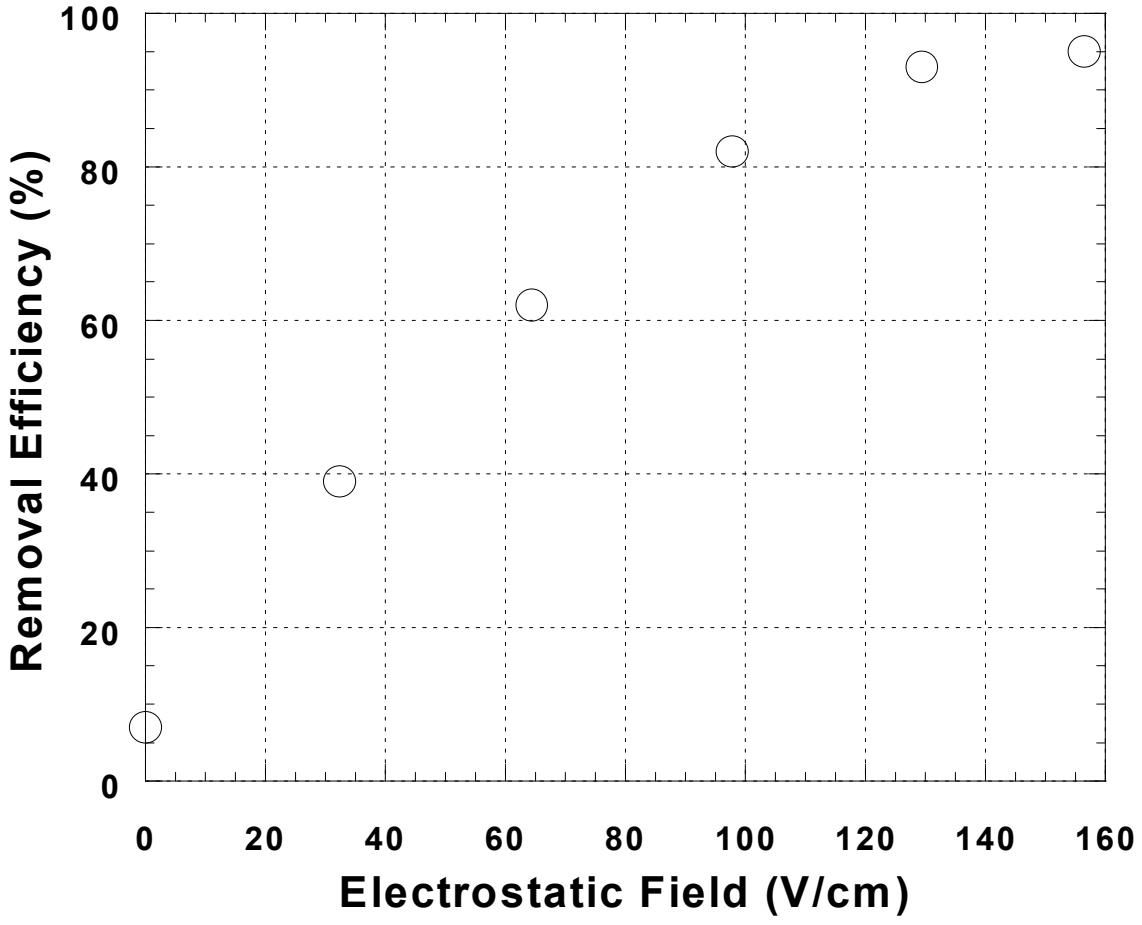

Figure 29. Removal efficiency as a function of time at various electrostatic field values (II). Experimental condition: pH = 6.6; Sample = 5SIIB03.

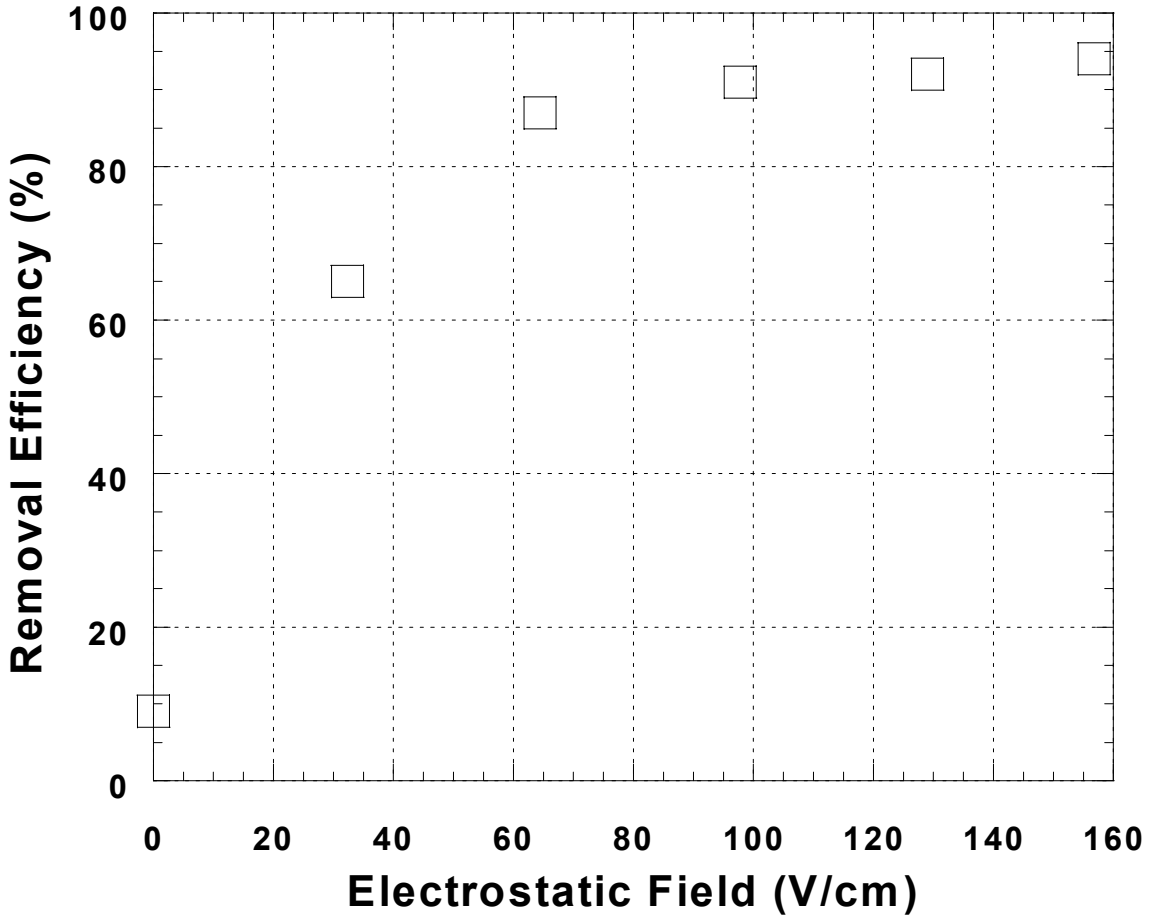

Figure 30. Removal efficiency as a function of time at various electrostatic field values.
Experimental condition: pH = 6.7; Sample = 5SIL02.

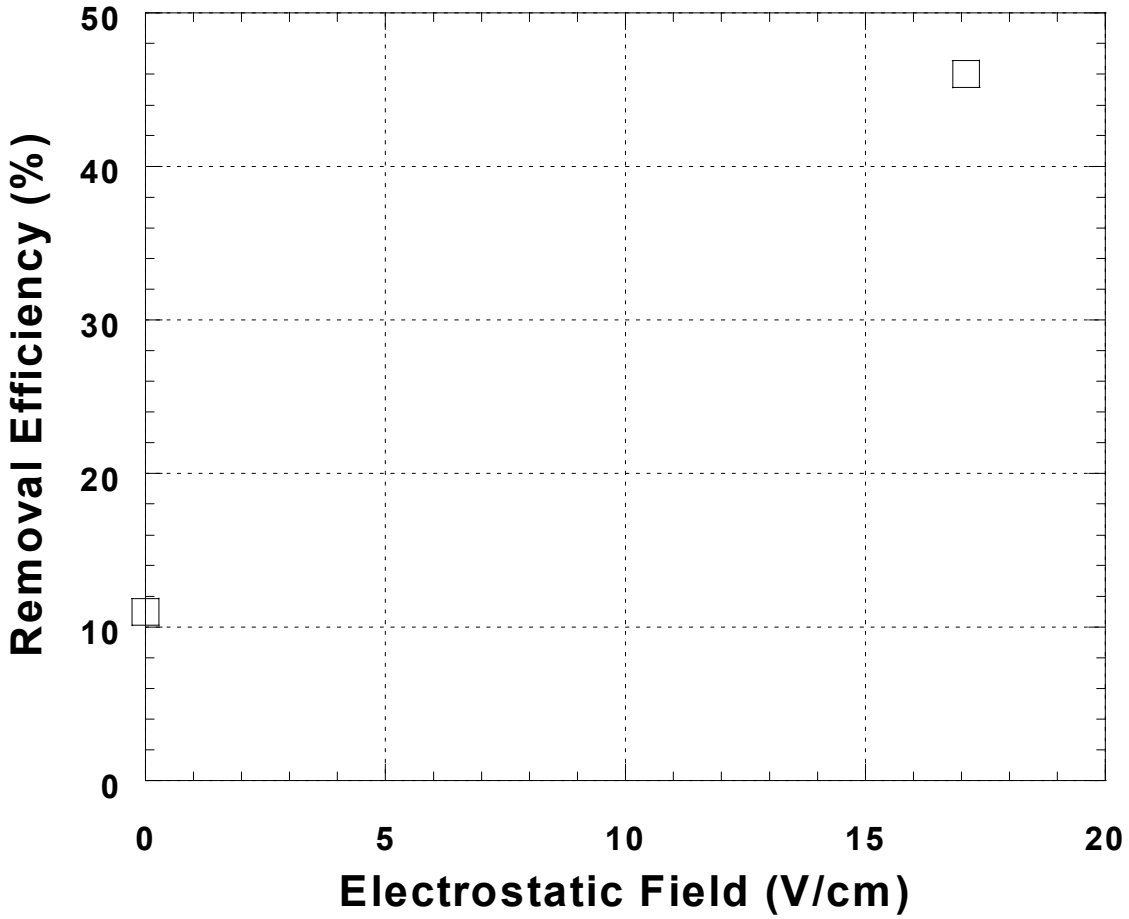

Figure 31. Removal efficiency as a function of time at various electrostatic field values. Experimental condition: pH = 7.9; Sample = MW3IB02.

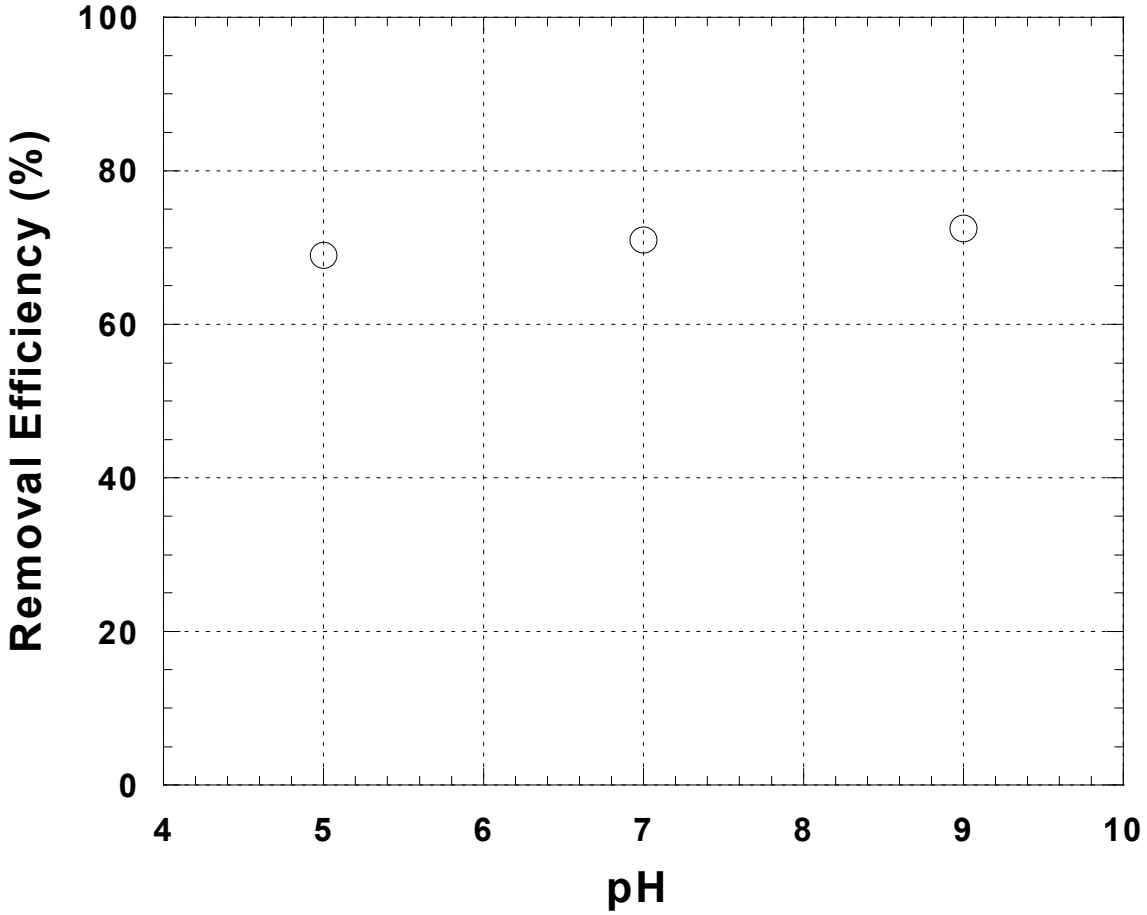

Figure 32. Steady state removal efficiency as a function of pH. Experimental conditions: pH = 5 (electrostatic field = 32.3V/cm); pH = 7 (electrostatic field = 48.4V/cm); pH = 9 (electrostatic field = 48.4V/cm); Sample = 10IB01.

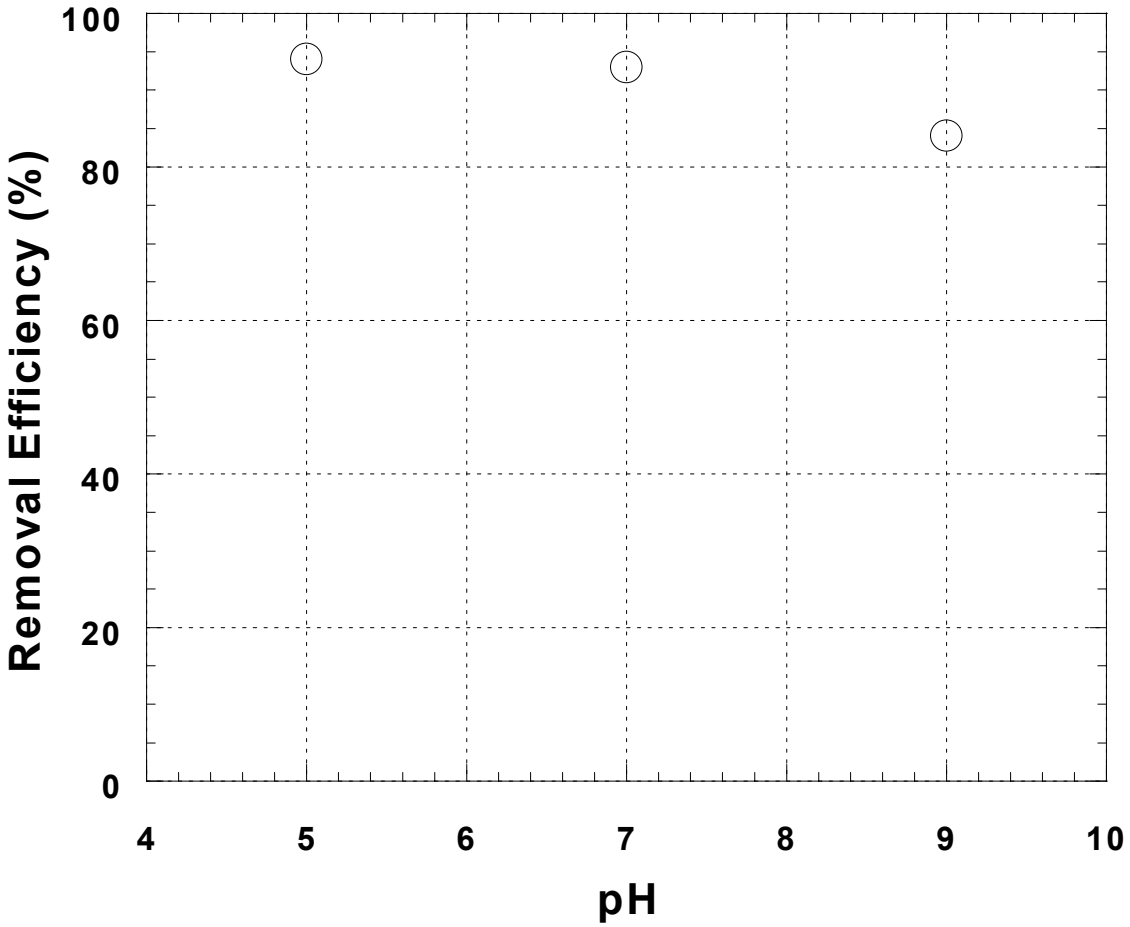

Figure 33. Steady state removal efficiency as a function of pH. Experimental condition: electrostatic field = 97.8V /cm; Sample = 5SIIB03.

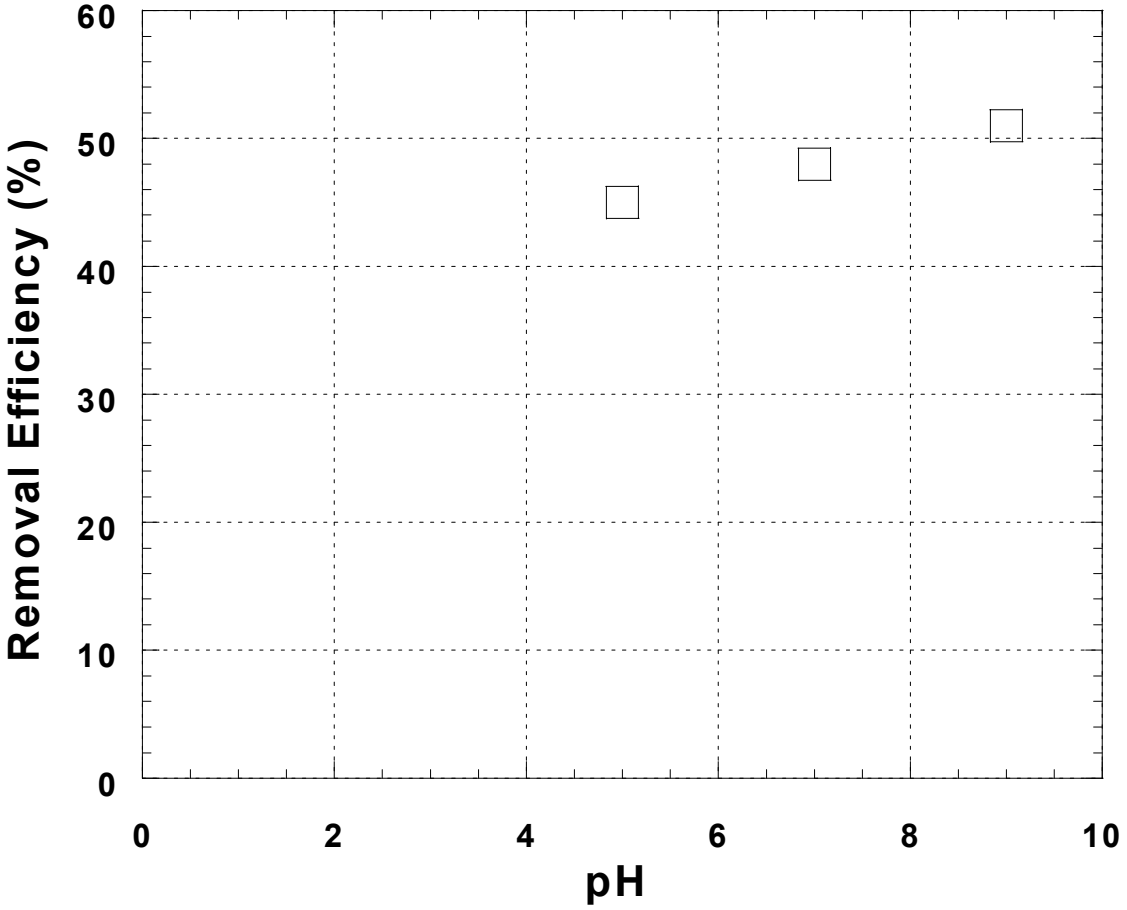

Figure 34. Steady state removal efficiency as a function of pH. Experimental conditions: pH = 5 (electrostatic field=10.3V/cm); pH = 7 (electrostatic field=13.2V/cm); pH = 9 (electrostatic field=14.8V/cm); Sample = MW3B02.

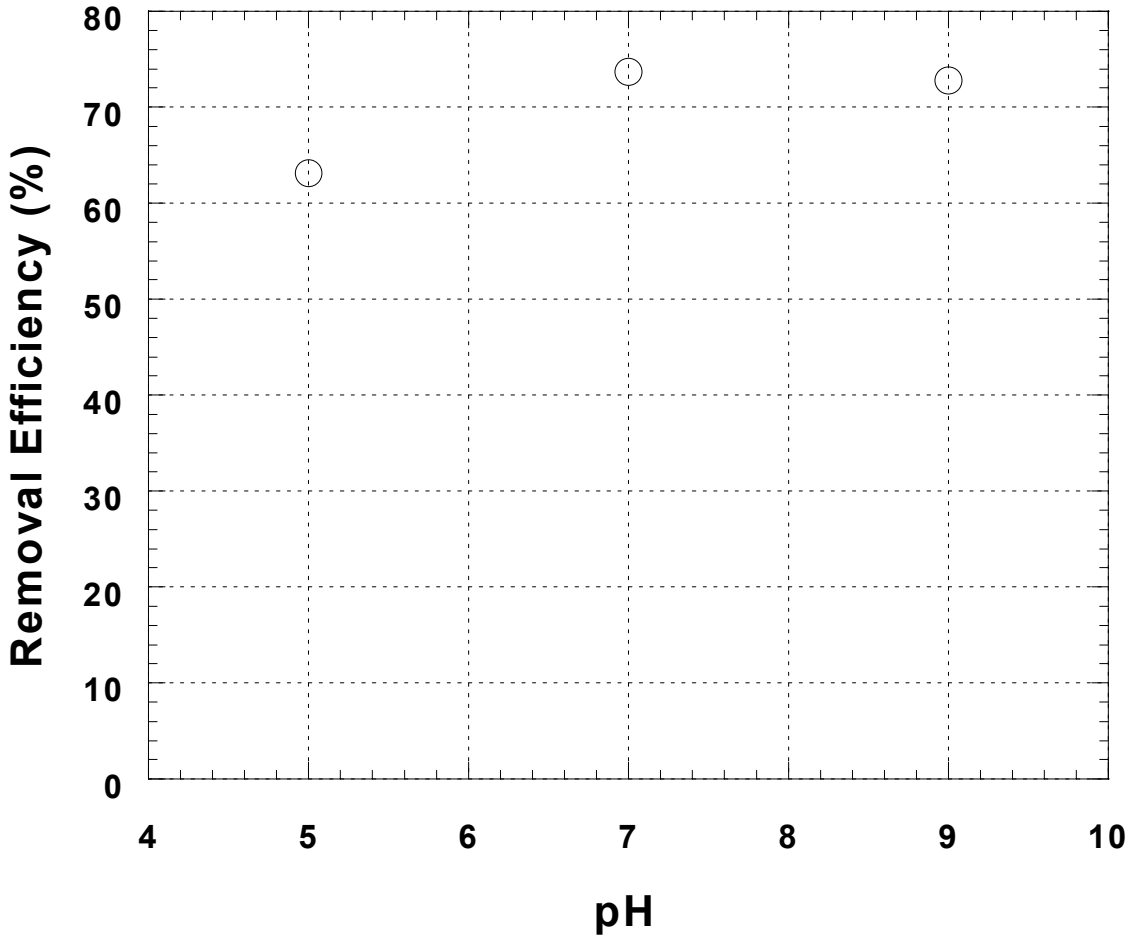

Figure 35. Steady state removal efficiency as a function of pH. Experimental conditions: pH = 5 (electrostatic field=32.3V/cm); pH = 7 (electrostatic field=48.4V/cm); pH = 9 (electrostatic field=48.4V/cm); Sample = 10IL01.

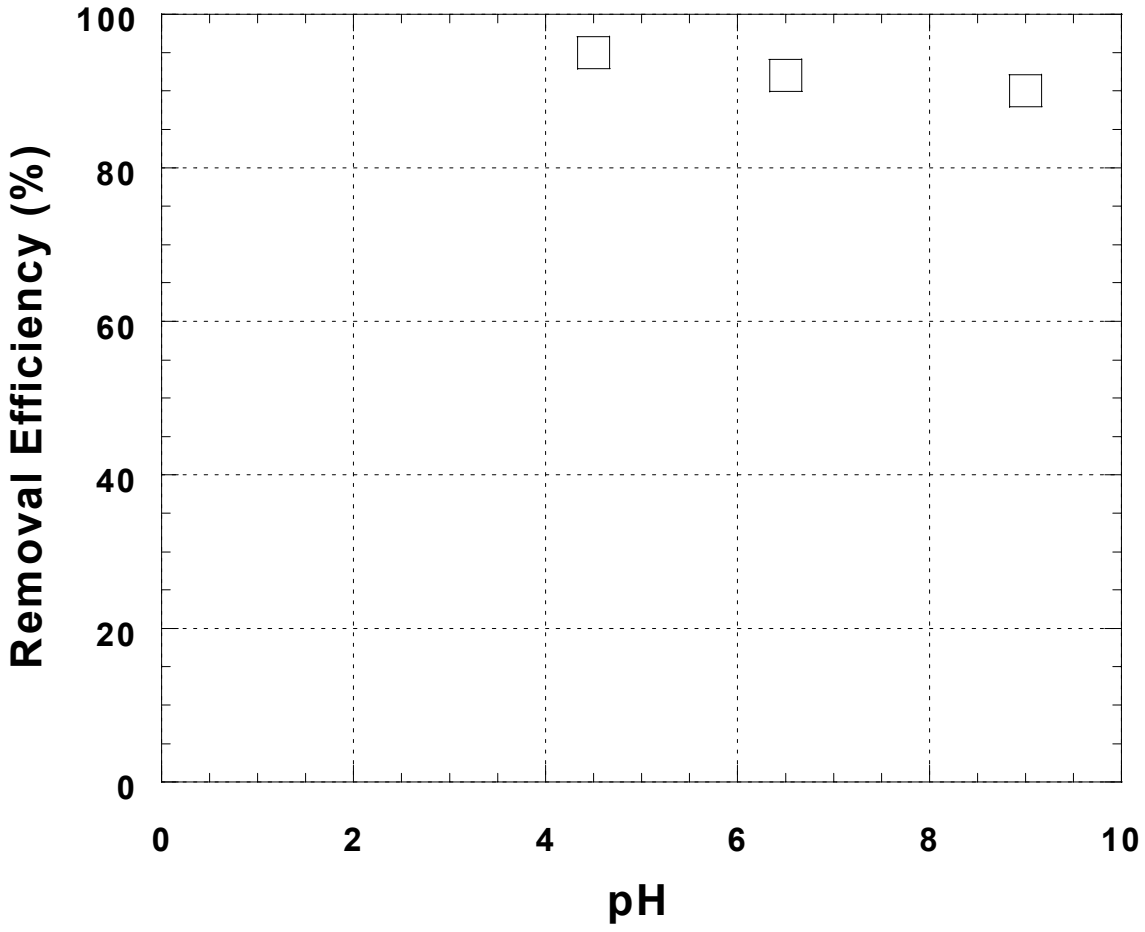

Figure 36. Steady state removal efficiency as a function of pH (I). Experimental condition (electrostatic field = 97.8 V/cm); Sample = 5SIL02.

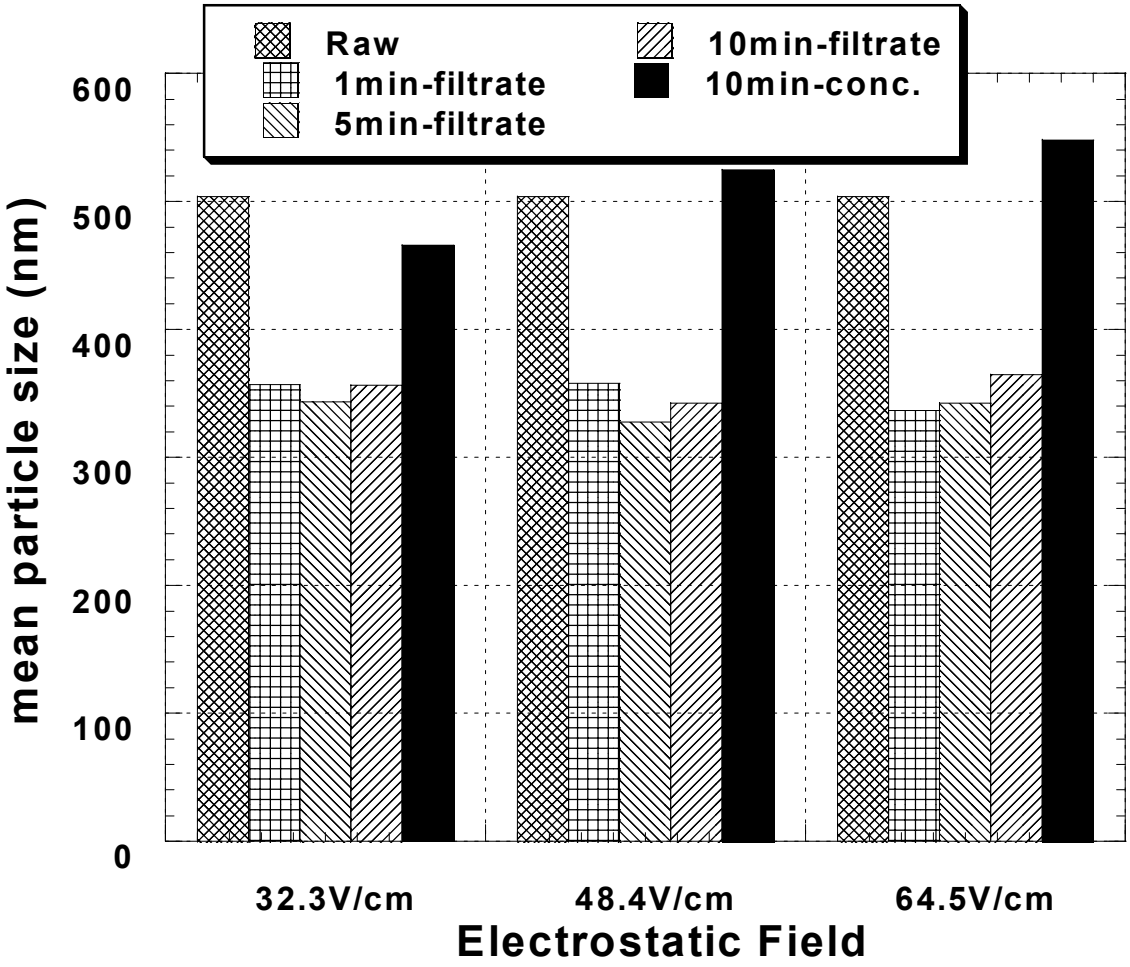

Figure 37. Distribution of particle size as affected by electrostatic field. Experimental condition: pH = 6.5; Sample = 10IB01.

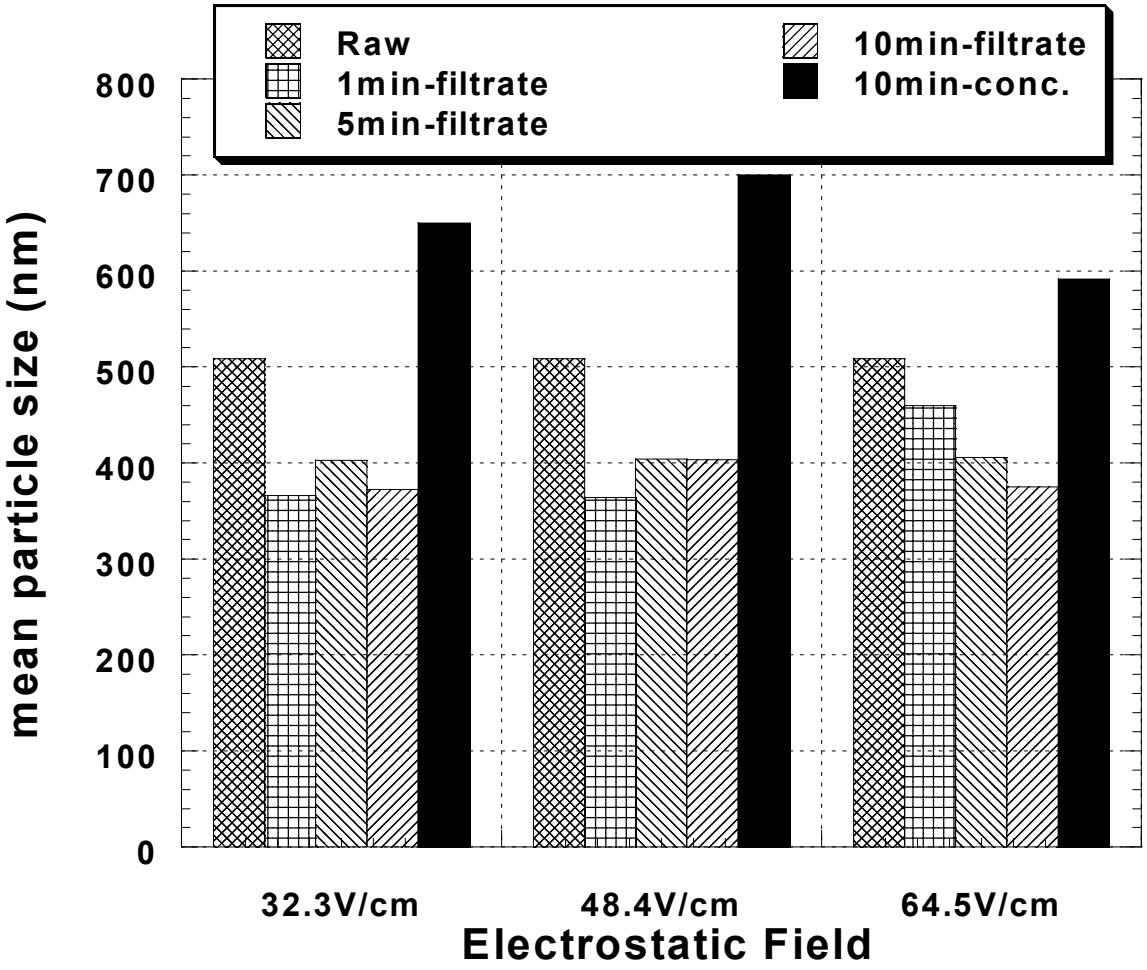

Figure 38. Distribution of particle size as affected by electrostatic field. Experimental condition: pH = 6.5; Sample = 10IL01.

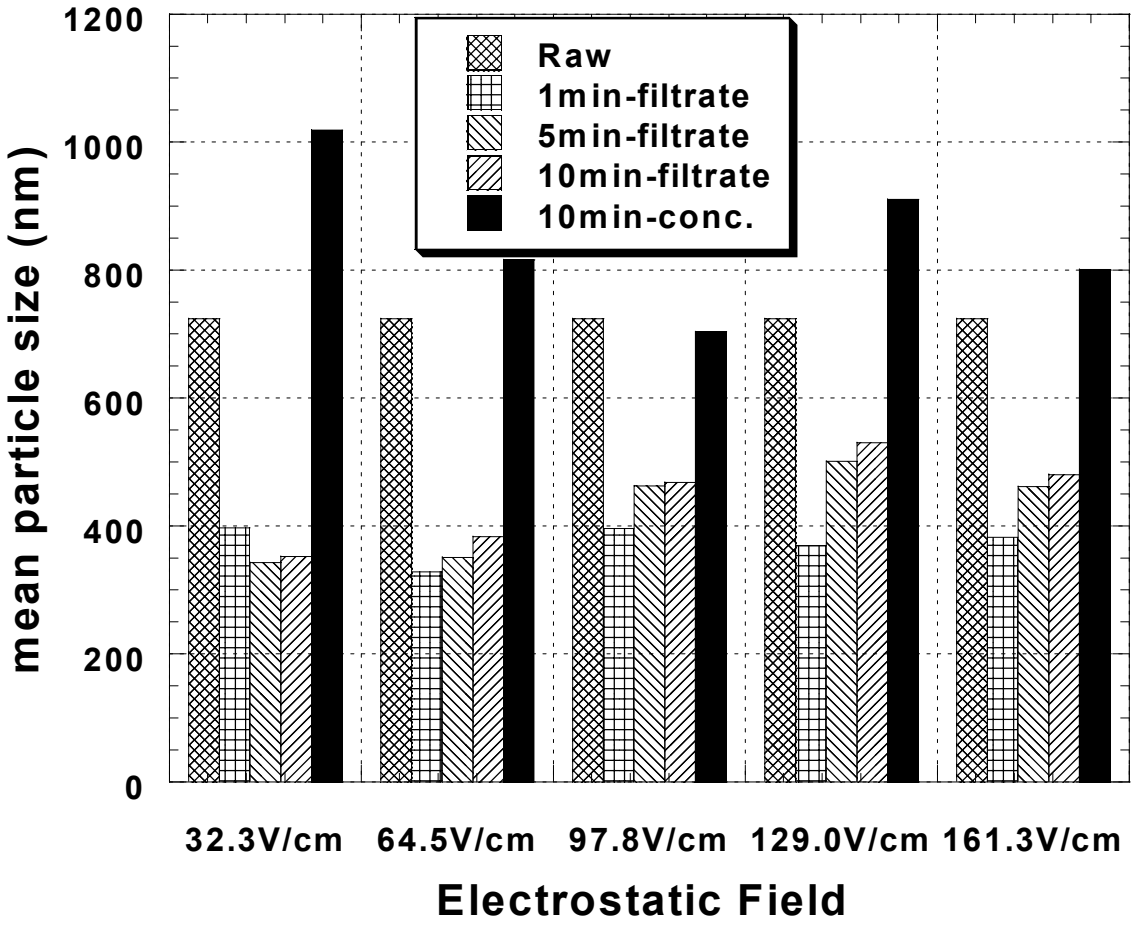

Figure 39. Distribution of particle as affected by electrostatic field. Experimental condition: pH = 6.6; Sample = 5SIIB03.

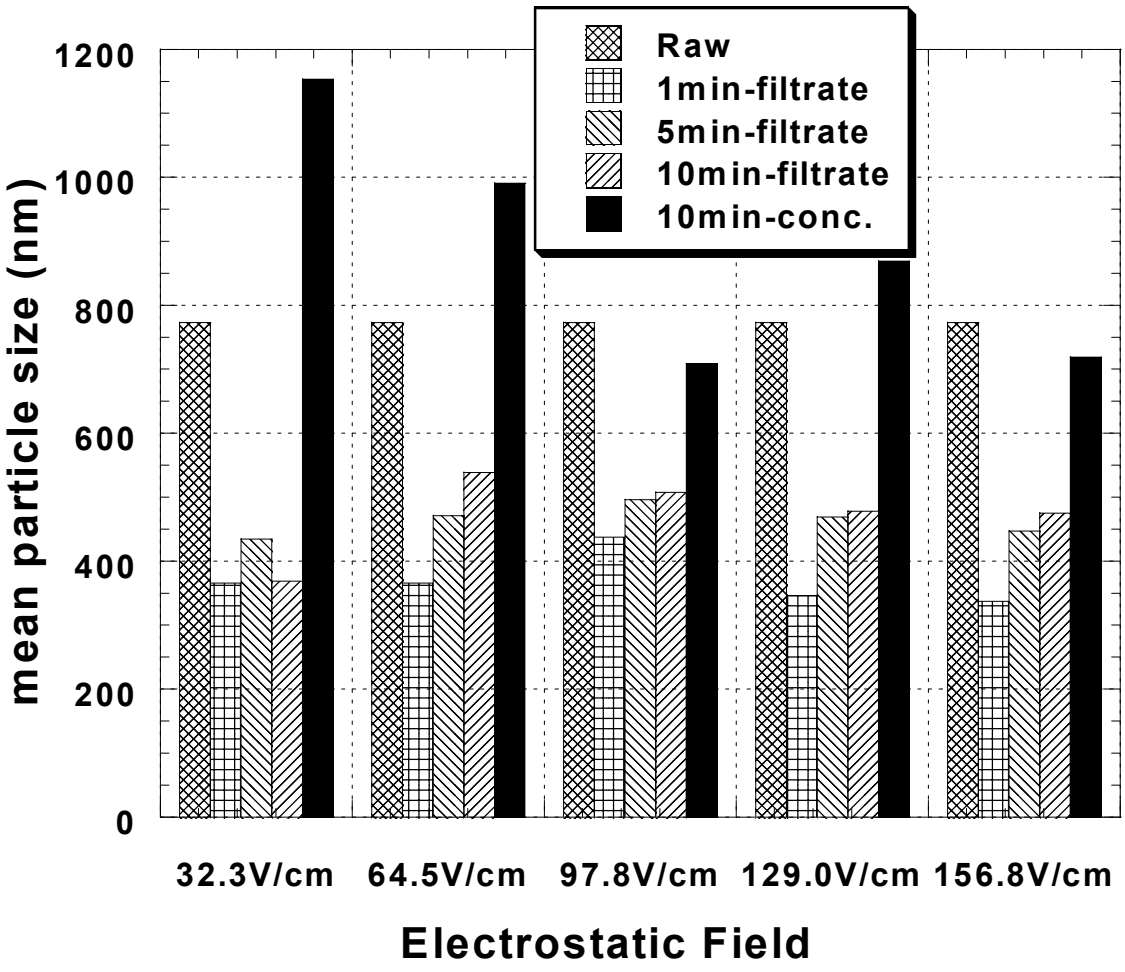

Figure 40. Distribution of particle size as affected by electrostatic field. Experimental condition: pH = 6.7; Sample = 5SIIL02.

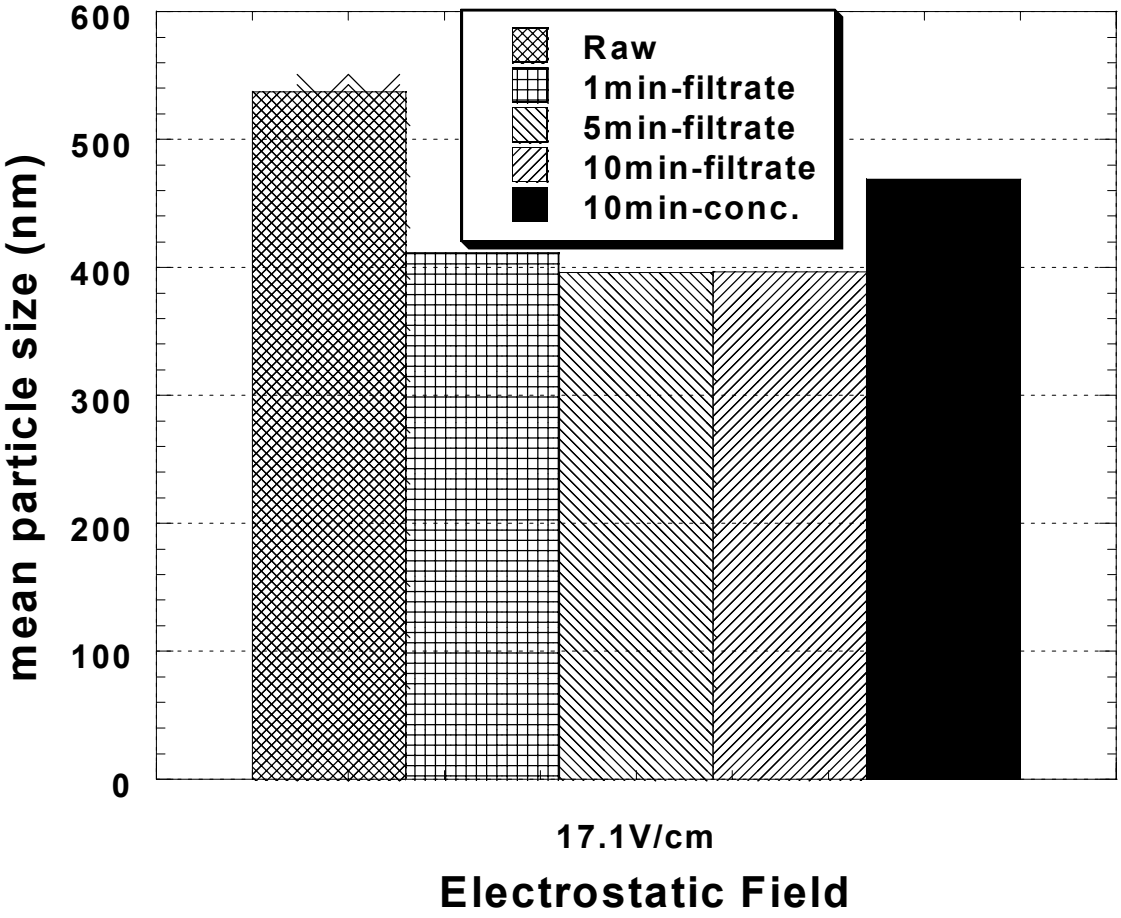

Figure 41. Distribution of particle size as affected by electrostatic field. Experimental condition: pH = 7.9; Sample = MW3IB01.

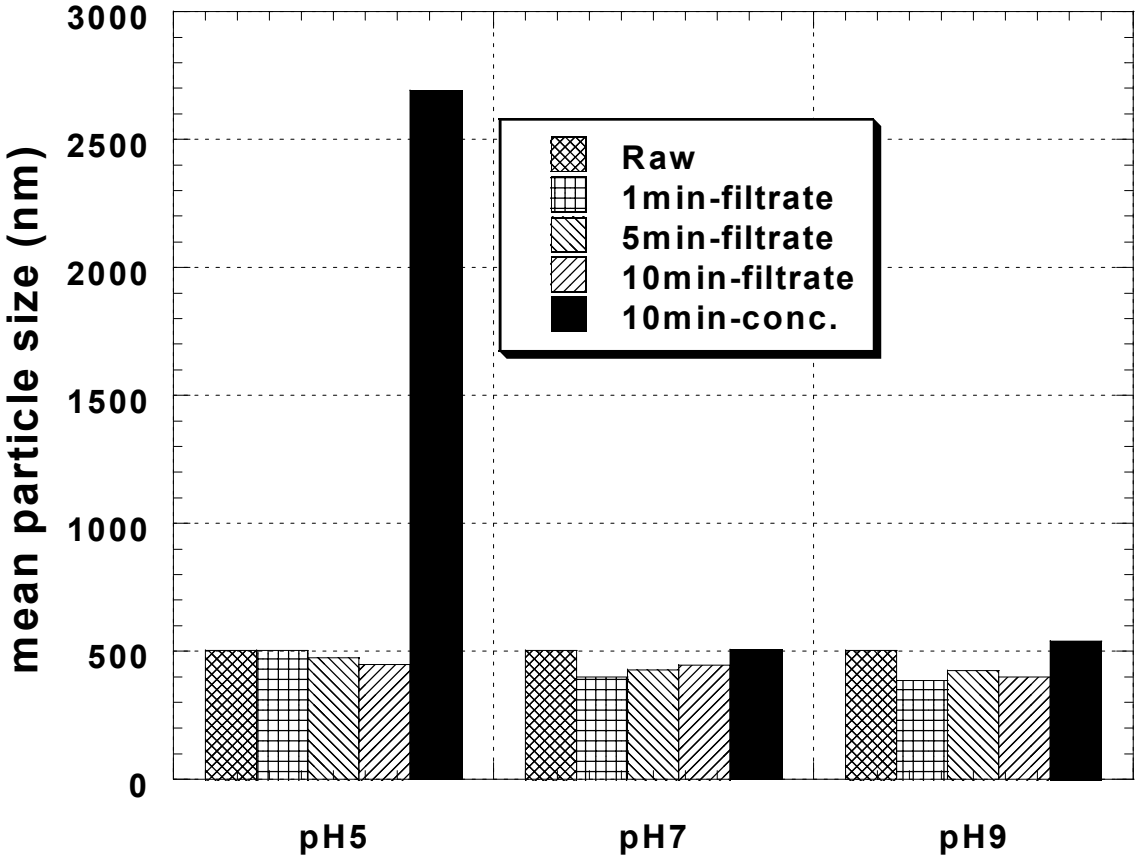

Figure 42. Distribution of particle size as affected by pH. Experimental conditions: pH = 5 (electrostatic field=32.3V/cm); pH = 7 (electrostatic field=48.4V/cm); pH = 9 (electrostatic field=48.4V/cm); Sample = 10IB01.

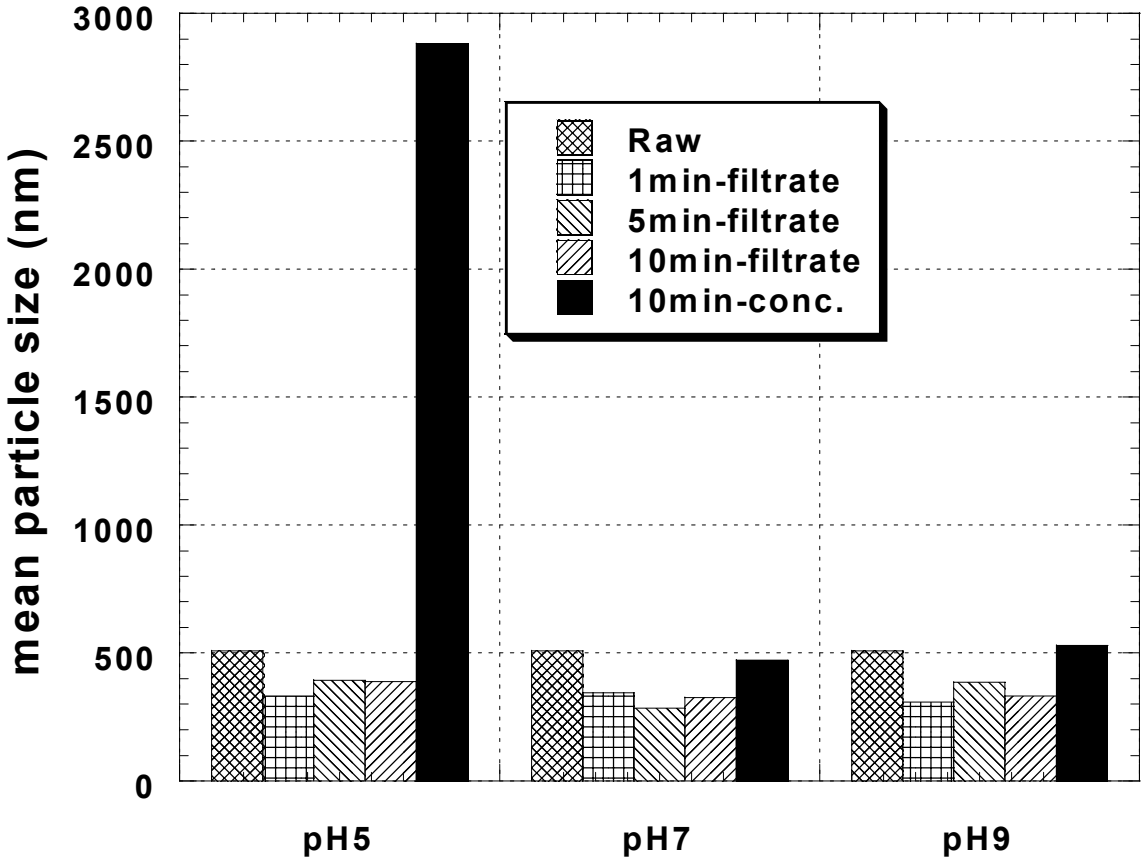

Figure 43. Distribution of particle size as affected by pH. Experimental conditions: pH = 5 (electrostatic field = 32.3 V/cm); pH = 7 (electrostatic field = 48.4 V/cm); pH = 9 (electrostatic field = 48.4 V/cm); Sample = 10IL01.

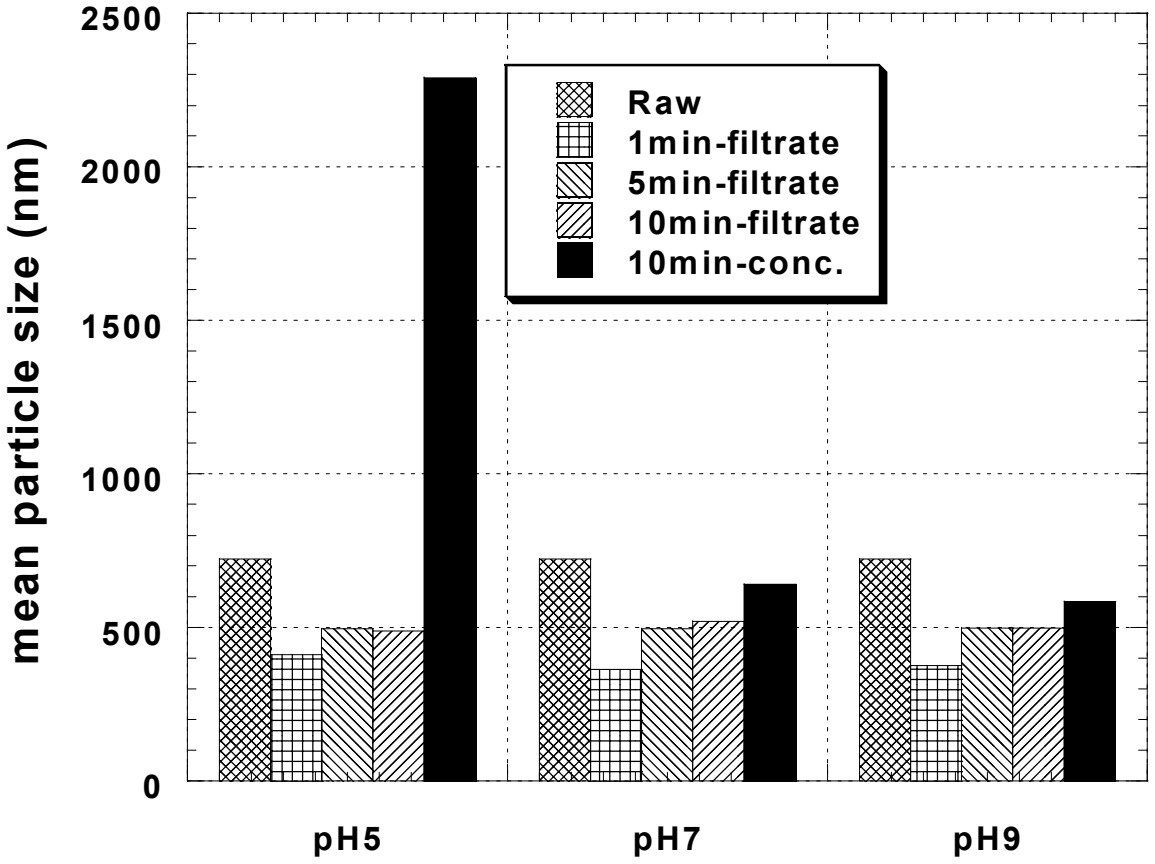

Figure 44. Distribution of particle size as affected by pH. Experimental conditions: electrostatic field = 97.8 V/cm; Sample = 5SIIB03.

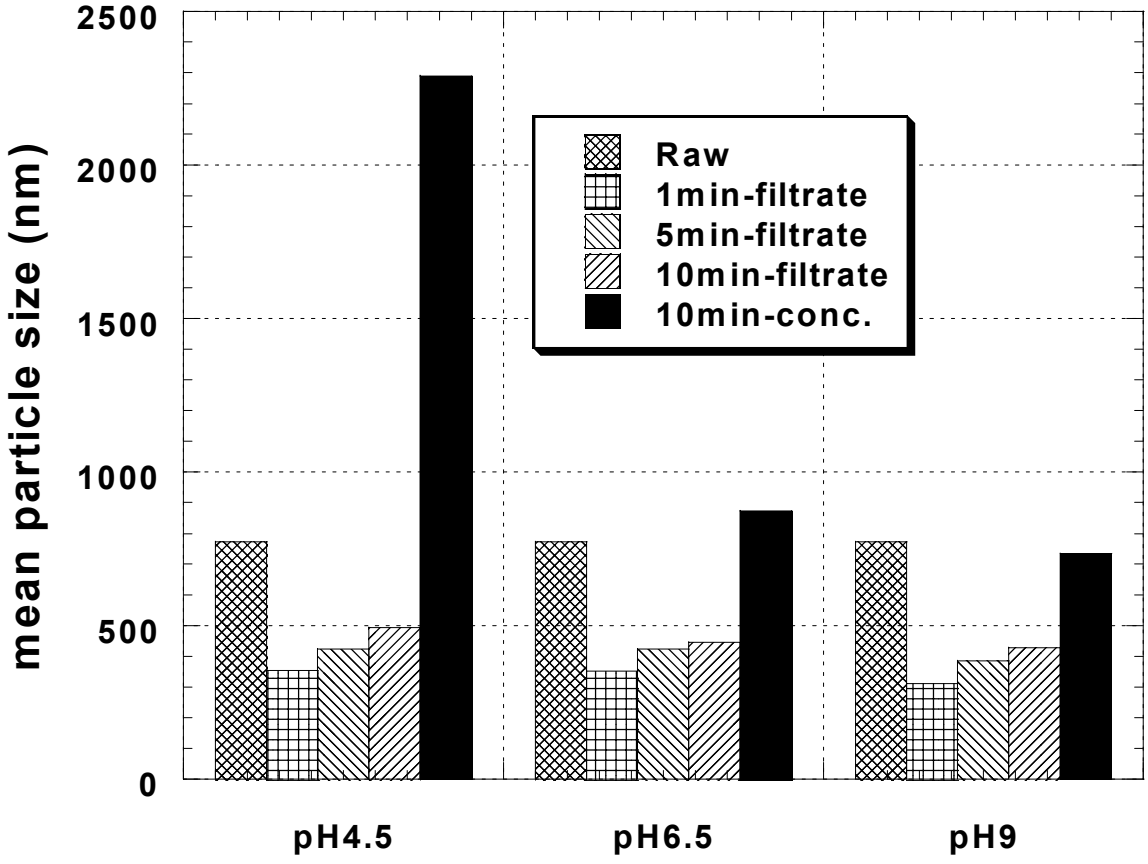

Figure 45. Distribution of particle size as affected by pH. Experimental condition: electrostatic field = 97.8 V/cm; Sample = 5SIIL02.

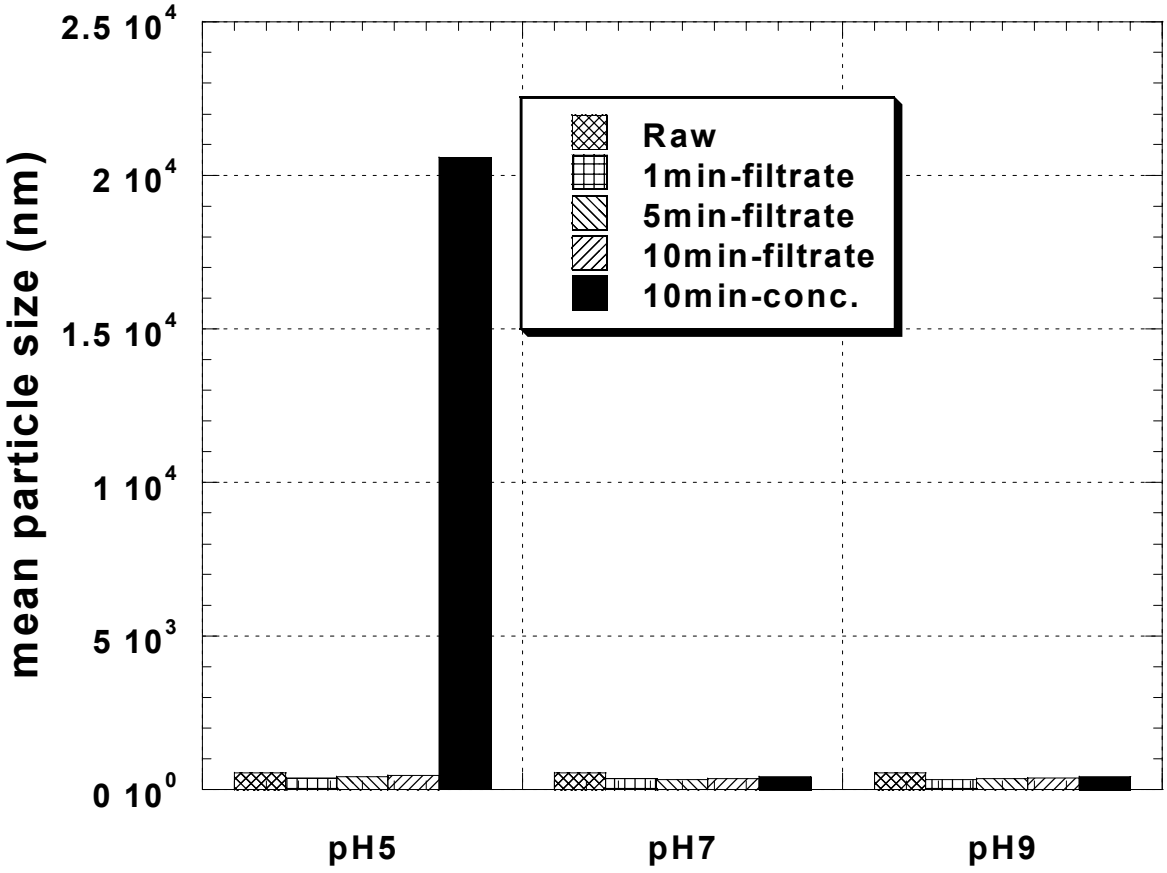

Figure 46. Distribution of particle size as affected by pH. Experimental conditions: pH = 5 (electrostatic field = 10.3 V/cm); pH = 7 (electrostatic field = 13.2 V/cm); pH = 9 (electrostatic field = 14.8 V/cm); Sample = MW3IB01.

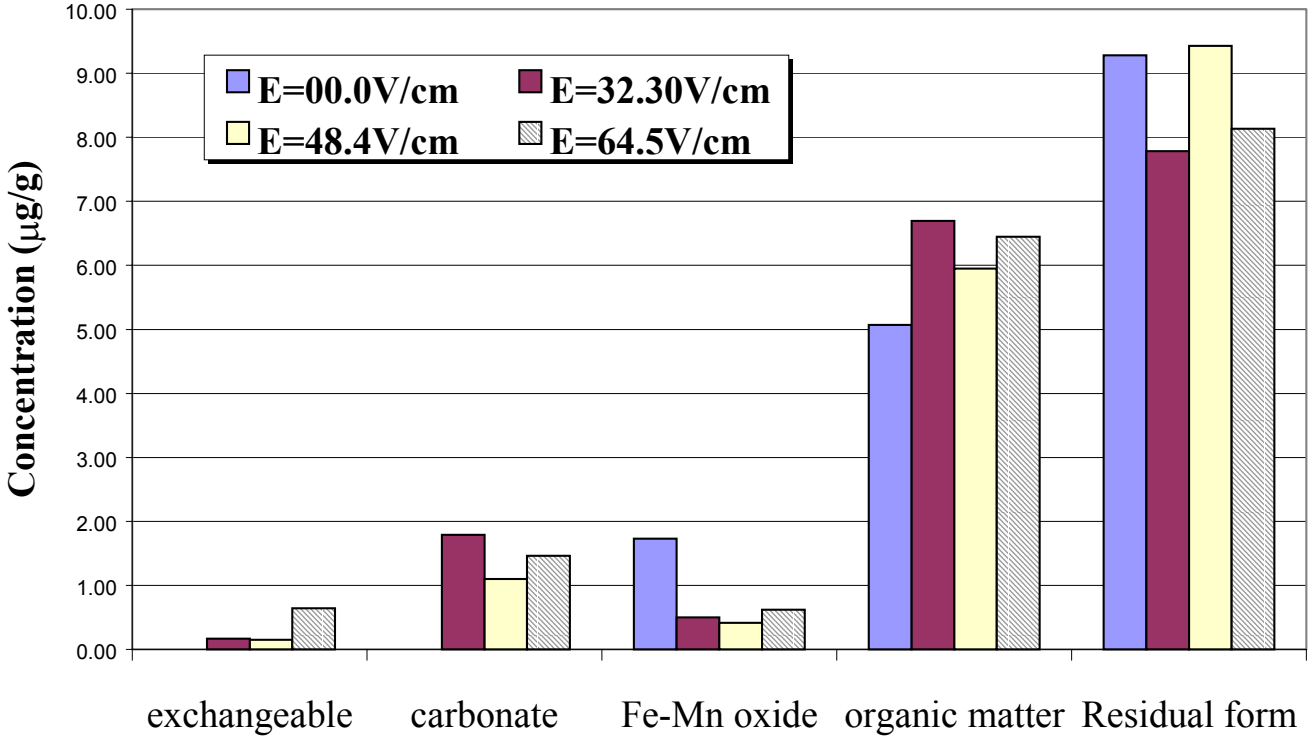

Figure 47. Distribution of lead species in particulate collected from well water sample 10IB01 as affected by electrostatic field. Experimental condition: pH = 6.5.

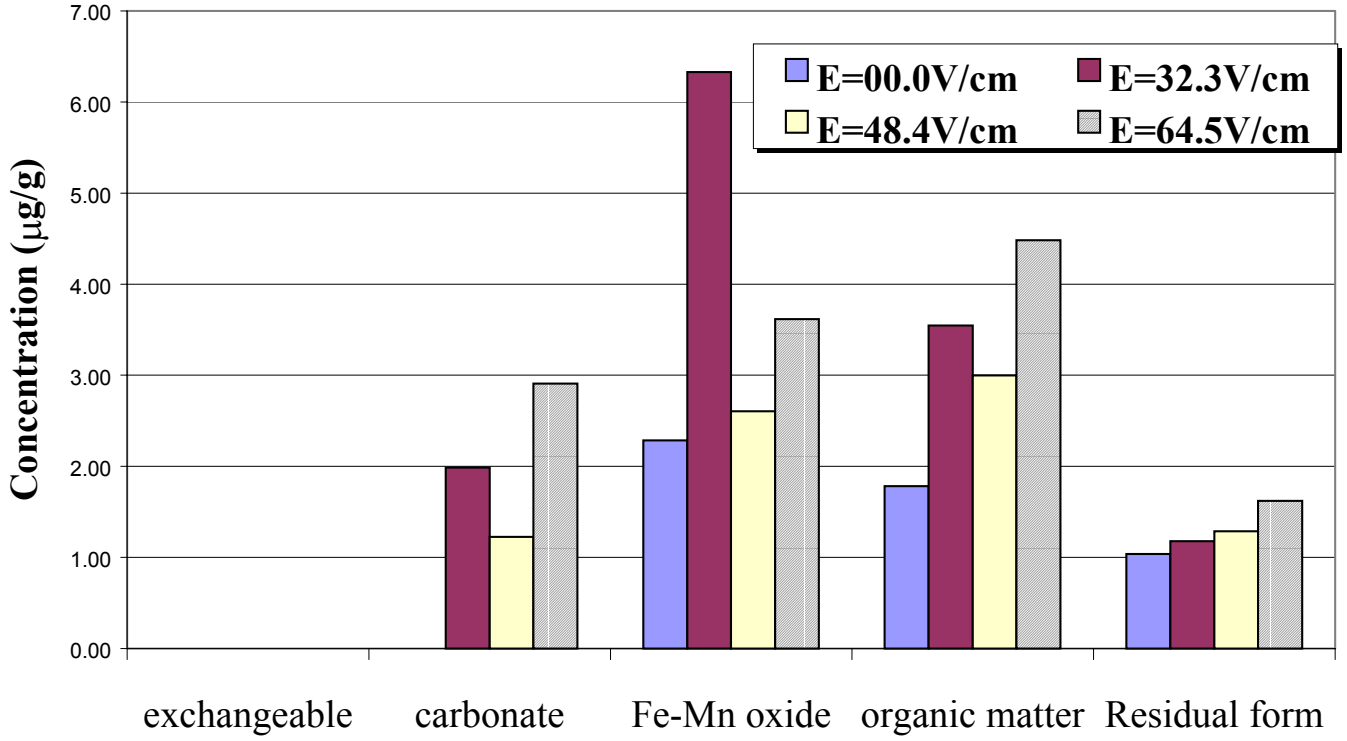

Figure 48. Distribution of lead species in particulate collected from well water sample 10IL01 as affected by electrostatic field. Experimental condition: pH = 6.5.

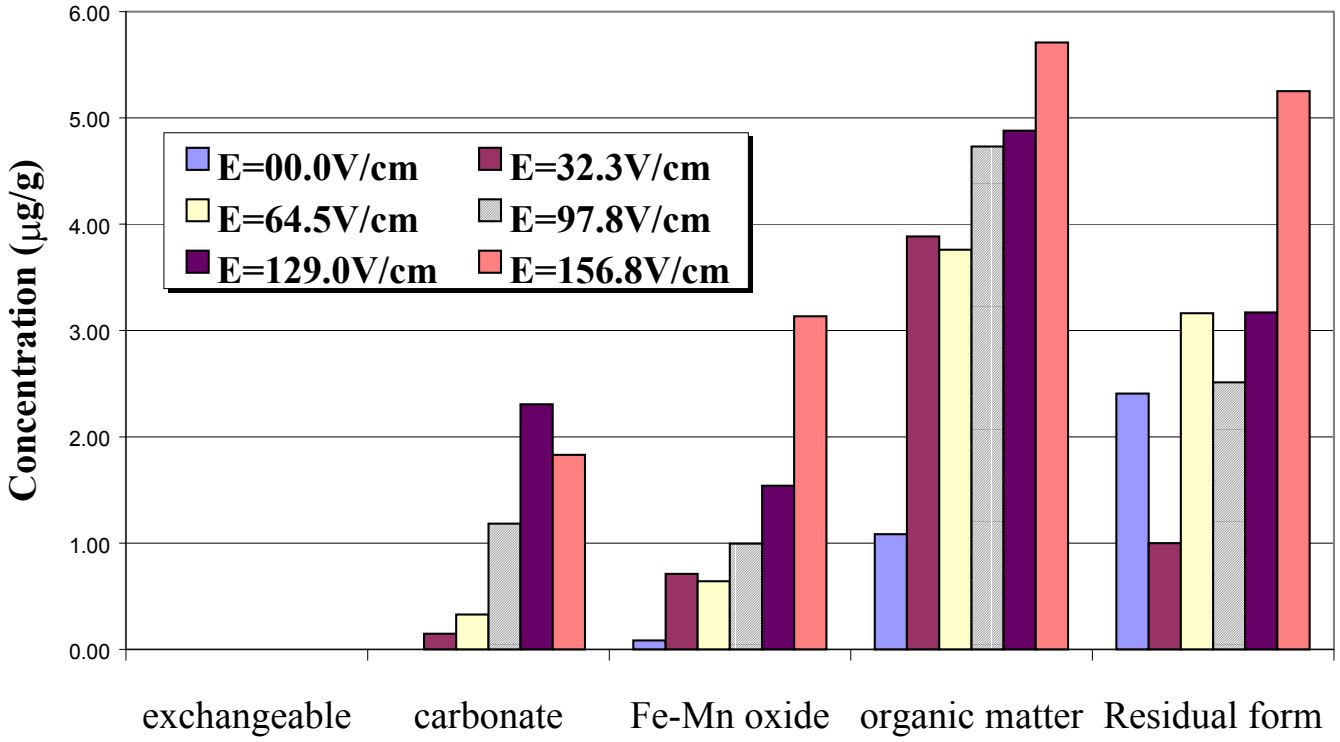

Figure 49. Distribution of lead species in particulate collected from well water sample 5SIIL02 as affected by electrostatic field. Experimental condition: pH = 6.7.

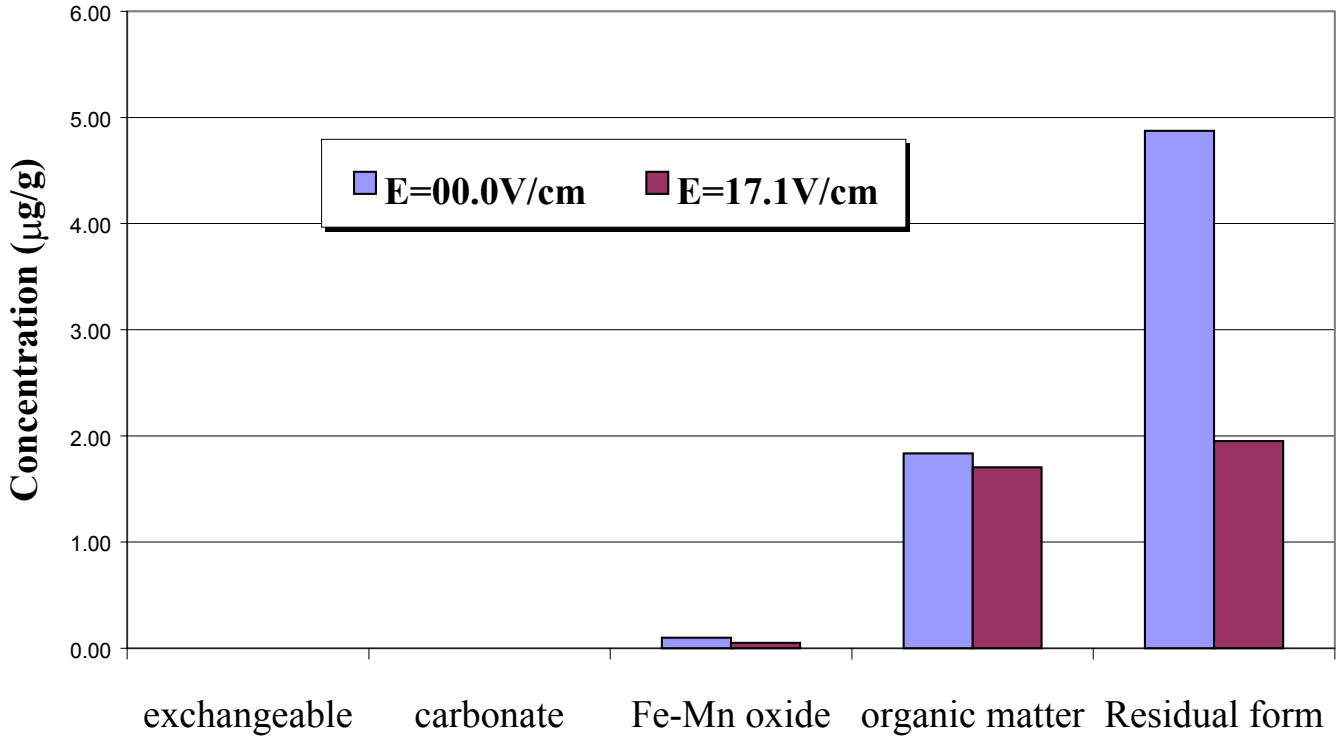

Figure 50. Distribution of lead species in particulate collected from well water sample MW3IB03 as affected by electrostatic field. Experimental conditions: pH = 7.9.

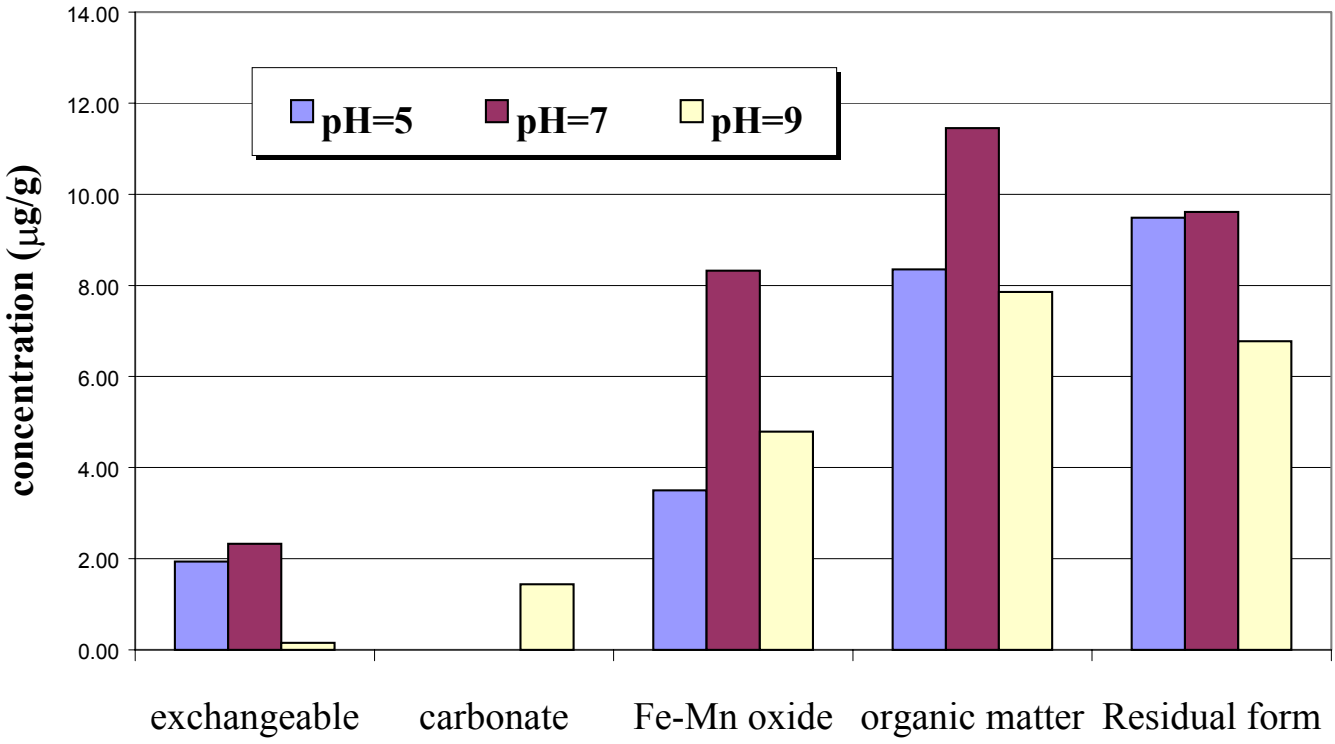

Figure 51. Distribution of lead species in particulate collected from well water sample 10IB01 as affected by pH. Experimental conditions: pH = 5 (electrostatic field = 32.3 V/cm); pH = 7 (electrostatic field = 48.4 V/cm); pH = 9 (electrostatic field = 64.5 V/cm).

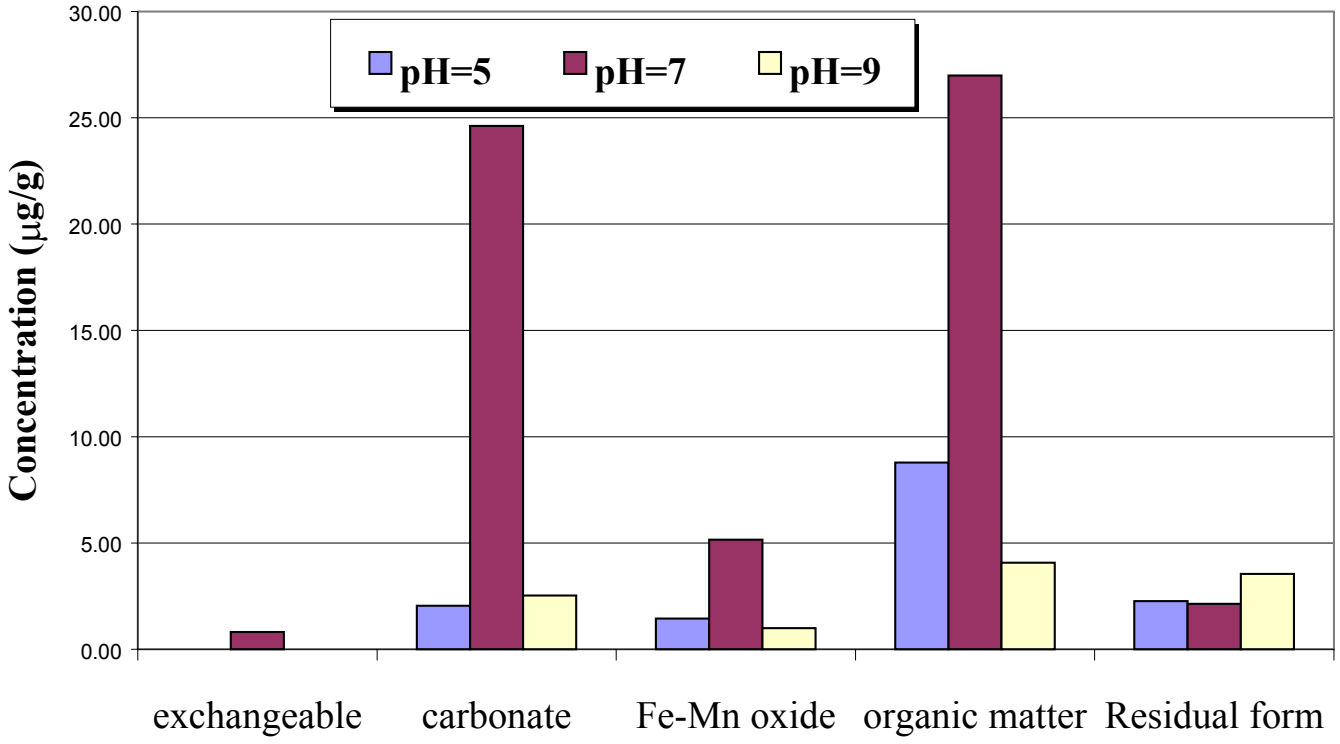

Figure 52. Distribution of lead species in particulate collected from well water sample 10IL01 as affected by pH. Experimental conditions: pH = 5 (electrostatic field = 32.3 V/cm); pH = 7 (electrostatic field = 48.4 V/cm); pH = 9 (electrostatic field = 48.4 V/cm).

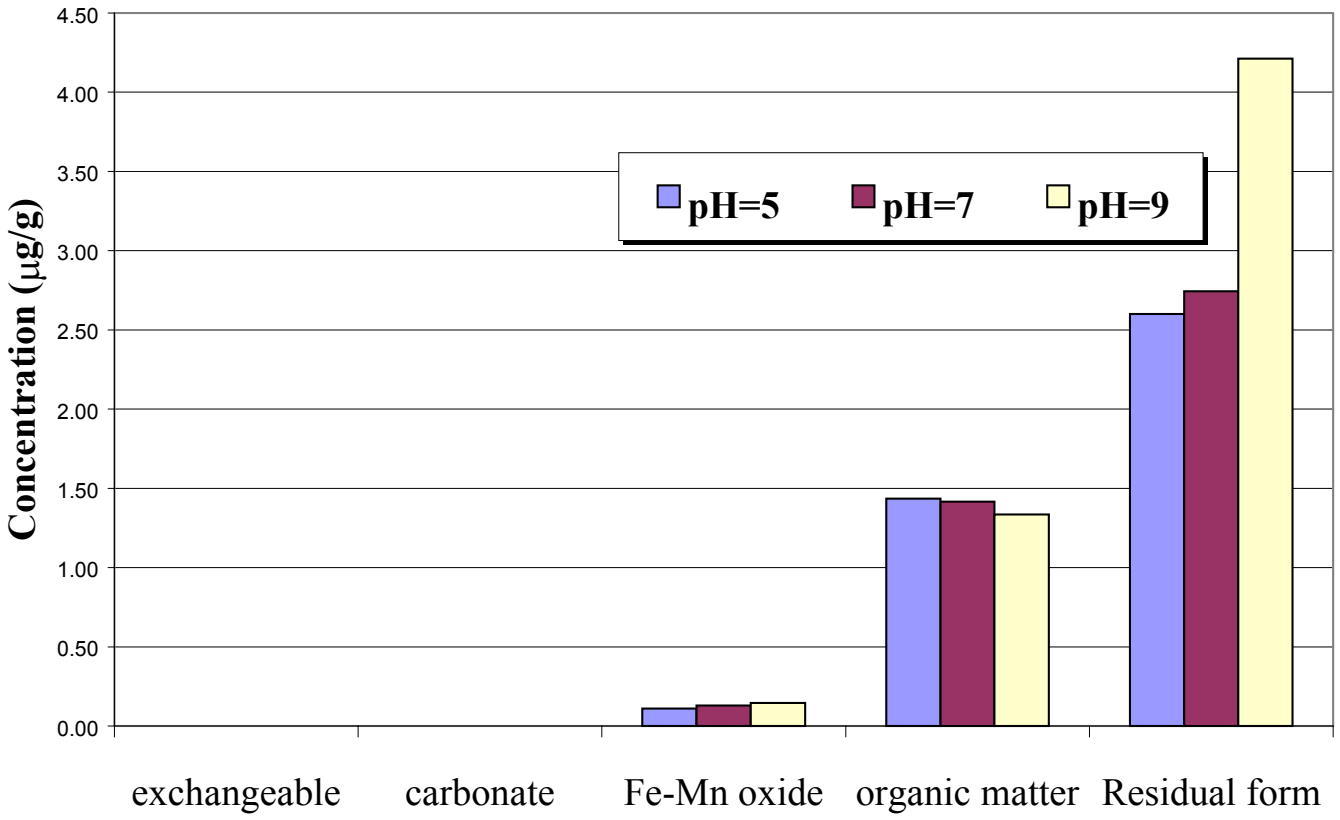

Figure 53. Distribution of lead species in particulate collected from well water sample 5SIIB03 as affected by pH. Experimental conditions: pH = 5 (electrostatic field = 97.8 V/cm); pH = 7 (electrostatic field = 97.8 V/cm); pH = 9 (electrostatic field = 97.8 V/cm).

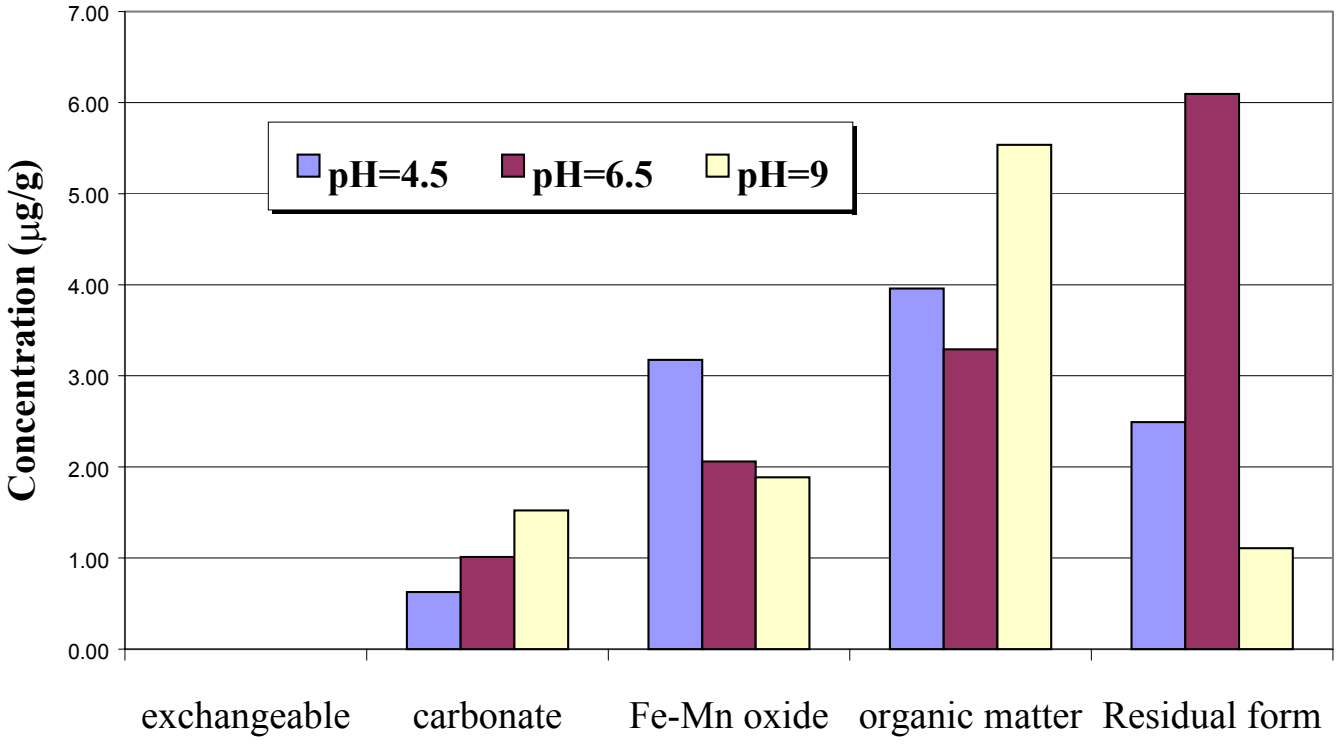

Figure 54. Distribution of lead species in particulate collected from well water sample 5SIIL02 as affected by pH. Experimental conditions: pH = 4.5 (electrostatic field = 97.8 V/cm); pH = 6.5 (electrostatic field = 97.8 V/cm); pH = 9.0 (electrostatic field = 97.8 V/cm).

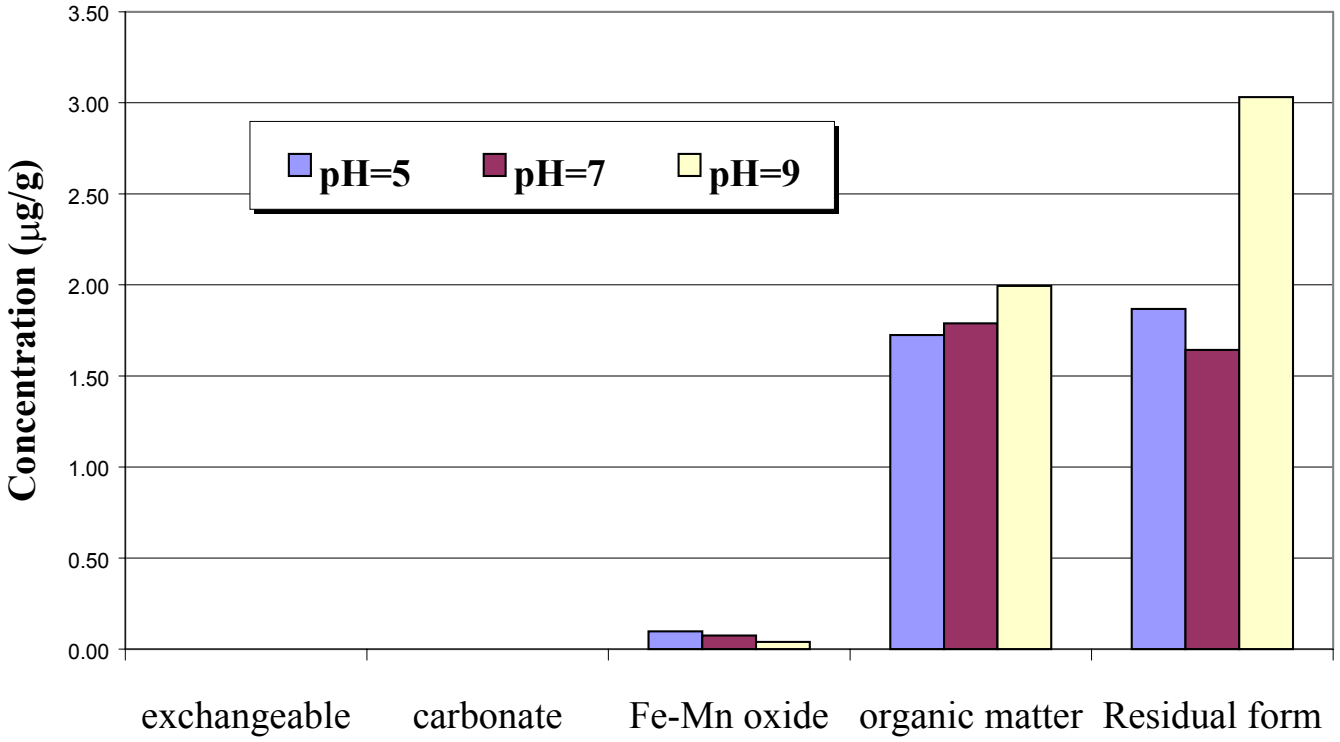

Figure 55. Distribution of lead species in particulate collected from well water sample as affected by pH. Experimental conditions: pH = 5 (electrostatic field = 10.3 V/cm); pH = 7 (electrostatic field = 13.2 V/cm); pH = 9 (electrostatic field = 14.8 V/cm).

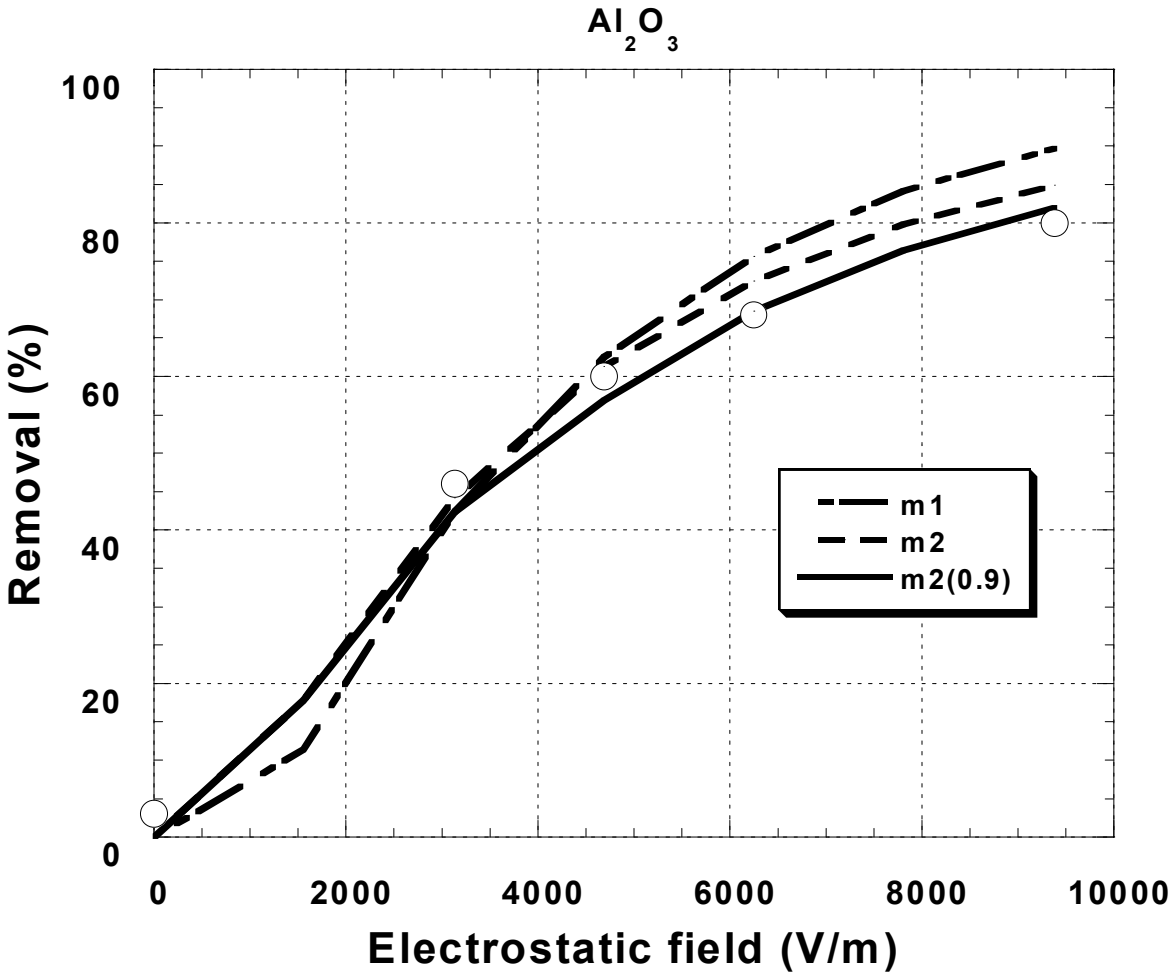

Figure 56. Predicting the removal of γ-Al_2O_3 as a function of applied electrostatic field. Theoretical values using Equations 15, 21 and 30 versus measured values.

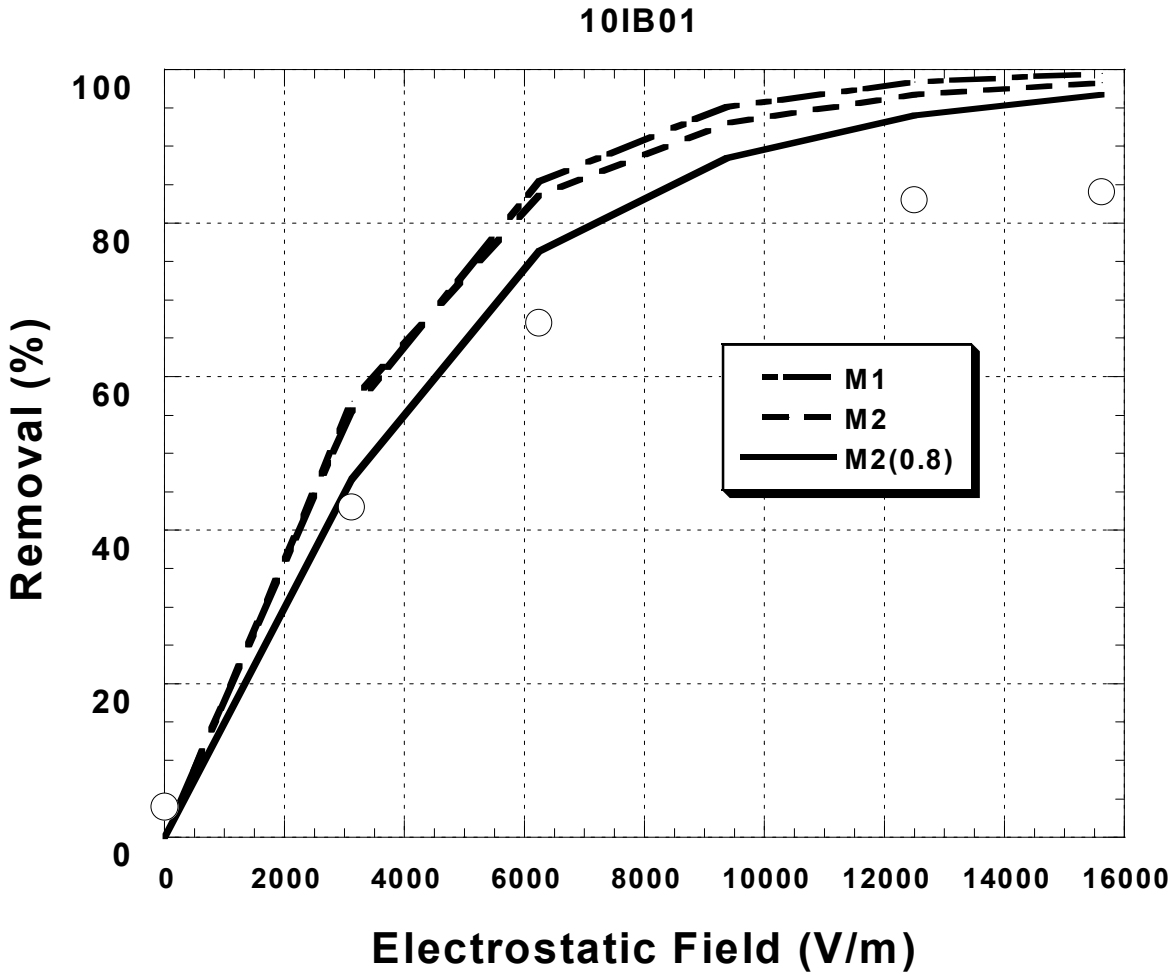

Figure 57. Predicting the removal of naturally occurring particles in well water sample 10IB01 as a function of applied electrostatic field. Theoretical values using equations 15, 21 and 30 versus measured values.

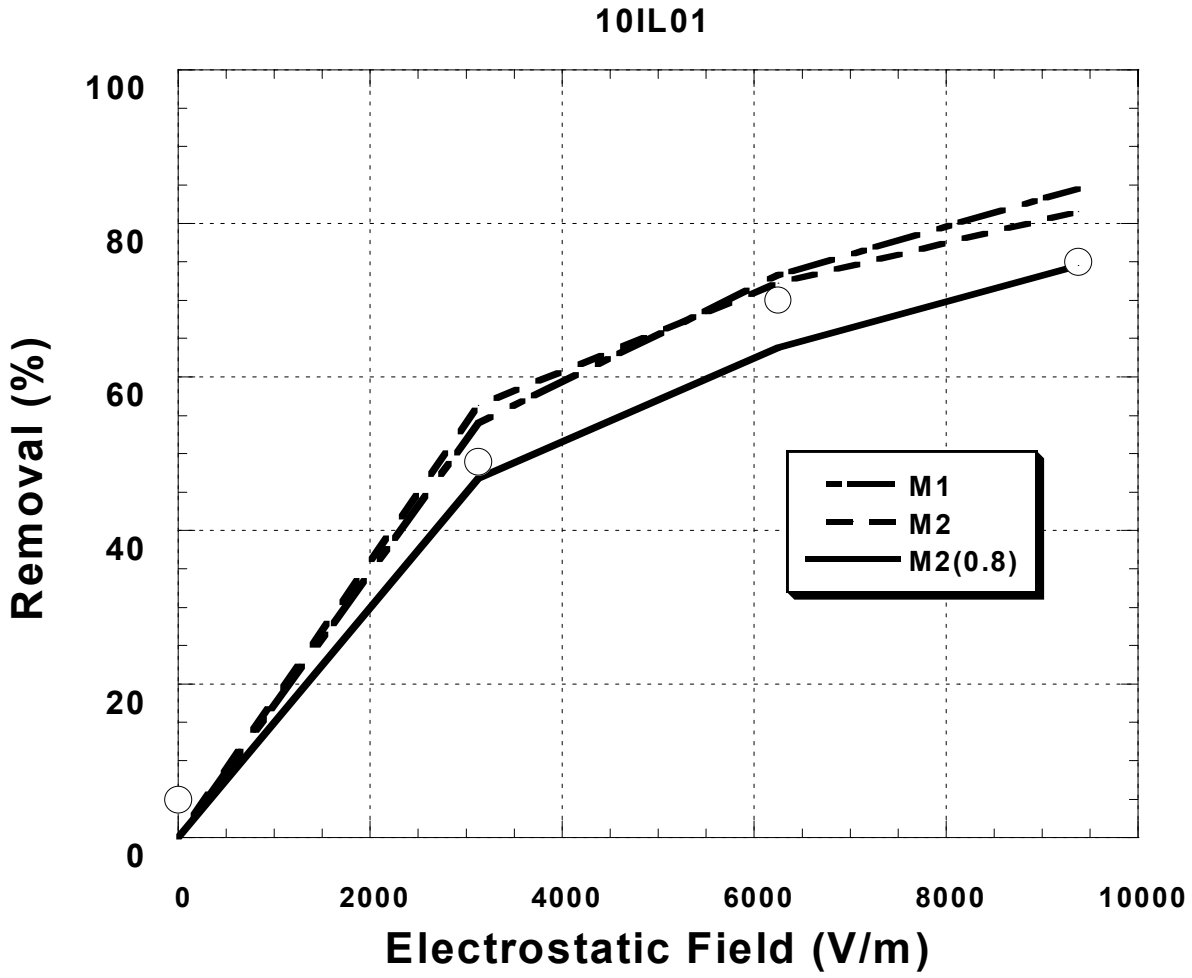

Figure 58. Predicting the removal of naturally occurring particles in well water sample 10IL0 as a function of applied electrostatic field. Theoretical values using equations 15, 21 and 30 versus measured values.

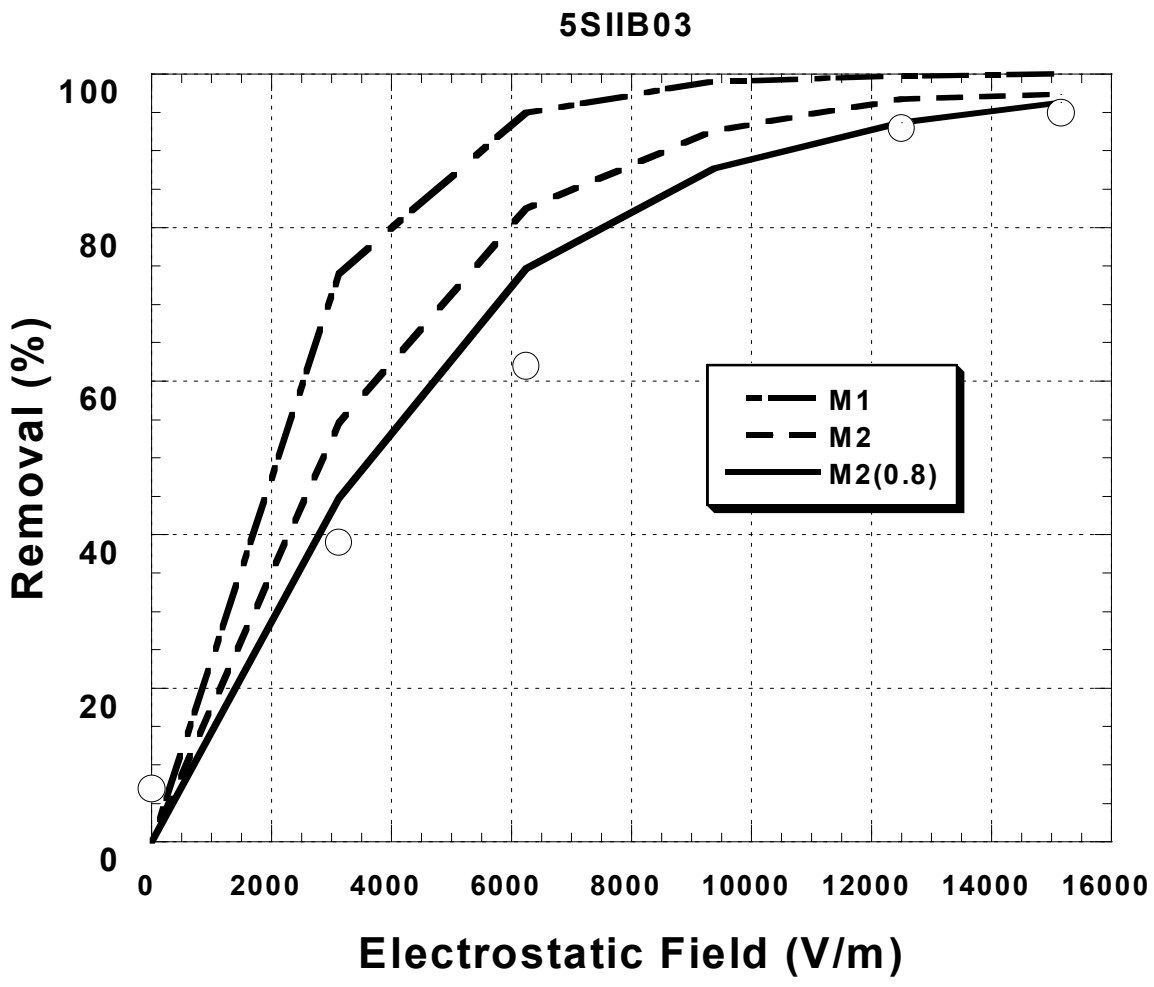

Figure 59. Predicting the removal of naturally occurring particles in well water sample 5SII03 as a function of applied electrostatic field. Theoretical values using equations 15, 21 and 30 versus measured values.

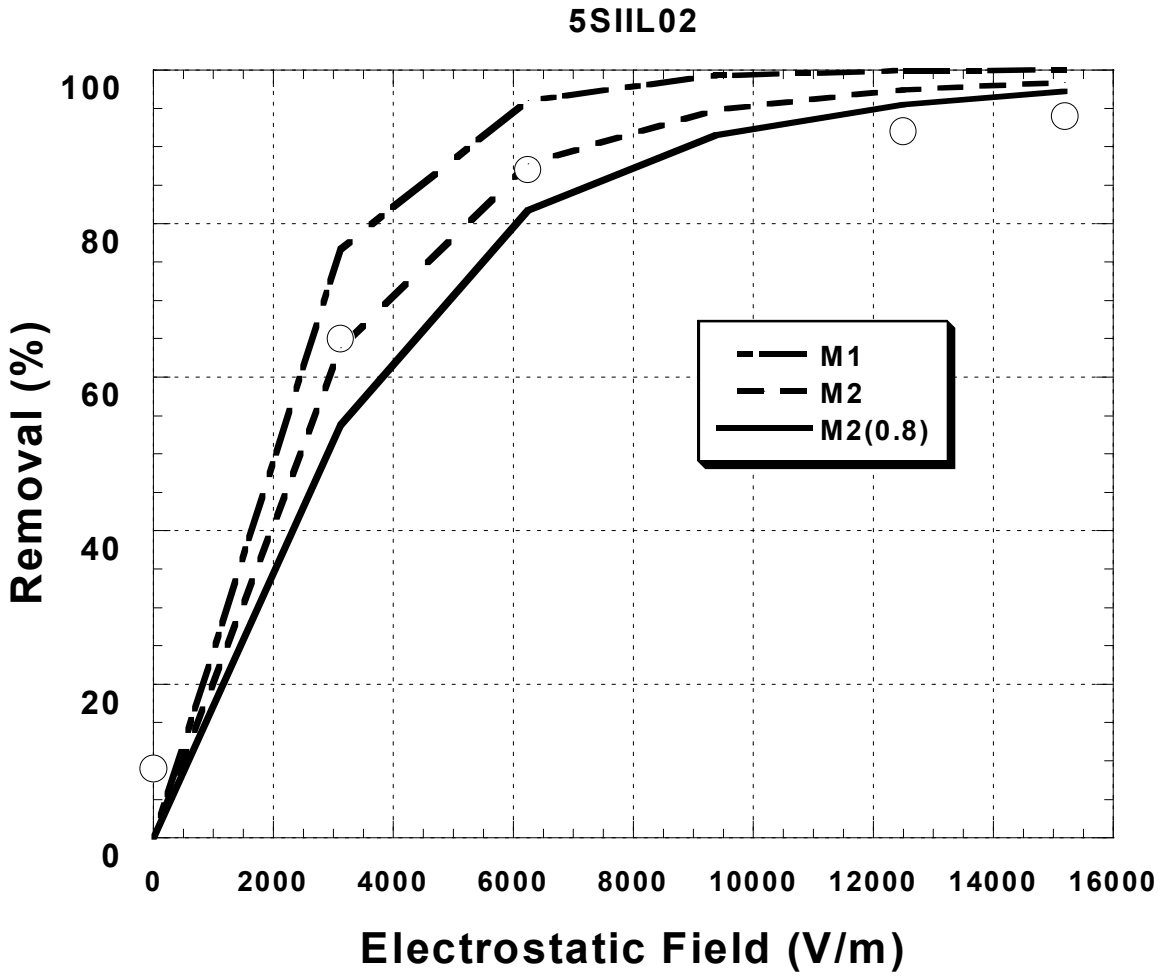

Figure 60. Predicting the removal of naturally occurring particles in well water sample 5IIL02 as a function of applied electrostatic field. Theoretical values using equations 15, 21 and 30 versus measured values.

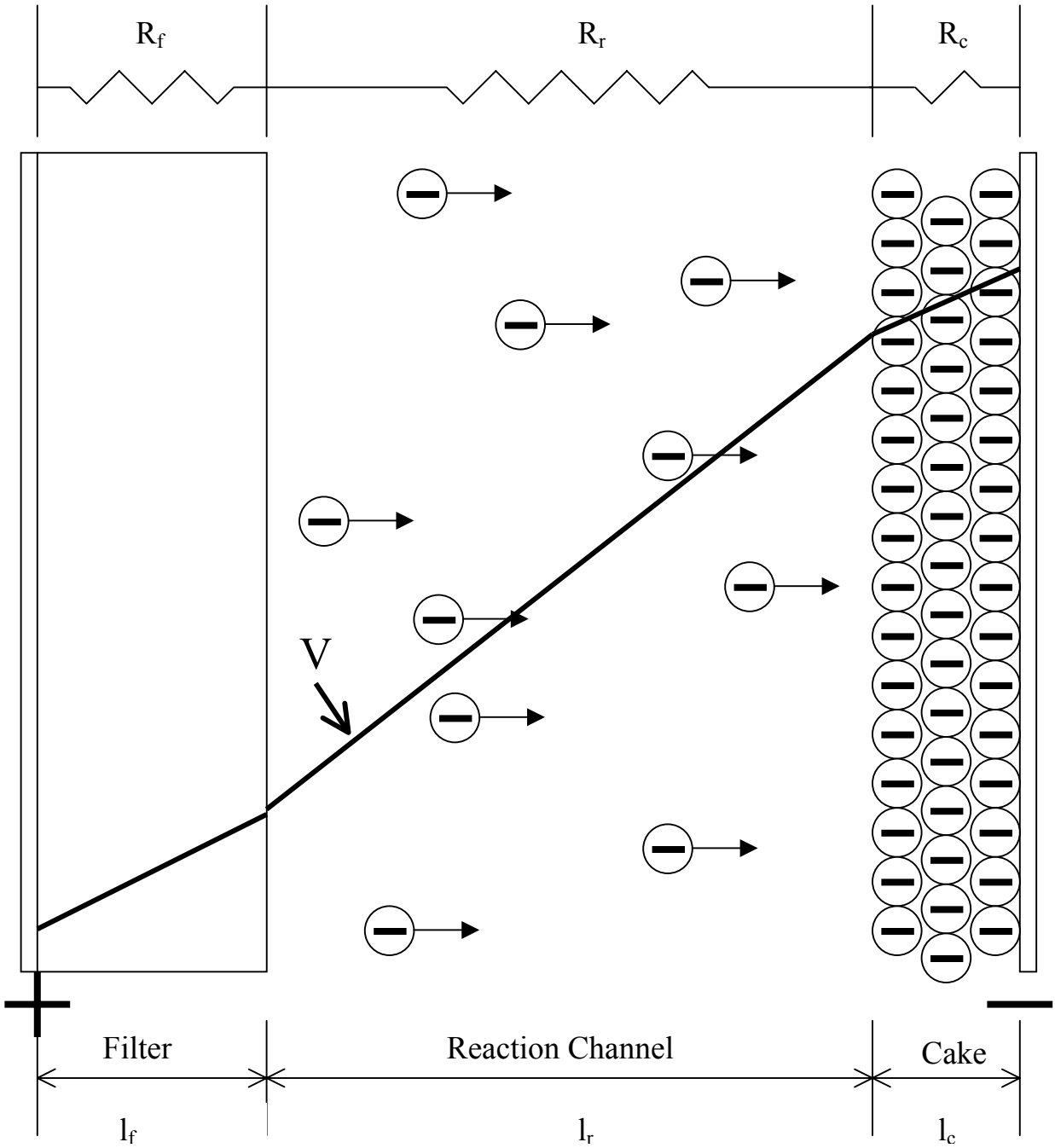

Figure 61. The concept of resistance distribution of the CFEF unit

Table A1. The effect of electrostatic field on the change of turbidity (I)

Time (min)	Turbidity (NTU)		
	E = 00.0 V/cm (V = 00)	E = 12.9 V/cm (V = 40)	E = 16.1 V/cm (V = 50)
0	29.0	29.0	29.0
1	28.0	27.6	27.2
2	28.0	26.4	26.8
3	28.0	26.1	26.4
4	28.0	25.7	25.4
5	28.0	25.9	24.6
6	28.0	26.1	24.0
7	28.0	25.9	24.0
8	28.0	25.5	24.0
9	28.0	25.1	23.8
10	28.0	25.7	23.9
11	28.0	25.6	23.8
12	28.0	25.6	24.1
13	28.0	25.6	23.7
14	28.0	25.6	23.6
15	28.0	25.2	23.8

Experimental conditions: [γ-Al_2O_3] = 100 mg/L; pump speed = 20% (or 0.77 L/min filtration rate); Initial pH = 5.6.

Table A2. The effect of electrostatic field on the removal of Al_2O_3 (II)

Time (min)	Removal Efficiency (%)		
	E = 00.0 V/cm (V = 00)	E = 12.9 V/cm (V = 40)	E = 16.1 V/cm (V = 50)
0	0	0	0
1	3	5	6
2	3	9	8
3	3	10	9
4	3	11	12
5	3	11	15
6	3	10	17
7	3	11	17
8	3	12	17
9	3	13	18
10	3	11	18
11	3	12	18
12	3	12	17
13	3	12	18
14	3	12	19
15	3	13	18

Experimental conditions: [γ-Al_2O_3] = 100 mg/L; pump speed = 20% (or 0.77 L/min filtration rate); Initial pH = 5.6. Removal Efficiency = $(T_0-T_i)/T_0*100\%$

T_0: Turbidity of filtrate at 0 minute

T_i: Turbidity of filtrate at i minute

Table A3. Effect of electrostatic field on the change of turbidity (III)

Time (min)	Turbidity (NTU)					
	E = 16.1 V/cm (V = 50)	E = 32.3 V/cm (V =100)	E = 48.4 V/cm (V =150)	E = 64.5 V/cm (V = 200)	E = 80.6 V/cm (V = 250)	E = 96.8 V/cm (V = 300)
0	30.8	28.5	28.5	28.5	28.5	28.5
1	28.9	16.0	14.6	14.1	15.0	13.4
2	26.7	14.7	12.3	14.2	14.4	14.6
3	26.5	14.4	12.1	14.3	13.0	10.9
4	25.4	14.7	12.2	14.3	12.0	11.4
5	25.0	14.9	12.5	11.5	11.1	10.2
6	24.8	14.6	12.0	12.5	10.4	9.4
7	24.9	14.8	12.0	11.6	9.8	8.1
8	24.1	15.1	12.2	10.4	8.9	7.1
9	23.2	15.2	11.9	9.6	8.3	6.5
10	23.7	15.3	11.5	9.2	8.0	5.7

Experimental condition: [γ-Al_2O_3] = 100 mg/L; pump speed = 15% (or 0.46 L/min filtration rate); Initial pH = 5.6

Table A4. Effect of electrostatic field on the removal of Al_2O_3 (IV)

Time (min)	Removal Efficiency (%)					
	E = 16.1 V/cm (V = 50)	E = 32.3 V/cm (V =100)	E = 48.4 V/cm (V =150)	E = 64.5 V/cm (V = 200)	E = 80.6 V/cm (V = 250)	E = 96.8 V/cm (V = 300)
0	0	0	0	0	0	0
1	6	44	49	51	47	53
2	13	48	57	50	49	49
3	14	49	58	50	54	62
4	18	48	57	50	58	60
5	19	48	56	60	61	64
6	19	49	58	56	64	67
7	19	48	58	59	66	72
8	22	47	57	64	69	75
9	25	47	58	66	71	77
10	23	46	60	68	72	80

Experimental condition: [γ-Al_2O_3] = 100 mg/L; pump speed = 15% (or 0.46 L/min filtration rate); Initial pH = 5.6. Removal Efficiency = $(T_0-T_i)/T_0*100\%$; T_0: Turbidity of filtrate at 0 minute; T_i: Turbidity of filtrate at i minute.

Table A5. The effect of concentration on the change of turbidity (I)

Time (min)	Turbidity (NTU)		
	C = 50mg/L	C =100mg/L	C = 200mg/L
0	16.0	30.8	58.1
1	16.0	28.9	52.4
2	16.0	26.7	52.3
3	15.1	26.5	51.6
4	14.3	25.4	48.6
5	13.3	25.0	47.4
6	13.1	24.8	45.6
7	13.7	24.9	44.1
8	13.0	24.1	43.6
9	13.5	23.2	43.9
10	13.1	23.7	44.7
11	13.0	23.7	45.2
12	12.3	23.1	45.2
13	12.1	23.0	44.5
14	11.9	22.4	43.5
15	11.3	21.9	43.6

Experimental conditions: pumping speed = 20% or 0.77 L/min filtration rate); E = 16.1 V/cm (or Voltage = 50 V).

Table A6. The effect of concentration on the removal of Al_2O_3 (II)

Time (min)	Removal Efficiency (%)		
	C = 50mg/L	C = 100mg/L	C = 200mg/L
0	0	0	0
1	0	6	10
2	0	13	10
3	6	14	11
4	11	18	16
5	17	19	18
6	18	19	22
7	14	19	24
8	19	22	25
9	16	25	24
10	18	23	23
11	19	23	22
12	23	25	22
13	24	25	23
14	26	27	25
15	29	29	25

Experimental conditions: pumping speed = 20% (or 0.77 L/min filtration rate); E = 16.1 V/cm (or Voltage = 50 V). Removal Efficiency = $(T_0-T_i)/T_0*100\%$
T_0: Turbidity of filtrate at 0 minute; T_i: Turbidity of filtrate at i minute.

Table A7. The effect of filtrate rate on the change of turbidity (I)

Time (min)	Turbidity (NTU)					
	Pump speed = 12 Q = 0.27 L/min	Pump speed =15 Q = 0.46 L/min	Pump speed =20 Q = 0.77L/min	Pump speed =25 Q = 1.08 L/min	Pump speed =30 Q = 1.39 L/min	Pump speed =35 Q = 1.70 L/min
0	28.5	28.5	28.5	28.5	28.5	28.5
1	22.1	13.4	14.6	16.2	19.7	21.5
2	20.9	14.6	13.0	15.6	16.3	18.2
3	13.8	10.9	12.4	15.2	16.2	16.5
4	13.6	11.4	12.6	14.4	16.1	16.3
5	13.2	10.2	11.0	14.4	15.9	16.4
6	12.0	9.4	11.3	14.1	15.8	16.2
7	10.9	8.1	11.1	13.8	15.0	15.9
8	9.6	7.1	10.7	14.0	15.7	15.7
9	8.1	6.5	10.6	14.0	15.2	15.7
10	7.1	5.7	10.4	13.5	15.6	15.5

Experimental conditions: [γ-Al_2O_3] = 100 mg/L; initial pH = 5.6; E = 96.8 V/cm (or Voltage = 300V)

Table A8. The effect of filtrate rate on the removal efficiency of Al_2O_3 (II)

Time (min)	Removal Efficiency (%)					
	Pump speed = 12 Q = 0.27 L/min	Pump speed =15 Q = 0.46 L/min	Pump speed =20 Q = 0.77L/min	Pump speed =25 Q = 1.08 L/min	Pump speed =30 Q = 1.39 L/min	Pump speed =35 Q = 1.70 L/min
0	00	00	00	00	00	00
1	22	53	49	43	31	25
2	27	49	54	45	43	36
3	52	62	56	47	43	42
4	52	60	56	49	44	43
5	54	64	61	49	44	42
6	58	67	60	51	45	43
7	62	72	61	52	47	44
8	66	75	62	51	45	45
9	71	77	63	51	47	45
10	75	80	64	53	45	46

Experimental condition: [γ-Al_2O_3] = 100 mg/L; initial pH = 5.6; E = 96.8 V/cm (or Voltage = 300V) Removal Efficiency: $(T_0-T_i)/T_0*100\%$; T_0: Turbidity of filtrate at 0 minute; T_i: Turbidity of filtrate at i minute.

Table A9. The effect of pH on the change of turbidity (I)

Time (min)	Turbidity (NTU)				
	pH = 4.0	pH = 5.0	pH = 6.0	pH = 7.0	pH = 8.0
0	29.7	29.7	29.7	29.7	29.7
1	15.5	23.9	16.3	16.4	19.7
2	11.6	11.9	11.5	15.4	10.7
3	10.2	7.8	9.4	15.0	14.0
4	9.9	8.0	10.3	15.2	15.8
5	8.7	8.5	11.4	16.8	17.0
6	7.9	9.1	11.9	17.5	16.2
7	7.1	9.1	11.8	16.9	16.3
8	6.4	9.2	11.8	16.6	16.7
9	6.0	9.1	11.5	16.4	16.2
10	5.7	9.5	11.2	16.2	15.9
11	5.4	8.1	11.4	16.1	16.1
12	5.1	6.9	10.9	15.9	16.5
13	4.7	6.7	11.7	16.0	16.3
14	4.7	6.9	11.3	16.2	16.3
15	5.0	7.2	11.2	16.0	16.1
16	4.7	7.4	10.7	15.9	16.1
17	4.9	7.6	10.6	16.3	16.2
18	4.8	7.6	10.5	15.8	16.2
19	4.8	7.8	11.1	16.1	16.7
20	4.7	8.2	11.1	16.3	16.6
21	5.1	8.9	10.9	16.2	16.3
22	4.9	8.3	10.7	16.2	16.0

Experimental conditions: [γ-Al_2O_3] = 100 mg/L; pump speed = 15% (or 0.46 L/min filtration rate); Voltage = 300 V.

Table A10. The effect of pH on the removal of Al_2O_3 (II)

Time (min)	Removal Efficiency (%)				
	pH = 4.0	pH = 5.0	pH = 6.0	pH = 7.0	pH = 8.0
0	0	0	0	0	0
1	48	20	45	45	34
2	61	60	61	48	64
3	66	74	68	49	53
4	67	73	65	49	47
5	71	71	62	43	43
6	73	70	60	41	45
7	76	69	60	43	45
8	78	69	60	44	44
9	80	69	61	45	45
10	81	68	62	45	46
11	82	73	62	46	46
12	83	77	63	46	44
13	84	77	61	46	45
14	84	77	62	45	45
15	83	76	62	46	46
16	84	75	64	46	46
17	84	74	64	45	45
18	84	74	65	47	45
19	84	74	63	46	44
20	84	73	63	45	44
21	83	70	63	45	45
22	84	72	64	45	46

Experimental conditions: [γ-Al_2O_3] = 100 mg/L; pump speed = 15% (or 0.46 L/min filtration rate); Voltage = 300 V. Removal Efficiency=$(T_0-T_i)/T_0*100\%$; T_0: Turbidity of filtrate at 0 minute; T_i: Turbidity of filtrate at i minute.

Table A11. The effect of electrostatic field on the change of turbidity(I)
Sample: 10IB01

Time (min)	Turbidity (NTU)					
	E = 00 V/cm (V = 00)	E = 32.3 V/cm (V = 100)	E = 64.5 V/cm (V = 200)	E = 96.8 V/cm (V = 300)	E = 129.1 V/cm (V = 400)	E = 161.3 V/cm (V = 500)
0	223	223	223	223	223	223
1	209	199	157	215	95	188
2	212	134	76	82	60	86
3	211	109	73	67	43	51
4	210	108	61	52	40	44
5	212	110	45	50	39	40
6	211	114	46	53	38	41
7	211	118	54	53	37	38
8	211	123	61	49	36	37
9	213	127	65	47	36	34
10	213	127	68	45	38	35

Table A12. The effect of electrostatic field on the removal efficiency (I)
Sample: 10IB01

Time (min)	Removal Efficiency (%)					
	E = 00 V/cm (V = 00)	E = 32.3 V/cm (V = 100)	E = 64.5 V/cm (V = 200)	E = 96.8 V/cm (V = 300)	E = 129.1 V/cm (V = 400)	E = 161.3 V/cm (V = 500)
0	0	0	0	0	0	0
1	6	11	30	4	57	16
2	5	40	65	63	73	62
3	5	51	67	70	81	77
4	6	52	73	77	82	80
5	5	51	80	77	82	82
6	5	49	79	76	83	82
7	5	47	76	76	84	83
8	5	45	73	78	84	83
9	4	43	71	79	84	85
10	4	43	69	80	83	84

Table A13. The effect of electrostatic field on the change of turbidity (II)
Sample: 10IB01

Time (min)	Turbidity (NTU)			
	E = 00 V/cm (V = 00)	E = 32.3 V/cm (V = 100)	E = 48.4 V/cm (V = 150)	E = 62.6 V/cm (V = 194)
0	799	799	799	799
1	628	740	710	632
2	682	480	542	460
3	689	391	387	354
4	715	355	323	297
5	709	330	290	247
6	712	313	270	210
7	710	292	270	204
8	705	304	262	202
9	720	335	271	199
10	717	344	272	196

Table A14. The effect of electrostatic field on the removal efficiency (II)
Sample: 10IB01

Time	Removal Efficiency (%)			
	E = 00 V/cm (V = 00)	E = 32.3 V/cm (V = 100)	E = 48.4 V/cm (V = 150)	E = 62.6 V/cm (V = 194)
0	0	0	0	0
1	21	7	11	21
2	15	40	32	42
3	14	51	52	56
4	11	56	60	63
5	11	59	64	69
6	11	61	66	74
7	11	63	66	74
8	12	62	67	75
9	10	58	66	75
10	10	57	66	75

Table A15. The effect of pH on the change of turbidity
Sample: 10IB01

Time (min)	Turbidity (NTU)		
	pH = 5	pH = 7	pH = 9
0	799	799	799
1	742	676	609
2	512	520	501
3	367	382	373
4	312	312	329
5	291	262	292
6	269	254	261
7	262	242	230
8	247	248	218
9	249	239	215
10	248	239	212

Experimental conditions: pH = 5 (electrostatic field = 32.3 V/cm); pH = 7 (electrostatic field = 48.4 V/cm); pH = 9 (electrostatic field = 48.4 V/cm).

Table A16. The effect of pH on the removal efficiency
Sample: 10IB01

Time (min)	iciency (%)		
	pH = 5	pH = 7	pH = 9
0	0	0	0
1	7	15	24
2	36	35	37
3	54	52	53
4	61	61	59
5	64	67	63
6	66	68	67
7	67	70	71
8	69	69	73
9	69	70	73
10	69	70	73

Experimental conditions: pH = 5 (electrostatic field = 32.3 V/cm); pH = 7 (electrostatic field = 48.4 V/cm); pH = 9 (electrostatic field = 48.4 V/cm).

Table A17. The effect of electrostatic field on the change of turbidity
Sample: 10IL01

Time (min)	Turbidity (NTU)			
	E = 00 V/cm (V = 00)	E = 32.3 V/cm (V = 100)	E = 48.4 V/cm (V = 150)	E = 64.5 V/cm (V = 200)
0	548	548	548	548
1	500	509	403	505
2	516	442	379	369
3	519	370	267	295
4	528	317	229	260
5	520	269	206	229
6	519	254	192	199
7	515	267	178	177
8	520	275	176	157
9	519	280	169	148
10	521	278	164	136

Table A18. The effect of electrostatic field on the removal efficiency
Sample: 10IL01

Time	Removal Efficiency (%)			
	E = 00 V/cm (V = 00)	E = 32.3 V/cm (V = 100)	E = 48.4 V/cm (V = 150)	E = 64.5 V/cm (V = 200)
0	0	0	0	0
1	9	7	26	8
2	6	19	31	33
3	5	32	51	46
4	4	42	58	53
5	5	51	62	58
6	5	54	65	64
7	6	51	68	68
8	5	50	68	71
9	5	49	69	73
10	5	49	70	75

Table A19. The effect of pH on the change of turbidity
Sample: 10IL01

Time (min)	Turbidity (NTU)		
	pH = 5	pH = 7	pH = 9
0	548	548	548
1	444	427	464
2	407	368	375
3	307	296	314
4	255	241	269
5	225	208	235
6	215	181	197
7	206	163	178
8	201	151	162
9	206	147	154
10	202	144	149

Experimental condition: pH = 5 (electrostatic field = 32.3 V/cm); pH = 7 (electrostatic field = 48.4 V/cm); pH = 9 (electrostatic field = 48.4 V/cm).

Table A20. The effect of pH on the removal efficiency
Sample: 10IL01

Time (min)	iciency (%)		
	pH = 5	pH = 7	pH = 9
0	0	0	0
1	19	22	15
2	26	33	32
3	44	46	43
4	53	56	51
5	59	62	57
6	61	67	64
7	62	70	68
8	63	72	70
9	62	73	72
10	63	74	73

Experimental condition: pH = 5 (electrostatic field = 32.3 V/cm); pH = 7 (electrostatic field = 48.4 V/cm); pH = 9 (electrostatic field = 48.4 V/cm).

Table A21. The effect of electrostatic field on the change of turbidity
Sample: 5SIIB03

Time (min)	Turbidity (NTU)					
	E = 00 V/cm (V = 00)	E = 32.3 V/cm (V = 100)	E = 64.5 V/cm (V = 200)	E = 96.8 V/cm (V = 300)	E = 129.1 V/cm (V = 400)	E = 156.5 V/cm (V = 485)
0	748	748	748	748	748	748
1	718	650	630	466	398	306
2	692	555	383	216	211	160
3	702	427	267	129	160	112
4	697	410	242	122	103	73
5	700	415	248	121	75	59
6	690	430	265	123	67	56
7	688	433	276	124	60	51
8	688	447	283	127	61	47
9	690	445	277	128	59	45
10	694	456	283	131	51	39

Table A22. The effect of electrostatic field on the removal efficiency
Sample: 5SIIB03

Time (min)	Removal Efficiency (%)					
	E = 00 V/cm (V = 00)	E = 32.3 V/cm (V = 100)	E = 64.5 V/cm (V = 200)	E = 96.8 V/cm (V = 300)	E = 129.1 V/cm (V = 400)	E = 156.5 V/cm (V = 485)
0	0	0	0	0	0	0
1	4	13	16	38	47	59
2	7	26	49	71	72	79
3	6	43	64	83	79	85
4	7	45	68	84	86	90
5	6	45	67	84	90	92
6	8	43	65	84	91	93
7	8	42	63	83	92	93
8	8	40	62	83	92	94
9	8	41	63	83	92	94
10	7	39	62	82	93	95

Table A23. The effect of pH on the change of turbidity
Sample: 5SIIB03

Time (min)	Turbidity (NTU)		
	pH = 5	pH = 7	pH = 9
0	748	748	748
1	522	452	704
2	148	151	336
3	109	131	291
4	101	124	243
5	94	105	201
6	71	93	167
7	57	86	158
8	53	76	145
9	48	64	140
10	45	56	120

Experimental condition: electrostatic field = 96.8 V/cm (or V = 300).

Table A24. The effect of pH on the removal efficiency
Sample: 5SIIB03

Time (min)	ficiency (%)		
	pH =5	pH =7	pH =9
0	0	0	0
1	30	40	6
2	80	80	55
3	85	82	61
4	86	83	68
5	87	86	73
6	90	88	78
7	92	88	79
8	93	90	81
9	94	91	81
10	94	93	84

Experimental conditions: electrostatic field = 96.8 V/cm (or V = 300).

Table A25. The effect of electrostatic field on the change of turbidity
Sample: 5SIIL02

Time (min)	Turbidity (NTU)					
	E = 00 V/cm (V = 00)	E = 32.3 V/cm (V = 100)	E = 64.5 V/cm (V = 200)	E = 96.8 V/cm (V = 300)	E = 129.1 V/cm (V = 400)	E = 156.8 V/cm (V = 486)
0	939	939	939	939	939	939
1	873	919	831	547	577	481
2	871	753	598	261	484	342
3	834	544	408	180	303	203
4	842	440	305	166	188	132
5	828	356	258	137	152	107
6	834	333	200	113	120	97
7	839	330	169	105	106	82
8	844	334	169	99	93	68
9	845	326	132	87	89	63
10	850	331	125	84	79	55

Table A26. The effect of electrostatic field on the removal efficiency
Sample: 5SIIL02

Time (min)	Removal Efficiency (%)					
	E = 00 V/cm (V = 00)	E = 32.3 V/cm (V = 100)	E = 64.5 V/cm (V = 200)	E = 96.8 V/cm (V = 300)	E = 129.1 V/cm (V = 400)	E = 156.8 V/cm (V = 486)
0	0	0	0	0	0	0
1	7	2	12	42	39	49
2	7	20	36	72	48	64
3	11	42	57	81	68	78
4	10	53	68	82	80	86
5	12	62	73	85	84	89
6	11	65	79	88	87	90
7	11	65	82	89	89	91
8	10	64	82	89	90	93
9	10	65	86	91	91	93
10	9	65	87	91	92	94

Table A27. The effect of pH on the change of turbidity
Sample: 5SIIL02

Time (min)	Turbidity (NTU)		
	pH = 4.5	pH = 6.5	pH = 9
0	939	939	939
1	346	664	629
2	158	418	505
3	165	208	254
4	153	169	207
5	126	159	190
6	103	131	168
7	82	112	146
8	62	98	129
9	56	86	112
10	50	78	95

Experimental conditions: electrostatic field = 96.8 V/cm (or V = 300).

Table A28. The effect of pH on the removal efficiency
Sample: 5SIIL02

Time (min)	ficiency (%)		
	pH = 4.5	pH = 6.5	pH = 9
0	0	0	0
1	63	29	33
2	83	55	46
3	82	78	73
4	84	82	78
5	87	83	80
6	89	86	82
7	91	88	84
8	93	90	86
9	94	91	88
10	95	92	90

Table A29. The effect of electrostatic field and pH on the change of turbidity
Sample: MW3IB02

Time (min)	Turbidity (NTU)				
	E = 00 V/cm (V = 00)	E = 17.1 V/cm (V = 53)	E = 10.3 V/cm (V = 32)	E = 13.2 V/cm (V = 41)	E = 14.8 V/cm (V = 46)
	pH = 7.9	pH = 7.9	pH = 5	pH = 7	pH = 9
0	582	582	582	582	582
1	499	559	559	496	569
2	534	521	469	436	492
3	545	434	400	399	433
4	551	375	366	387	376
5	548	346	352	364	344
6	538	335	335	344	339
7	506	328	335	333	320
8	550	318	322	319	304
9	536	320	325	314	292
10	514	312	322	303	287

Table A30. The effect of electrostatic field and pH on the removal efficiency
Sample: MW3IB02

Time (min)	Removal Efficiency (%)				
	E = 00 V/cm (V = 00)	E = 17.1 V/cm (V = 53)	E = 10.3 V/cm (V = 32)	E = 13.2 V/cm (V = 41)	E = 14.8 V/cm (V = 46)
	pH = 7..9	pH = 7.9	pH = 5	pH = 7	pH = 9
0	0	0	0	0	0
1	14	4	4	15	2
2	8	10	19	25	15
3	6	25	31	31	26
4	5	36	37	34	35
5	6	41	40	37	41
6	8	42	42	41	42
7	13	44	42	43	45
8	5	45	45	45	48
9	8	45	44	46	50
10	12	46	45	48	51

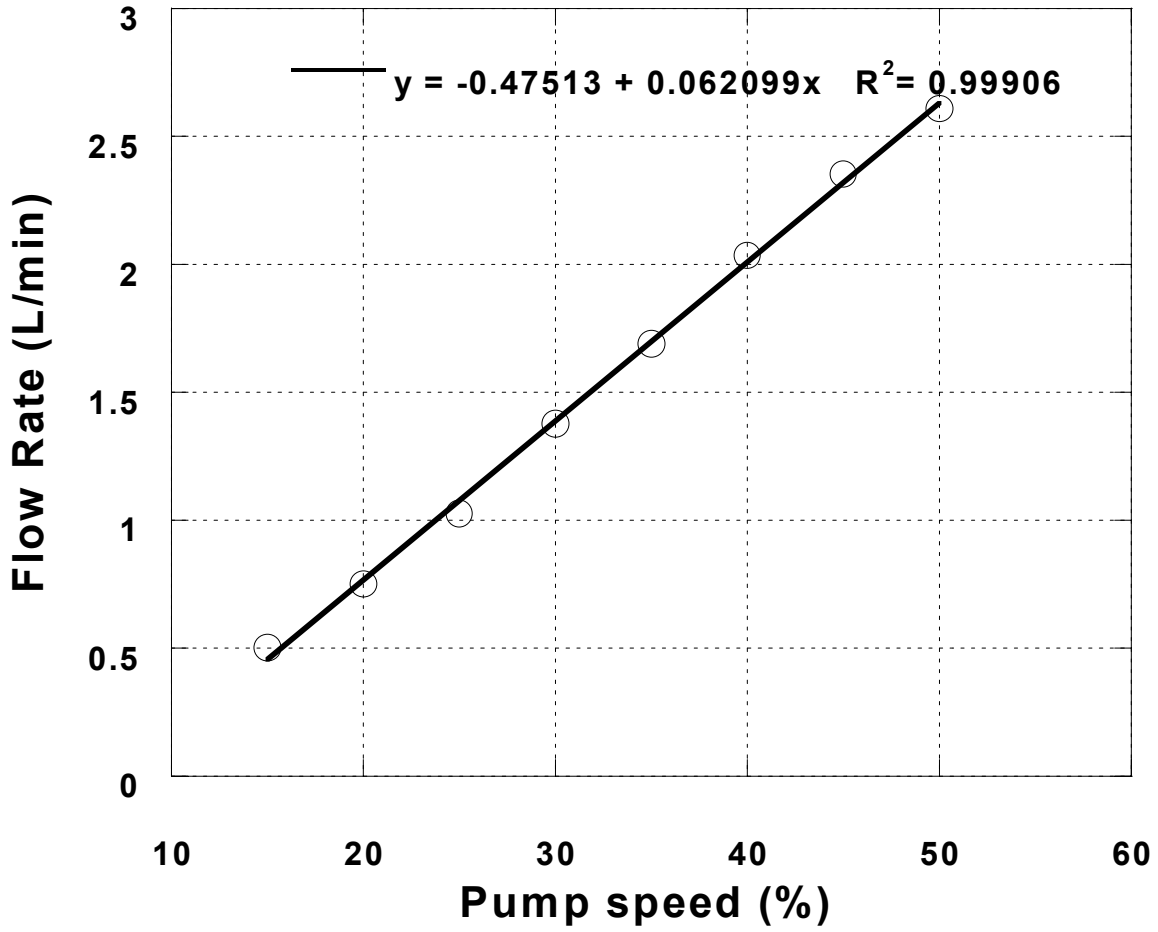

Figure A1. Filtration flow rate versus pumping speed

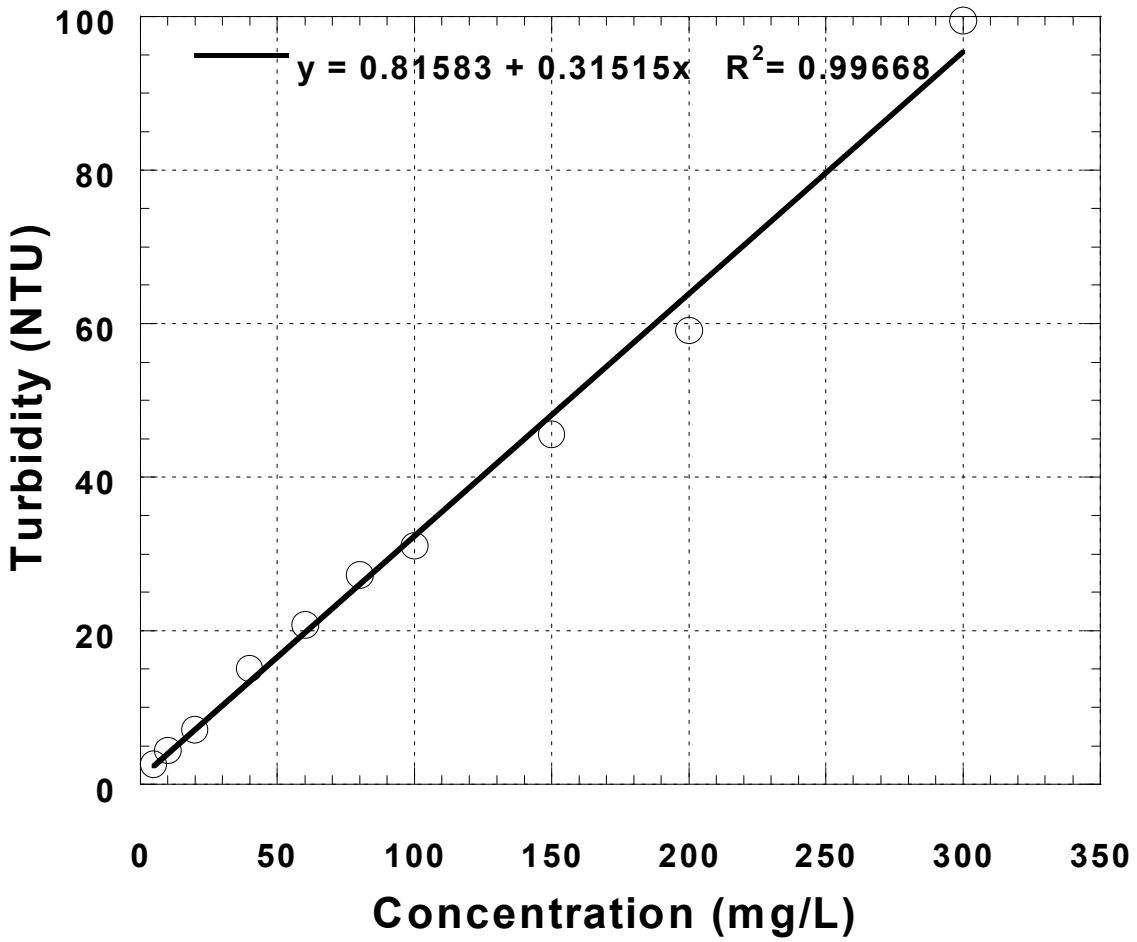

Figure A2. Calibration curve for γ-Al_2O_3 as measured by turbidity (NTU)

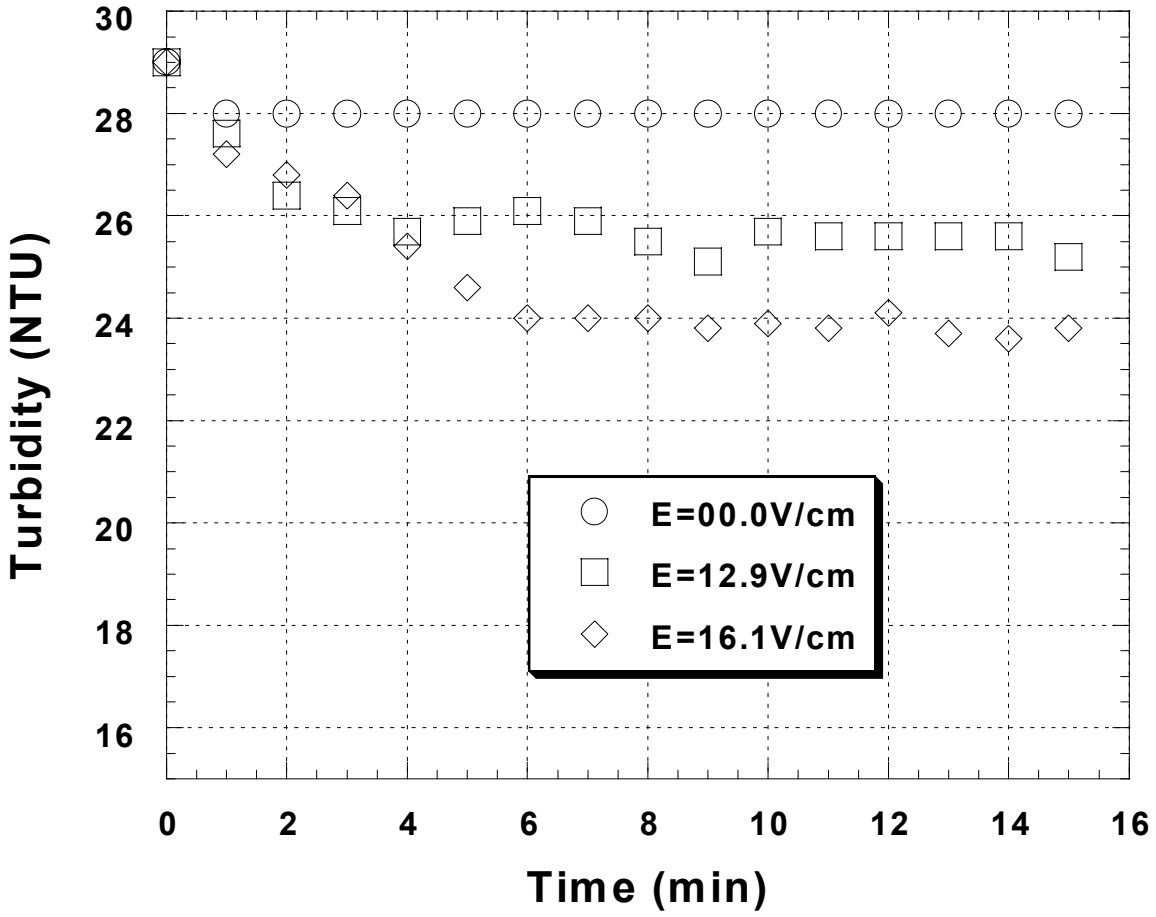

Figure A3. Effect of electrostatic field (I). Experimental conditions: 100 mg /L γ-Al_2O_3; pumping speed 20% (or filtration rate 0.77 mL/min).

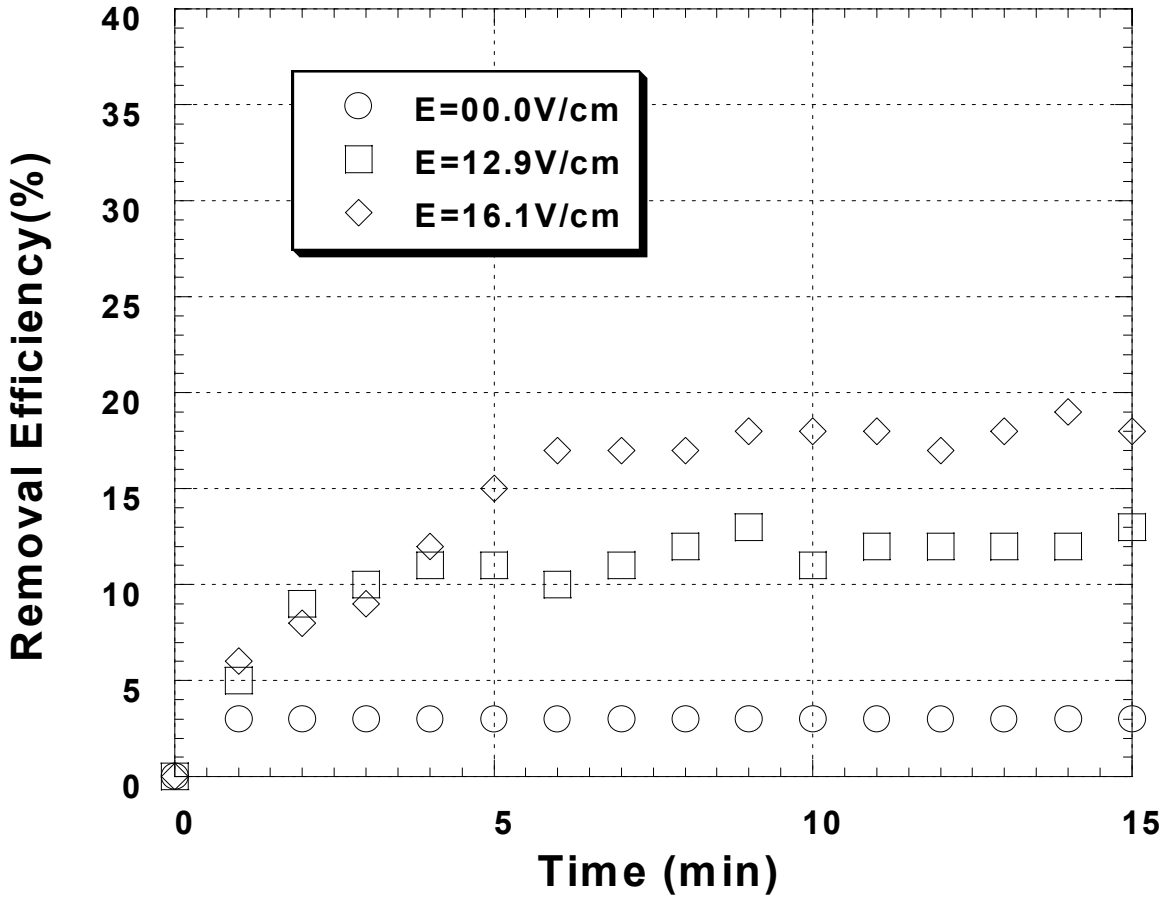

Figure A4. Effect of electrostatic field (II). Experimental conditions: 100 mg /L γ-Al_2O_3; pumping speed 20% (or filtration rate 0.77 mL/min).

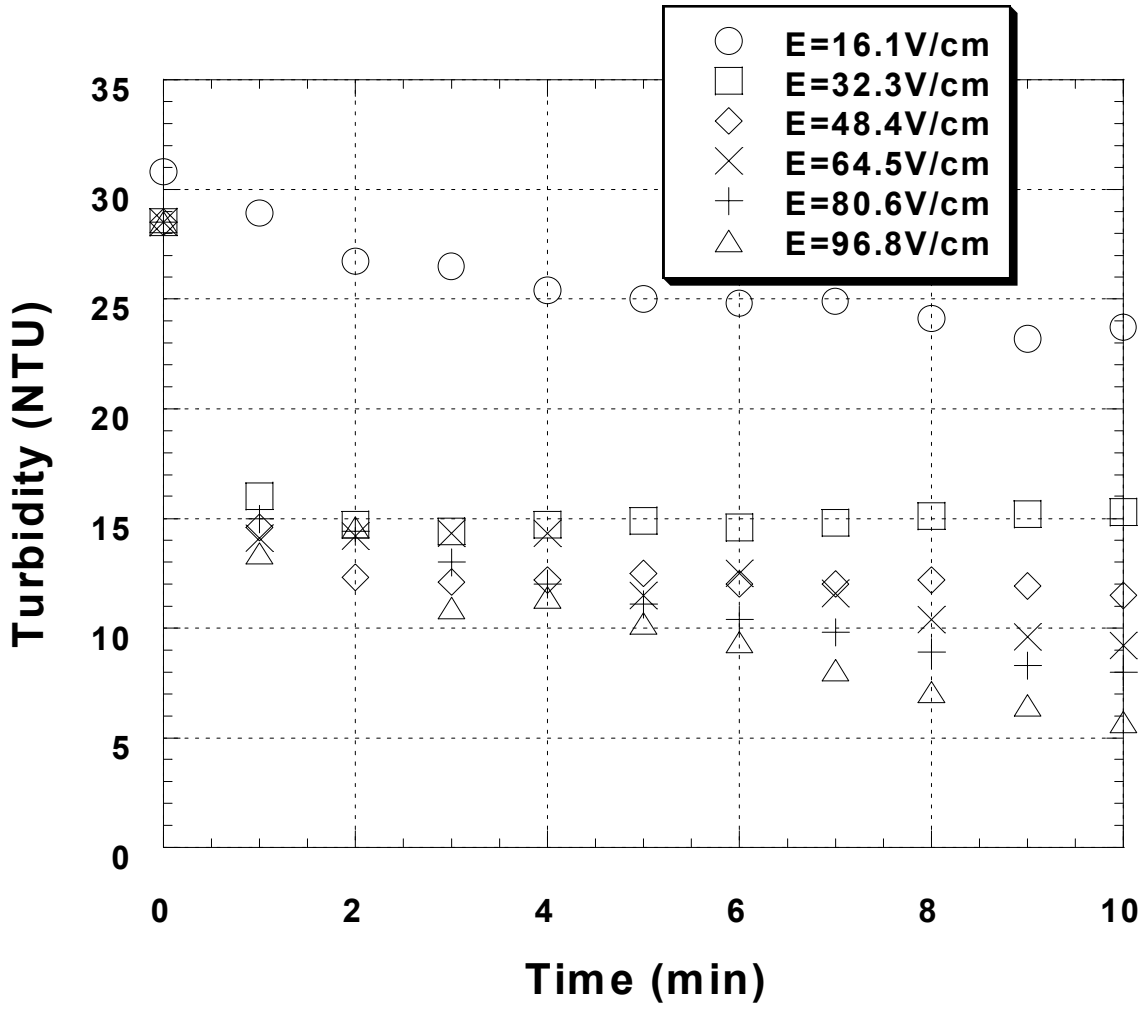

Figure A5. Effect of electrostatic field (III). Experimental conditions: 100 mg /L γ-Al_2O_3; pumping speed 15% (or filtration rate 0.46 mL/min).

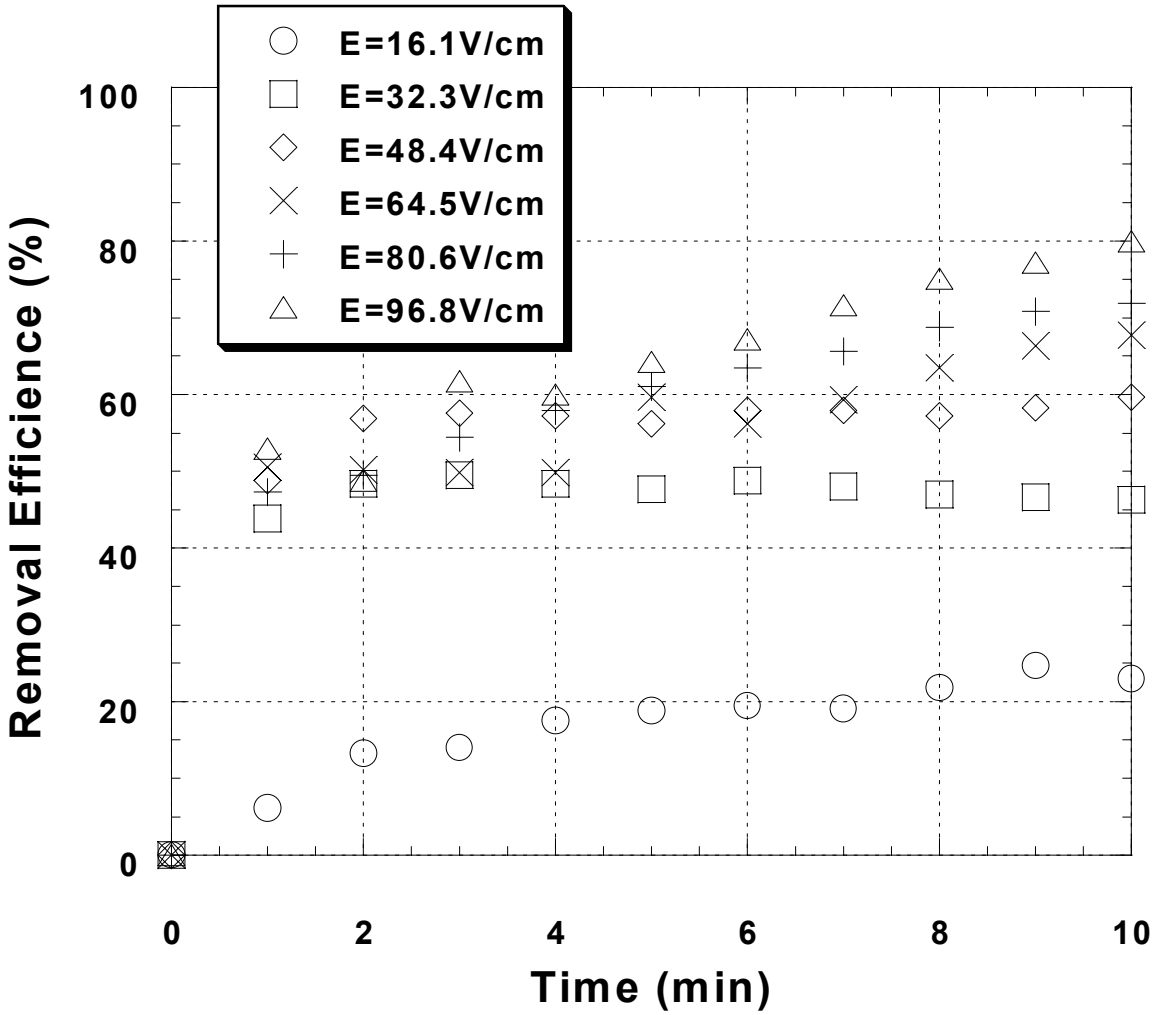

Figure A6. Effect of electrostatic field (IV). Experimental conditions: 100 mg /L γ-Al_2O_3; pumping speed 15% (or filtration rate 0.46 mL/min).

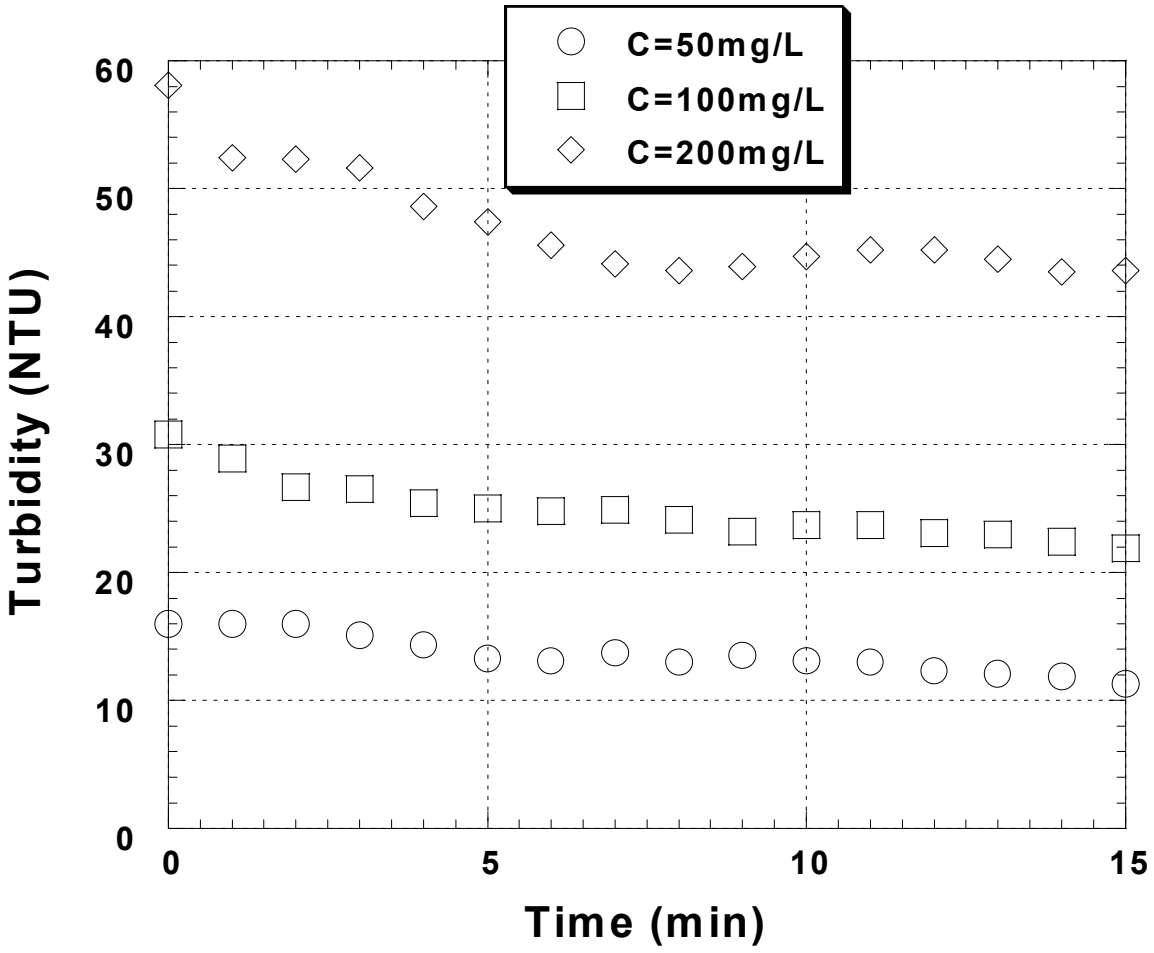

Figure A7. Effect of γ-Al_2O_3 concentration (I). Experimental conditions: pumping speed 15% (or filtration rate 0.46 mL/min); E = 16.1V/cm.

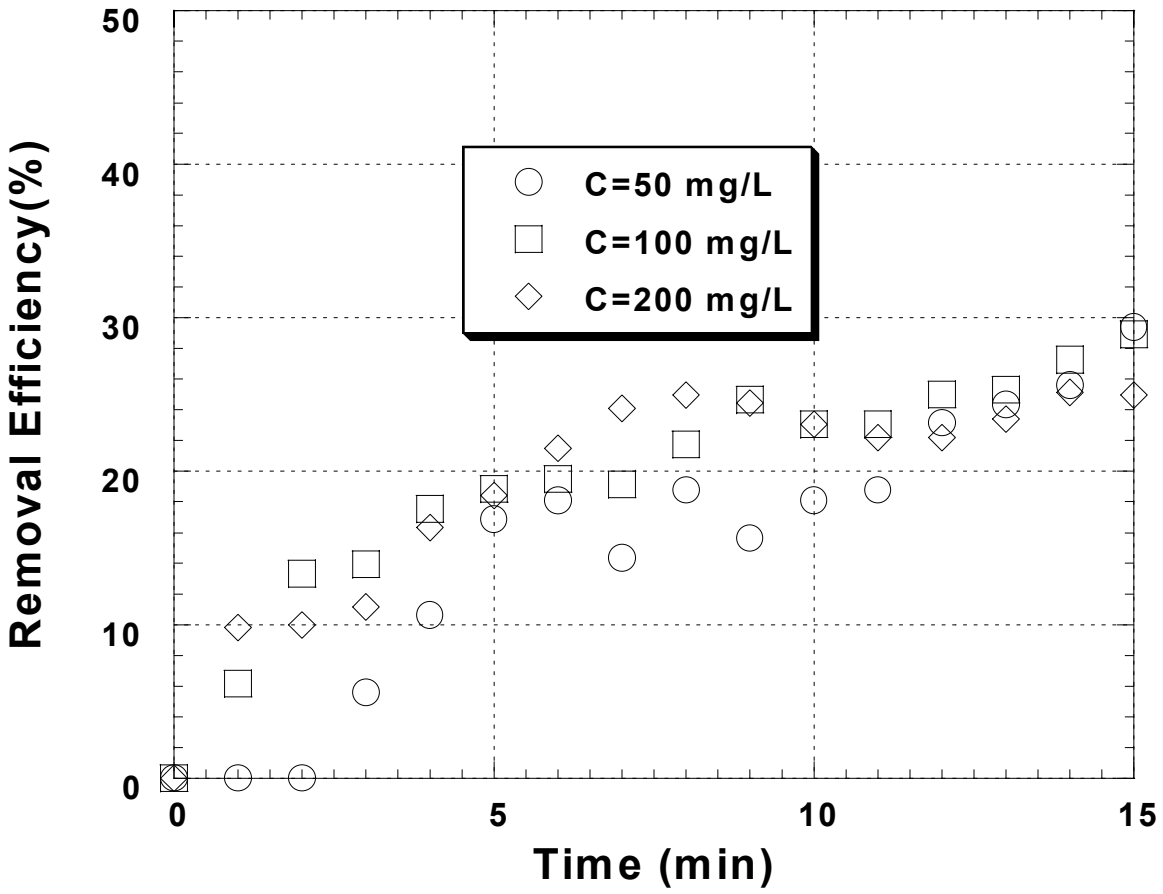

Figure A8. Effect of γ-Al_2O_3 concentration (II). Experimental conditions: pumping speed 15% (or filtration rate 0.46 mL/min); E = 16.1V/cm.

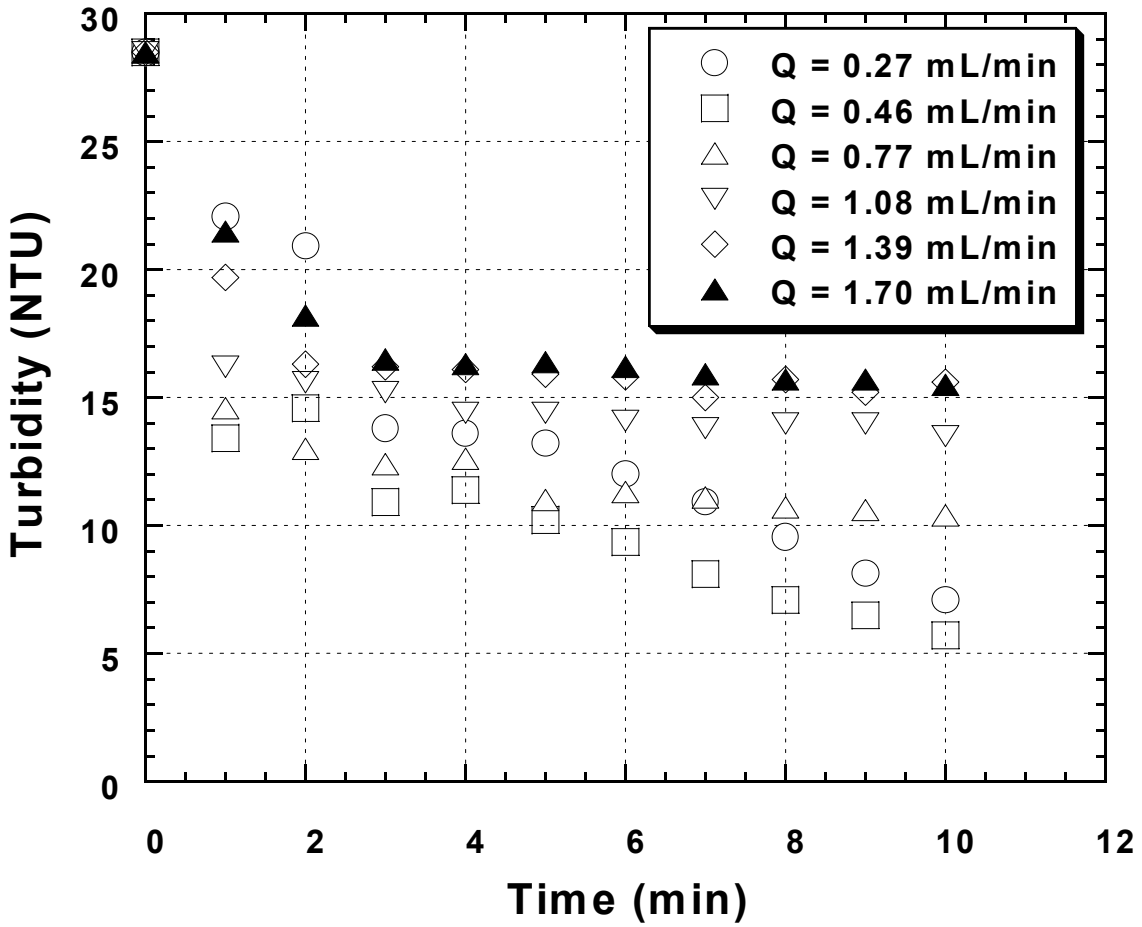

Figure A9. Effect of filtration rate on change of turbidity. Experimental conditions: 100mg/L γ-Al2O3; initial pH = 5.6; E = 96.8V/cm

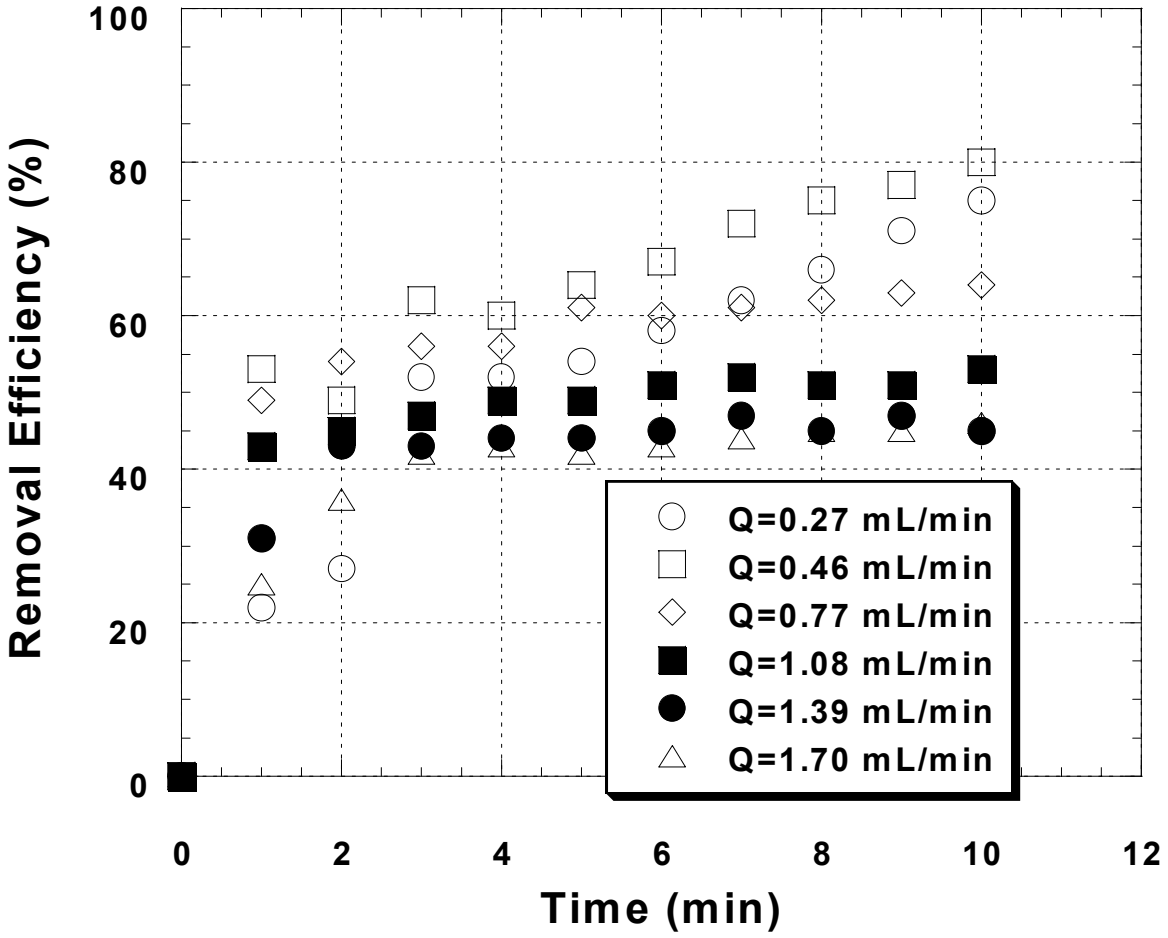

Figure A10. Effect of filtration rate on removal of colloidal particles (I). Experimental conditions: 100 mg/L γ-Al_2O_3; initial pH = 5.6; E = 96.8V/cm.

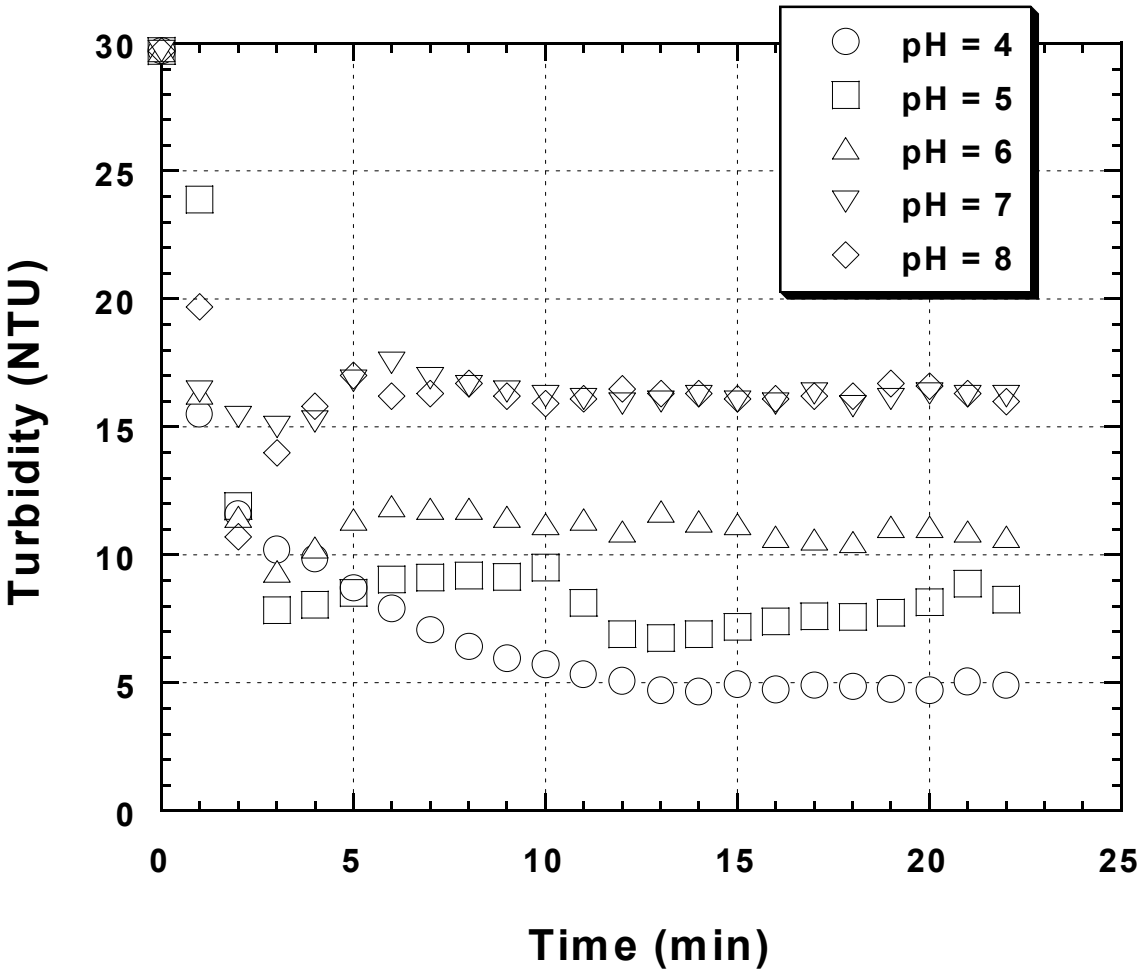

Figure A11. Effect of pH on the change of turbidity. Experimental conditions: 100mg/L γ-Al2O3; pumping speed 15% (or filtration rate 0.46 mL/min); E = 96.8V/cm.

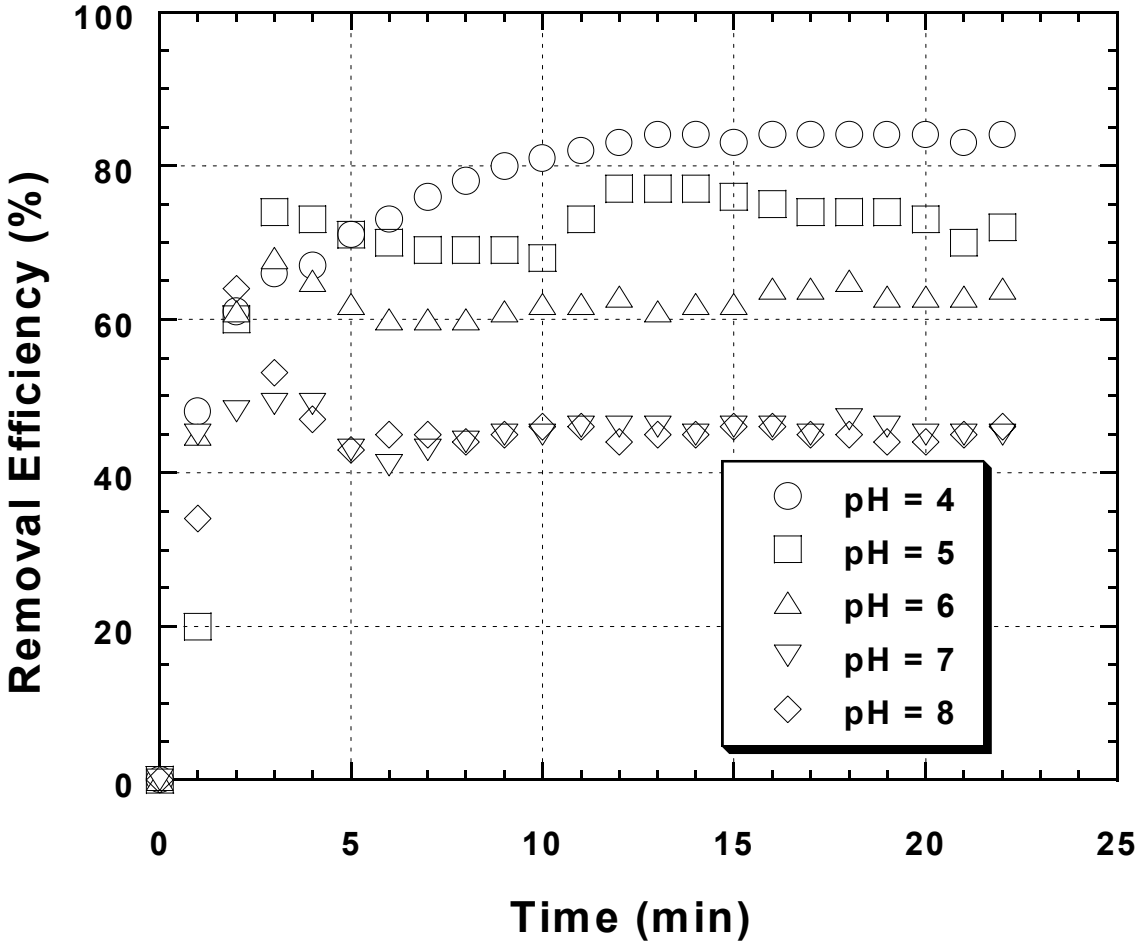

Figure A12. Effect of pH on the removal of colloidal particles (I). Experimental conditions: 100mg/L γ-Al_2O_3; pumping speeding 15% (or filtration rate 0.46 mL/min); E = 96.8V/cm.

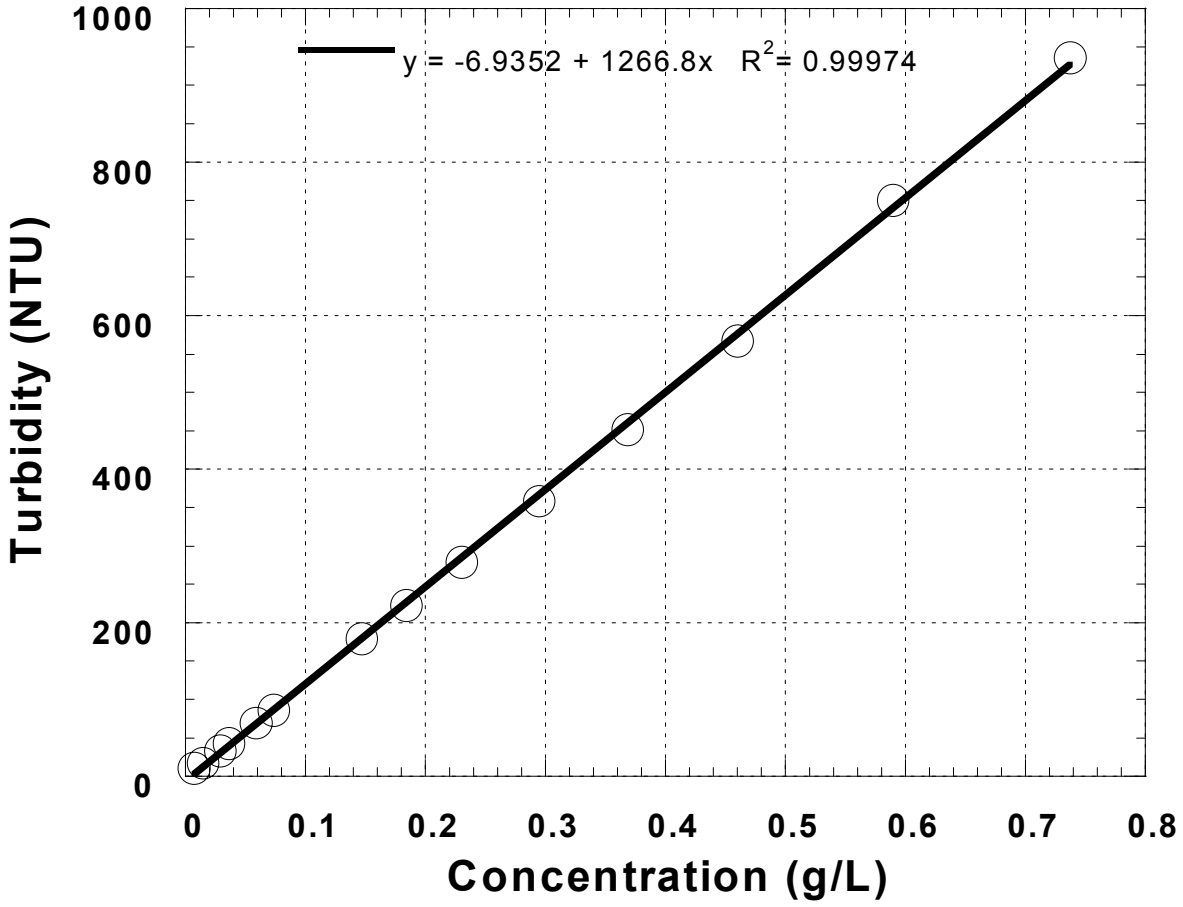

Figure A13. Calibration curve for turbidity (NTU) and particulate concentration of well water. (Well #10, bailing sample, 10IB01)

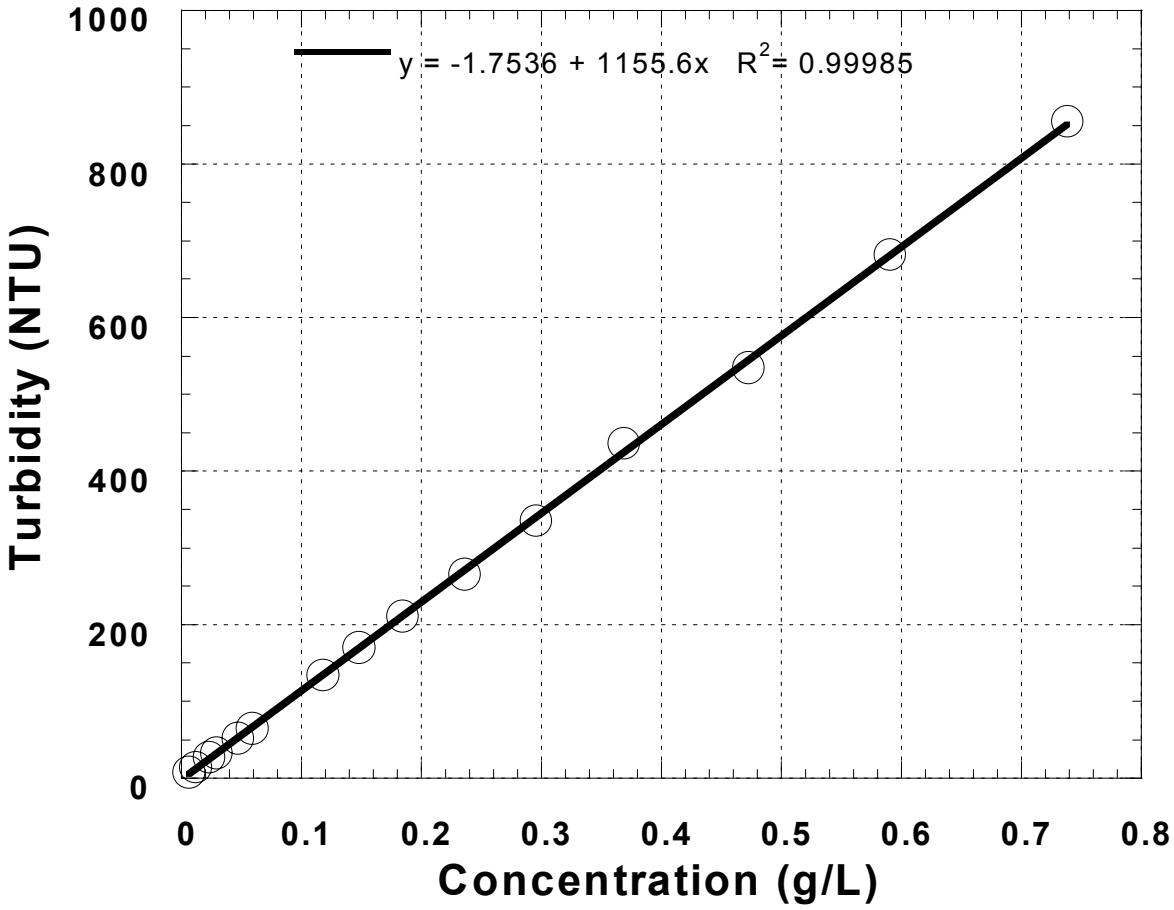

Figure A14. Calibration curve for turbidity (NTU) and particulate concentration of well water. (Well#10, low flow purging sample, 10IL01)

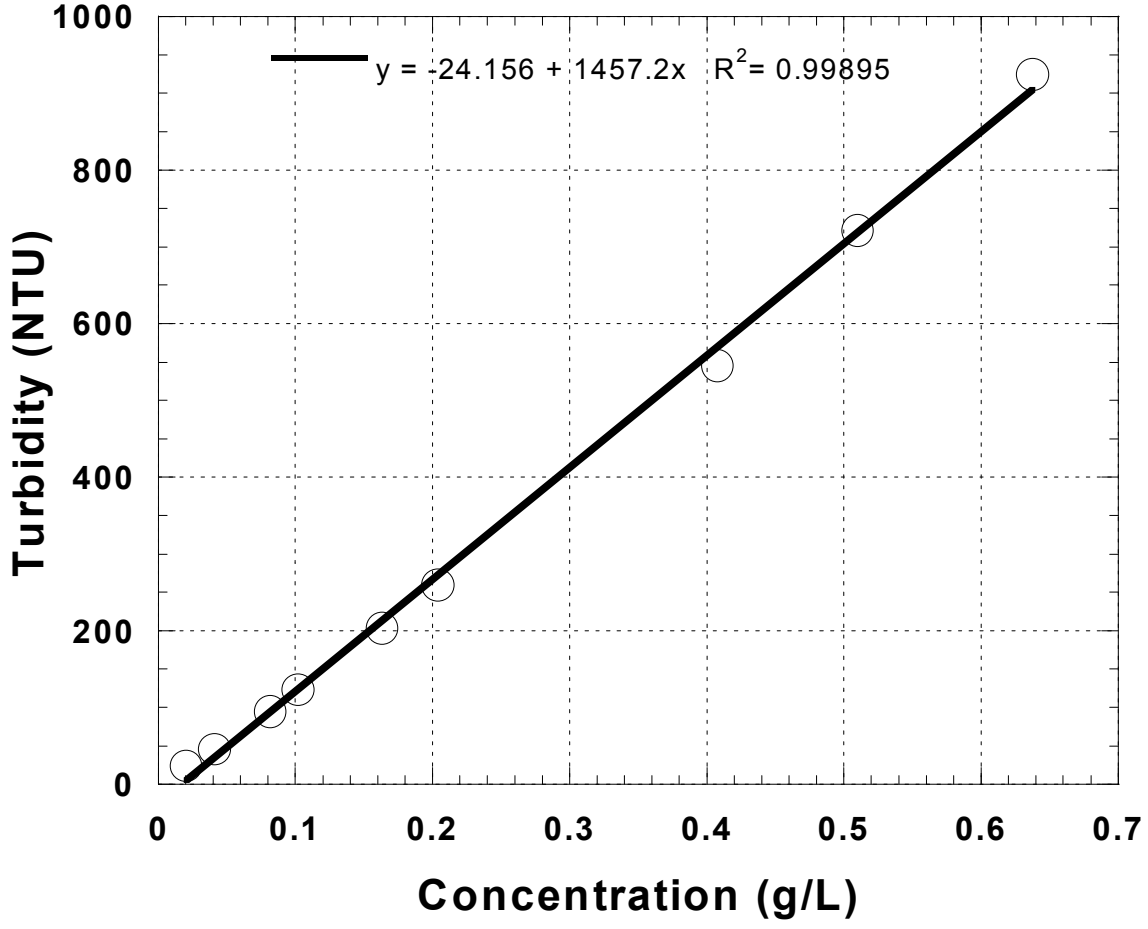

Figure A15. Calibration curve for turbidity (NTU) and particulate concentration of well water. (Well#5S, bailing sample, 5SIB01).

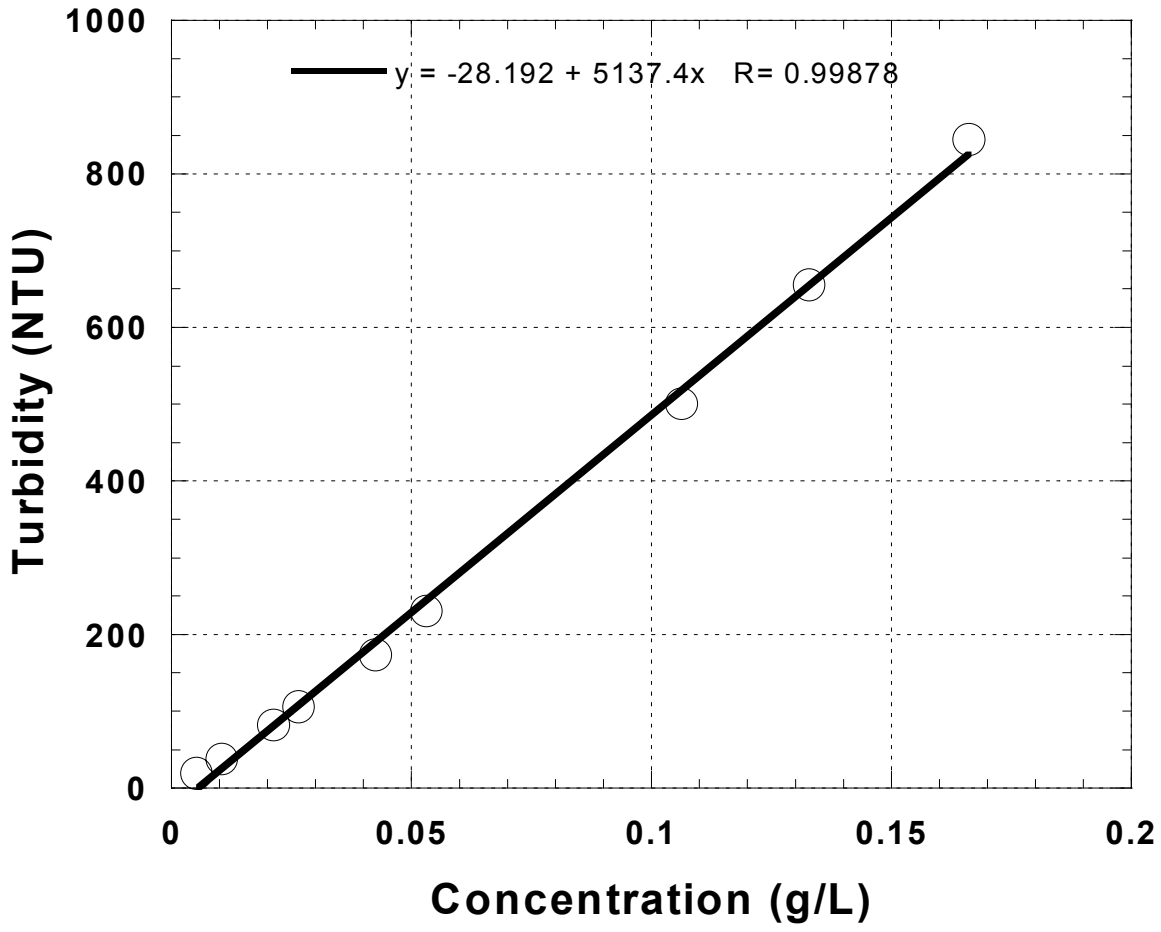

Figure A16. Calibration curve for turbidity (NTU) and particulate concentration of well water. (Well#5S, low flow purging sample, 5SIL02).

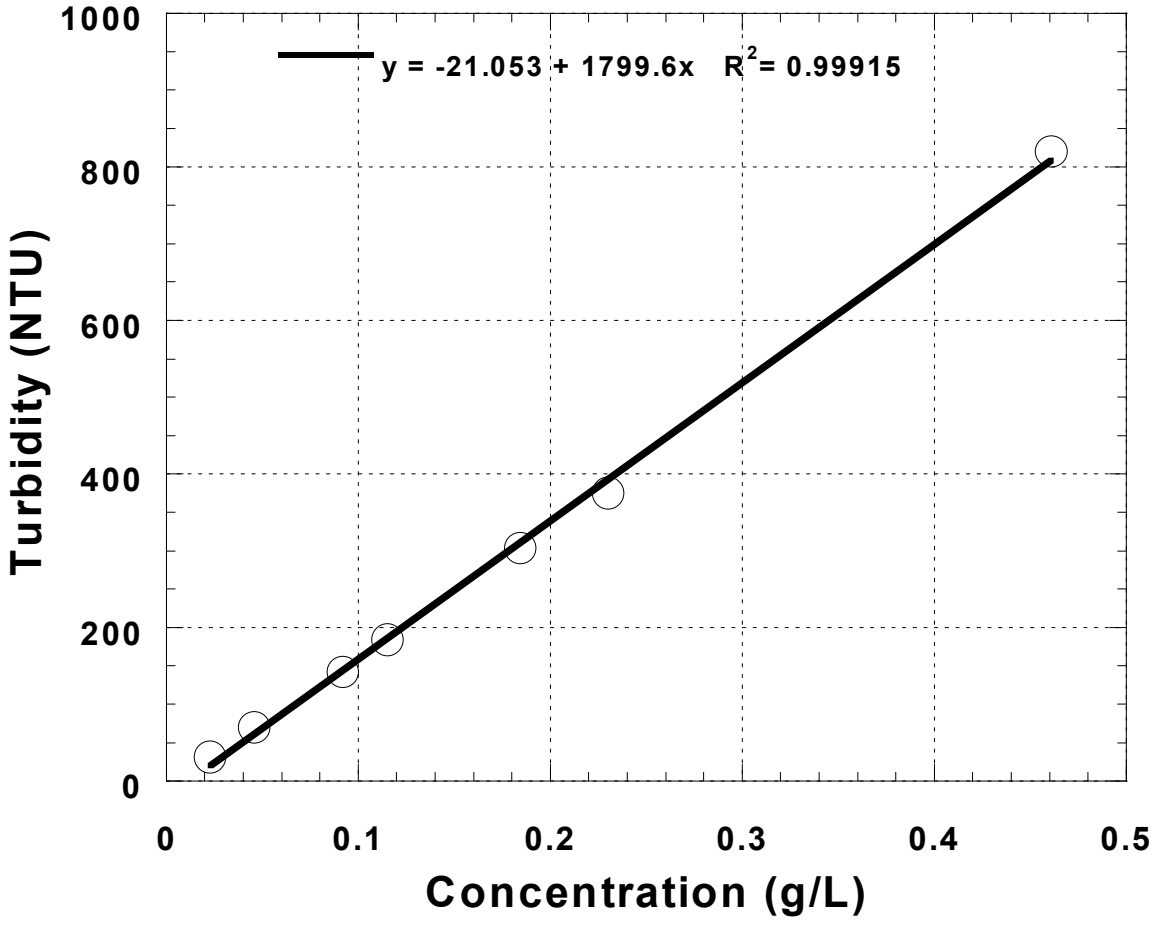

Figure A17. Calibration curve for turbidity (NTU) and particulate concentration of well water. (Well#5S, bailing sample, 5SIIB03).

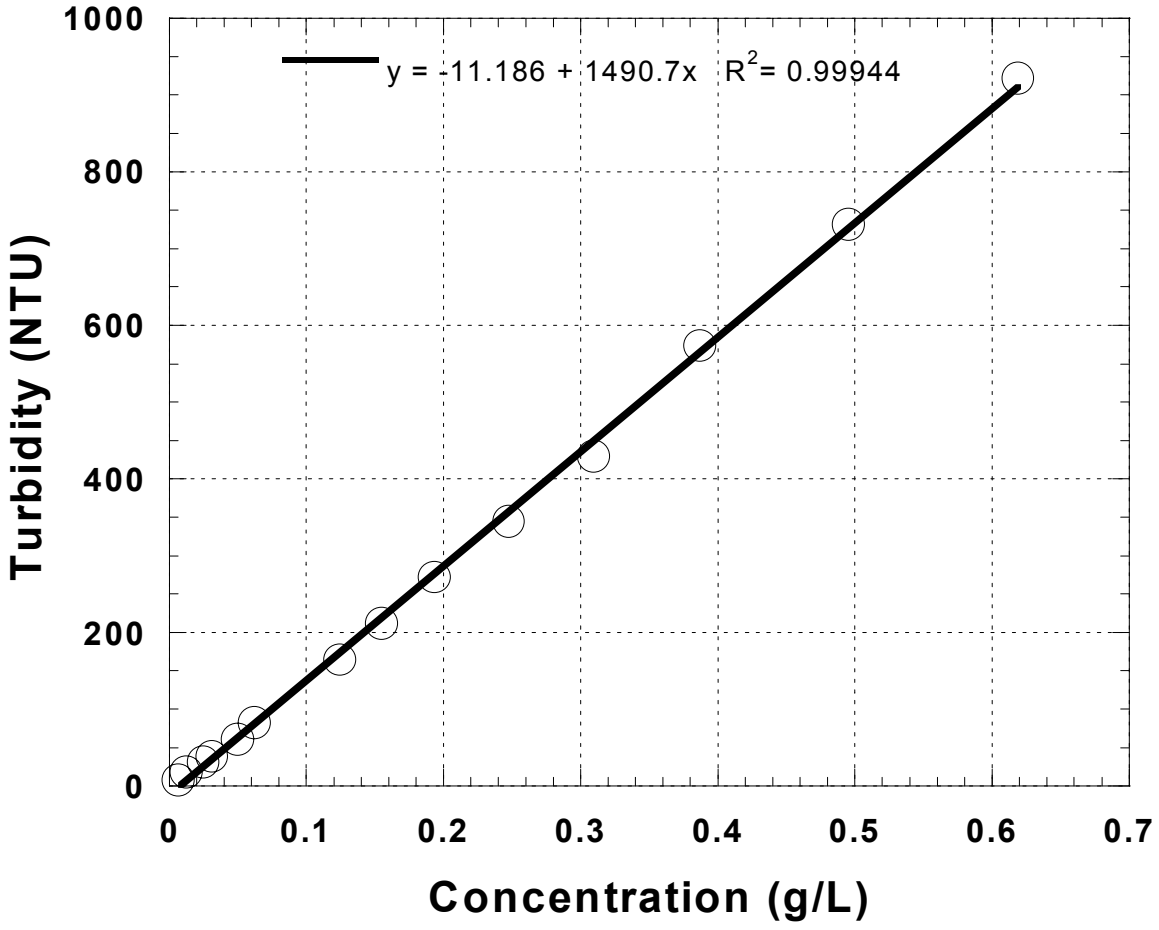

Figure A18. Calibration curve for turbidity (NTU) and particulate concentration of well water. (Well#5S, low flow purging sample, 5SIIL01).

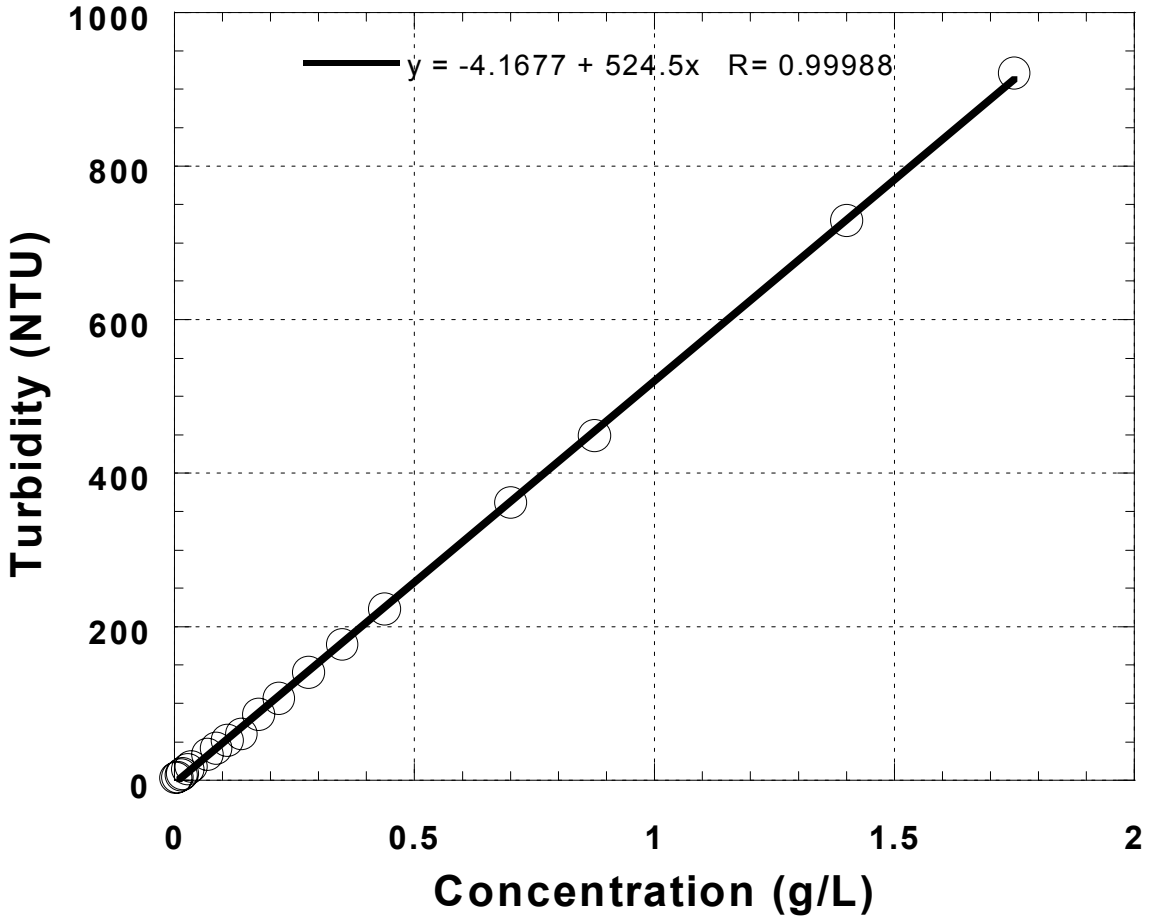

Figure A19. Calibration curve for turbidity (NTU) and particulate concentration of well water. (Well#MW3, bailing sample, MW3IB03).

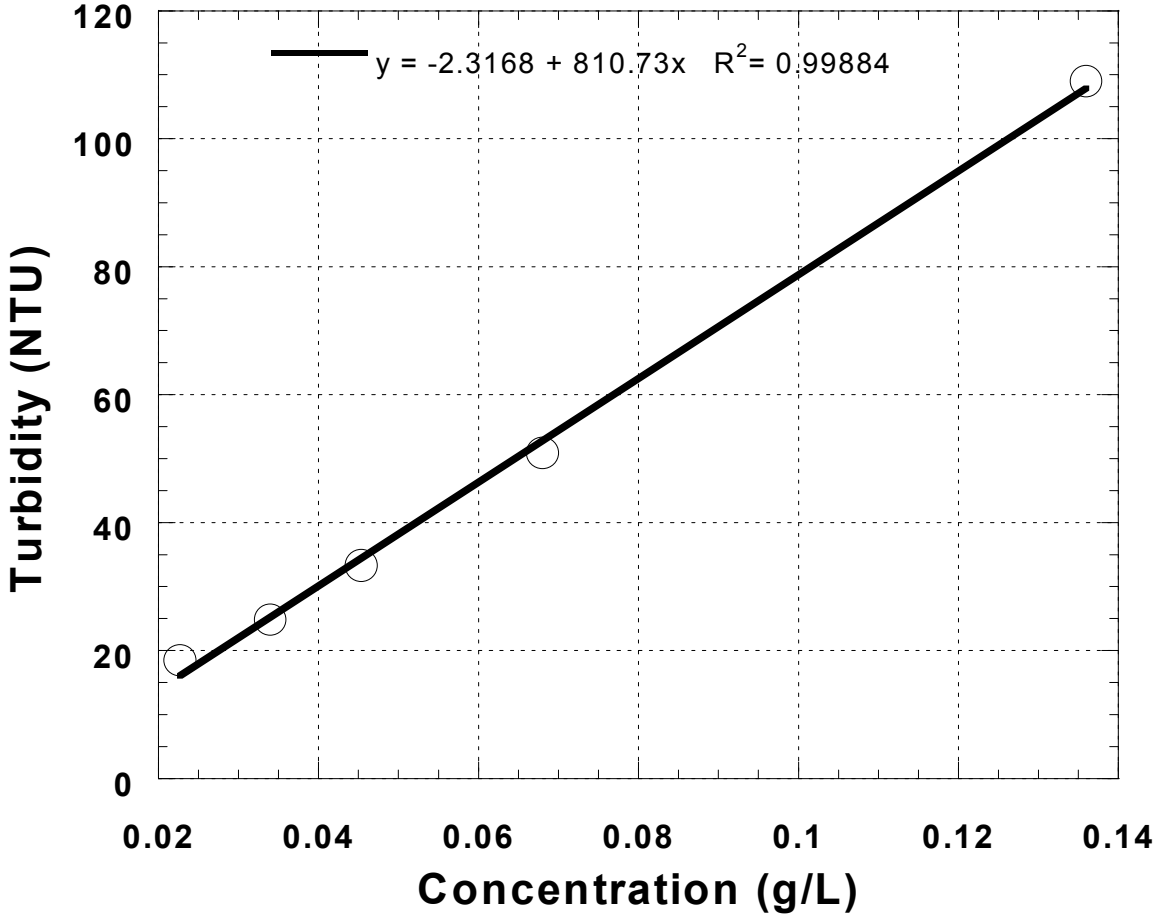

Figure A20. Calibration curve for turbidity (NTU) and particulate concentration of well water. (Well#MW3, low flow purging sample, MW3IL01).

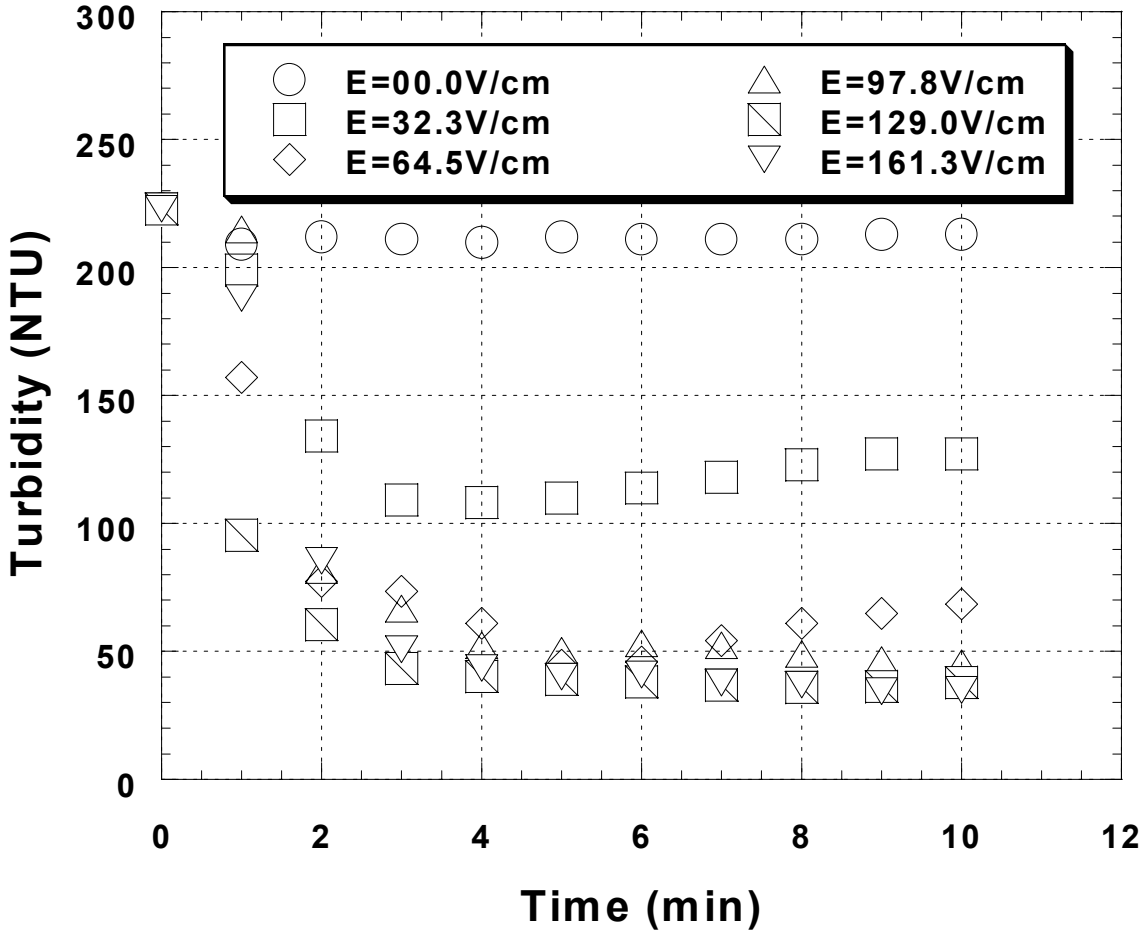

Figure A21. Change of filtrate turbidity as a function of time under various electrostatic field values (I). Experimental condition: pH = 6.5; Sample = 10IB01.

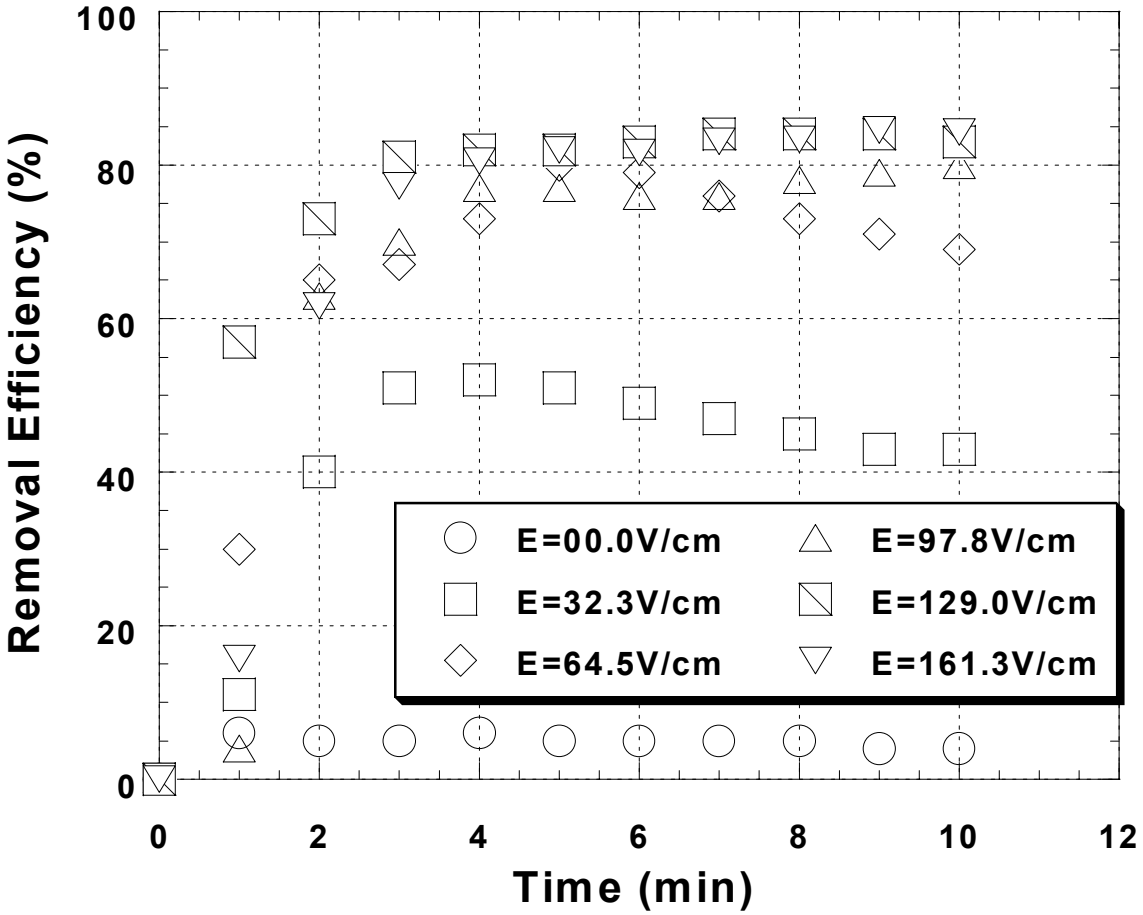

Figure A22. Change of filtrate turbidity as a function of time under various electrostatic field values (II). Experimental condition: pH = 6.5; Sample = 10IB01.

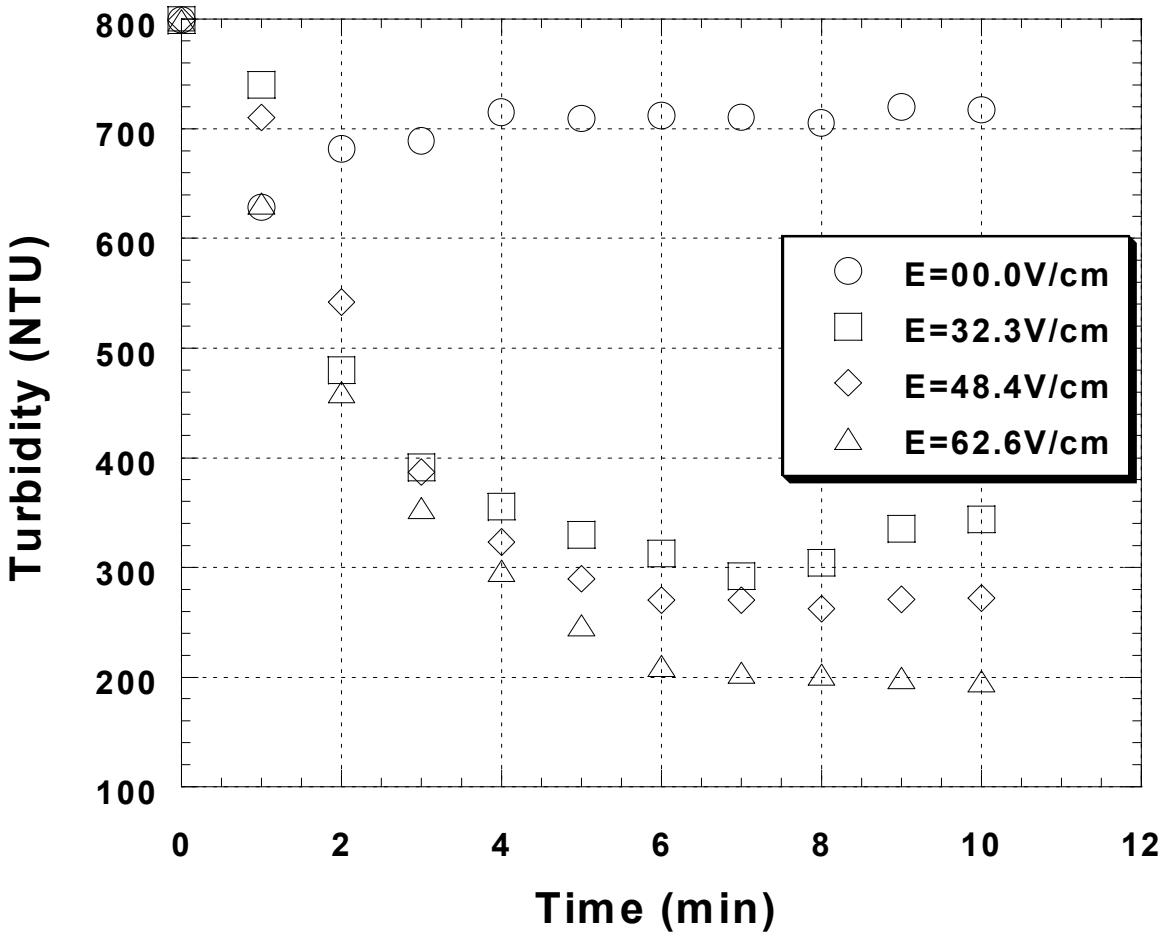

Figure A23. Change of filtrate turbidity as a function of time under various electrostatic field values (II). Experimental condition: pH = 6.5; Sample = 10IB01.

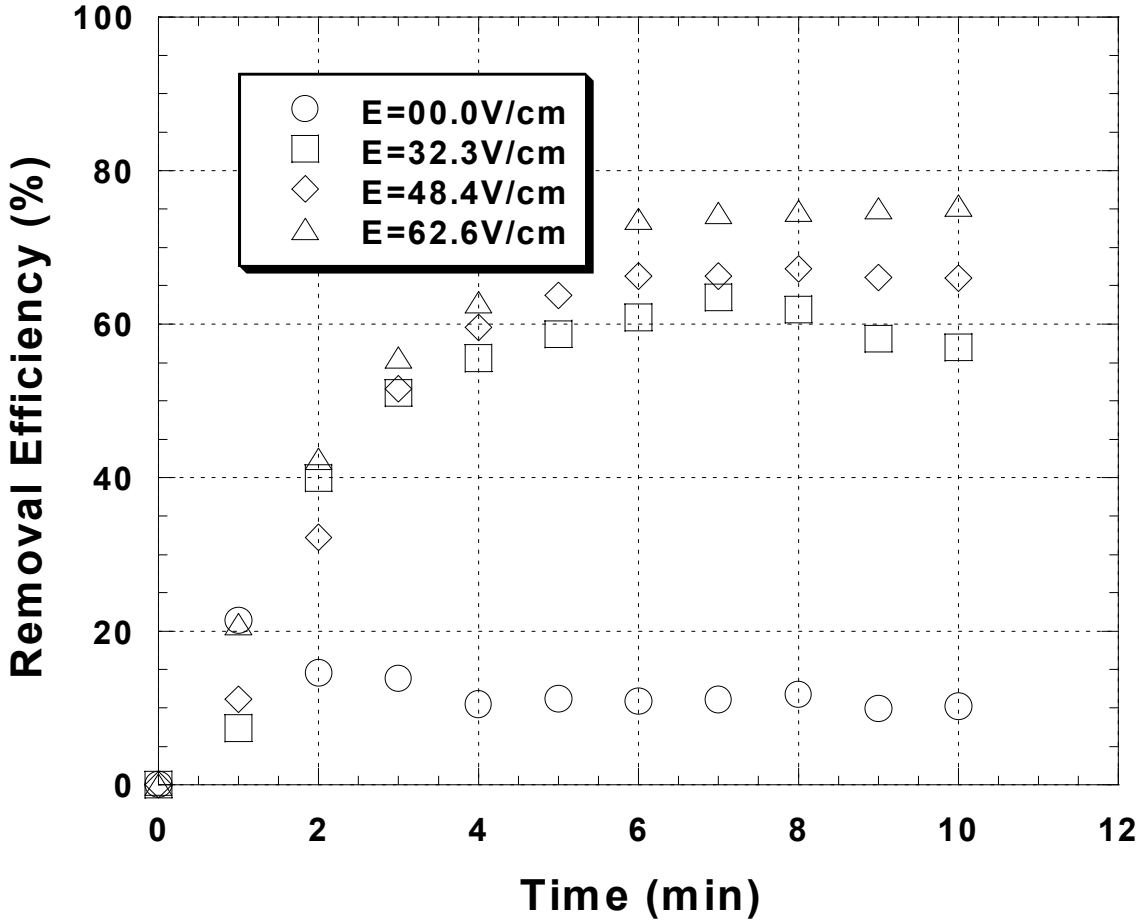

Figure A24. Change of filtrate turbidity as a function of time under various electrostatic field values (III). Experimental condition: pH = 6.5; Sample = 10IB01.

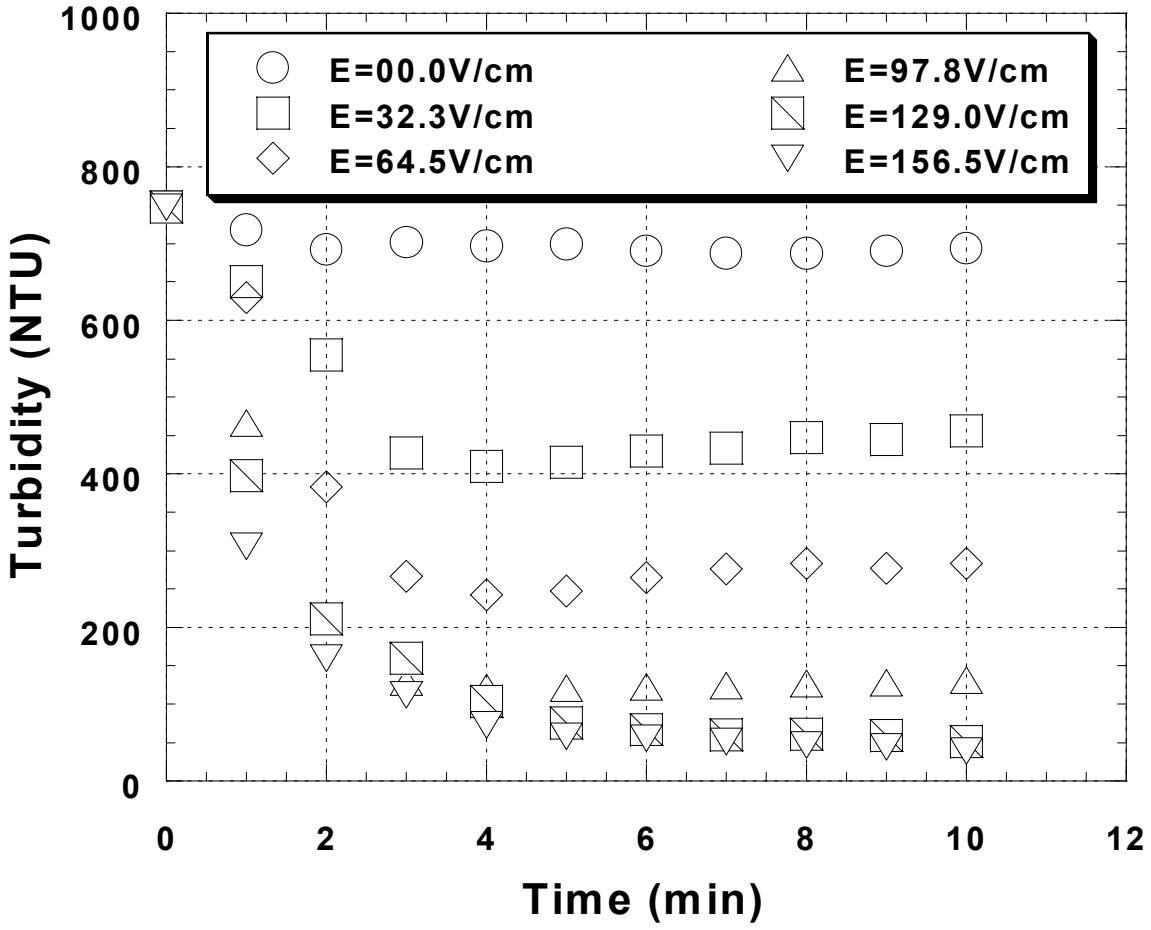

Figure A25. Turbidity changes as a function of time at various electrostatic field values. Experimental condition: pH = 6.6; Sample = 5SIIB03.

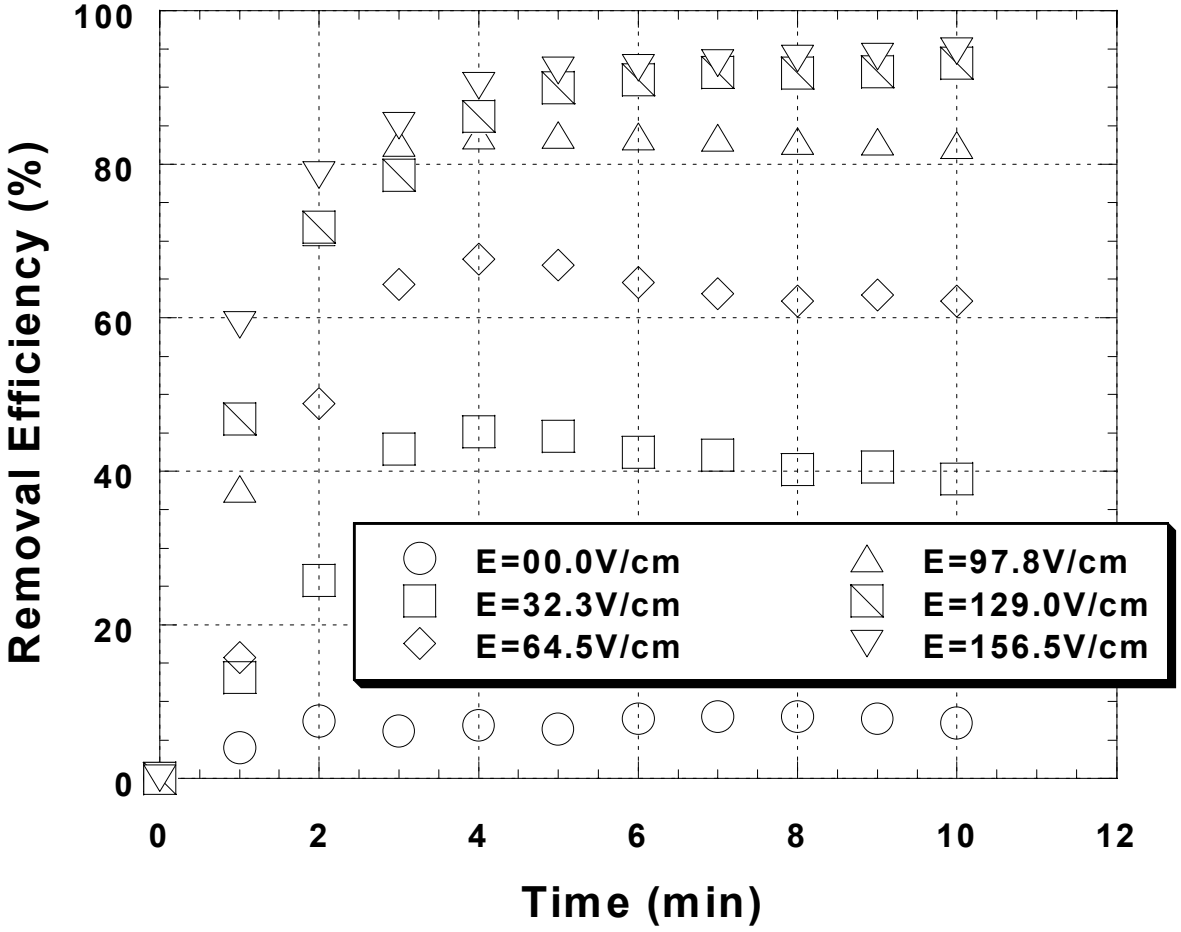

Figure A26. Removal efficiency as a function of time at various electrostatic field values (I). Experimental condition: pH = 6.6; Sample = 5SIIB03.

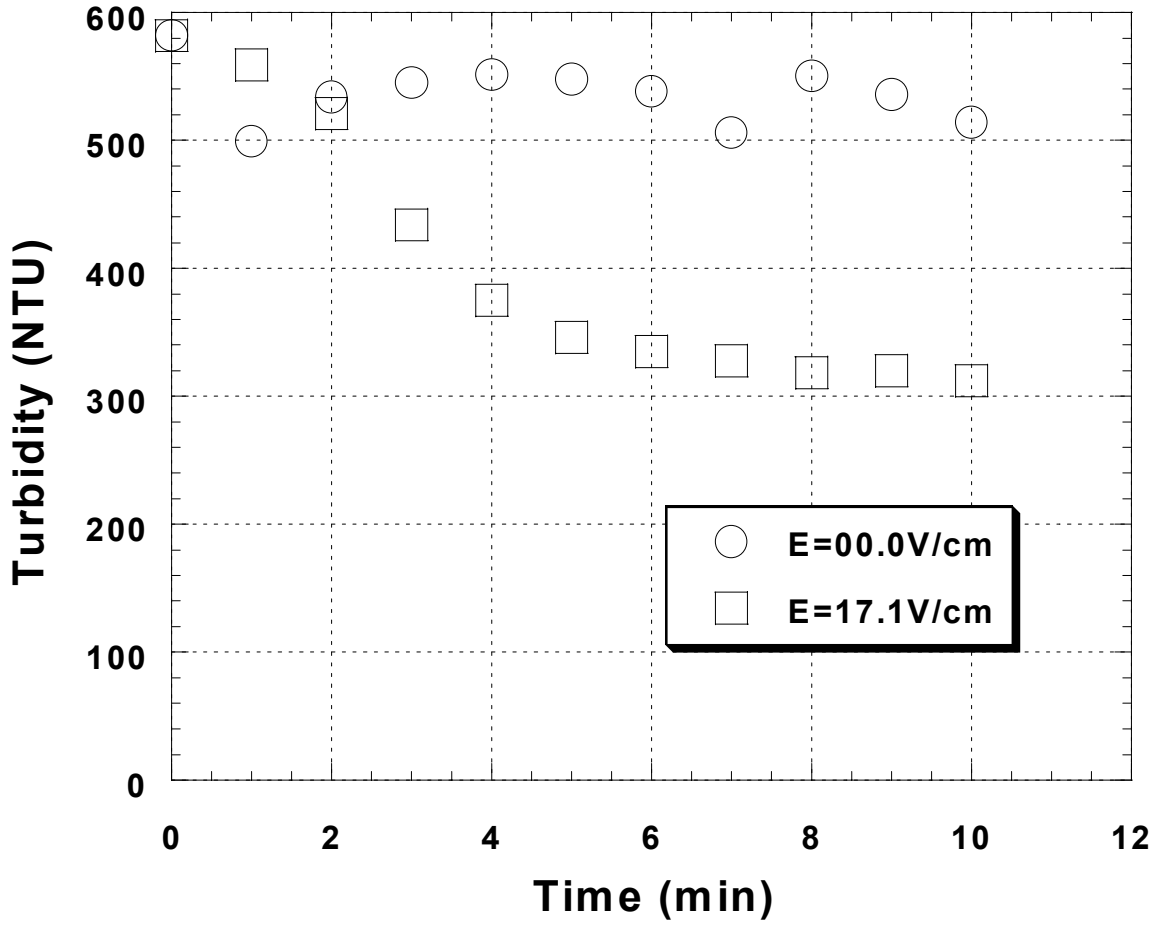

Figure A27. Turbidity changes as a function of time at various electrostatic field values. Experimental condition: pH = 7.9; Sample = MW3IB02.

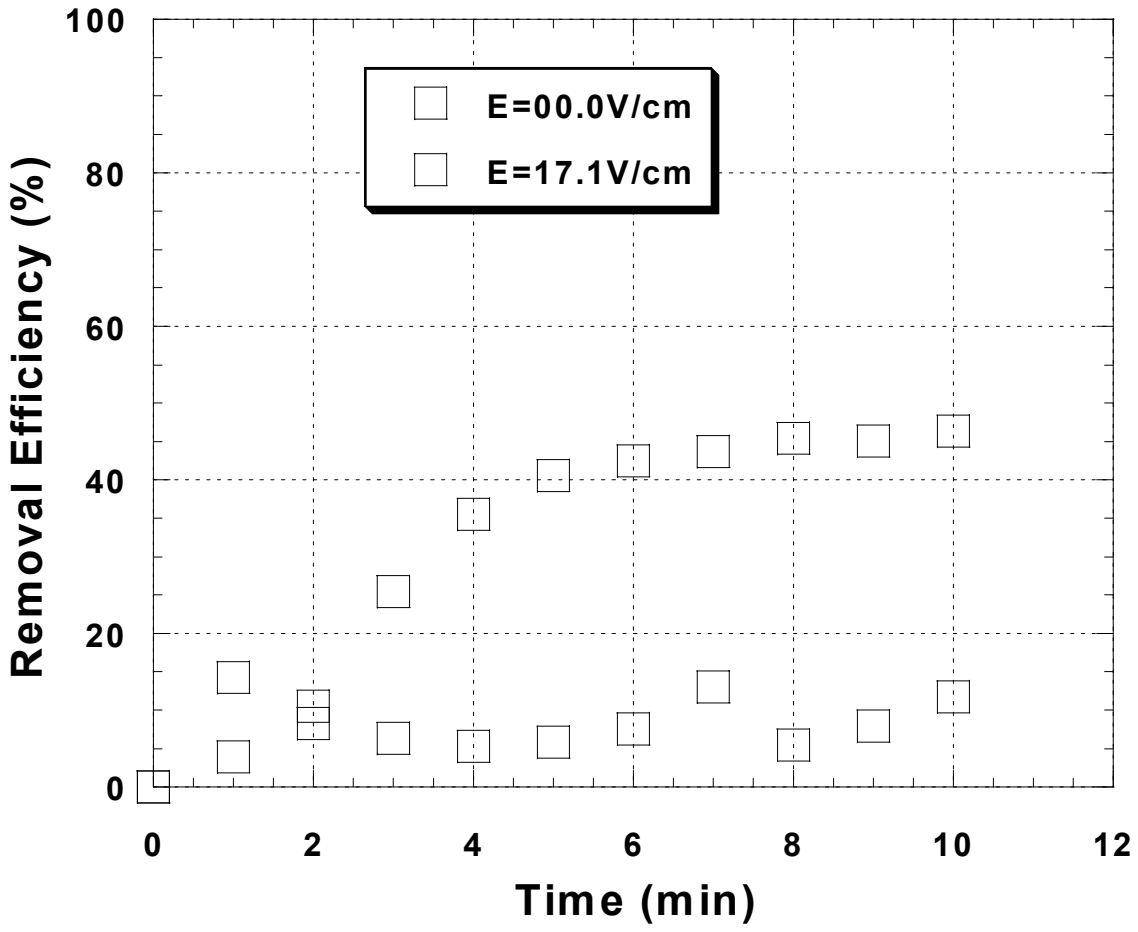

Figure A28. Removal efficiency as a function of time at various electrostatic field values (I). Experimental condition: pH = 7.9; Sample = MW3IB02.

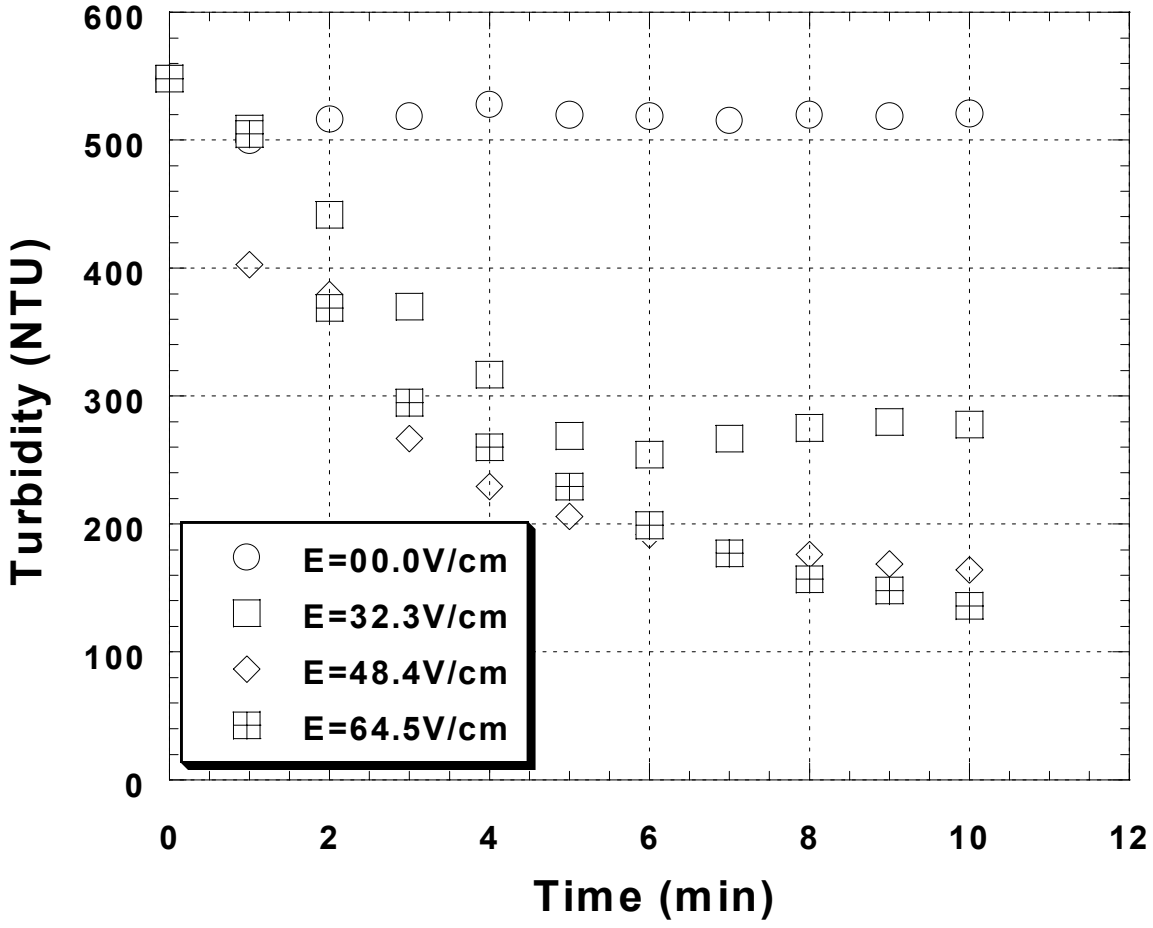

Figure A29. Turbidity changes as a function of time at various electrostatic field values. Experimental condition: pH = 5; Sample = 10IL01.

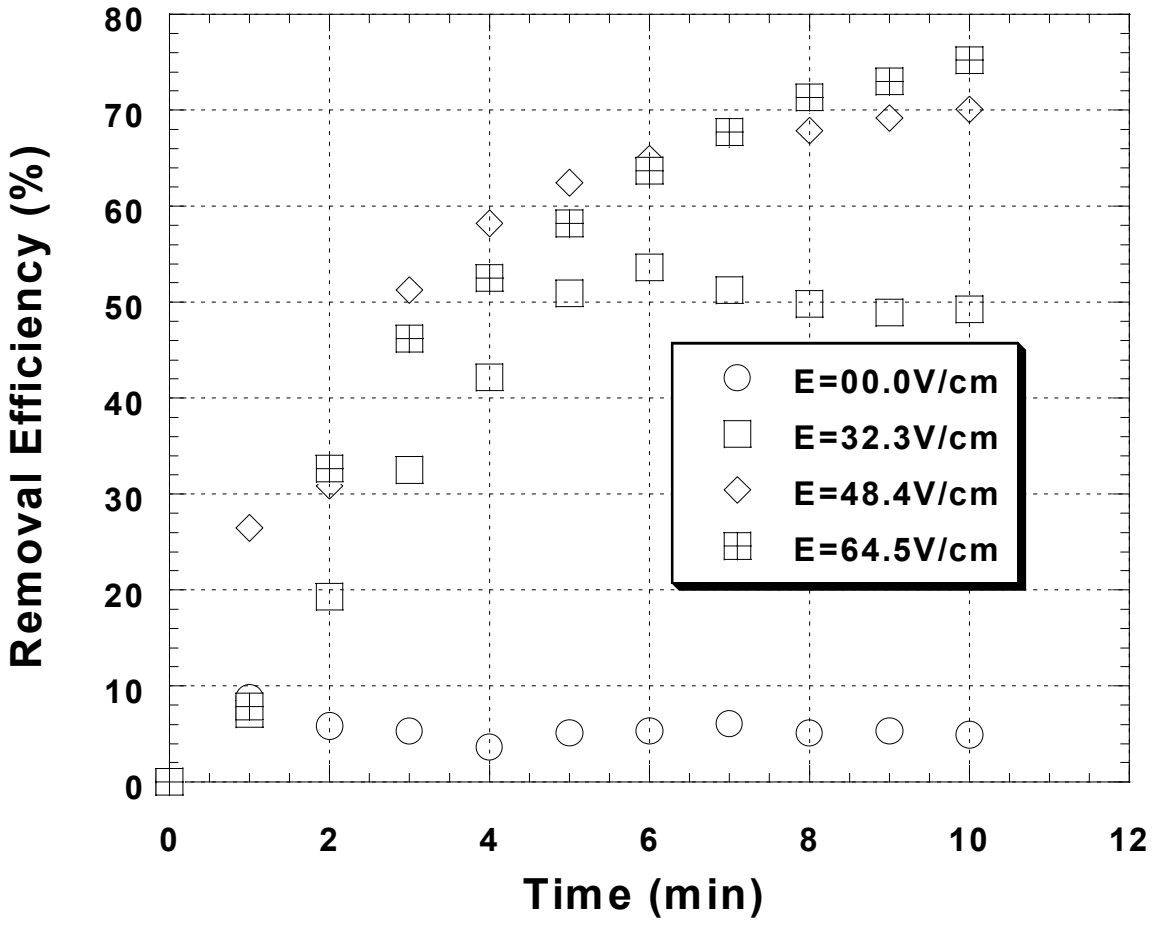

Figure A30. Removal efficiency as a function of time at various electrostatic field values (I). Experimental condition: pH = 5; Sample = 10IL01.

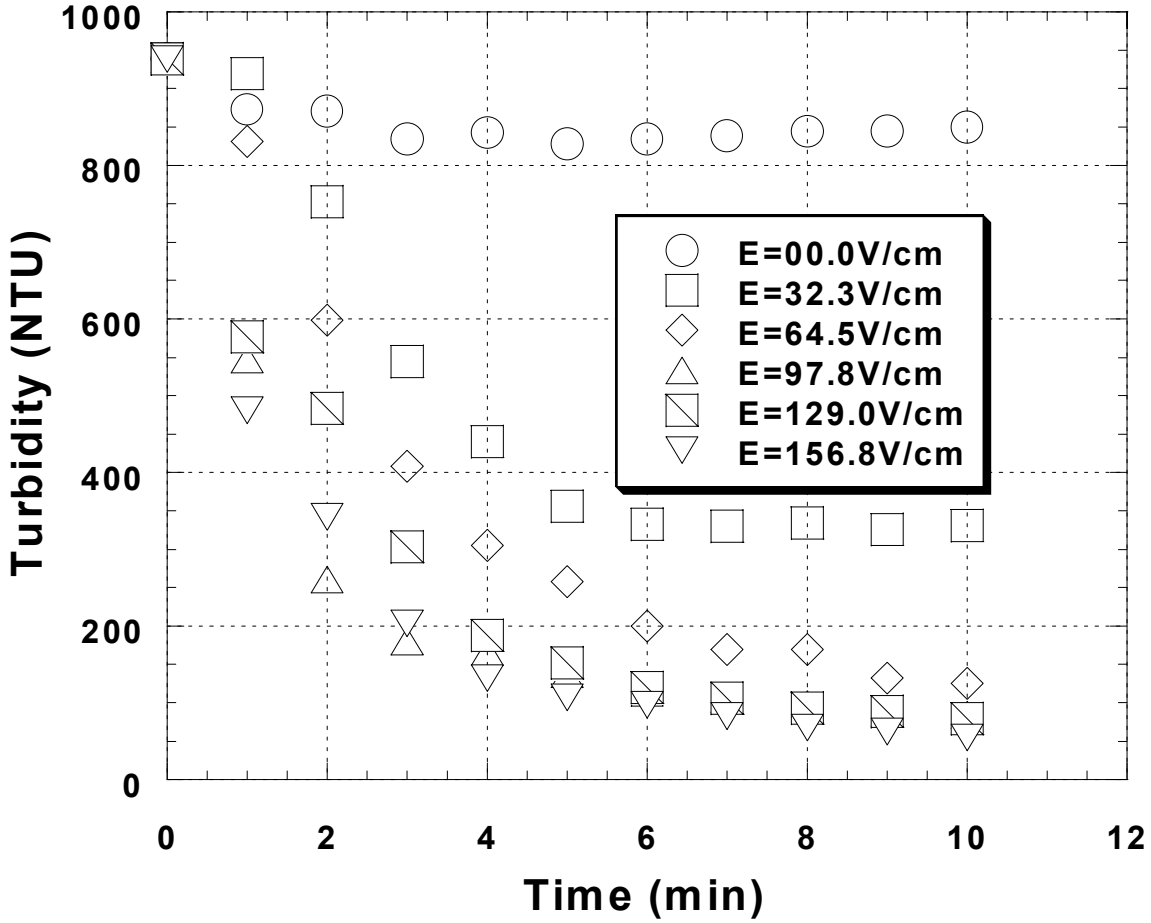

Figure A31. Turbidity changes as a function of time at various electrostatic field values. Experimental condition: pH = 6.7; Sample = 5SIIL02.

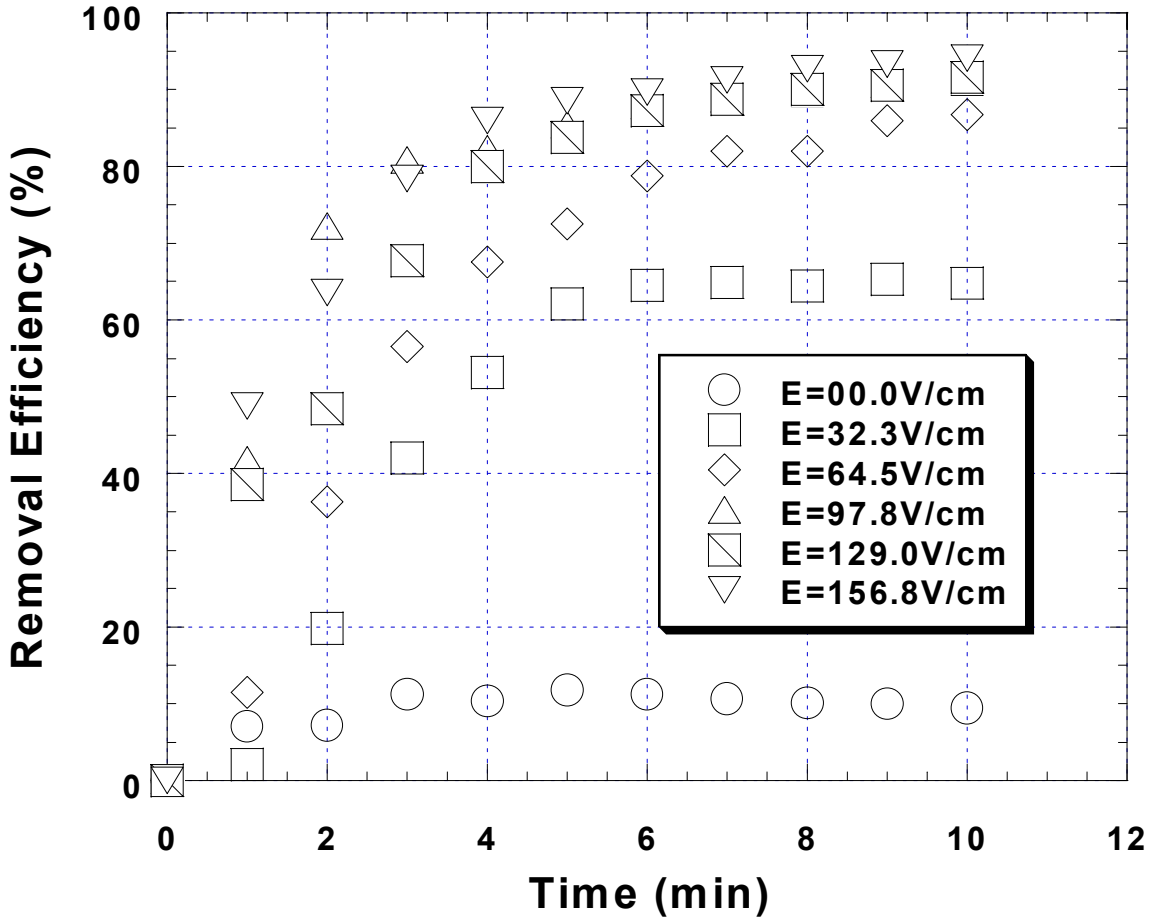

Figure A32. Removal efficiency as a function of time at various electrostatic field values (I). Experimental condition: pH = 6.7; Sample = 5SIL02.

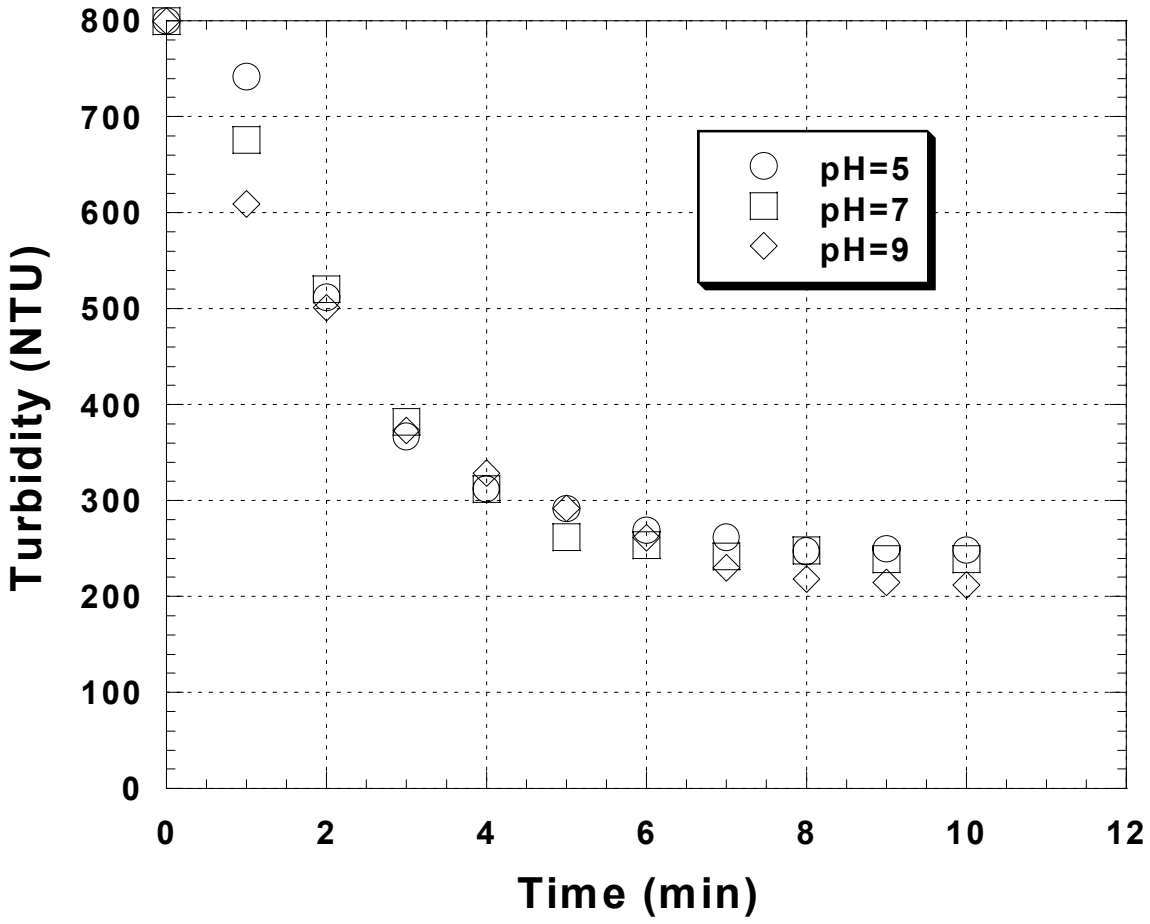

Figure A33. Change of turbidity as a function of time at various pH values. Experimental conditions: pH = 5 (electrostatic field = 32.3V/cm); pH = 7 (electrostatic field = 48.4V/cm); pH = 9 (electrostatic field = 48.4V/cm); Sample = 10IB01.

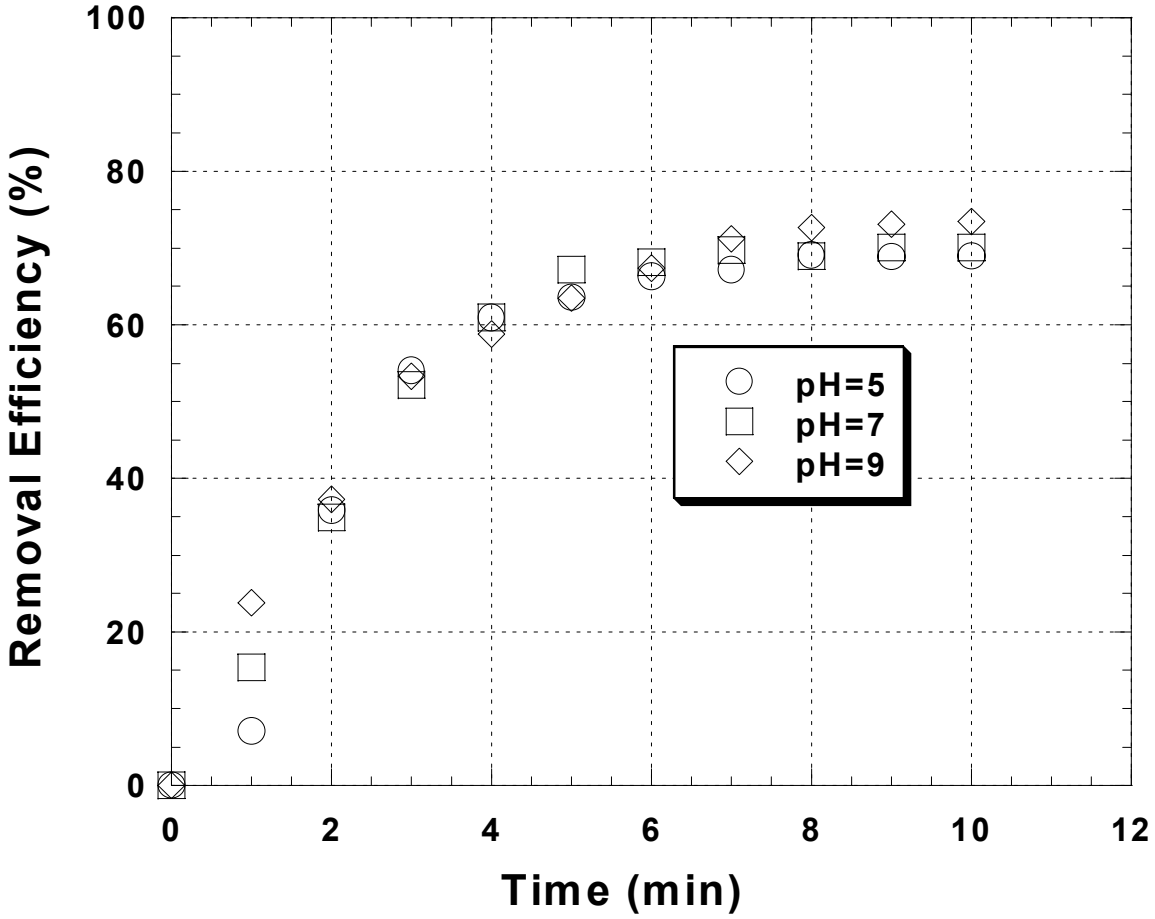

Figure A34. Removal efficiency as a function of time at various pH values (I). Experimental conditions: pH = 5 (electrostatic field = 32.3V/cm); pH = 7 (electrostatic field = 48.4V/cm); pH = 9 (electrostatic field = 48.4V/cm); Sample = 10IB01.

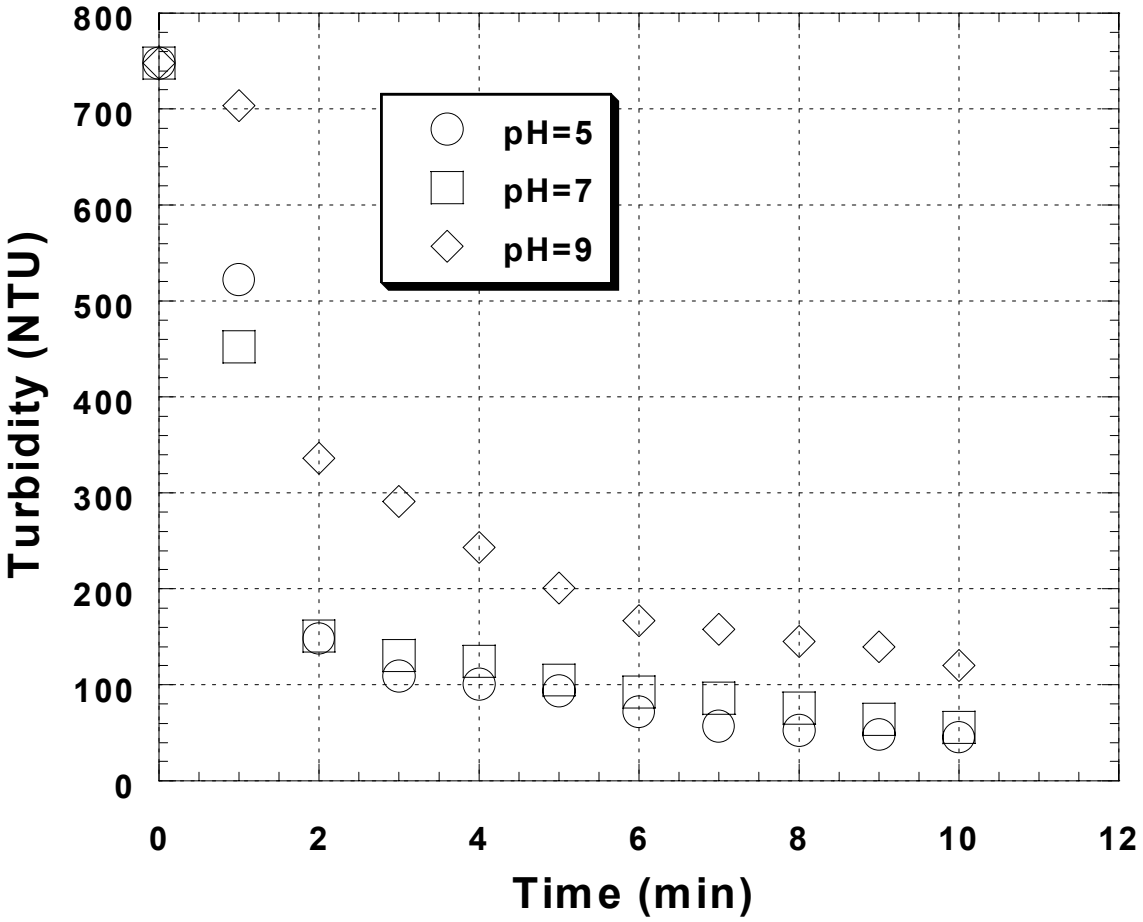

Figure A35. Turbidity changes as a function of time at various pH values. Experimental condition: electrostatic field = 97.8 V/cm; Sample = 5IIB03.

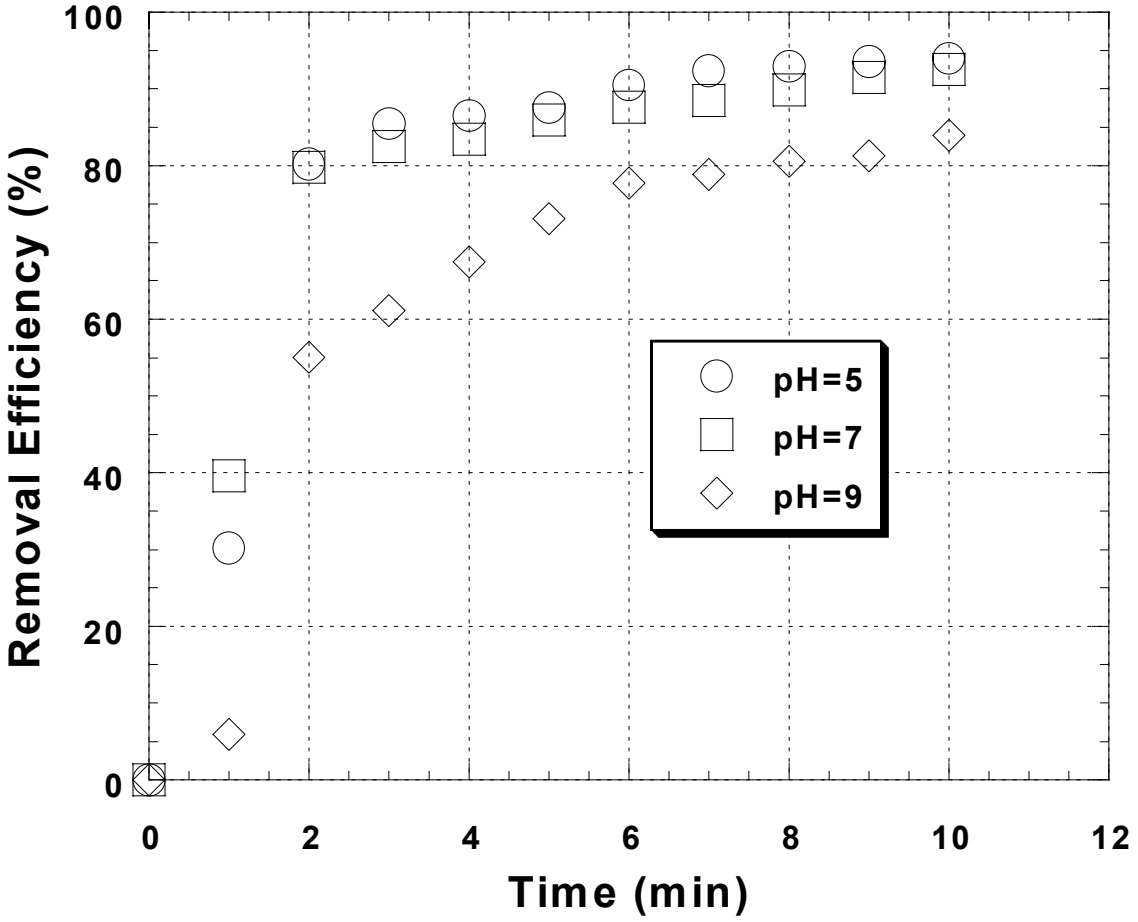

Figure A36. Removal efficiency as a function of time at various pH values (I). Experimental condition: electrostatic field = 97.8 V/cm; Sample = 5SIIB03.

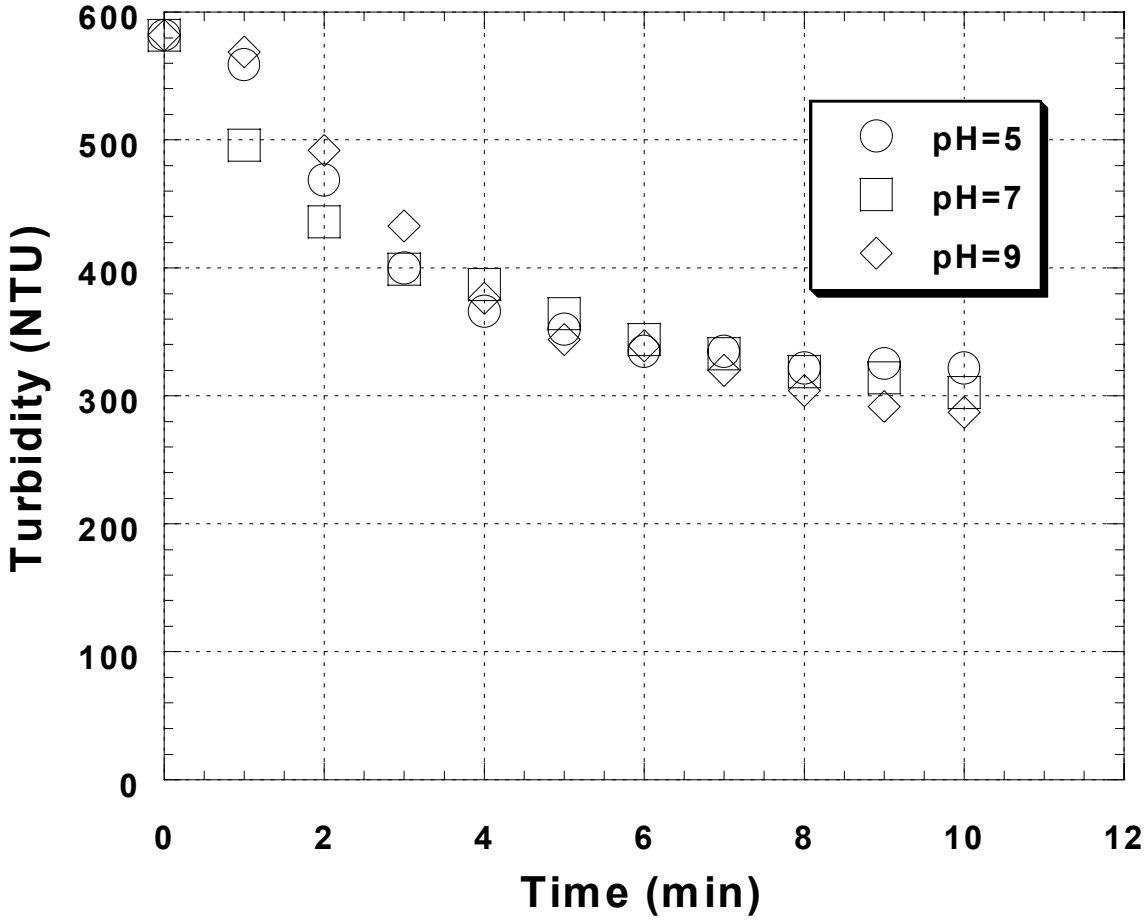

Figure A37. Turbidity changes as a function of time at various pH values. Experimental conditions: pH = 5 (electrostatic field=10.3V/cm); pH = 7 (electrostatic field=13.2V/cm); pH = 9 (electrostatic field=14.8V/cm); Sample = MW3IB02.

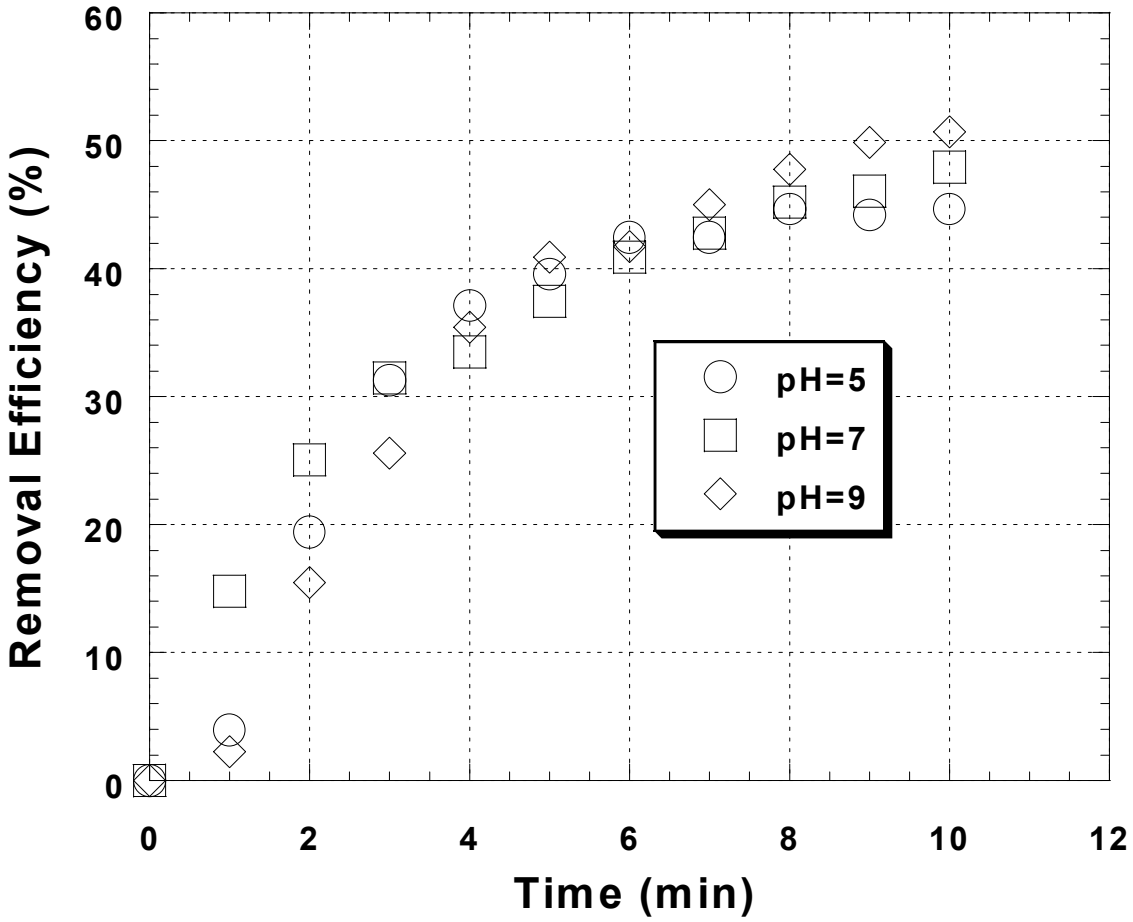

Figure A38. Removal efficiency as a function of time at various pH values (I). Experimental conditions: pH = 5 (electrostatic field=10.3V/cm); pH = 7 (electrostatic field=13.2V/cm); pH = 9 (electrostatic field=14.8V/cm); Sample = MW3IB02.

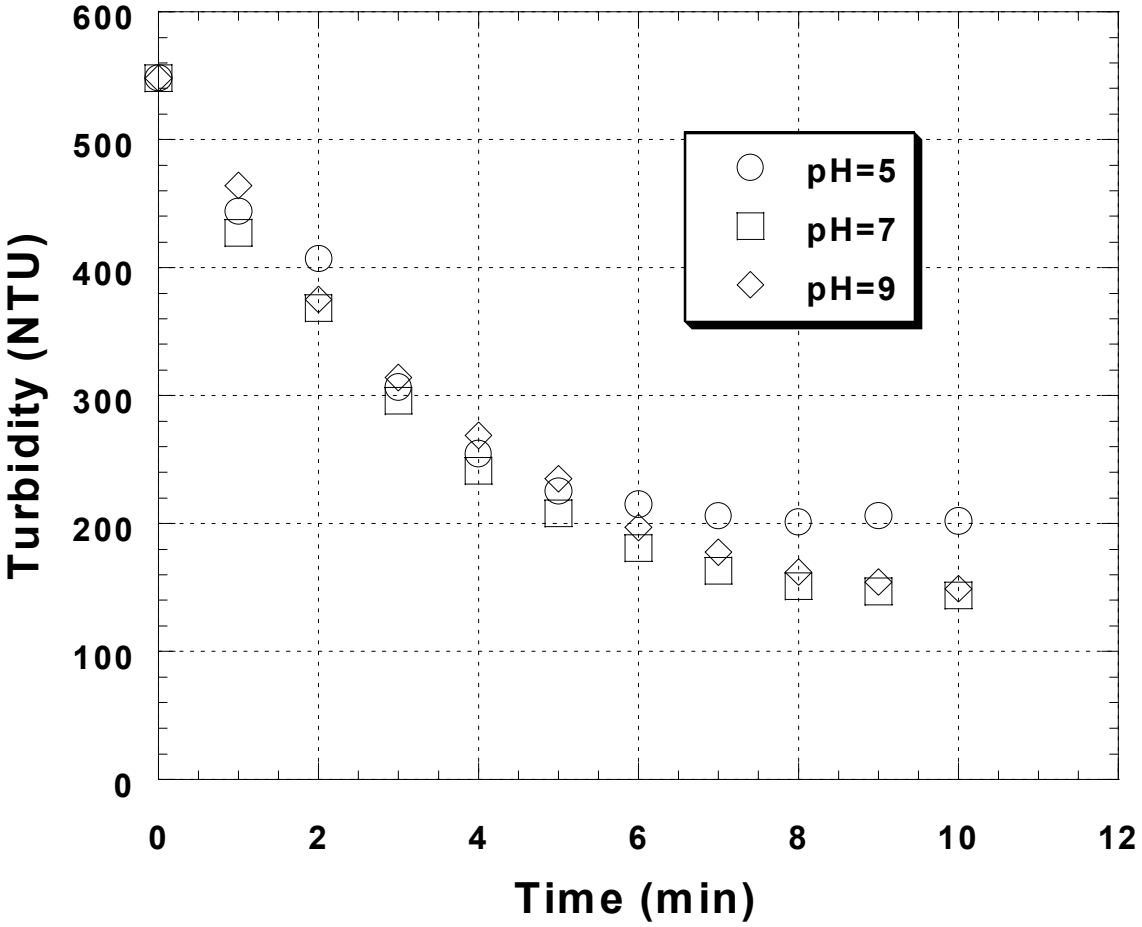

Figure A39 Turbidity changes as a function of time at various pH values. Experimental conditions: pH = 5 (electrostatic field = 32.3V/cm); pH = 7 (electrostatic field = 48.4V/cm); pH = 9 (electrostatic field = 48.4V/cm); Sample = 10IL01.

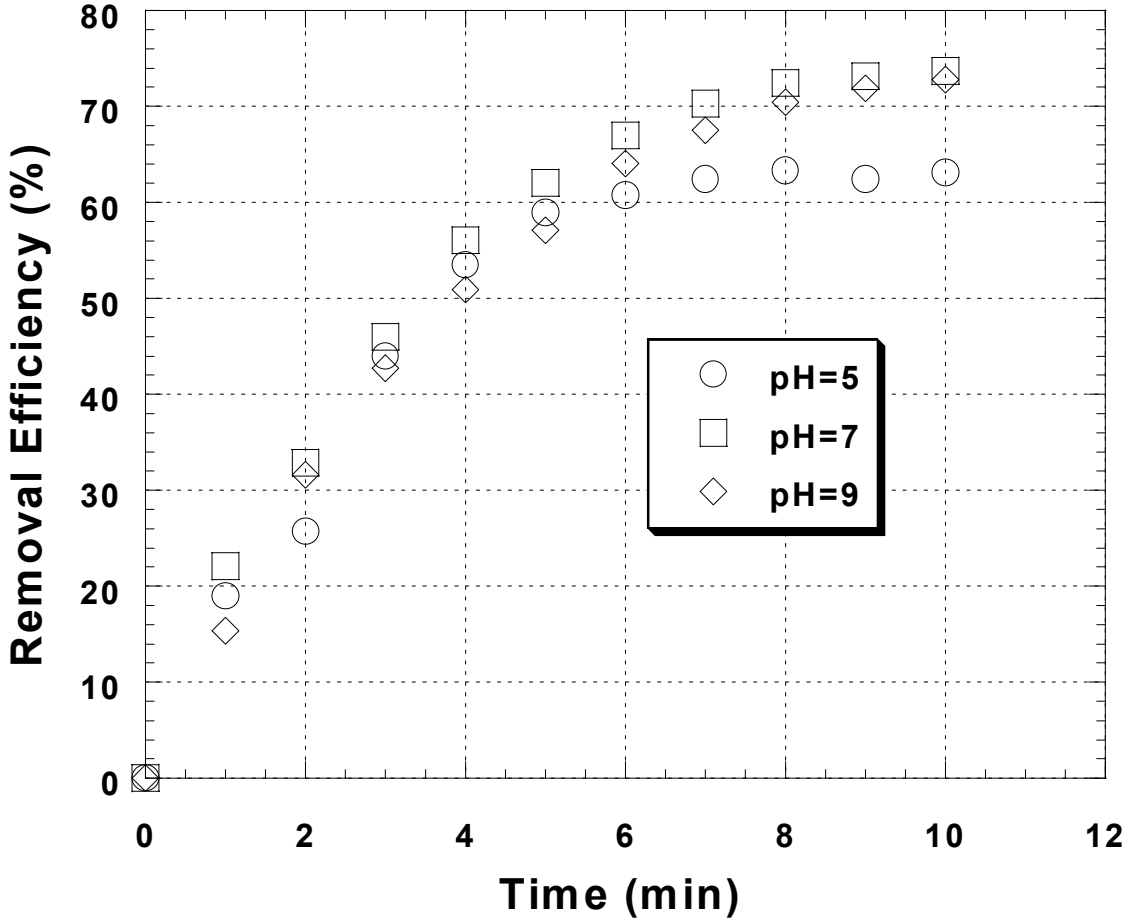

Figure A40. Removal efficiency as a function of time at various pH values (I). Experimental conditions: pH = 5 (electrostatic field=32.3V/cm); pH = 7 (electrostatic field=48.4V/cm); pH = 9 (electrostatic field=48.4V/cm); Sample = 10IL01.

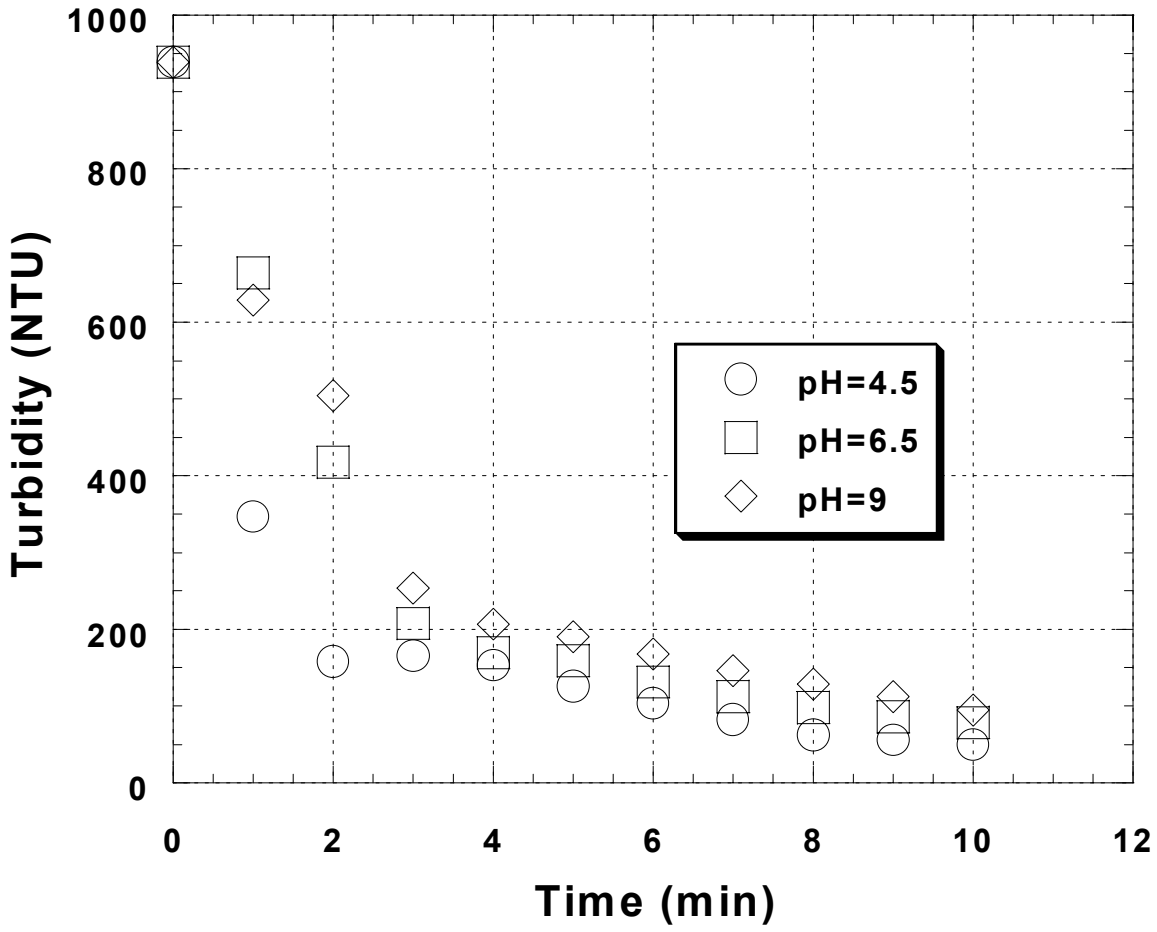

Figure A41. Turbidity changes as a function of time a t various pH values. Experimental condition: electrostatic field = 97.8 V/cm; Sample = 5SIL02.

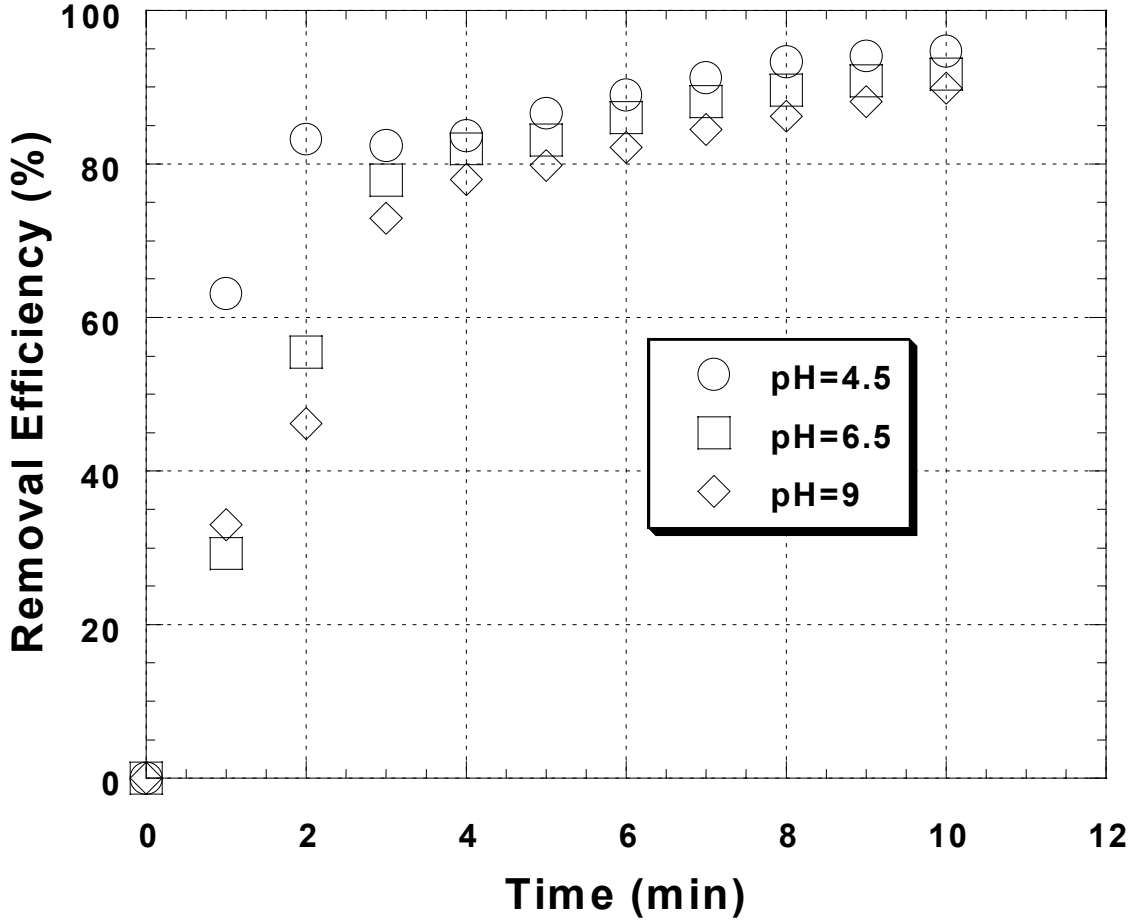

Figure A42. Removal efficiency as a function of time at various pH values (I). Experimental condition: electrostatic field = 97.8 V/cm; Sample = 5SIL02.

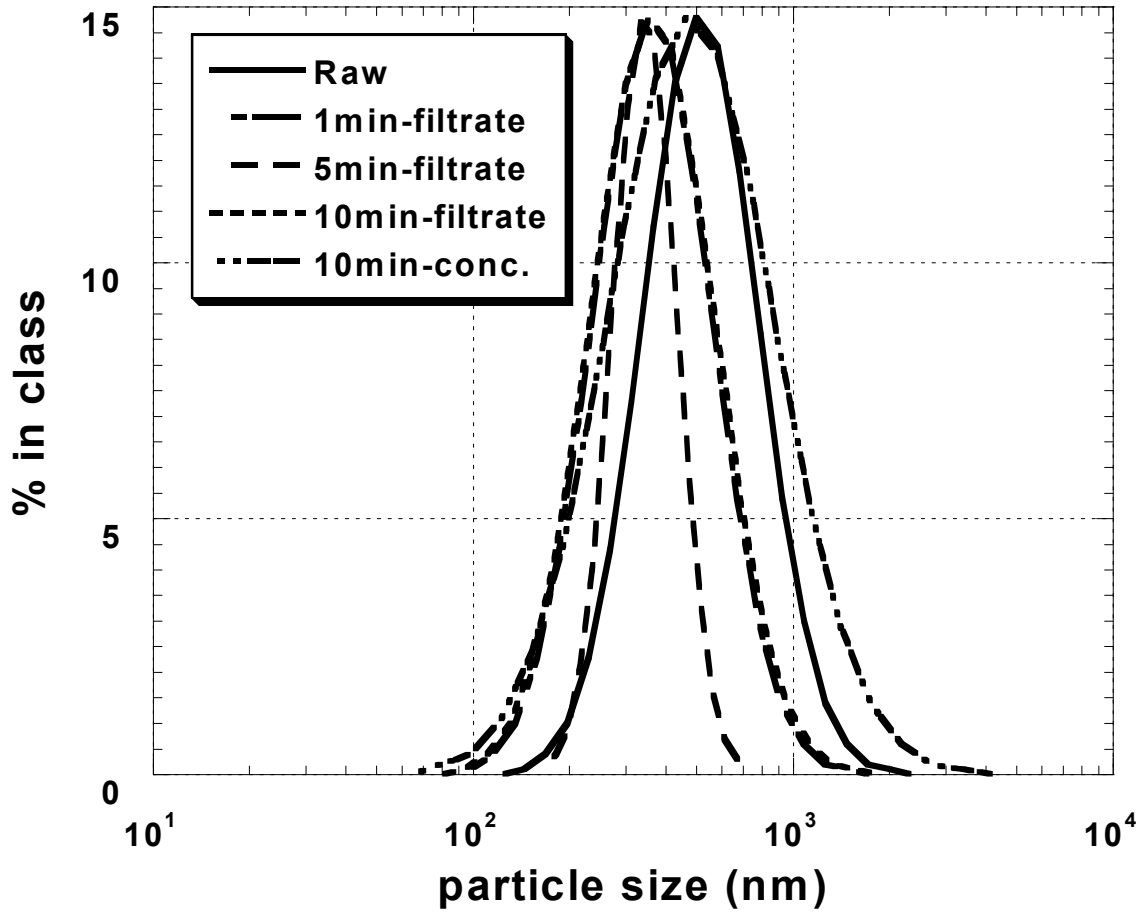

Figure A43. Changes in particle size distribution during filtration operation. Experimental conditions: Electrostatic field = 32.3 V/cm; pH = 6.5; Sample: 10IB01

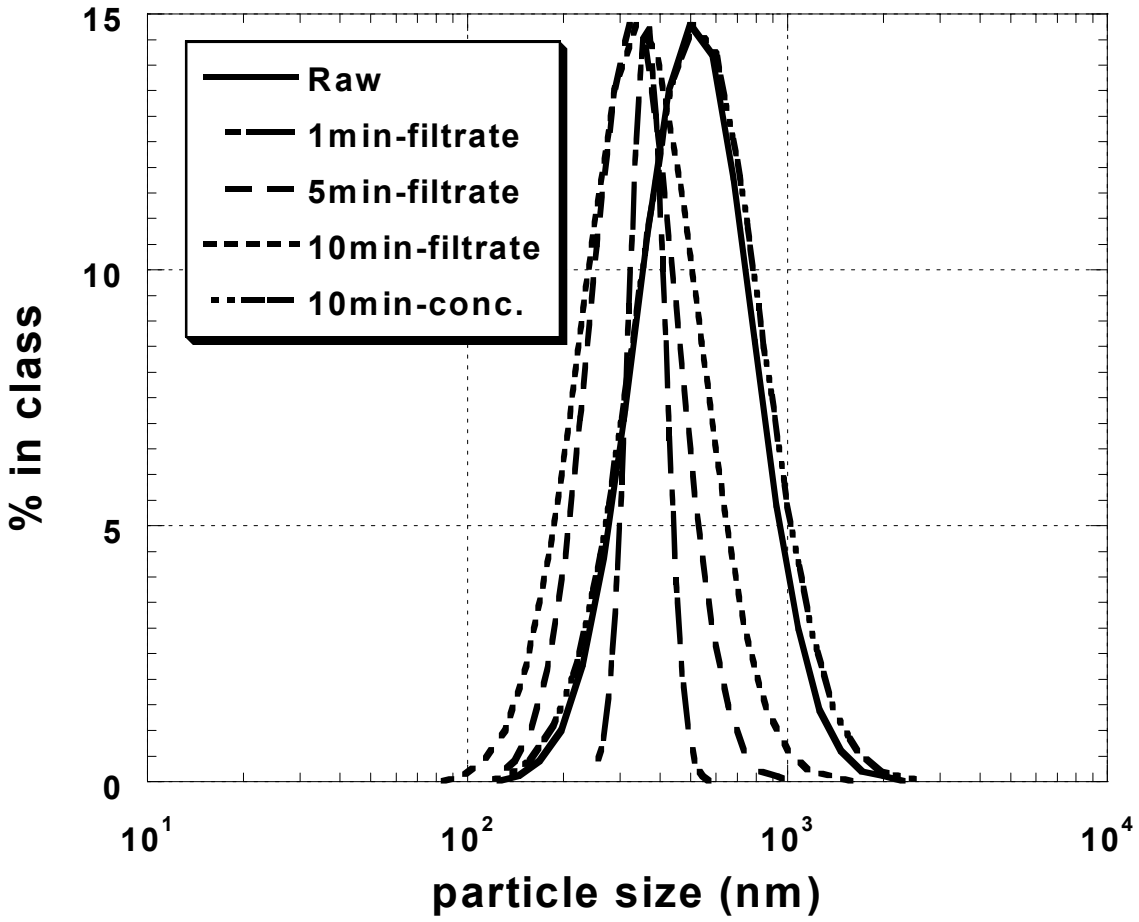

Figure A44. Changes in particle size distribution during filtration operation. Experimental conditions: electrostatic field = 48.4 V/cm; pH = 6.5; Sample = 10IB01.

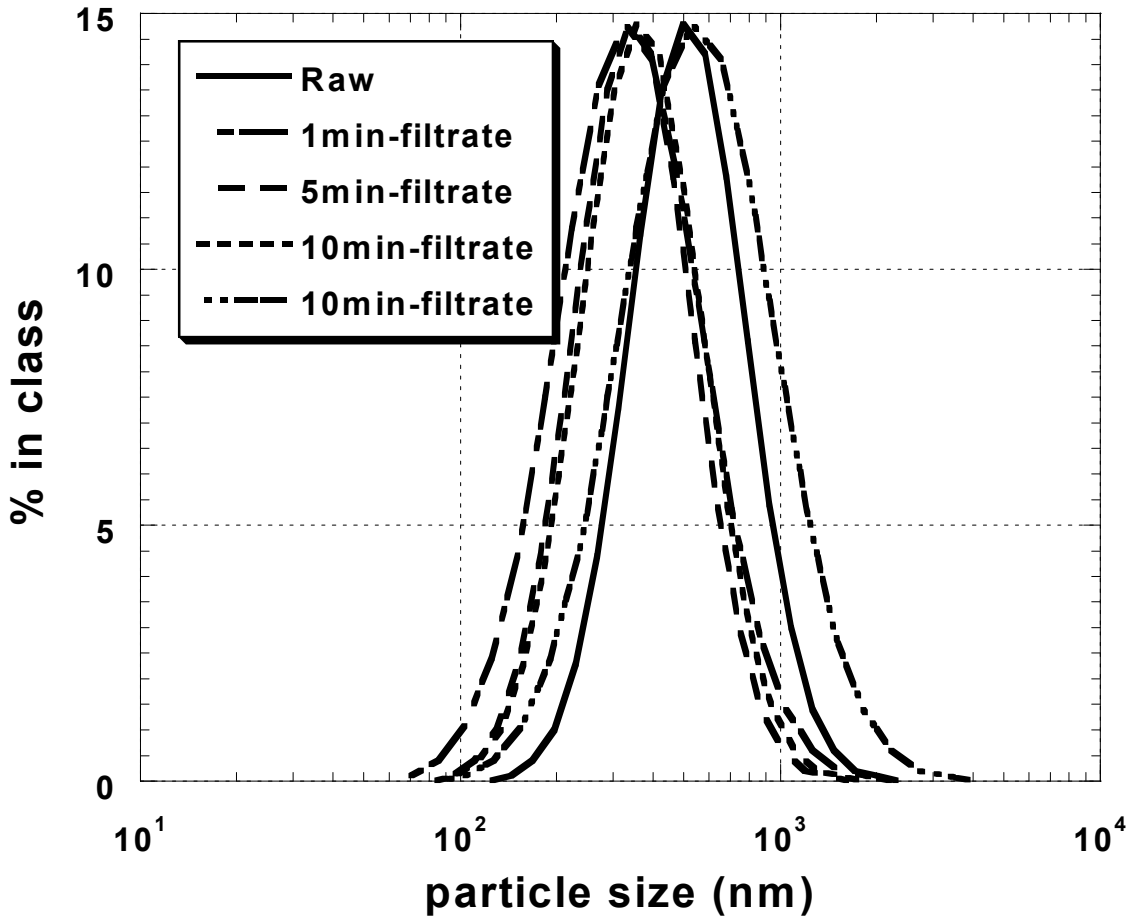

Figure A45. Changes in particle size distribution during filtration operation. Experimental conditions: electrostatic field = 64.5 V/cm; pH = 6.5; Sample = 10IB01.

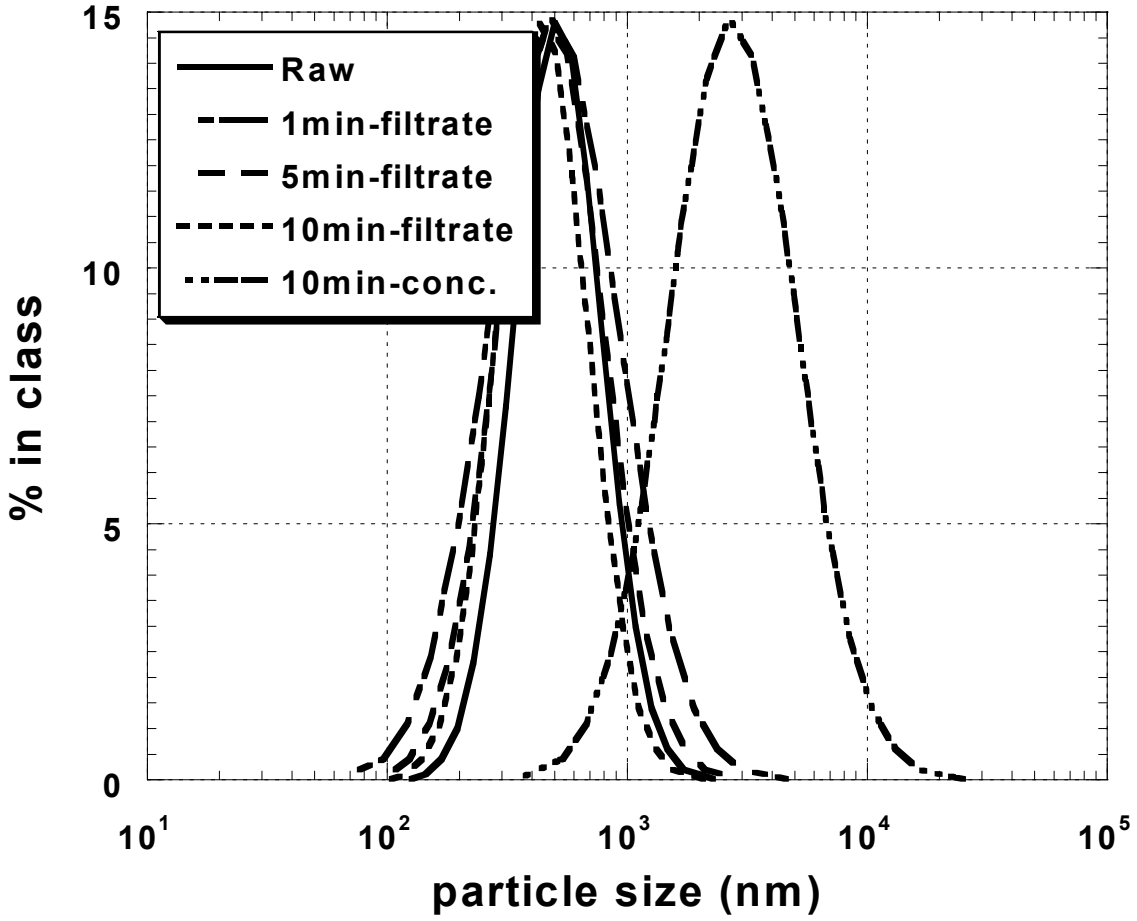

Figure A46. Changes in particle size distribution during filtration operation. Experimental conditions: pH = 5; electrostatic field = 32.3 V/cm; Sample = 10IB01.

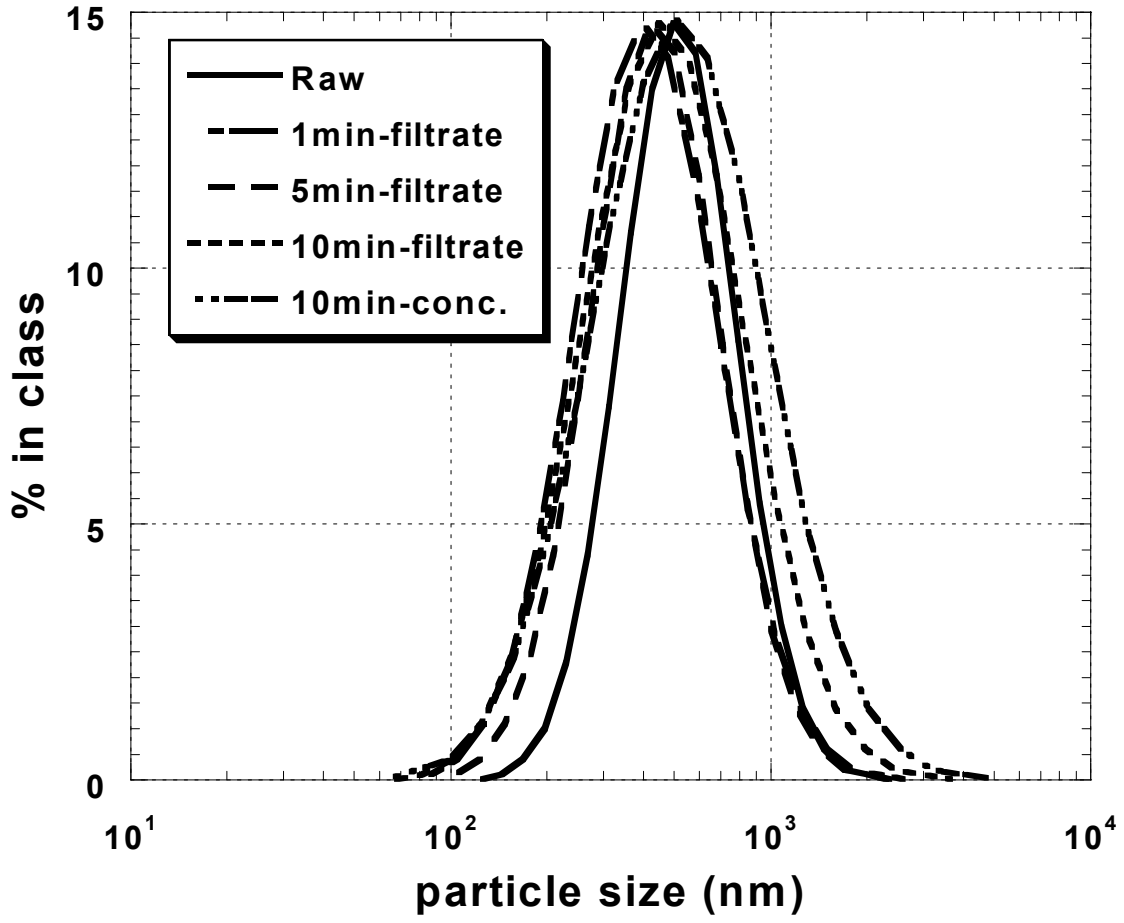

Figure A47. Changes in particle size distribution during filtration operation. Experimental conditions: pH = 7; electrostatic field = 48.4 V/cm; Sample = 10IB01.

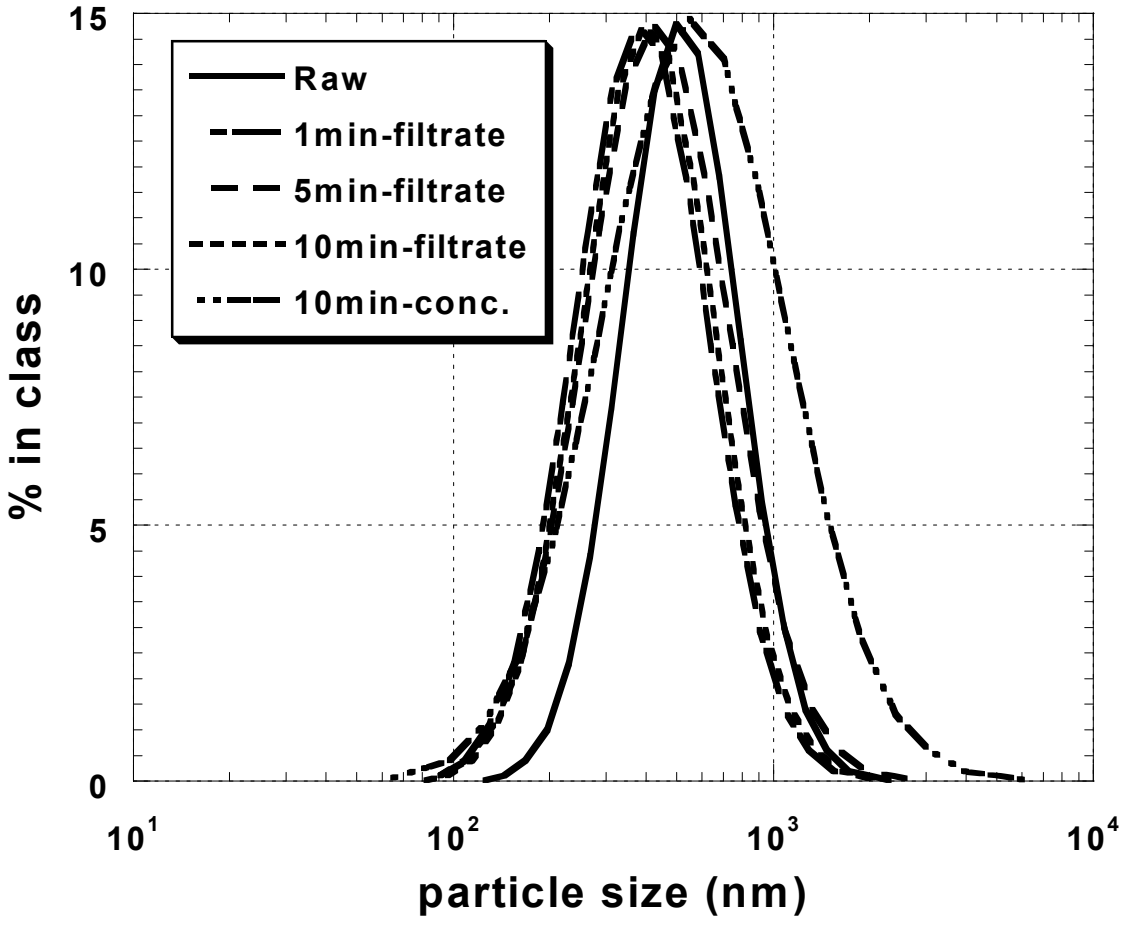

Figure A48. Changes in particle size distribution during filtration operation. Experimental conditions: pH = 9; electrostatic field = 48.4 V/cm; Sample = 10IB01.

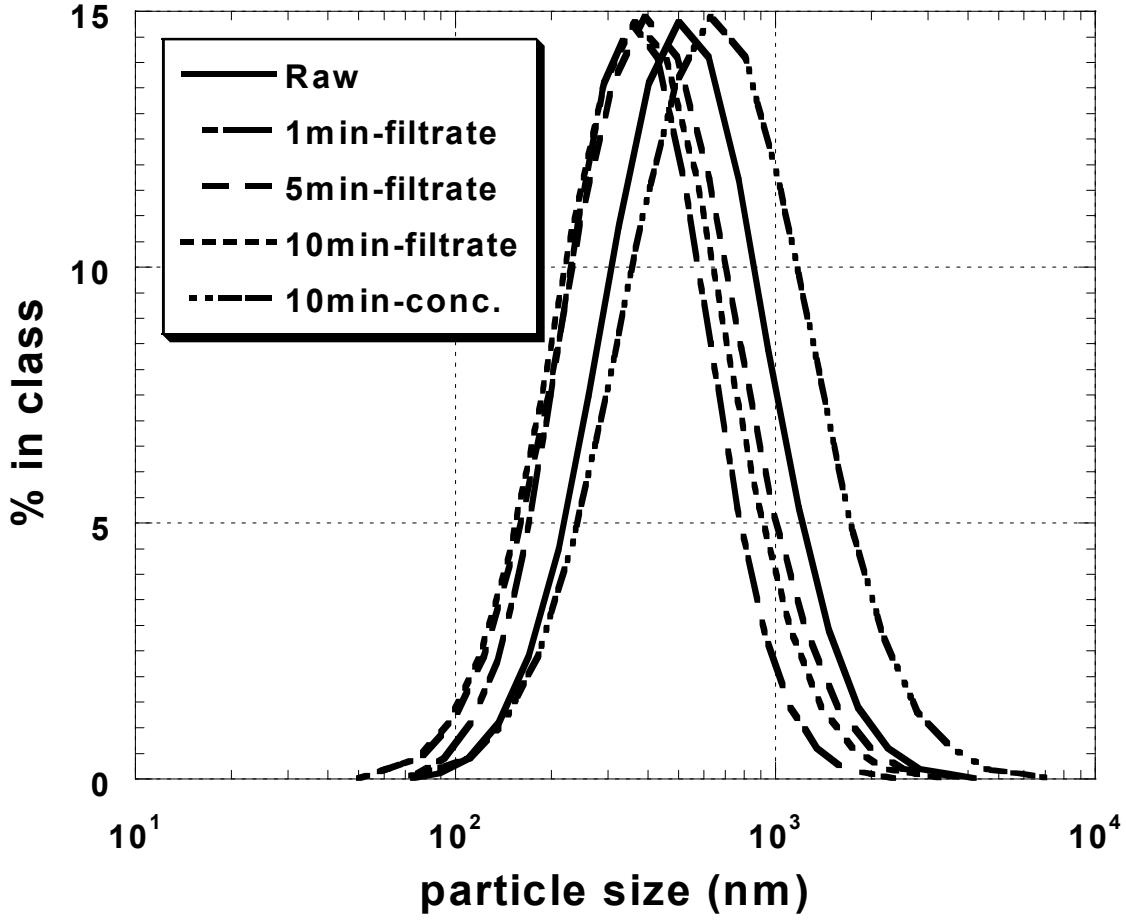

Figure A49. Changes in particle size distribution during filtration operation. Experimental conditions: electrostatic field = 32.3 V/cm; pH = 6.5; Sample = 10IL01.

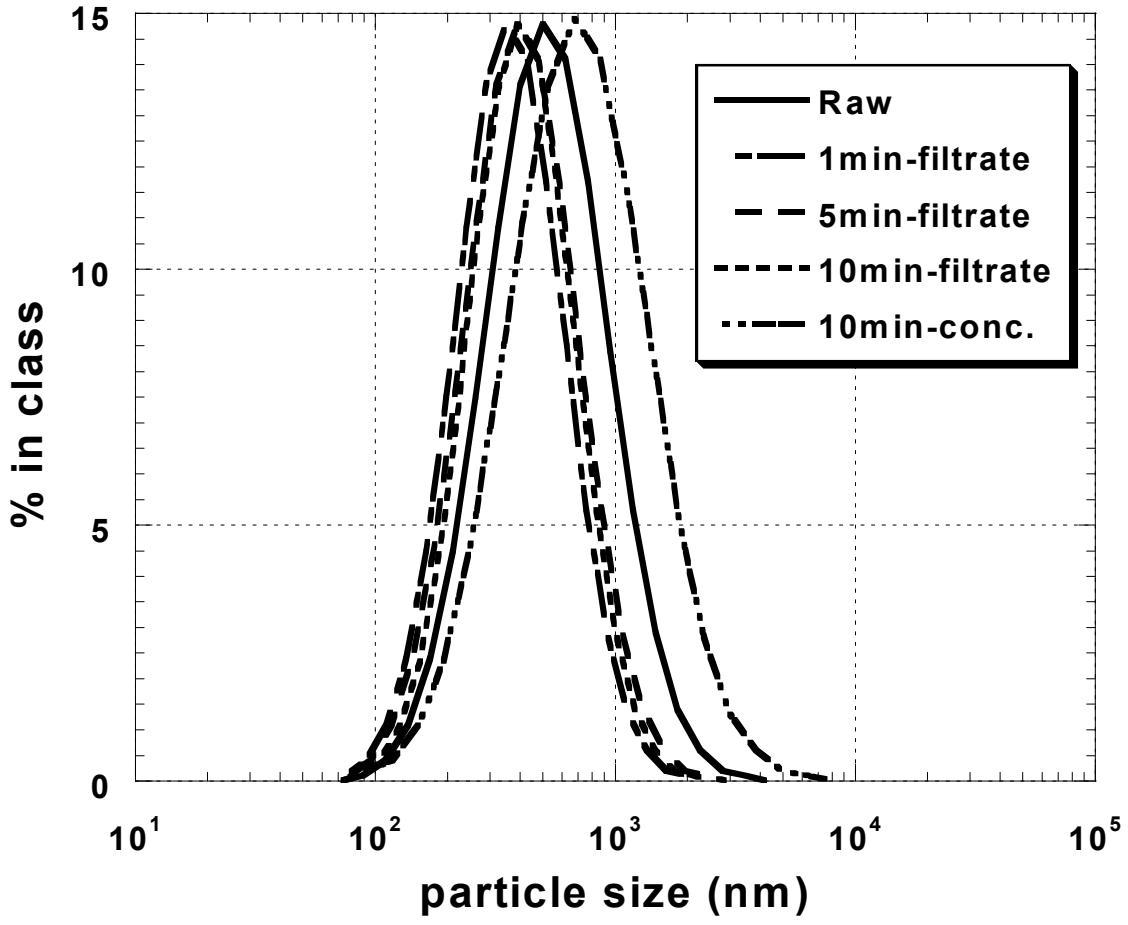

Figure A50. Changes in particle size distribution during filtration operation. Experimental conditions: electrostatic field = 48.4 V/cm; pH = 6.5; Sample = 10IL01.

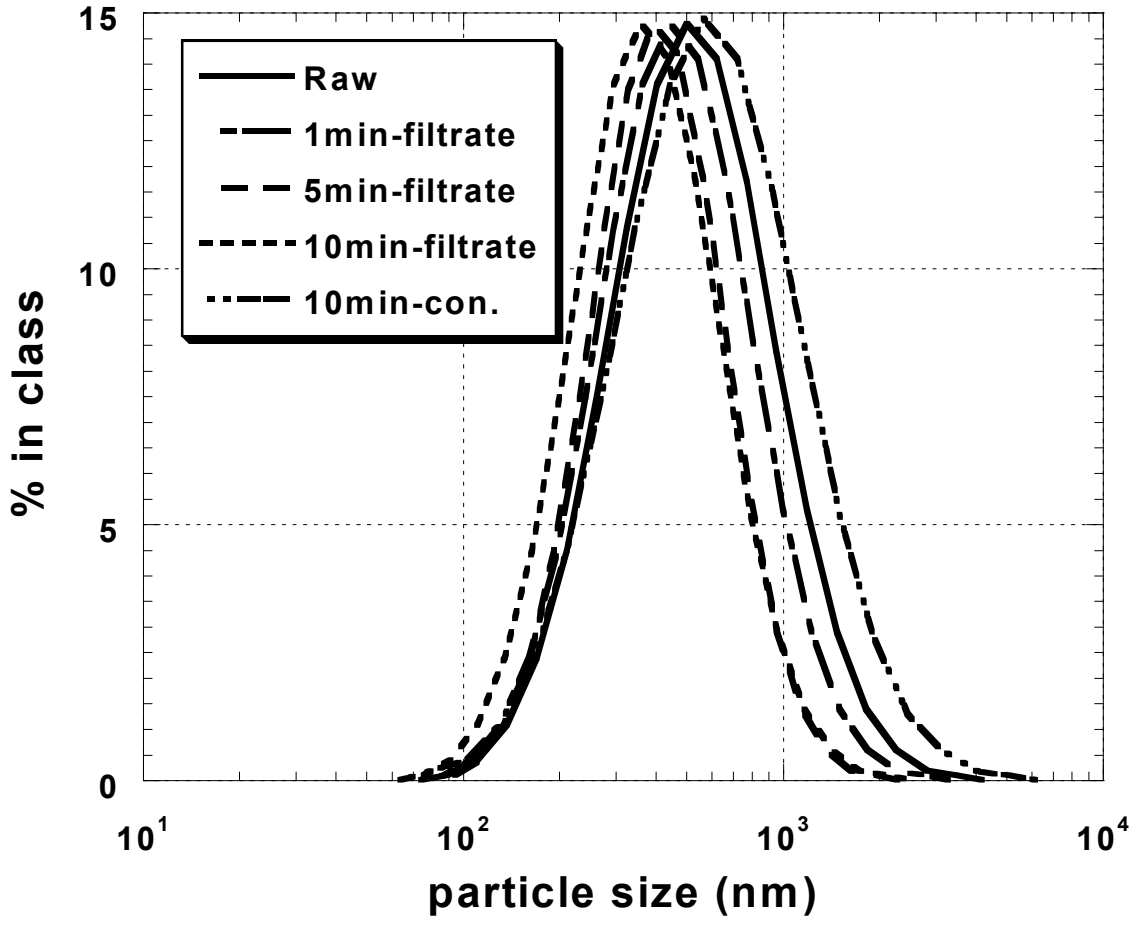

Figure A51. Changes in particle size distribution during filtration operation. Experimental conditions: electrostatic field = 64.5 V/cm; pH = 6.5; Sample = 10IL01.

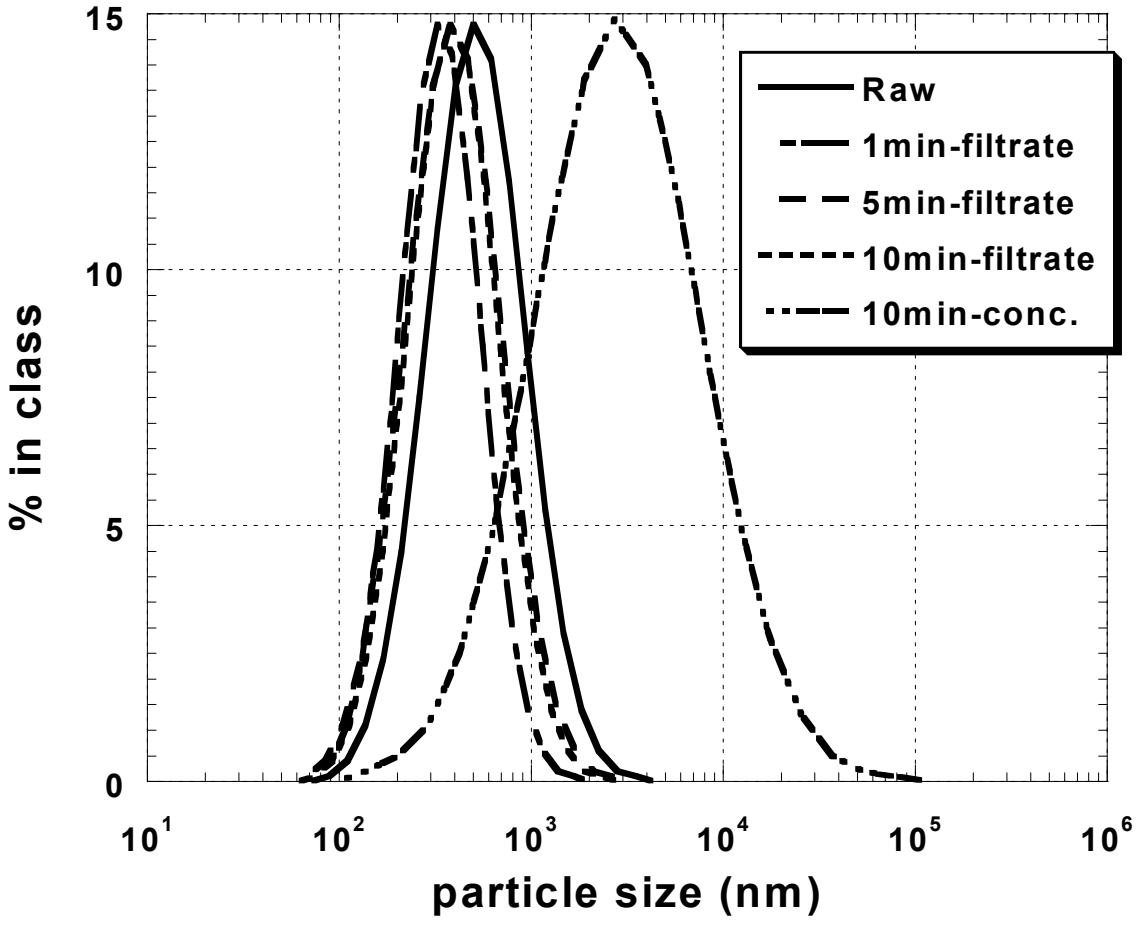

Figure A52. Changes in particle size distribution during filtration operation. Experimental conditions: pH = 5; electrostatic field = 32.3 V/cm; Sample = 10IL01.

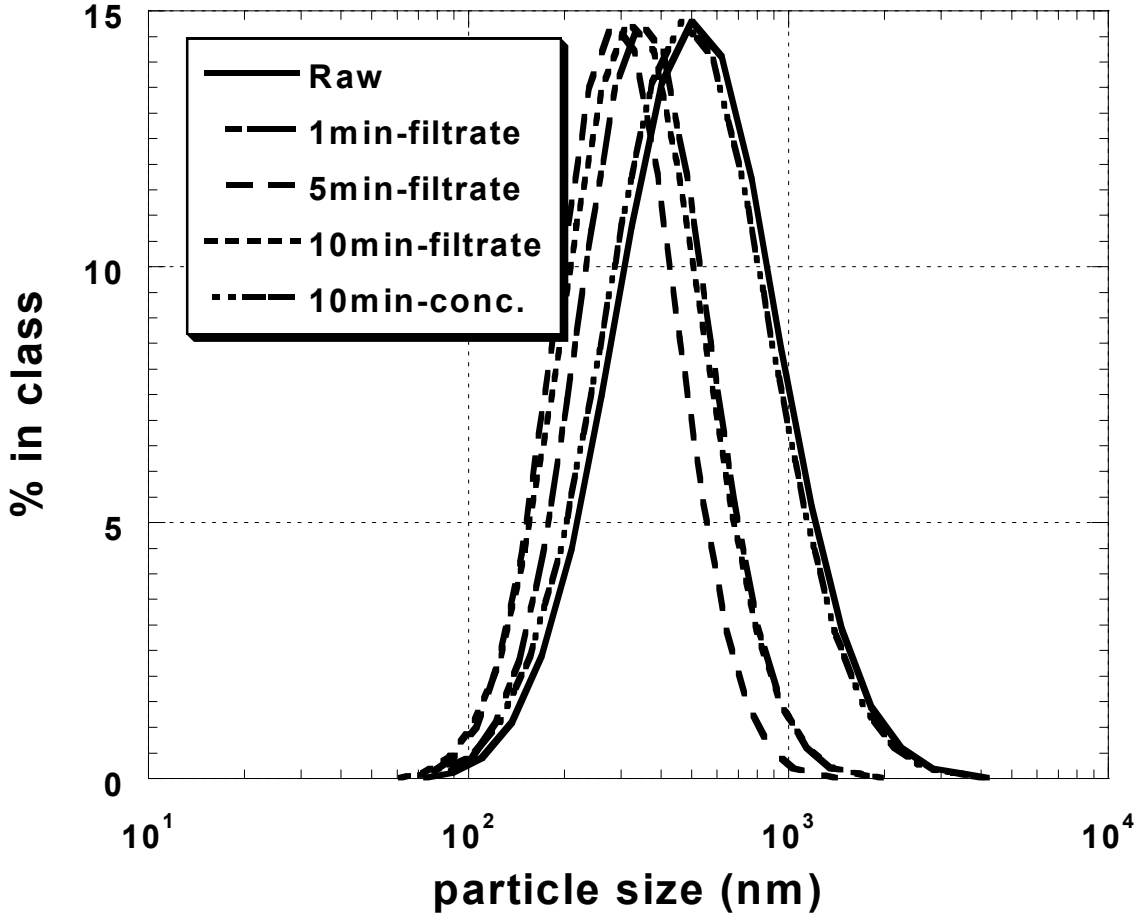

Figure A53. Changes in particle size distribution during filtration operation. Experimental conditions: pH = 7; electrostatic field = 48.4 V/cm; Sample = 10IL01.

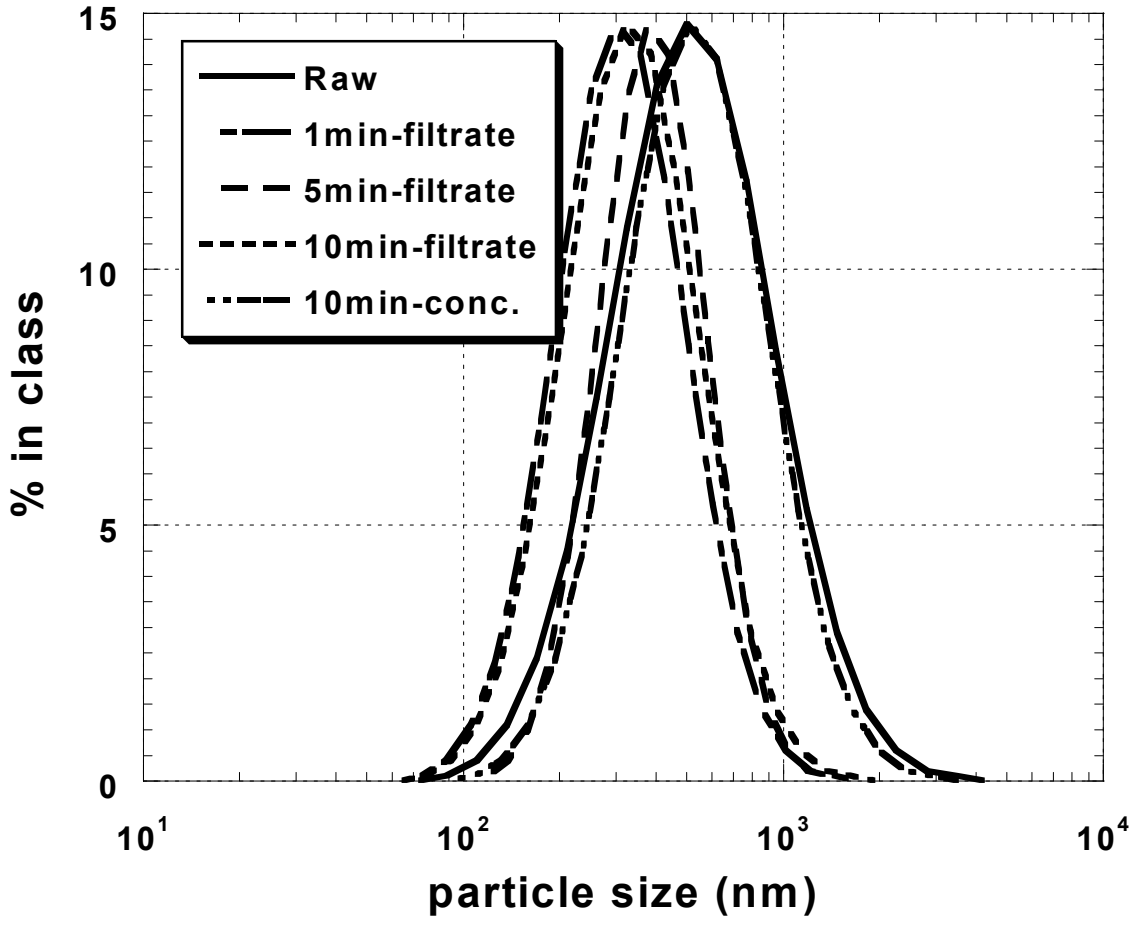

Figure A54. Changes in particle size distribution during filtration operation. Experimental conditions: pH = 9; electrostatic field = 48.4 V/cm; Sample = 10IL01.

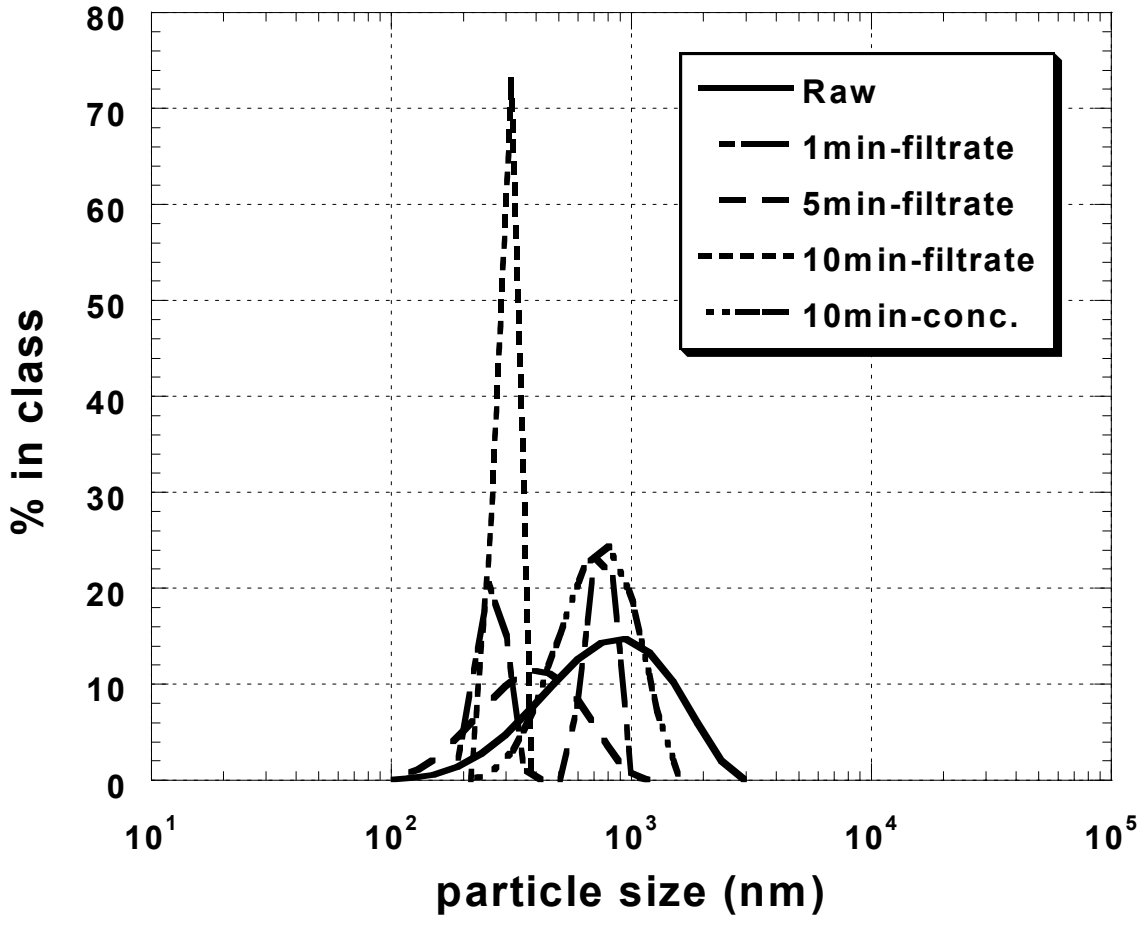

Figure A55. Changes in particle size distribution during filtration operation. Experimental conditions: electrostatic field = 32.3 V/cm; pH = 6.6; Sample = 5SIIB03.

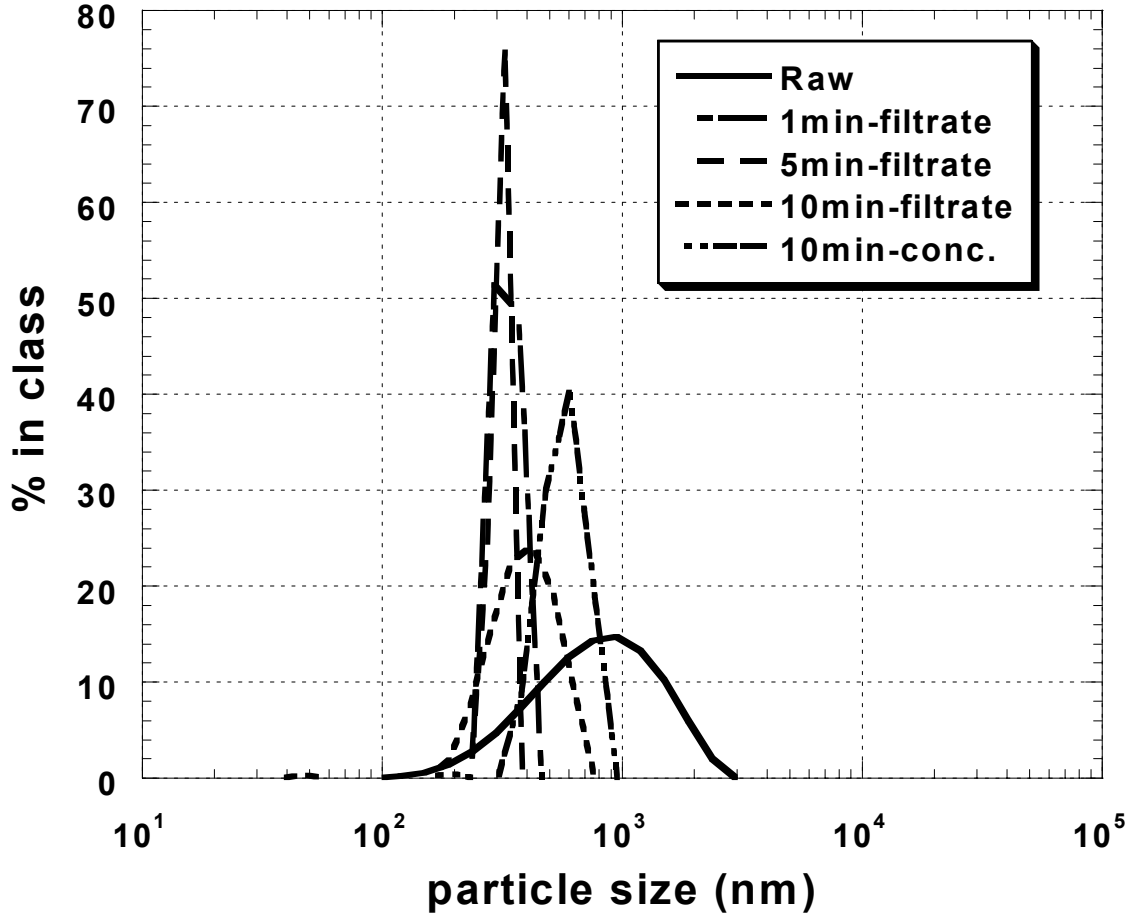

Figure A56. Changes in particle size distribution during filtration operation. Experiment conditions: electrostatic field = 64.5 V/cm; pH = 6.6; Sample = 5SIIB03.

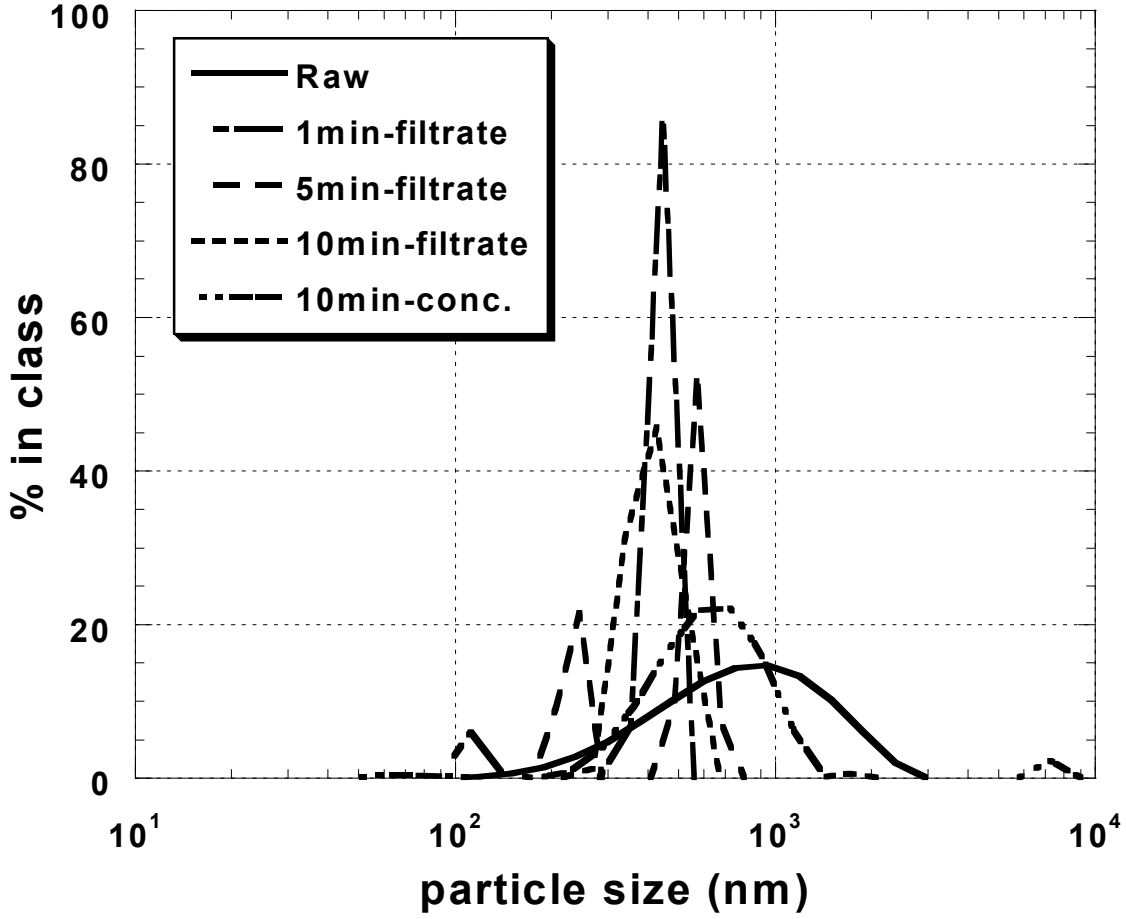

Figure A57. Changes in particle size distribution during filtration operation. Experimental conditions: electrostatic field = 97.8 V/cm; pH = 6.6; Sample = 5SIIB03.

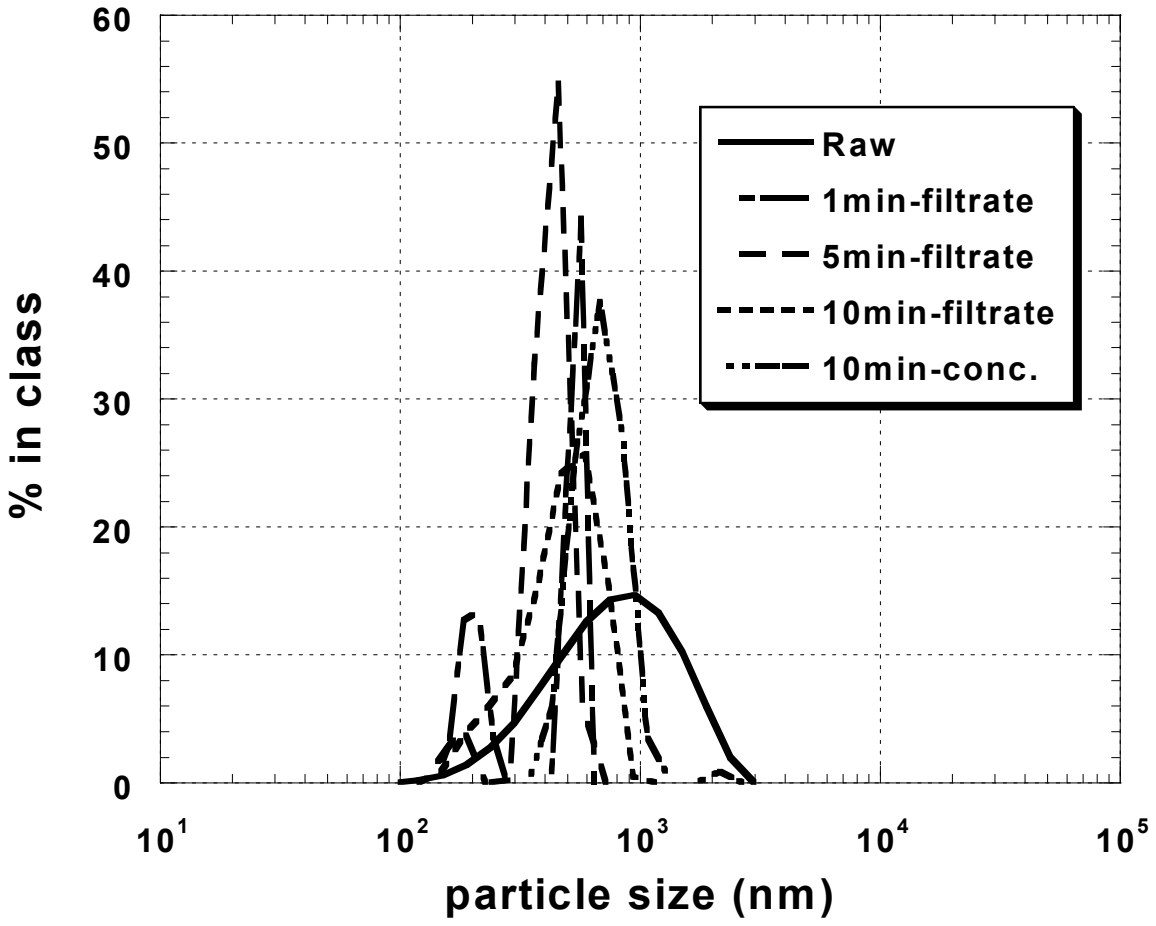

Figure A58. Changes in particle size distribution during filtration operation. Eexperimental conditions: electrostatic field = 129 V/cm; pH = 6.6; Sample = 5SIIB03.

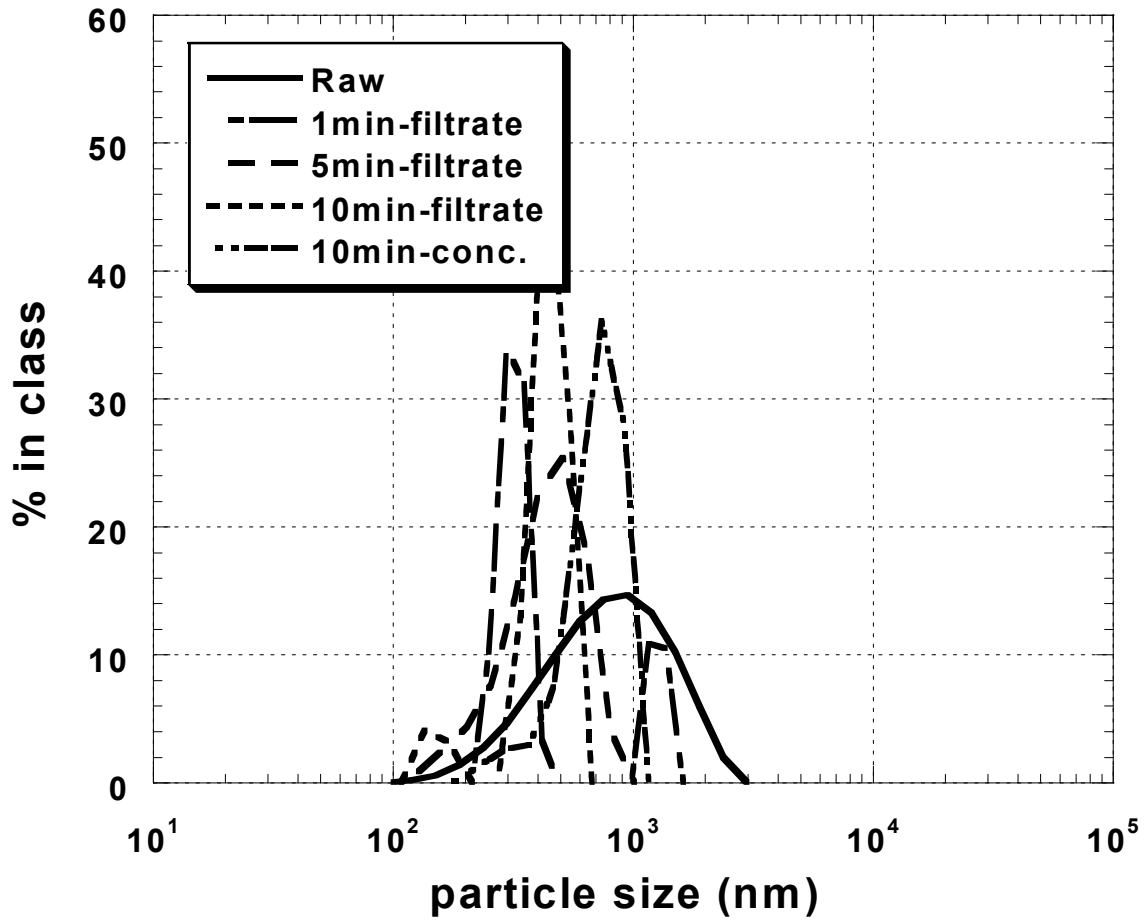

Figure A59. Changes in particle size distribution during filtration operation. Experimental conditions: electrostatic field = 156.8 V/cm; pH = 6.6; Sample = 5SIIB03.

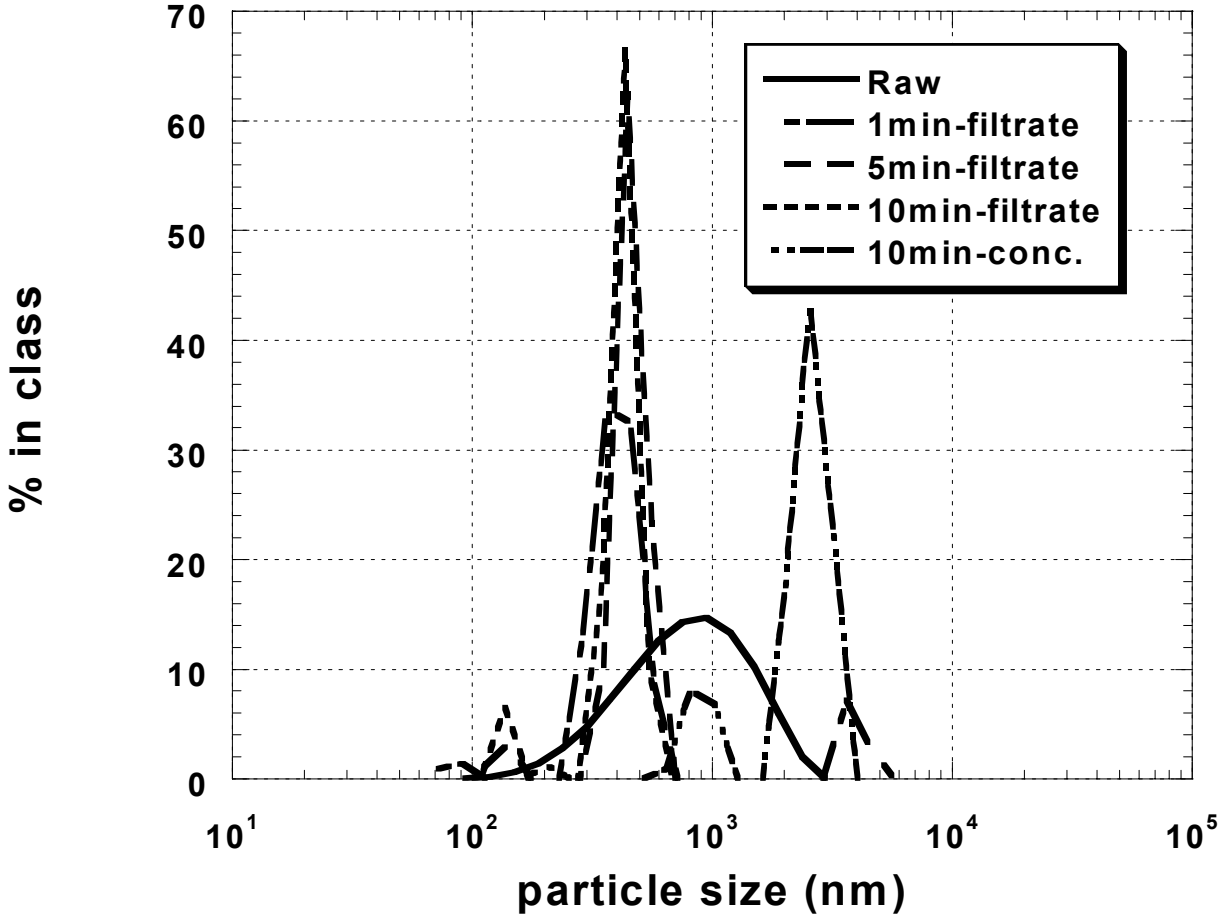

Figure A60. Changes in particle size distribution during filtration operation. Experimental conditions: pH = 5; electrostatic field = 97.8 V/cm; Sample = 5SIIB03.

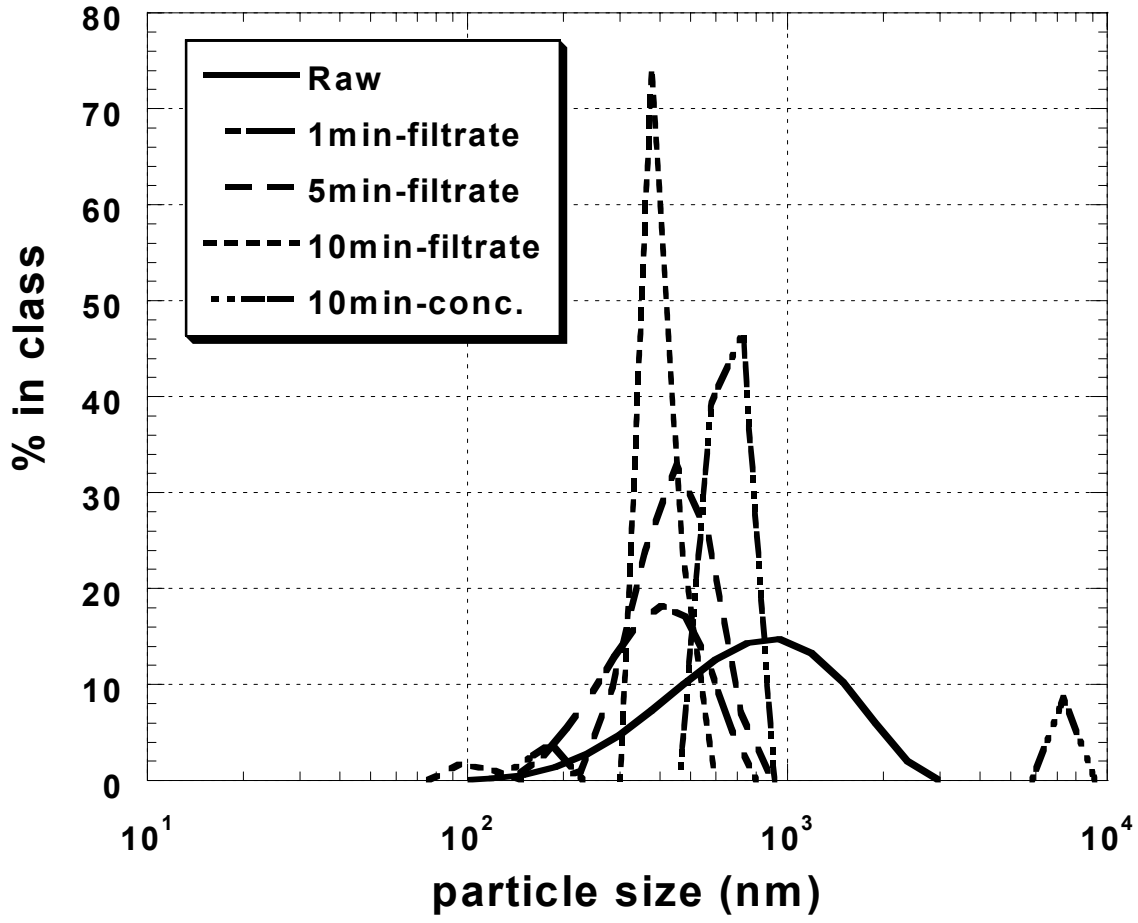

Figure A61. Changes in particle size distribution during filtration operation. Experimental conditions: pH = 7; electrostatic field = 97.8 V/cm; Sample = 5SIIB03.

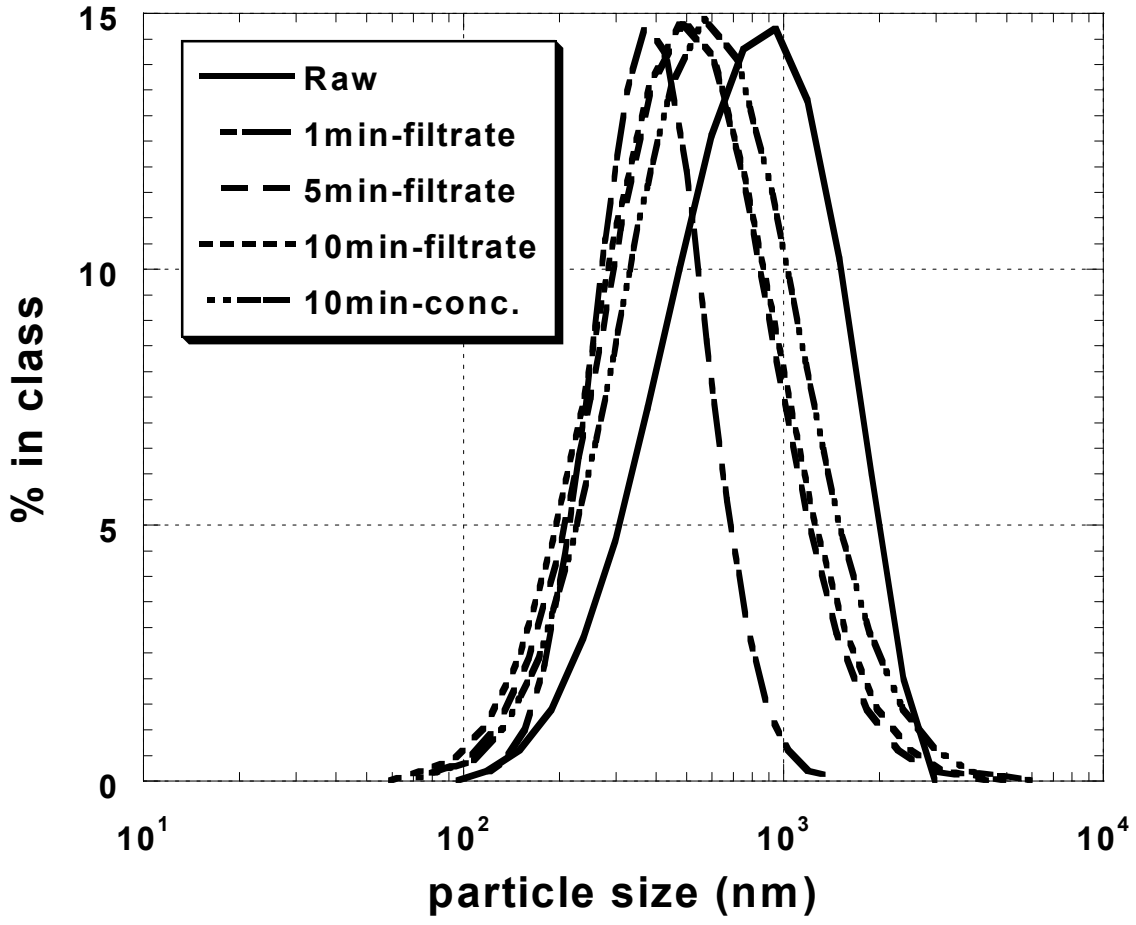

Figure A62. Changes in particle size distribution during filtration operation. Experimental conditions: pH = 9; electrostatic field = 97.8 V/cm; Sample = 5SIIB03.

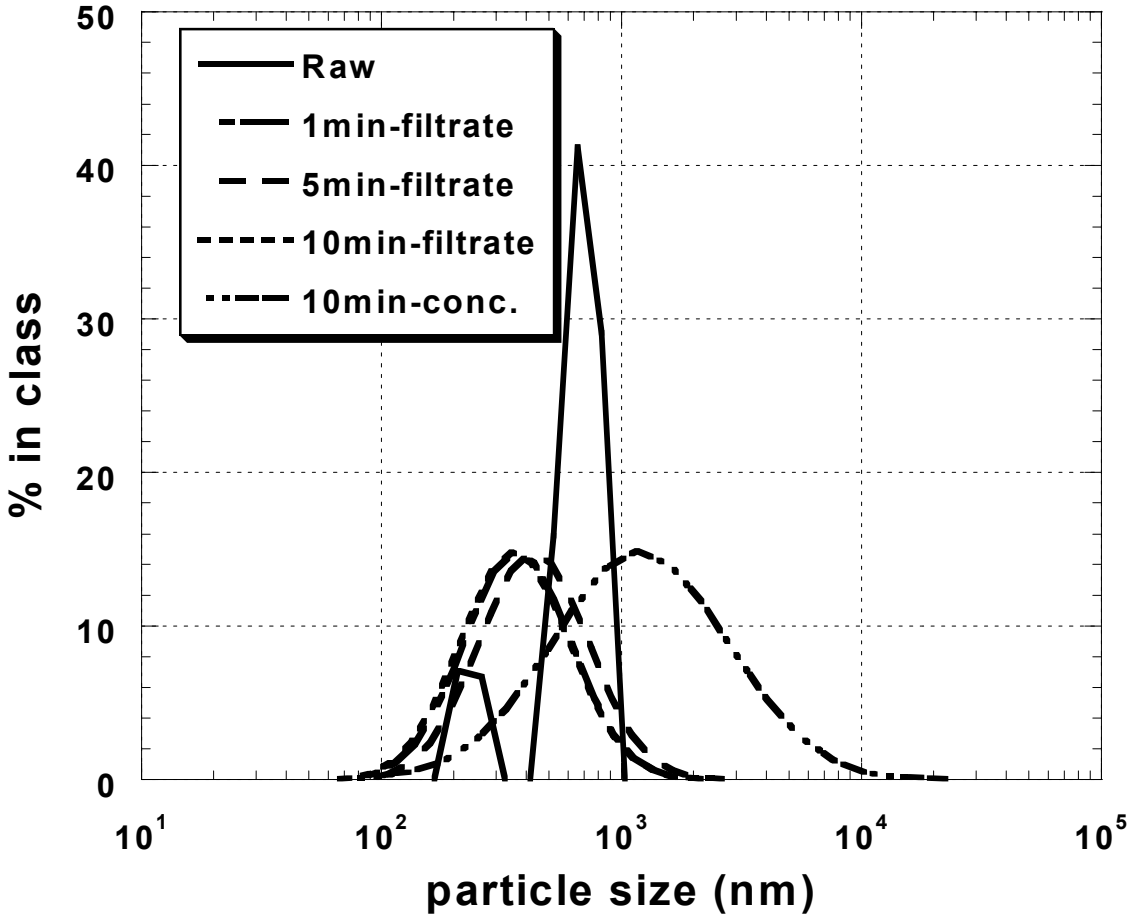

Figure A63. Changes in particle size distribution during filtration operation. Experimental conditions: electrostatic field = 32.3 V/cm; pH = 6.7; Sample = 5SIIL02.

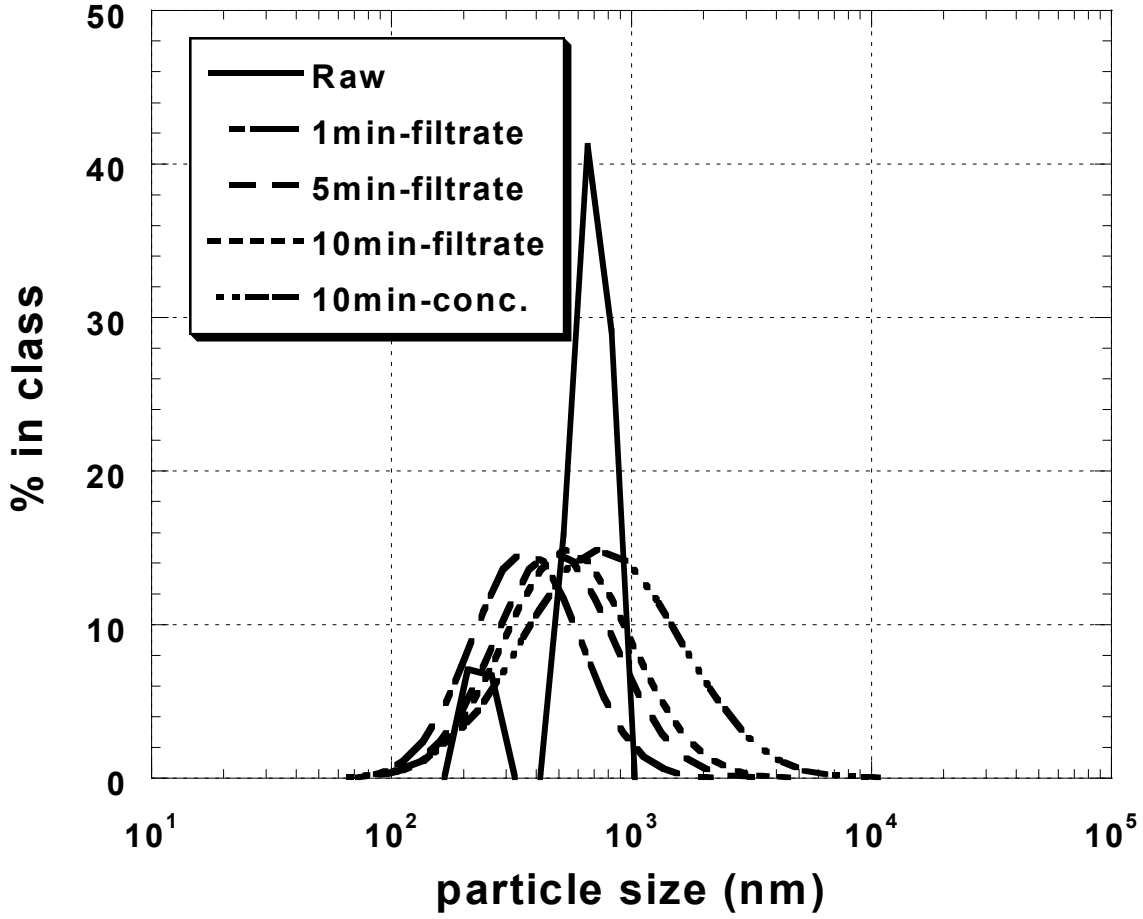

Figure A64. Changes in particle size distribution during filtration operation. Experimental conditions: electrostatic field = 64.5 V/cm; pH = 6.7; Sample = 5SIIL02.

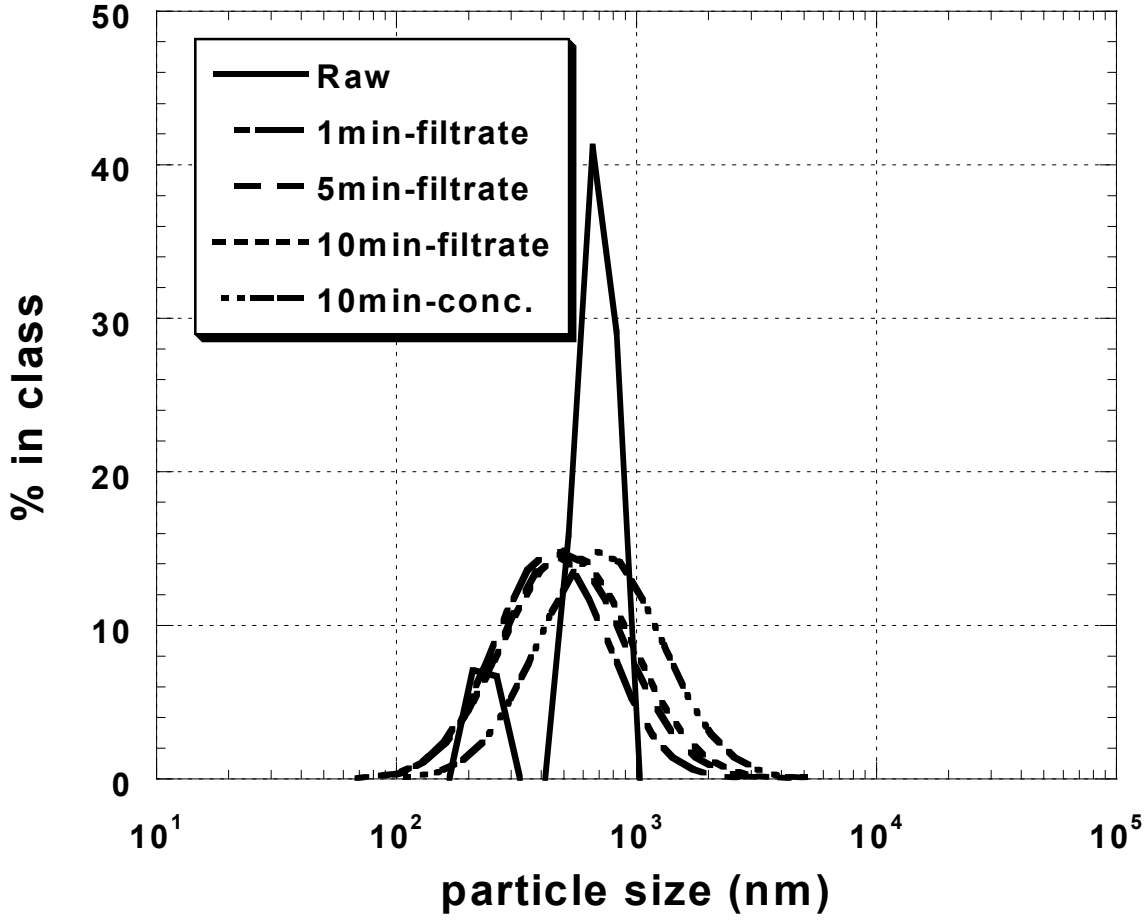

Figure A65. Changes in particle size distribution during filtration operation. Experimental conditions: electrostatic field = 97.8 V/cm; pH = 6.7; Sample = 5SIIL02.

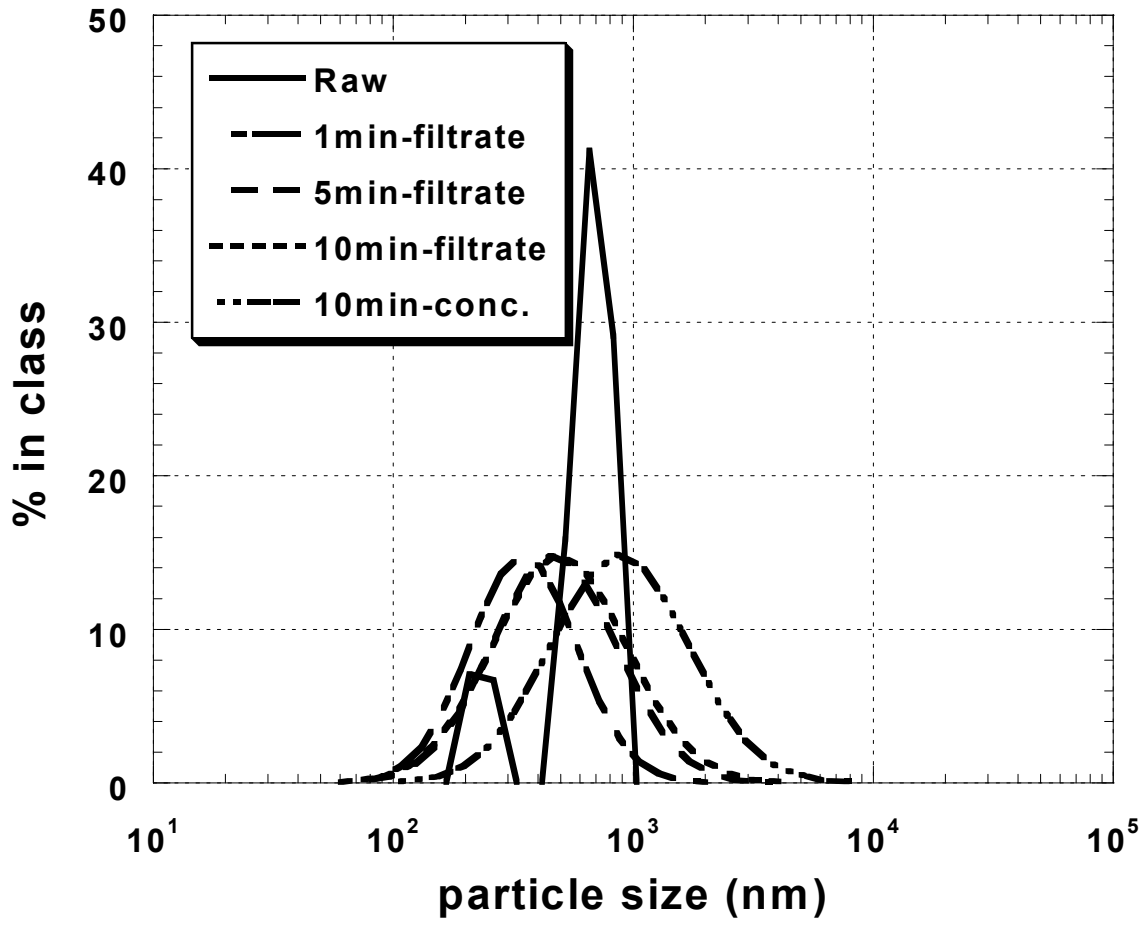

Figure A66. Changes in particle size distribution during filtration operation. Experimental conditions: electrostatic field = 129 V/cm; pH = 6.7; Sample = 5SIIL02.

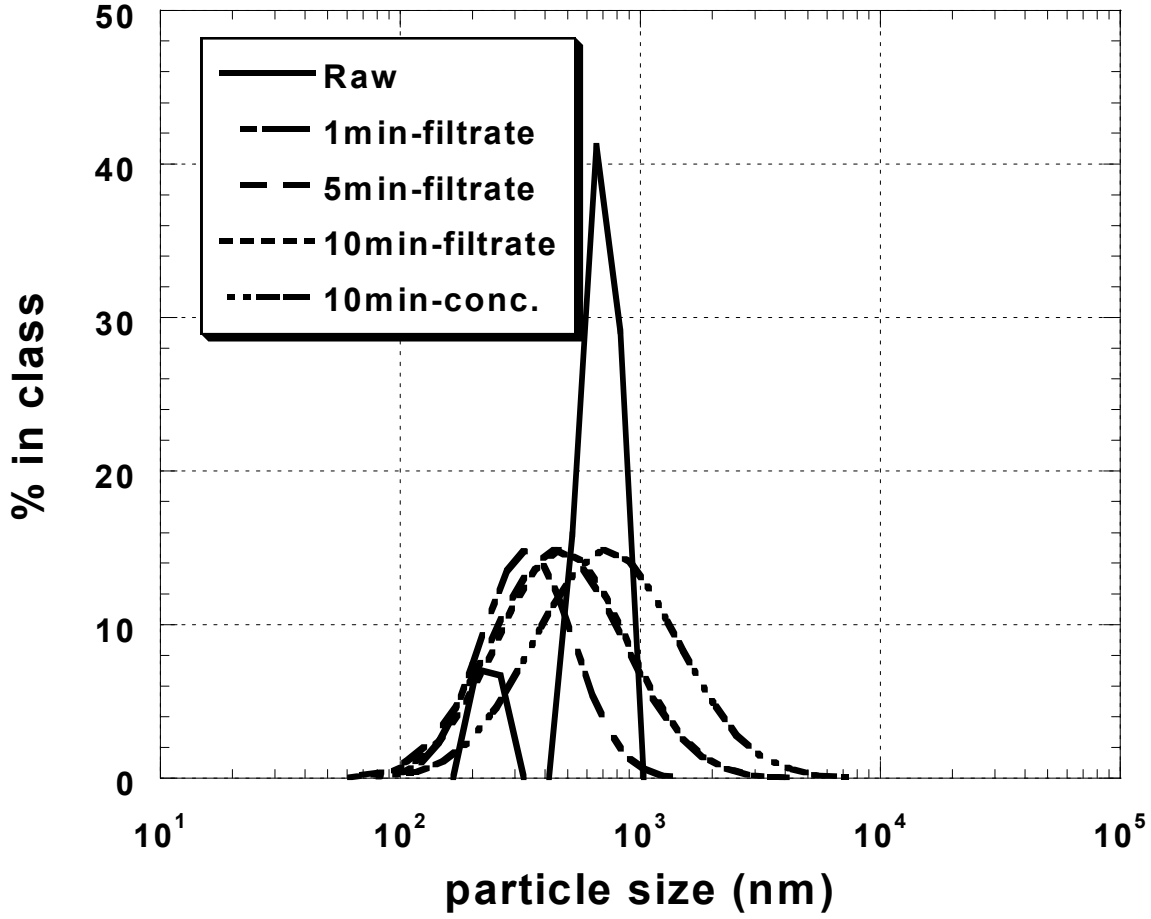

Figure A67. Changes in particle size distribution during filtration operation. Experimental conditions: electrostatic field = 156.8 V/cm; pH = 6.7; Sample = 5SIIL02.

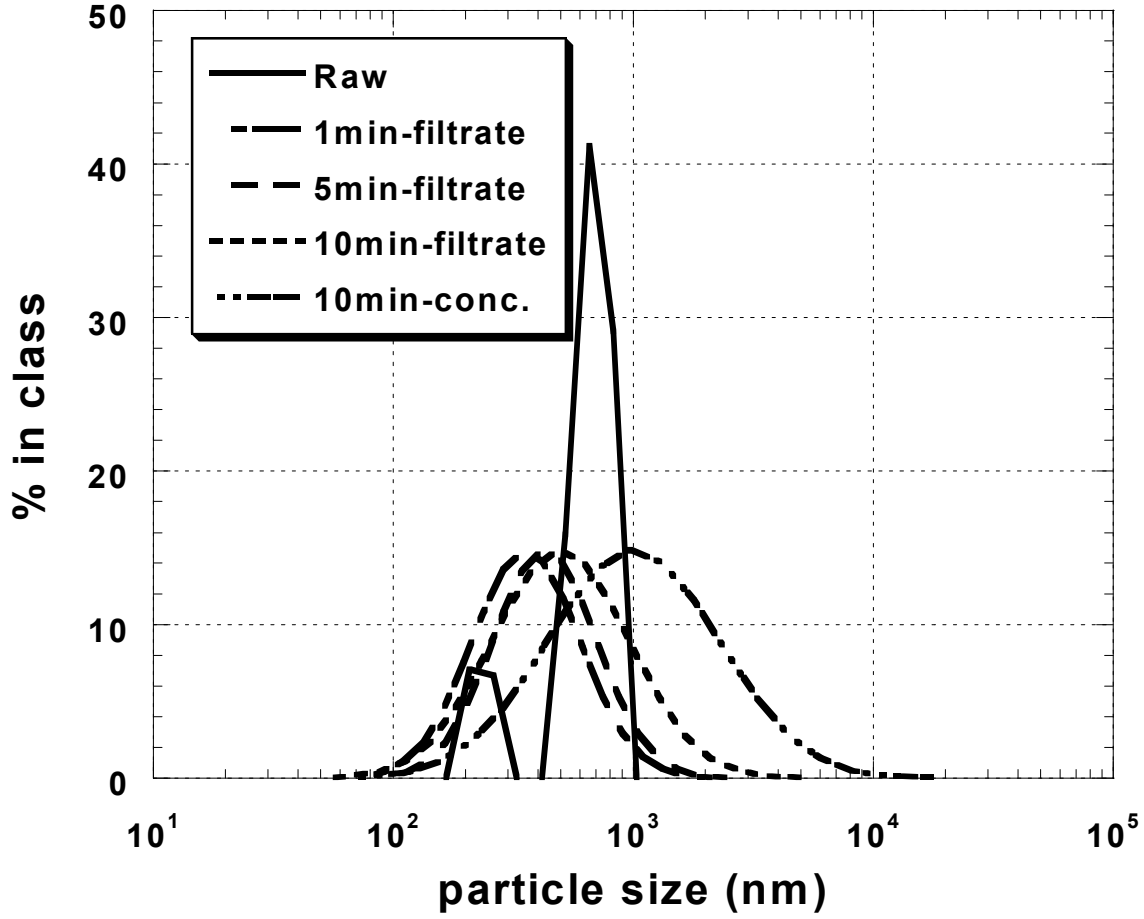

Figure A68. Changes in particle size distribution during filtration operation. Experimental conditions: pH = 4.5; electrostatic field = 97.8 V/cm; Sample = 5SIIL02.

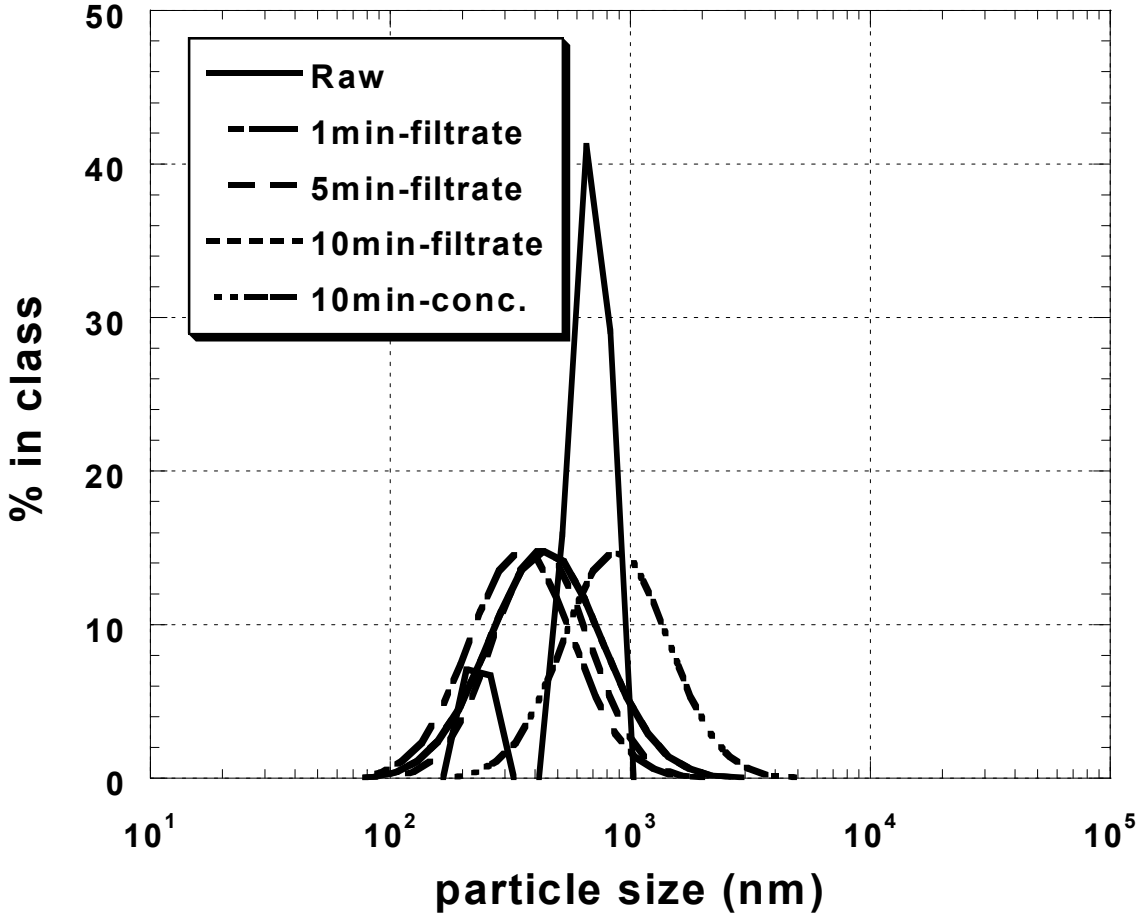

Figure A69. Changes in particle size distribution during filtration operation. Experimental conditions: pH = 6.5, electrostatic field = 97.8 V/cm; Sample = 5SIIL02.

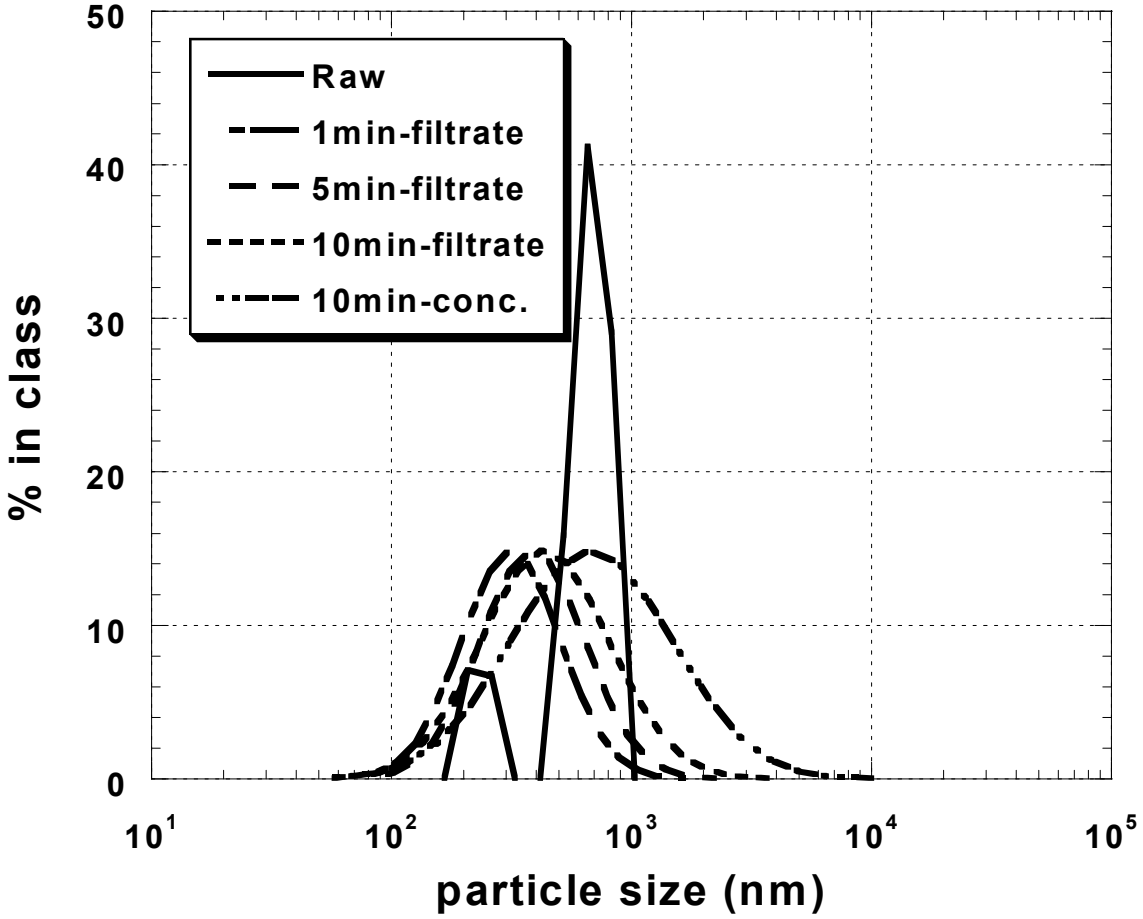

Figure A70. Changes in particle size distribution during filtration operation. Experimental conditions: pH = 9; electrostatic field = 97.8 V/cm; Sample = 5SIIL02.

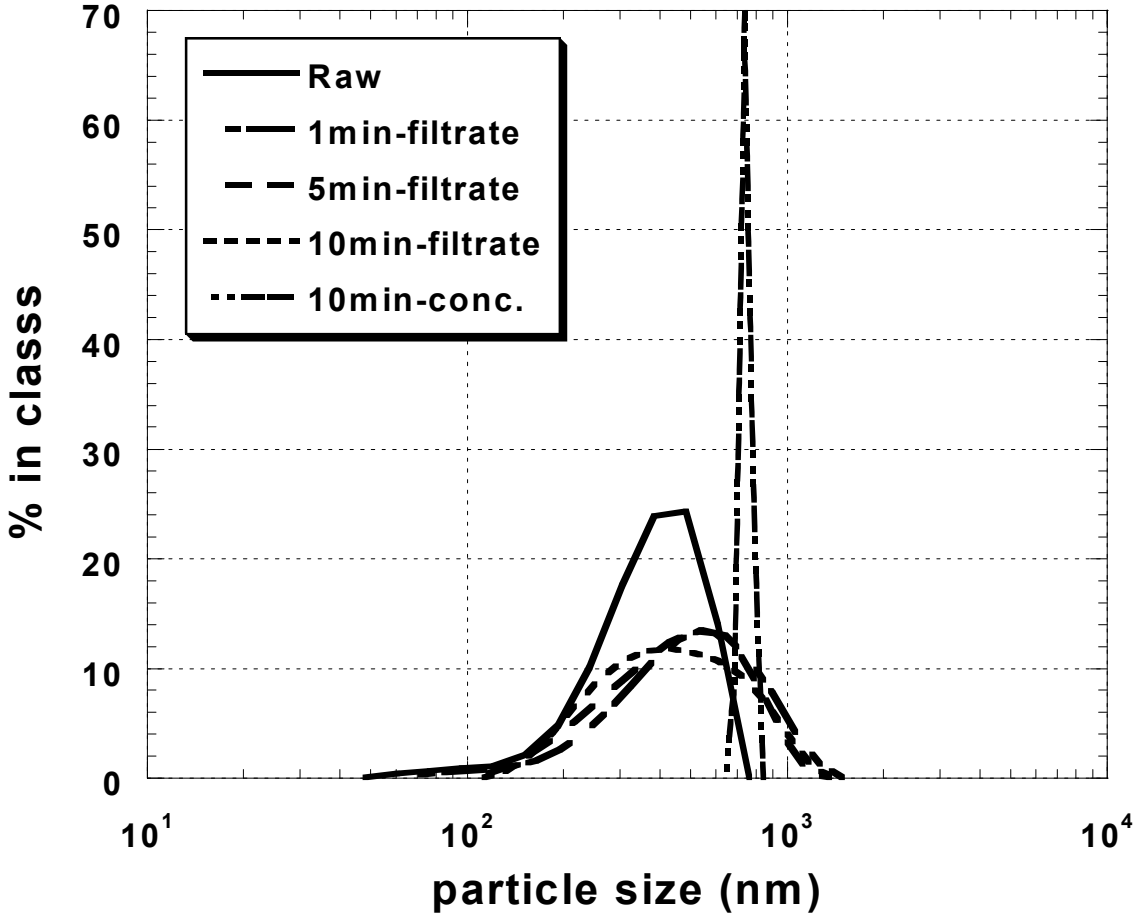

Figure A71. Changes in particle size distribution during filtration operation. Experimental conditions: electrostatic field = 17.1 V/cm; pH = 7.9; Sample = MW3IB01.

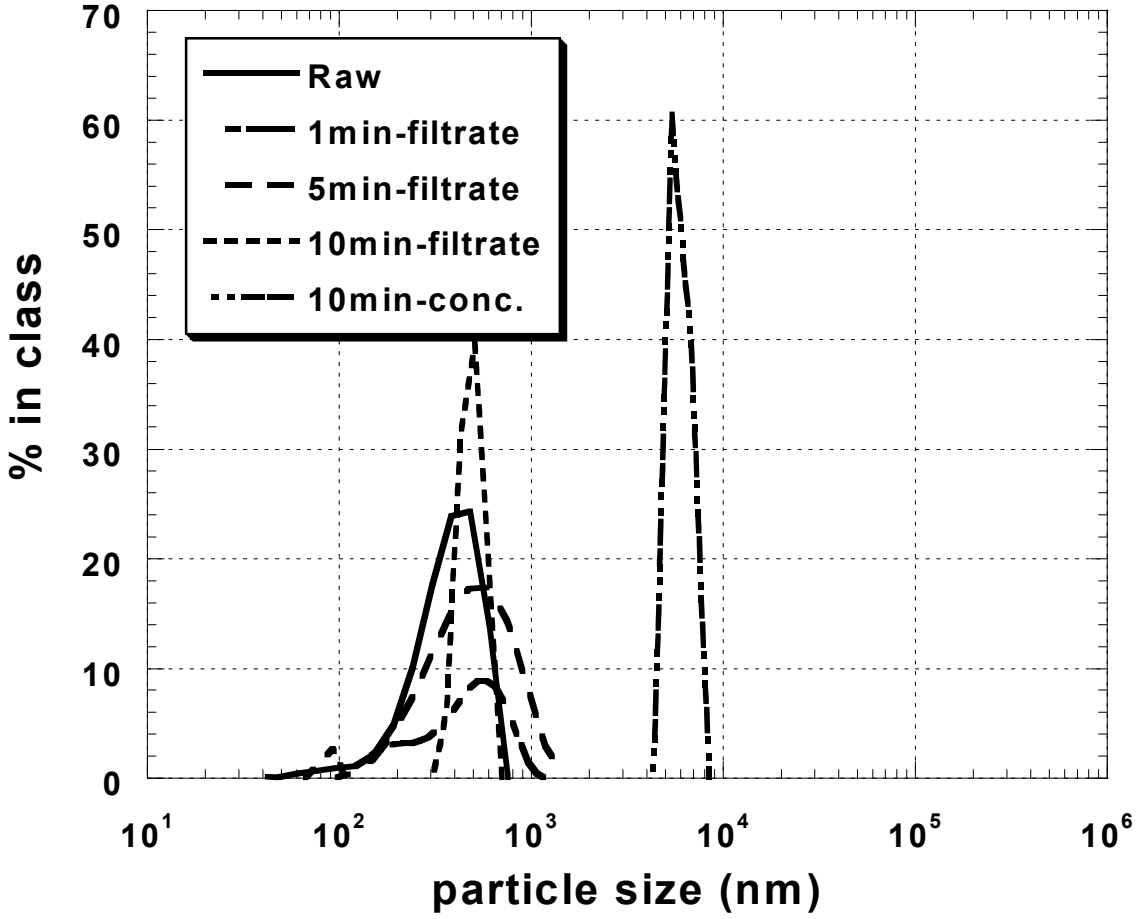

Figure A72. Changes in particle size distribution during filtration operation. Experimental conditions: pH = 5; electrostatic field = 10.3 V/cm; Sample = MW3IB01.

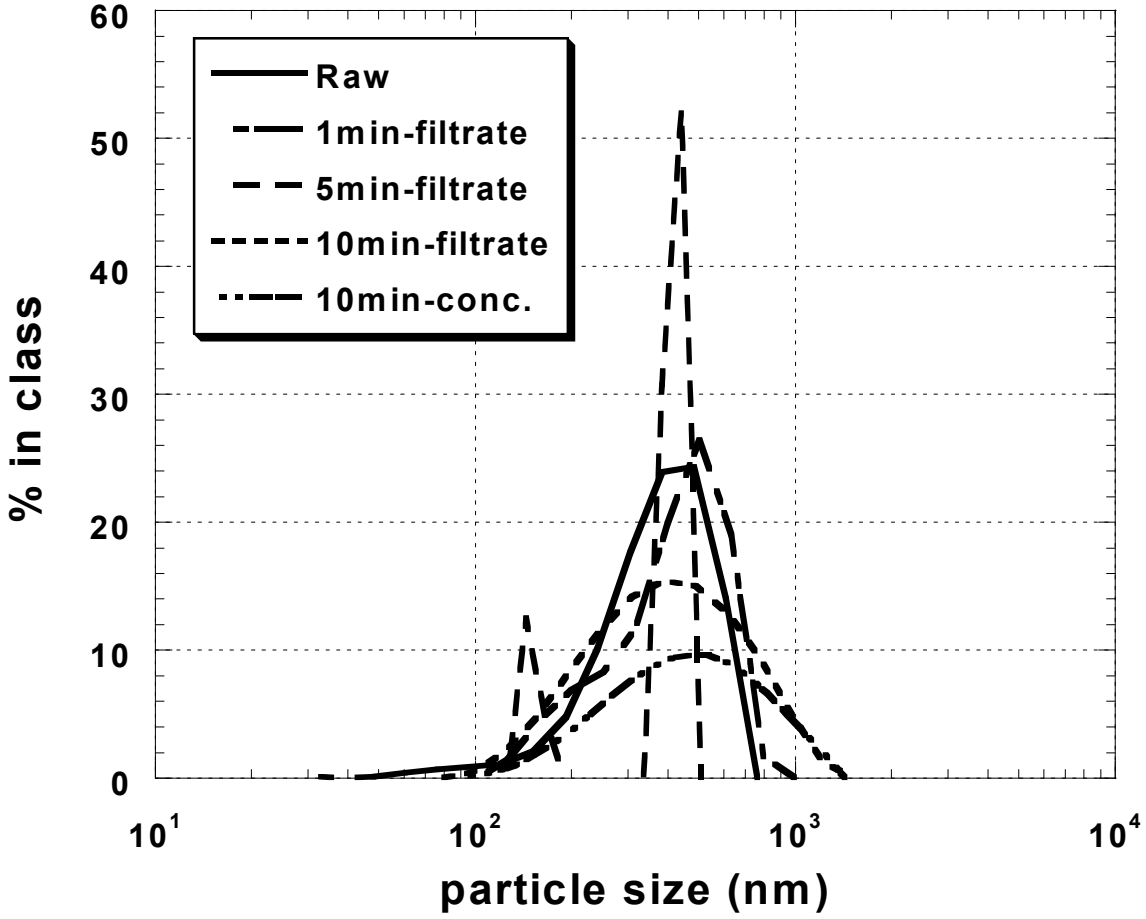

Figure A73. Changes in particle size distribution during filtration operation. Experimental conditions: pH = 7; electrostatic field = 13.2V /cm; Sample = MW3IB01.

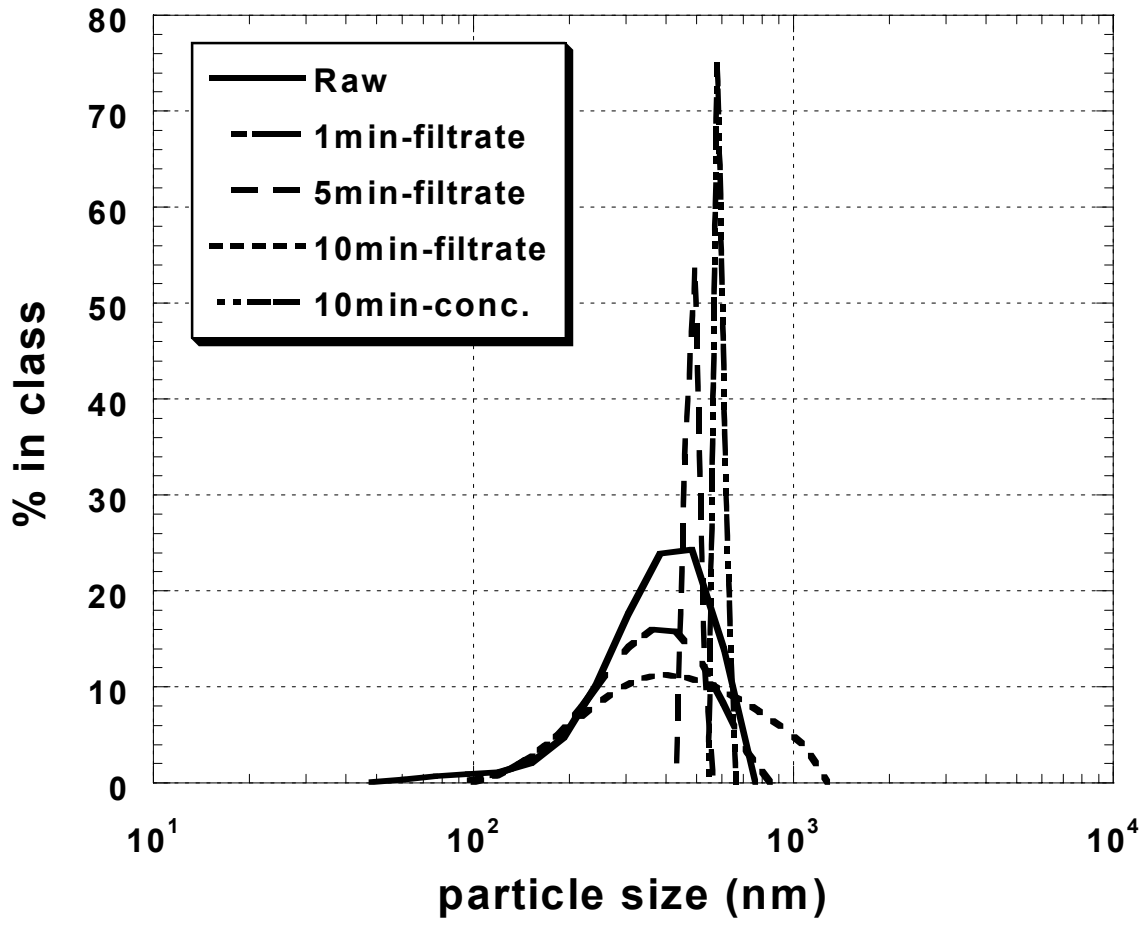

Figure A74. Changes in particle size distribution during filtration operation. Experimental conditions: pH = 9; electrostatic field = 14.8 V/cm; Sample = MW3IB01.

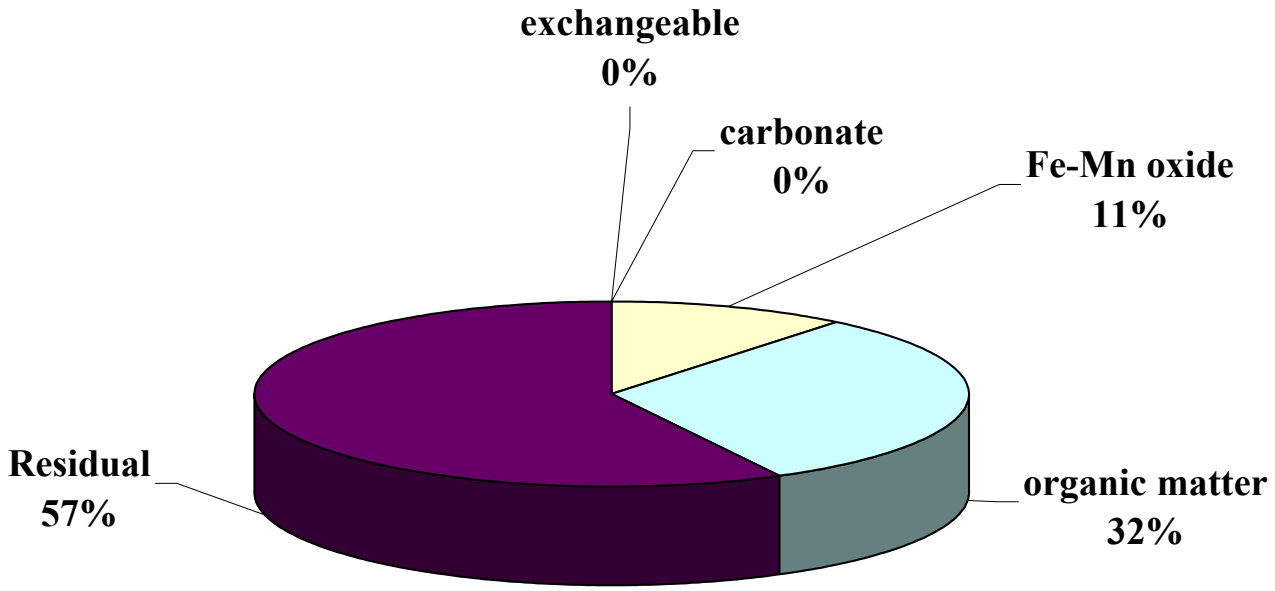

Figure A75. Distribution of lead species in particulate collected from well water sample 10IB01.

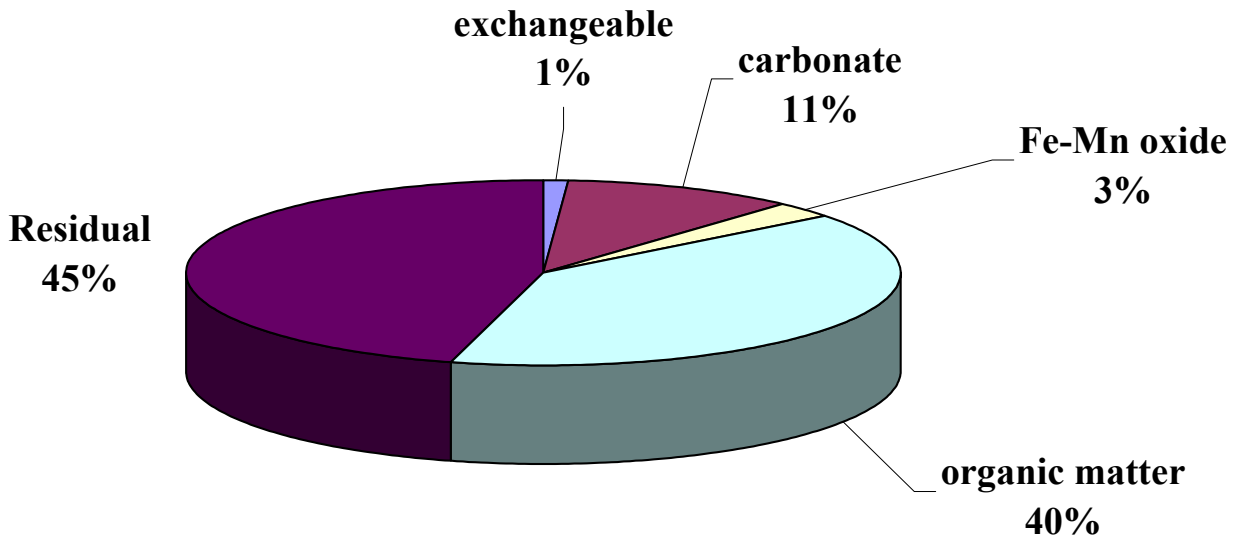

Figure A76. Distribution of lead species in particulate collected from well water sample 10IB01 at constant pH value. Experimental conditions: electrostatic field = 32.3 V/cm; pH = 6.5.

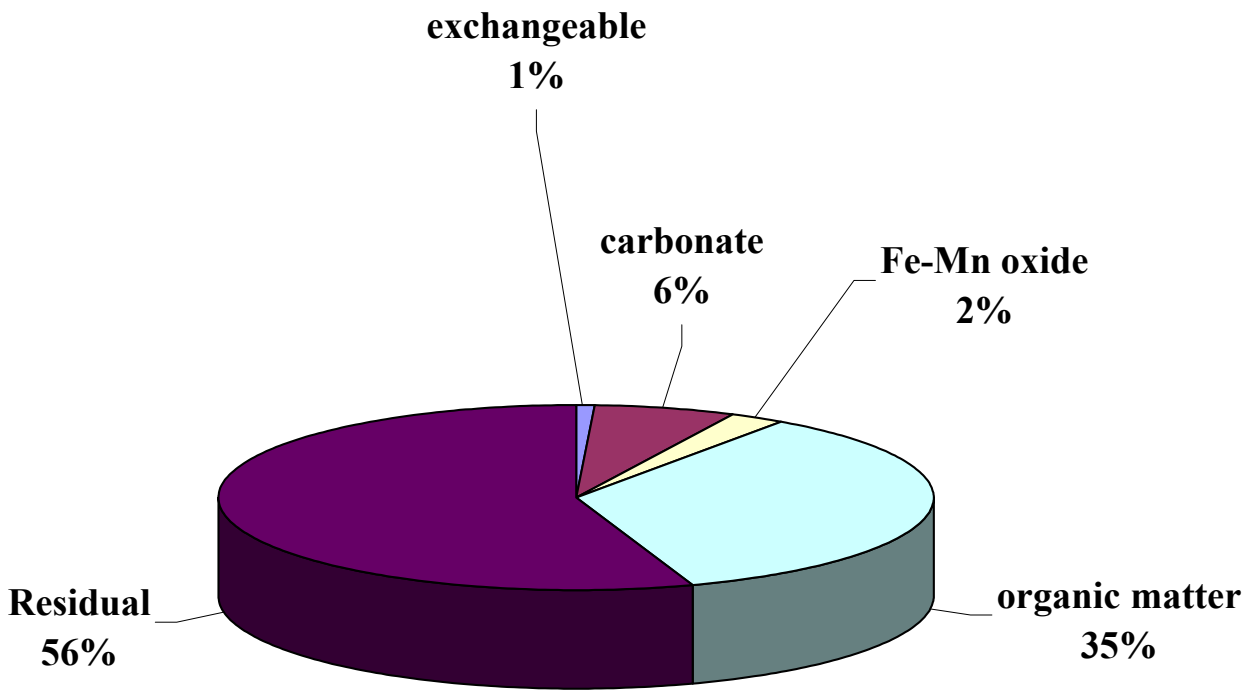

Figure A77. Distribution of lead species in particulate collected from well water sample 10IB01 at constant value. Experimental conditions: electrostatic field = 48.4 V/cm; pH = 6.5.

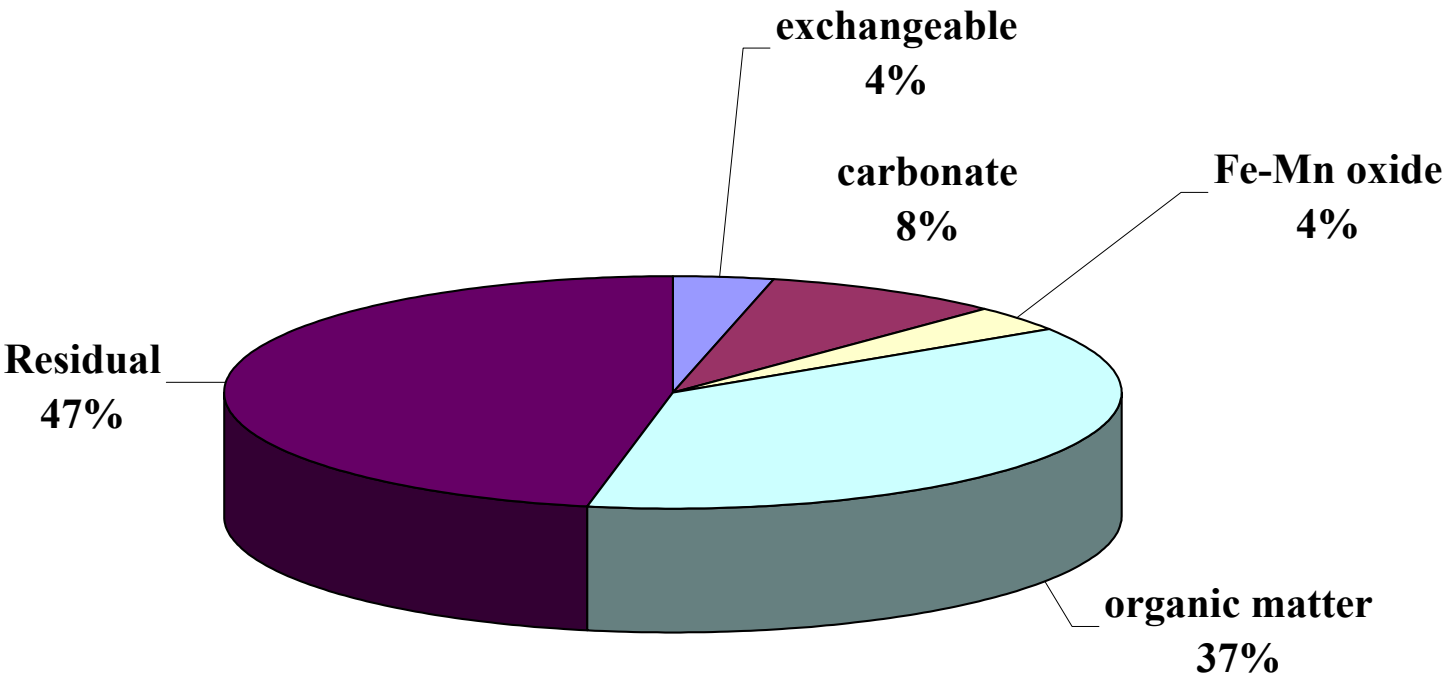

Figure A78. Distribution of lead species in particulate collected from water sample 10IB01 at constant pH value. Experimental conditions: electrostatic field = 64.5 V/cm; pH = 6.5.

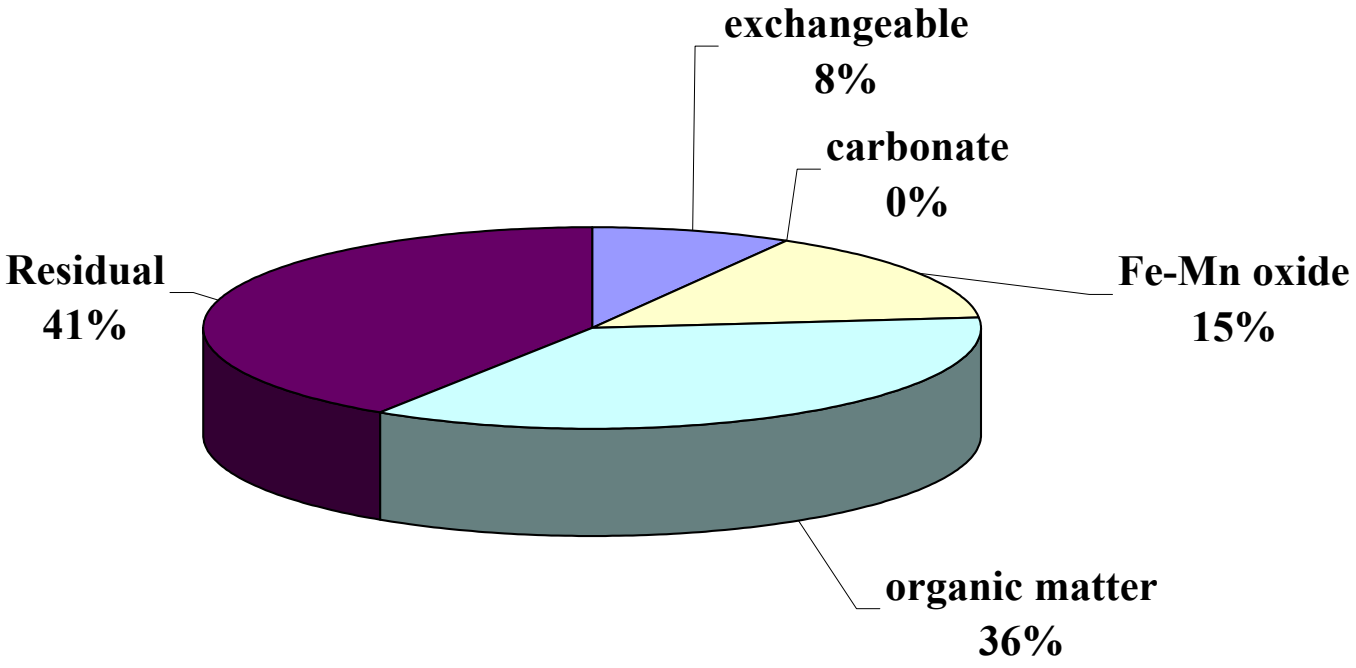

Figure A79. Distribution of lead species in particulate collected from well water sample 10IB01 at constant electrostatic field. Experimental conditions: electrostatic field = 32.3V/cm; pH = 5.

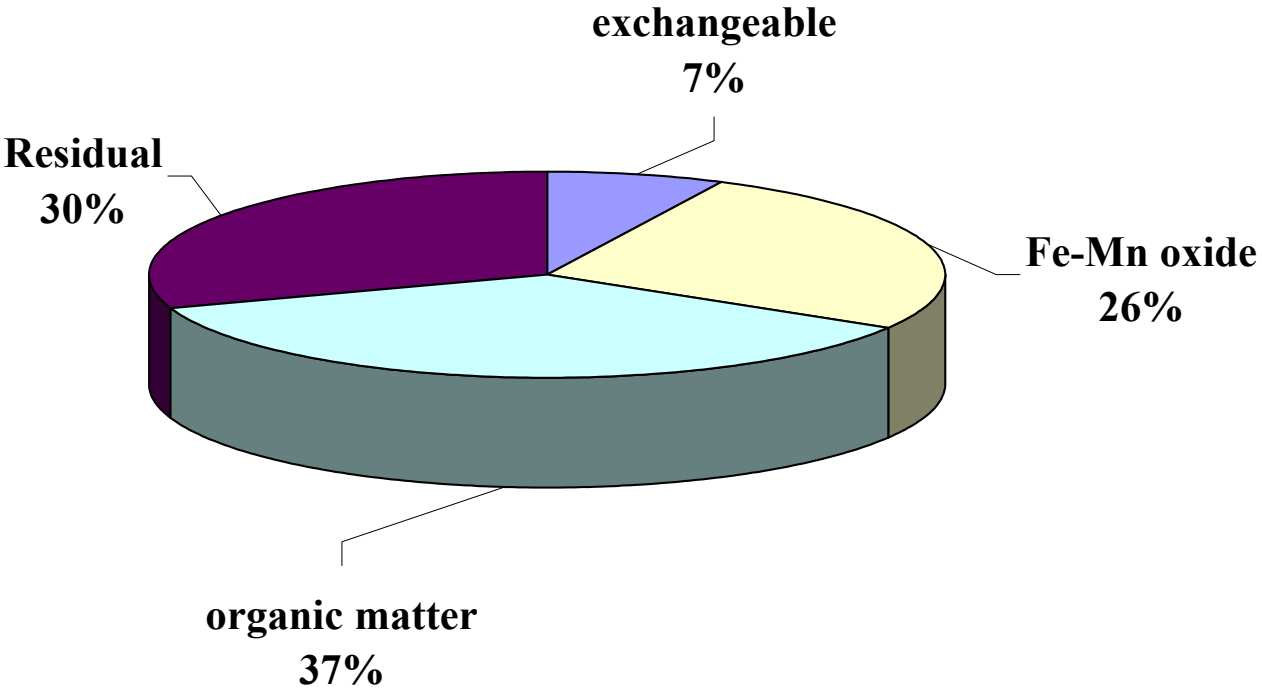

Figure A80. Distribution of lead species in particulate collected from well water sample 10IB01 at constant electrostatic field. Experimental conditions: electrostatic field = 48.4 V/cm; pH = 7.

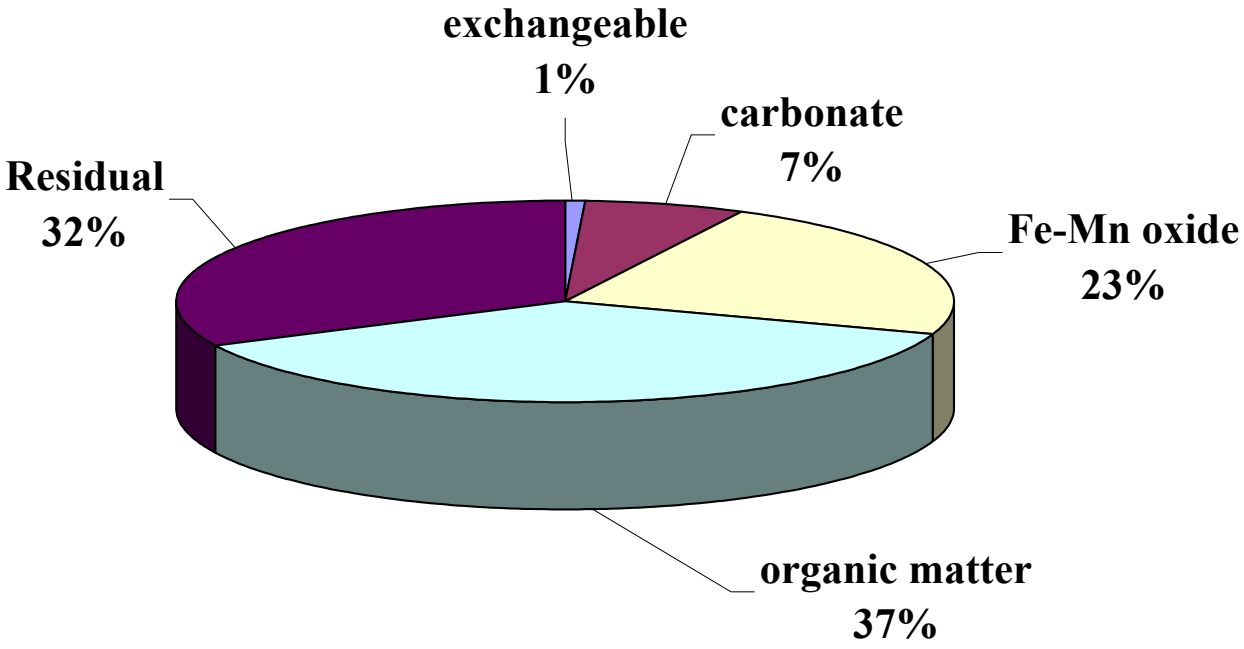

Figure A81. Distribution of lead species in particulate collected from well water sample 10IB01 at constant electrostatic field. Experimental conditions: electrostatic field = 64.5 V/cm; pH = 9.

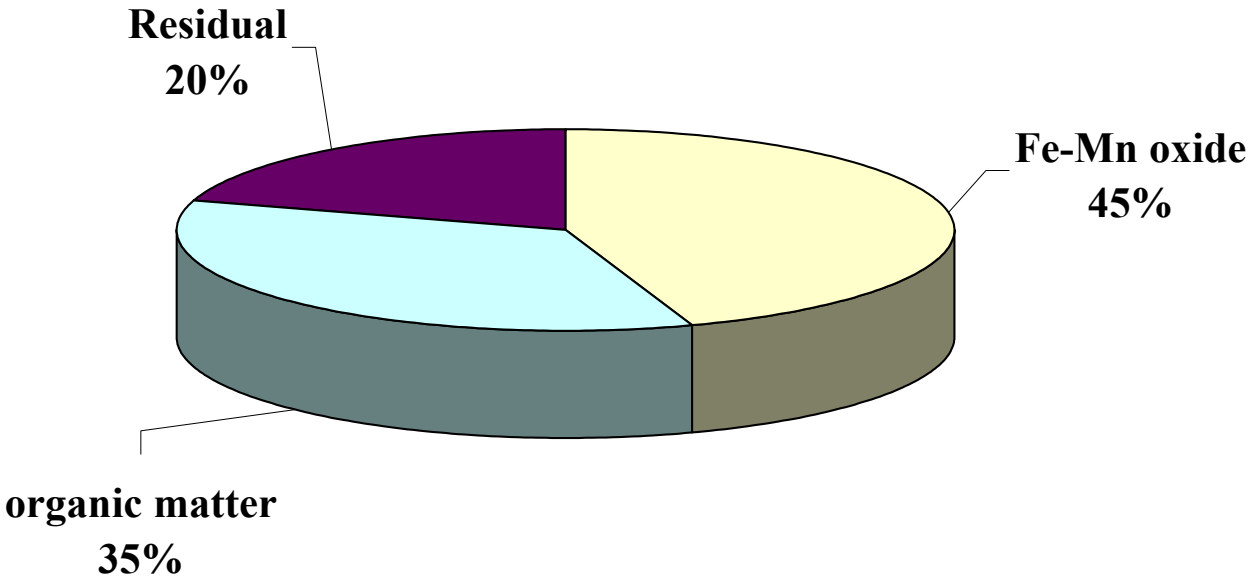

Figure A82. Distribution of lead species in particulate collected from well sample 10IL01.

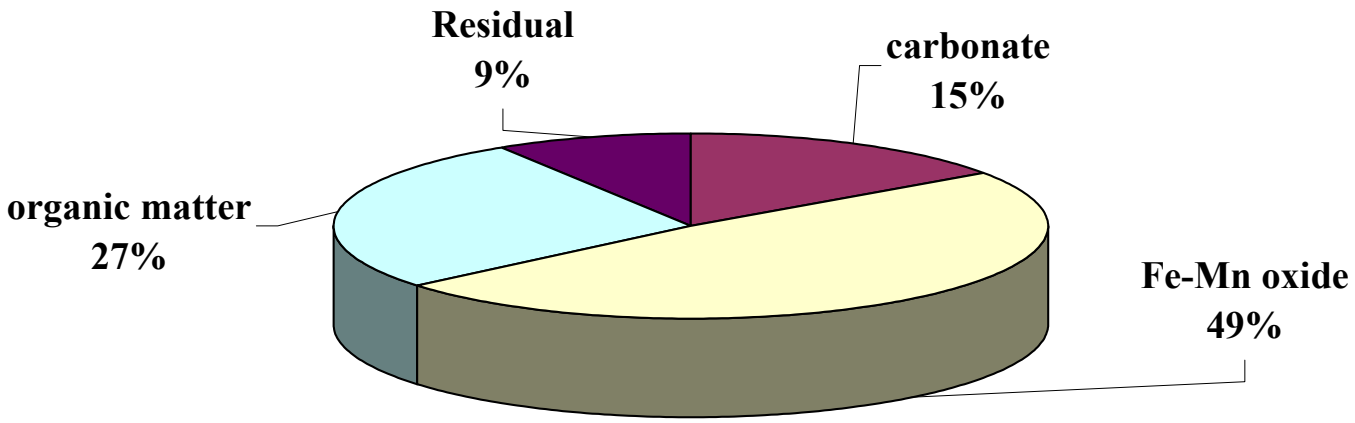

Figure A83. Distribution of lead species in particulate collected from well water sample 10IL01 at constant pH value. Experimental conditions: electrostatic field = 32.3 V/cm; pH = 6.5.

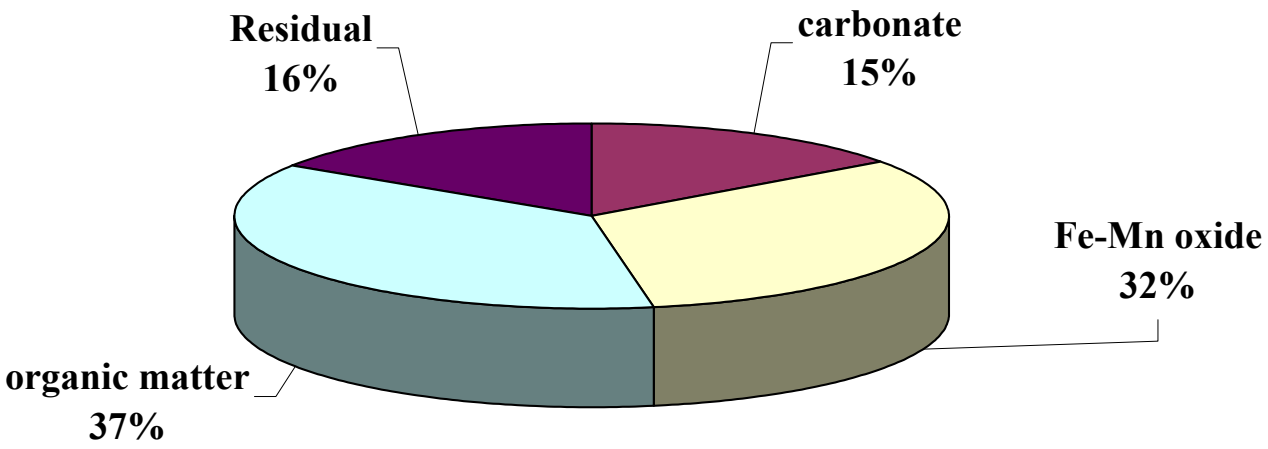

Figure A84. Distribution of lead species in particulate collected from well water sample 10IL01 at constant pH value. Experimental conditions: electrostatic field = 48.4 V/cm; pH = 6.5.

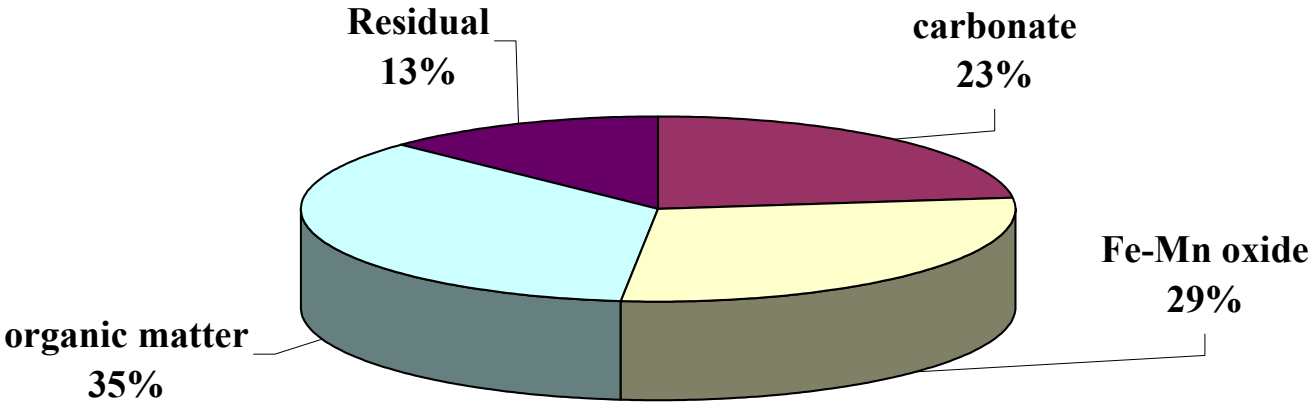

Figure A85. Distribution of lead species in particulate collected from well water sample 10IL01 at constant pH value. Experimental conditions: electrostatic field = 64.5 V/cm; pH = 6.5.

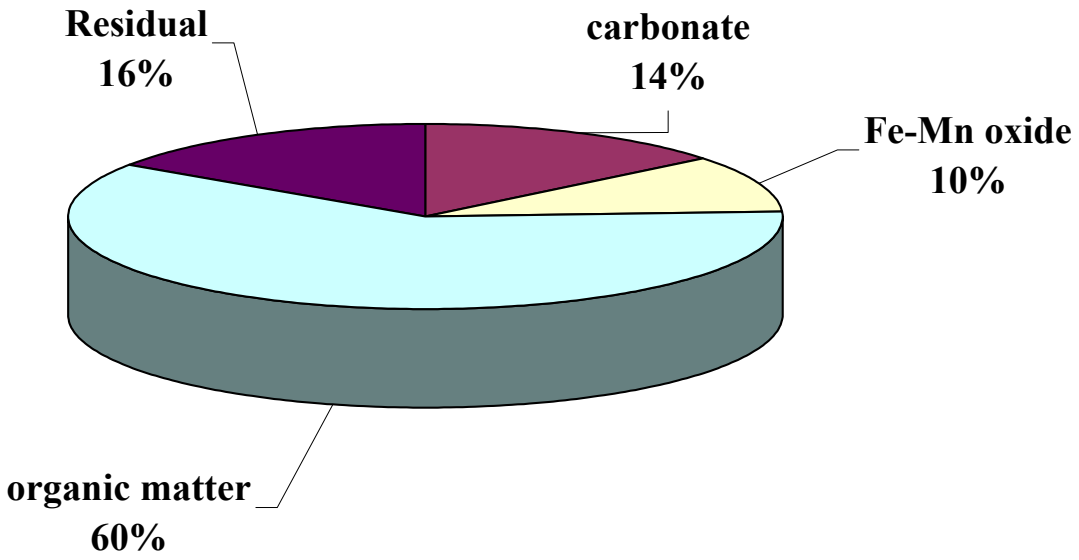

Figure A86. Distribution of lead species in particulate collected from well water sample 10IL01 at constant electrostatic field. Experimental conditions: pH = 5; electrostatic field = 32.3 V/cm.

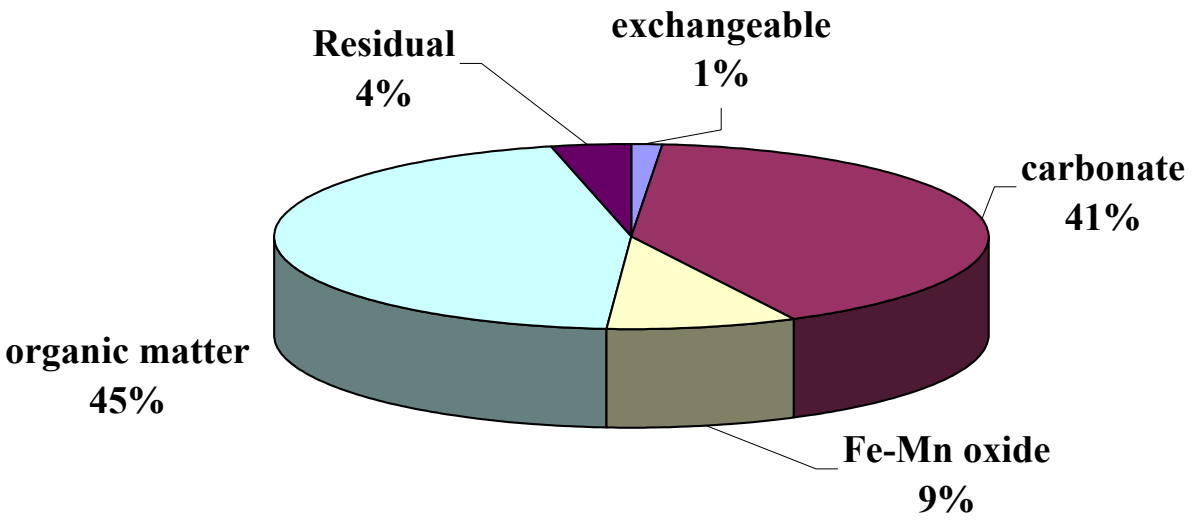

Figure A87. Distribution of lead species in particulate collected from well water sample 10IL01 at constant electrostatic field. Experimental conditions: pH = 7; electrostatic field = 48.4 V/cm.

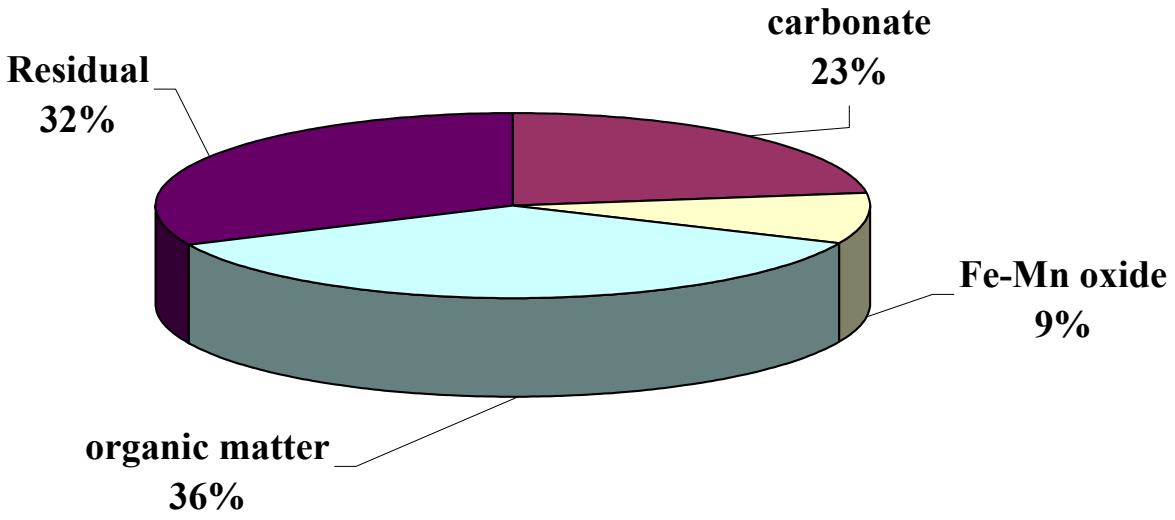

Figure A88. Distribution of lead species in particulate collected from well water sample 10IL01 at constant electrostatic field. Experimental conditions: pH = 9; electrostatic field = 48.4 V/cm.

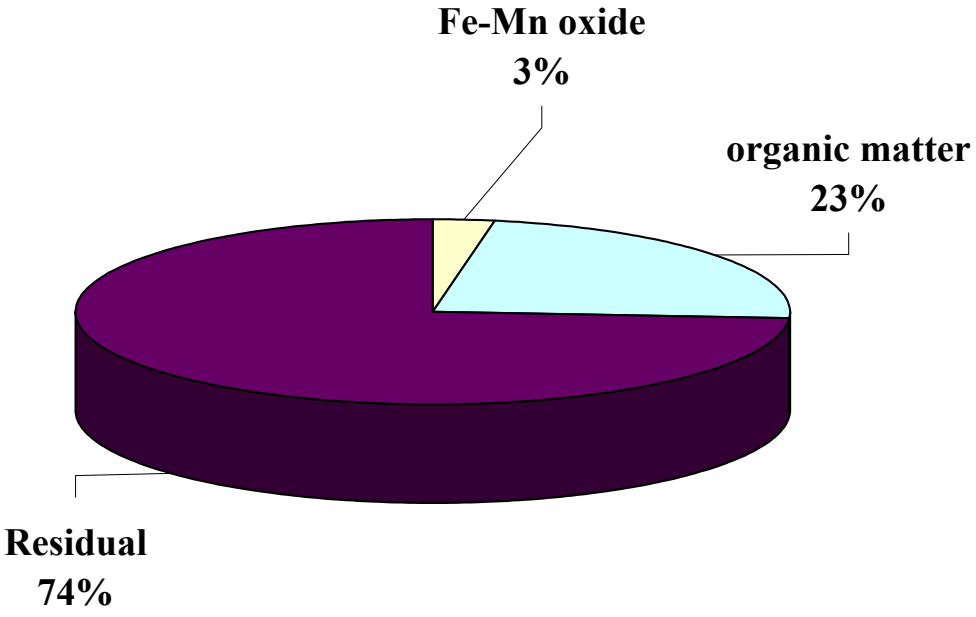

Figure A89. Distribution of lead species in particulate collected from well water sample 5SIIB03.

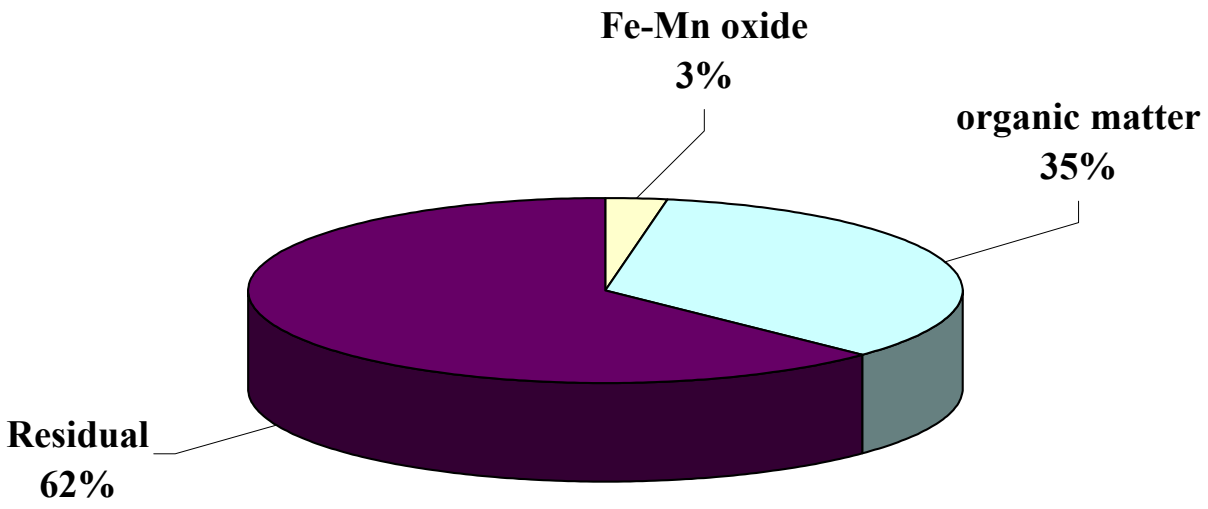

Figure A90. Distribution of lead species in particulate collected from well water sample 5SIIB03 at constant electrostatic field. Experimental conditions: pH = 5; electrostatic field = 97.8 V/cm.

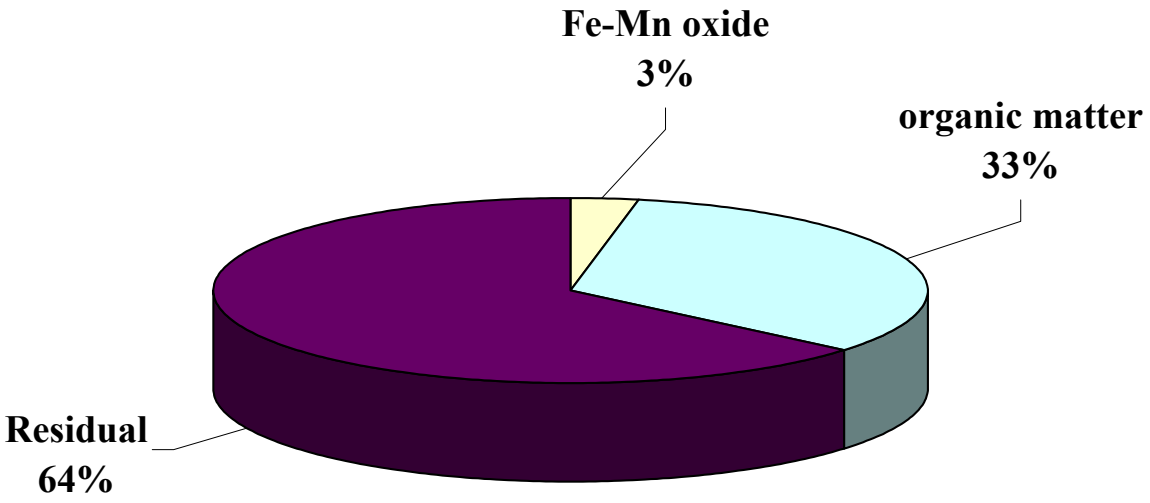

Figure A91. Distribution of lead species in particulate collected from well water sample 5SIIB03 at constant electrostatic field. Experimental conditions: pH = 7; electrostatic field = 97.8 V/cm.

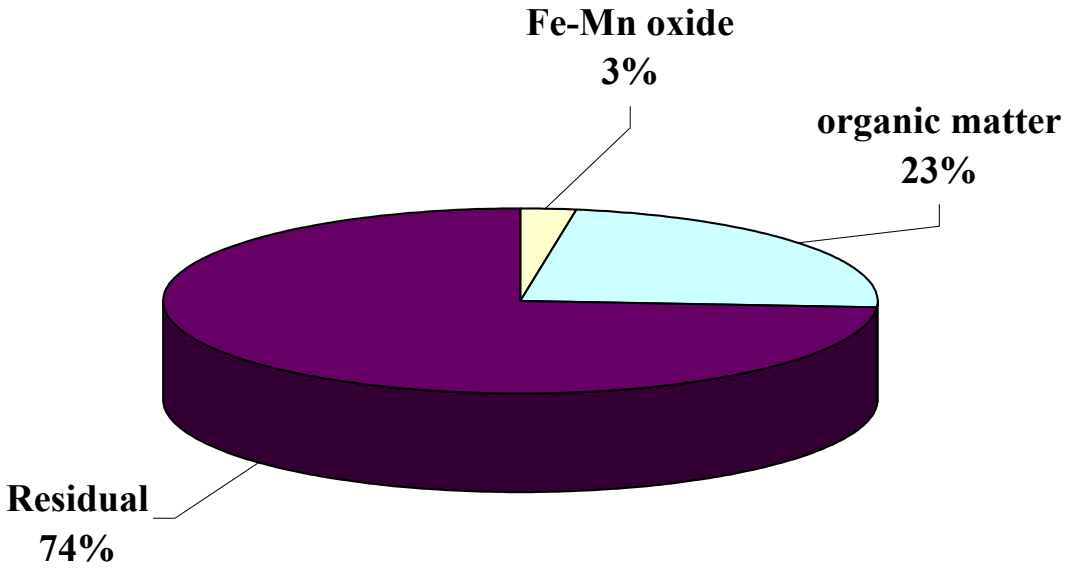

Figure A92. Distribution of lead species in particulate collected from well water sample 5SIIB03 at constant electrostatic field. Experimental conditions: pH = 9; electrostatic field = 97.8 V/cm.

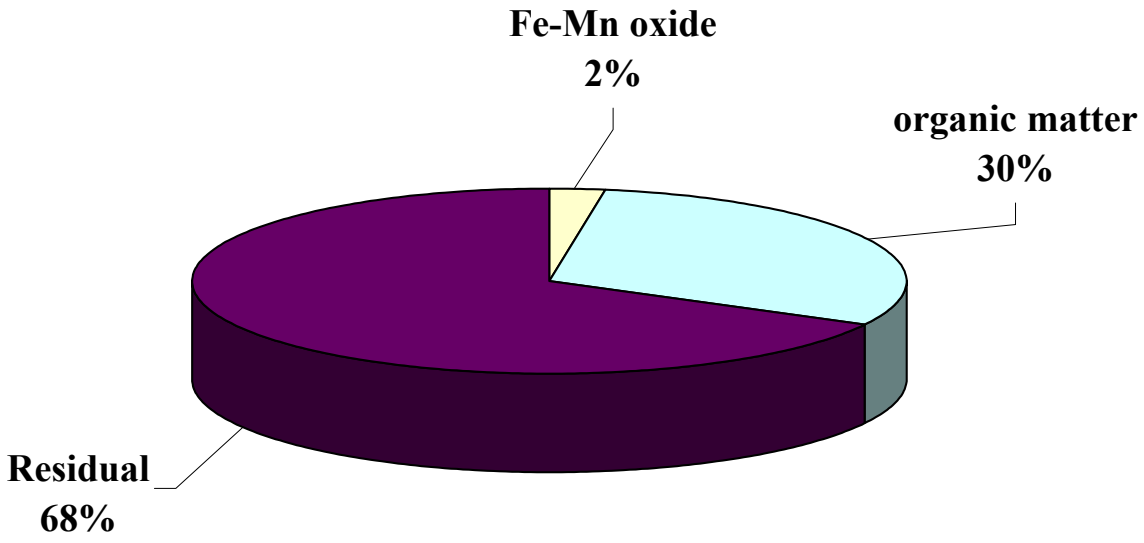

Figure A93. Distribution of lead species in particulate collected from well water sample 5SIIL02.

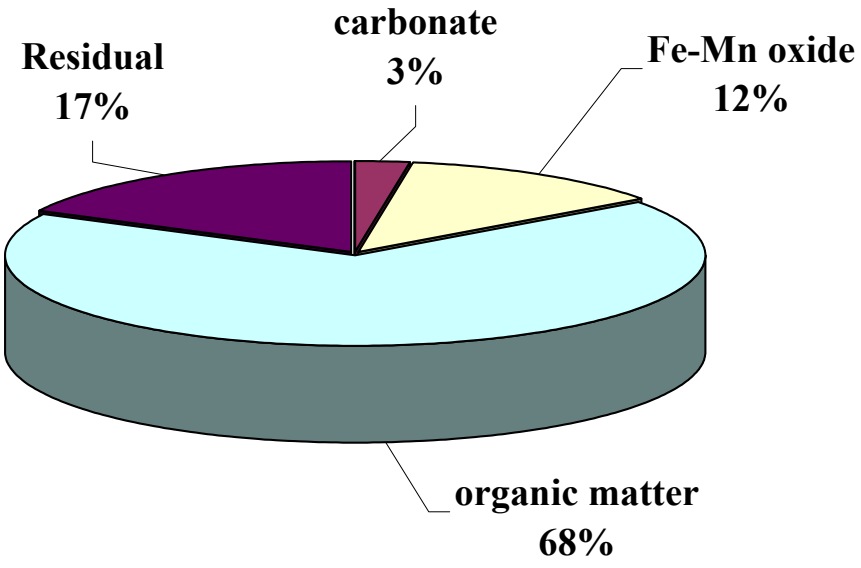

Figure A94. Distribution of lead species in particulate collected from well water sample 5SIIL02 at constant pH values. Experimental conditions: electrostatic field = 32.3 V/cm; pH = 6.7.

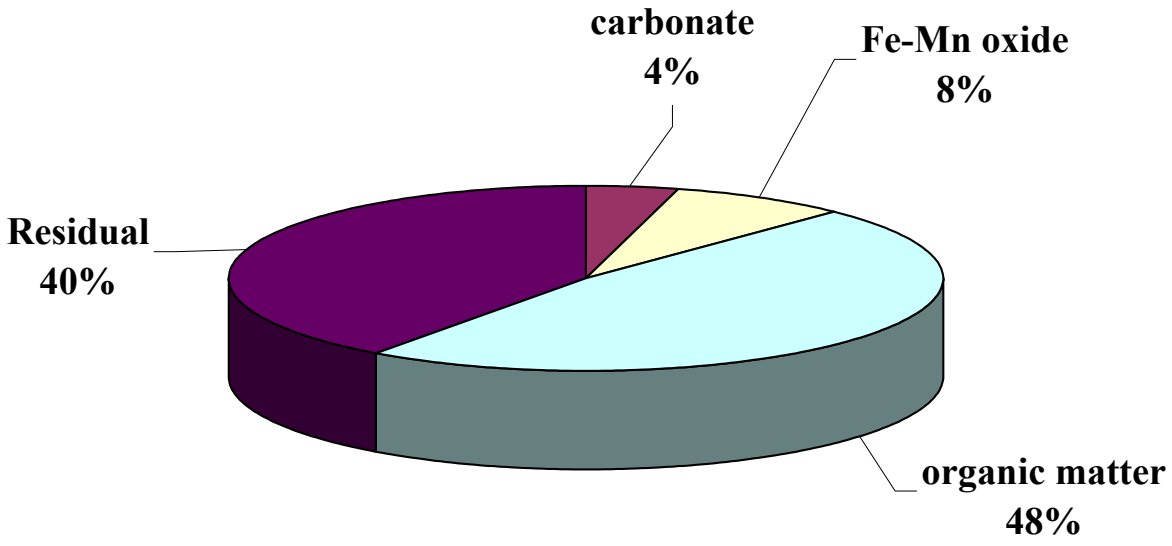

Figure A95. Distribution of lead species in particulate collected from well water sample 5SIIL02 at constant pH values. Experimental conditions: electrostatic field = 64.5 V/cm; pH = 6.7.

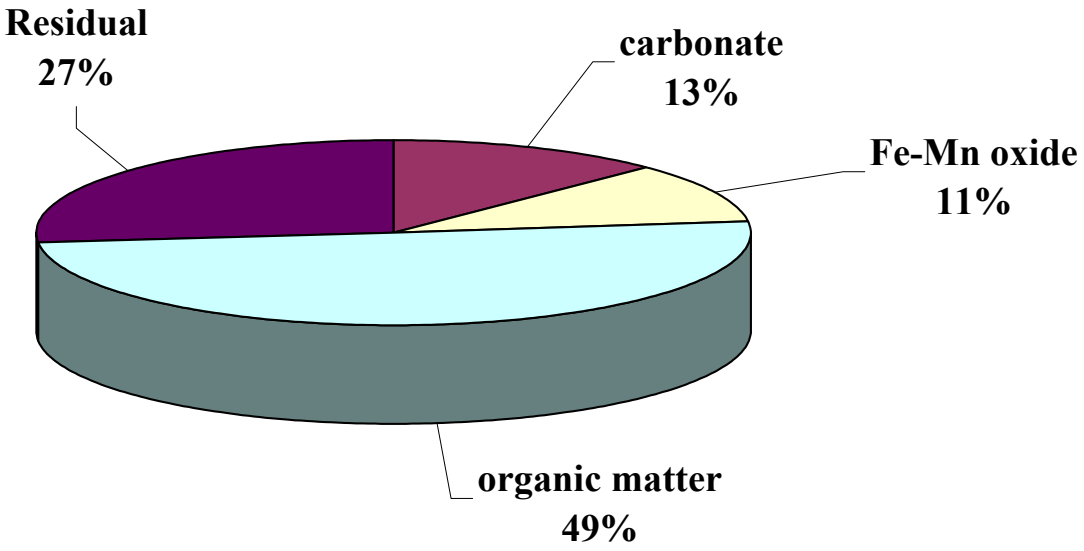

Figure A96. Distribution of lead species in particulate collected from well water sample 5SIIL02 at constant pH values. Experimental conditions: electrostatic field = 97.8 V/cm; pH = 6.7.

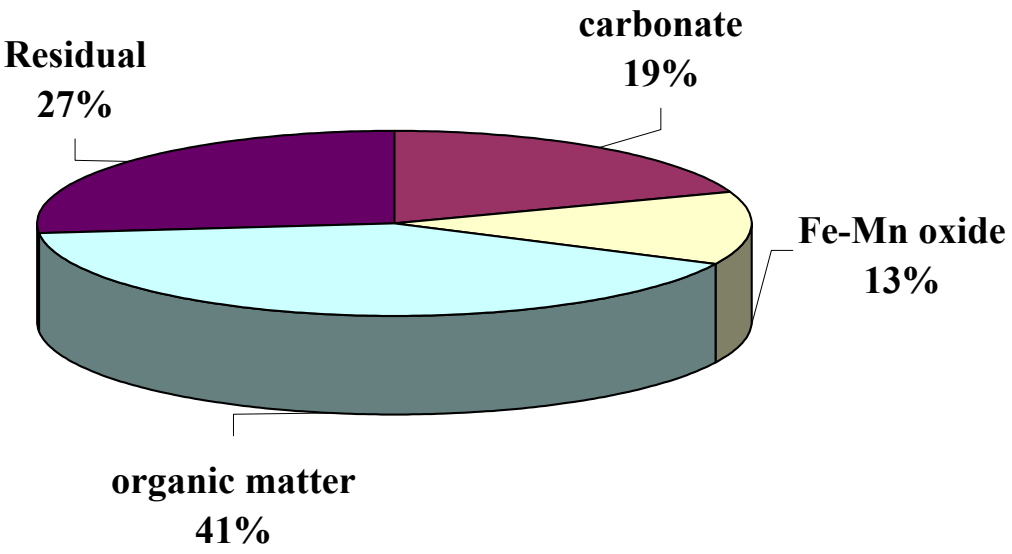

Figure A97. Distribution of lead species in particulate collected from well water sample 5SIIL02 at constant pH values. Experimental conditions: electrostatic field = 129.0 V/cm; pH = 6.7.

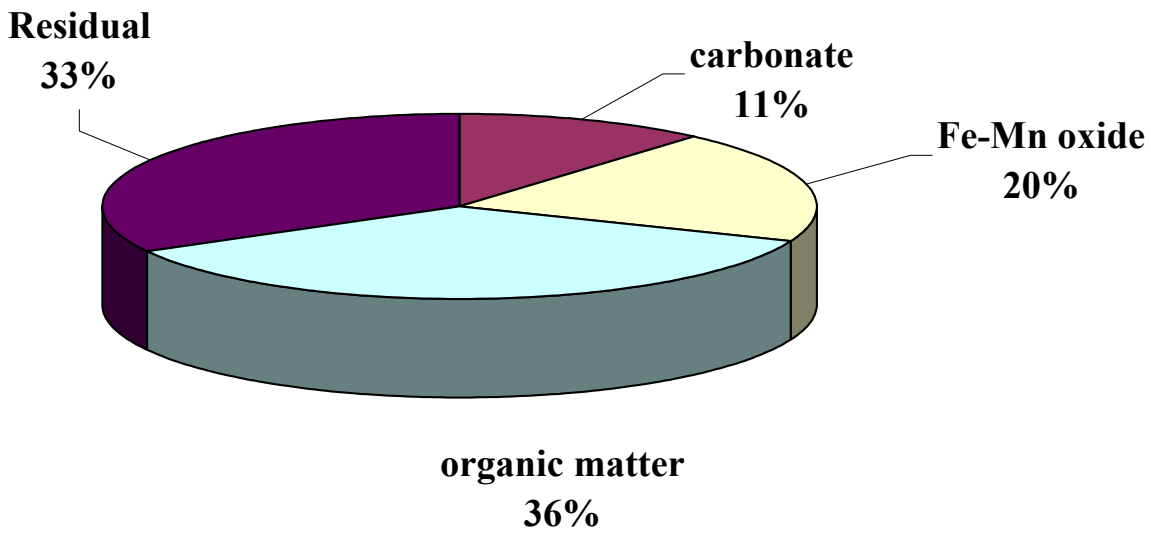

Figure A98. Distribution of lead species in particulate collected from well water sample 5SIIL02 at constant pH values. Experimental conditions: electrostatic field = 156.8 V/cm; pH = 6.7.

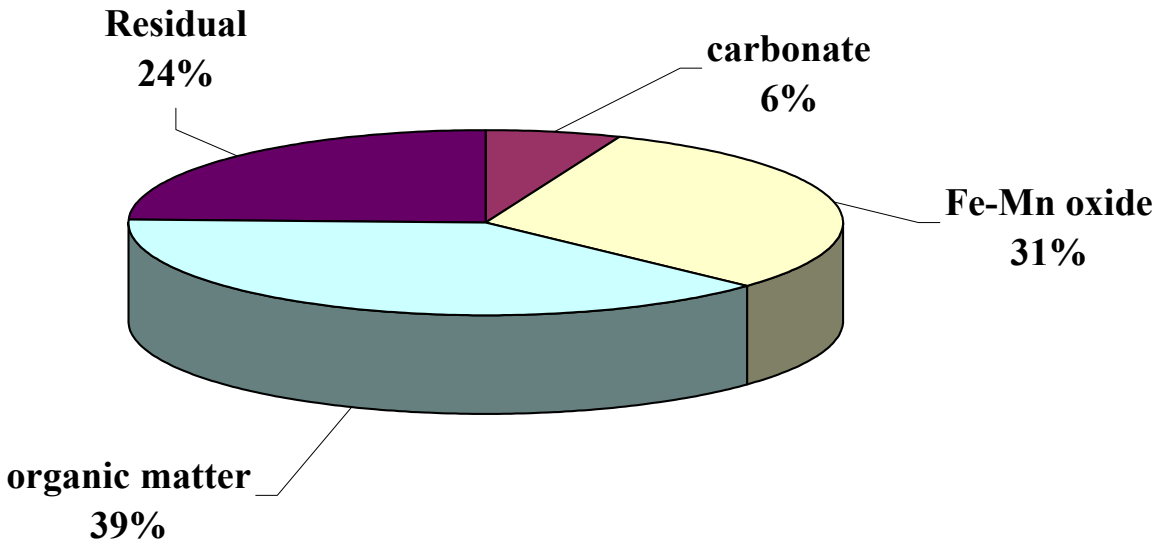

Figure A99. Distribution of lead species in particulate collected from well water sample 5SIIL02 at constant electrostatic field. Experimental conditions: pH = 4.5; electrostatic field = 97.8 V/cm.

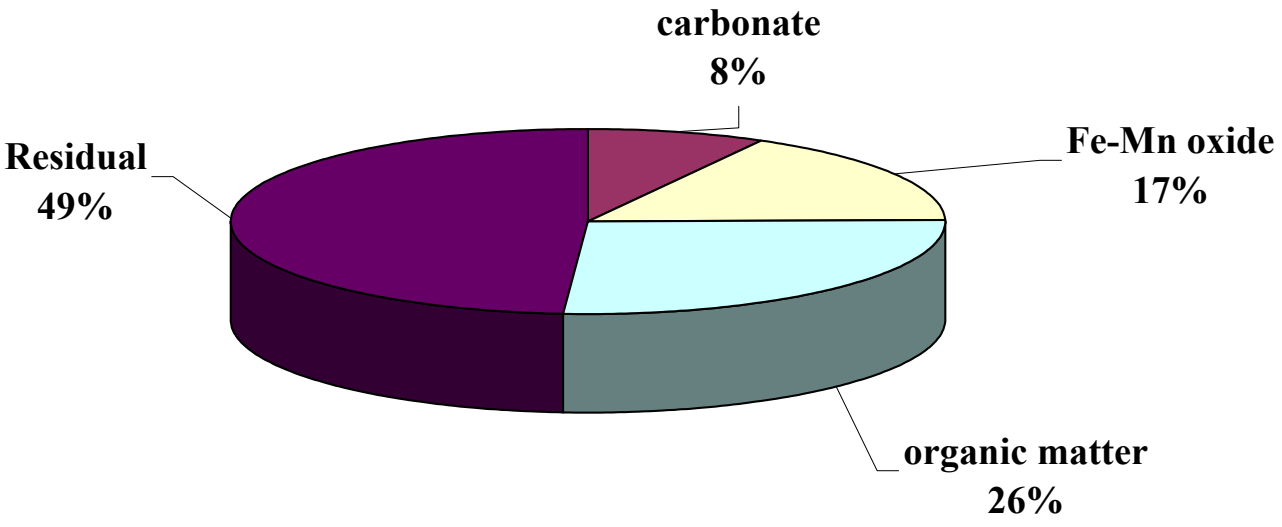

Figure A100. Distribution of lead species in particulate collected from well water sample 5SIIL02 at constant electrostatic field. Experimental conditions: pH = 6.5; electrostatic field = 97.8 V/cm.

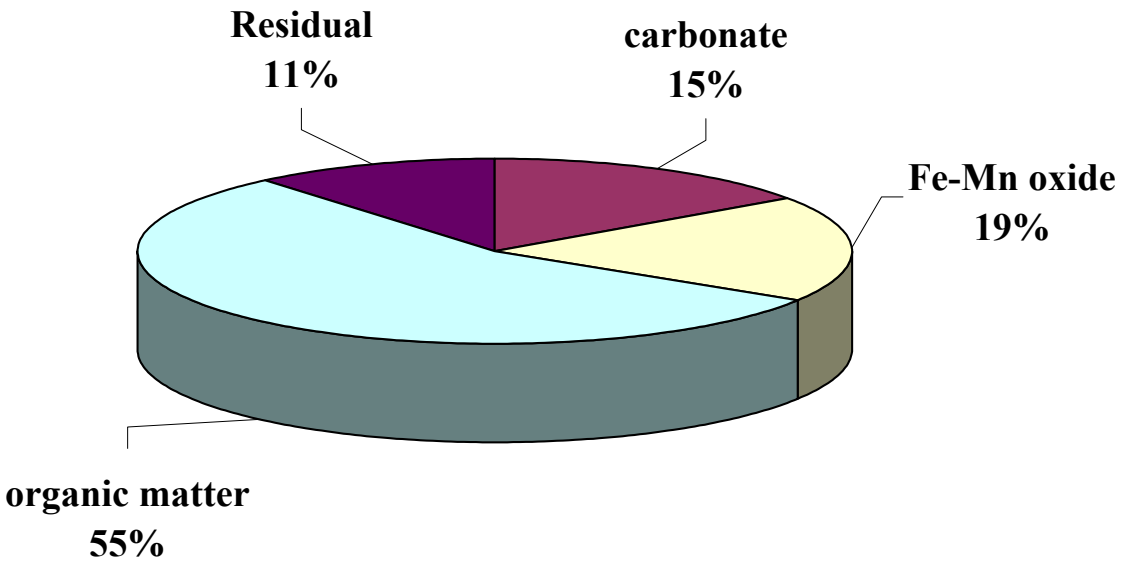

Figure A101. Distribution of lead species in particulate collected from well water sample 5SIIL02 at constant electrostatic field. Experimental conditions: pH = 9; electrostatic field = 97.8 V/cm.

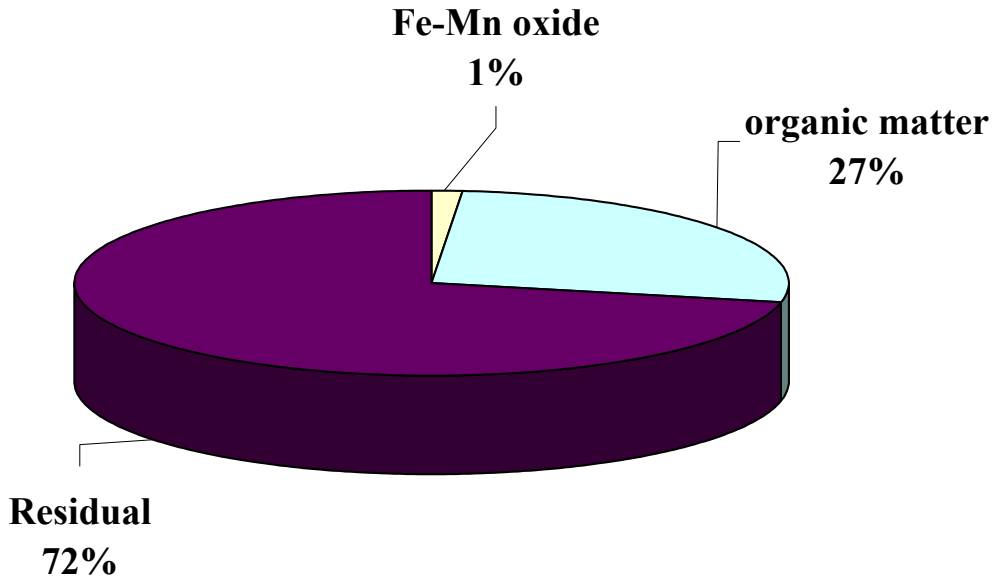

Figure A102. Distribution of lead species in particulate collected from well water sample MW3IB03.

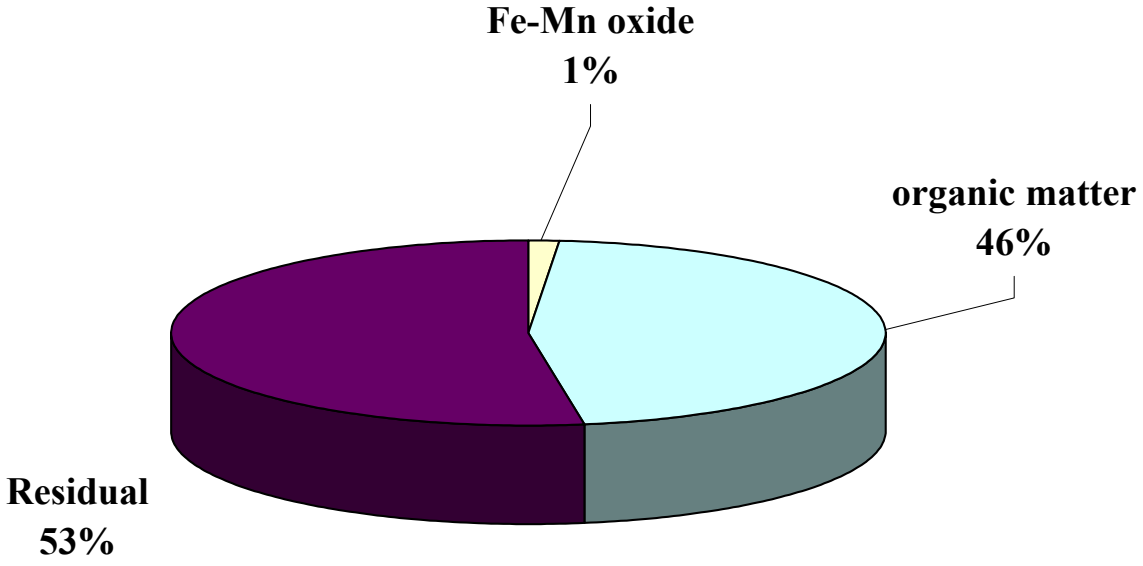

Figure A103. Distribution of lead species in particulate collected from well water sample MW3IB03. Experimental conditions: electrostatic field = 17.1 V/cm; pH = 7.9.

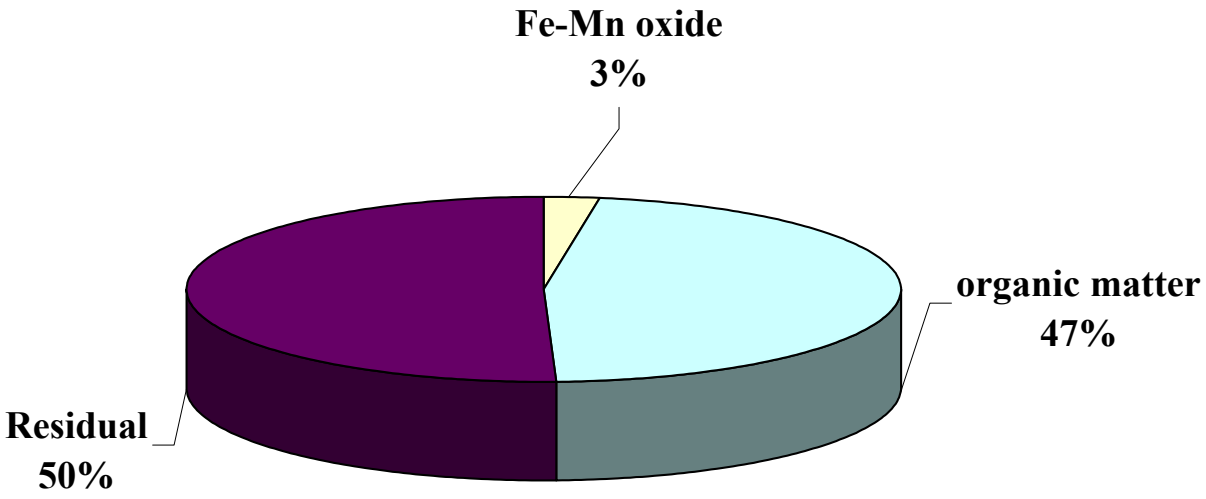

Figure A104. Distribution of lead species in particulate collected from well water sample MW3IM03 at constant electrostatic field. Experimental conditions: pH = 5; electrostatic field = 10.3 V/cm.

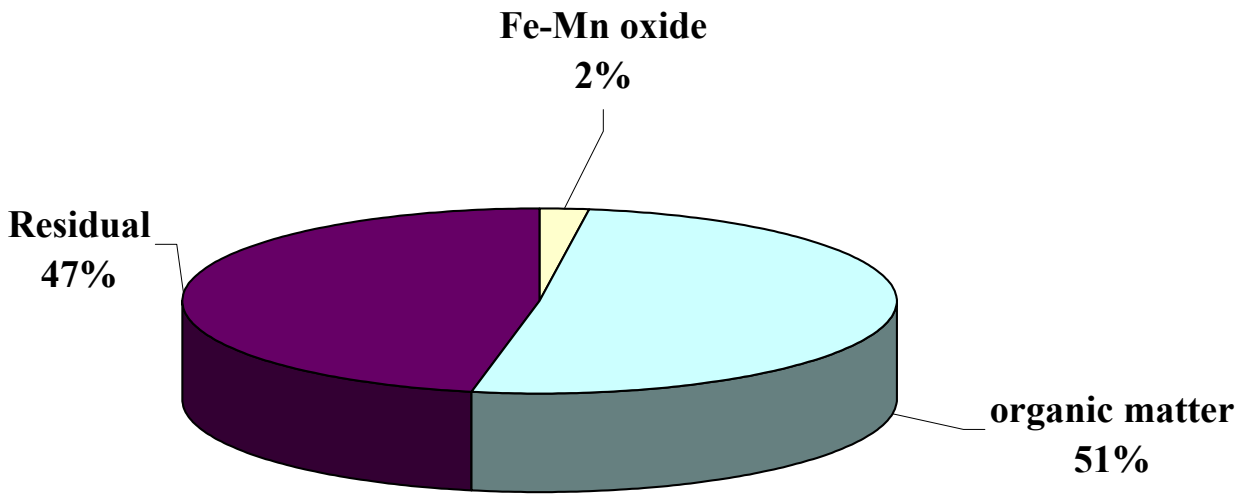

Figure A105. Distribution of lead species in particulate collected from well water sample MW3IM03 at constant electrostatic field. Experimental conditions: pH = 7; electrostatic field = 13.2 V/cm.

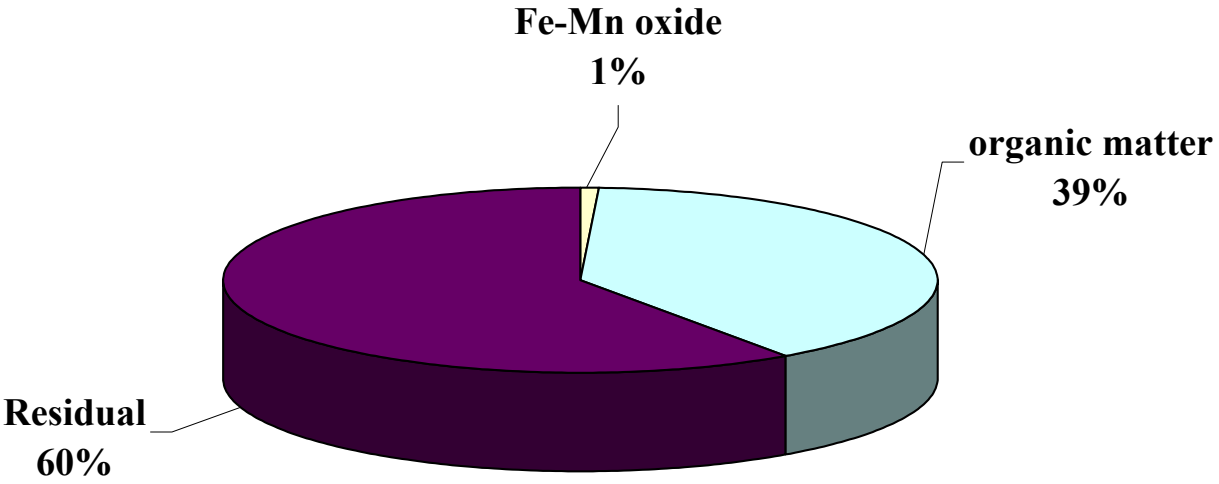

Figure A106. Distribution of lead species in particulate collected from well water sample MW3IM03 at constant electrostatic field. Experimental conditions: pH = 9; electrostatic field = 14.8 V/cm.